# PROTONATION OF METAL-SULFUR COMPLEXES: SYNTHETIC AND MECHANISTIC STUDIES

by

**Ahmed Ali Swadi Alwaaly**

A thesis submitted in partial fulfillment

of the requirements for the degree of

Doctor of Philosophy

University of Newcastle

School of Chemistry

**05 / 06 / 2015**

I certify that the work contained in this thesis submitted by me for the degree of PhD is my own original work; except where due reference is made to other authors; and has not been previously submitted for a degree at this or any other university.

Signed

**Ahmed Alwaaly**

Acknowledgements

I would first like to thank Prof. Richard A. Henderson for his guidance, encouragement, support during these years and patience have been invaluable.

Thank you to my follow PhD student Thaer Al-Rammahi for his help.

Thanks for all the members' staff who helped. Dr. Kieth Izod, Dr. Simon Doherty, Dr. John Errington, Dr. Corrine Willes for the NMR, Dr. Ross Harrington, Dr. William Clegg, Dr. Paul Waddell and Dr. Michael Probert for the X-ray crystallography and Richard Baron for the CHN analysis.

Finally I would like to thank my family back home and my wife and my friends for their support and encouragement.

# Abstract


## Protonation of metal-sulfur complexes: synthetic and mechanistic studies

Nickel and iron are present in certain metalloenzymes (e.g. nitrogenases, hydrogenases and carbon monoxide dehydrogenase) and also in some industrial catalysts (e.g. isomerization and hydrocyanation catalysts) where the substrate transformations also involve reactions with acids. Understanding the protonation of simple nickel and iron complexes is important in establishing the mechanisms of these natural and industrial catalysts, this thesis will focus on kinetic studies of the protonation mechanisms of various nickel and iron complexes.

The complexes $[Ni(S_2CR)(triphos)]BPh_4$ {R = Me, Et or $Bu^n$; triphos = $PhP(CH_2CH_2PPh_2)_2$} and $[Ni(S_2CC_6H_4R'\text{-}4)(triphos)]BPh_4$ (R′ = H, Me, Cl or OMe) were synthesised and characterised by spectroscopy, and for R = Et; R′ = Me, H, Cl or OMe the X-ray crystal structures were determined. The crystallography shows that the nickel is trigonal bipyramidal with the dithioate ligand being bidentate and spanning equatorial and axial positions. The protonation reactions of all $[Ni(S_2CR)(triphos)]^+$ and $[Ni(S_2CC_6H_4R'\text{-}4)(triphos)]^+$ with HCl to form $[Ni(HS_2CR)(triphos)]^+$, $[Ni(HS_2CC_6H_4R'\text{-}4)(triphos)]^+$ in MeCN have been studied . In all cases the rates of protonation are slow and the rate law is complicated. The kinetics are consistent with two coupled equilibria where initially the HCl binds to a sulfur through hydrogen bonding, and this is followed by intramolecular proton transfer to the sulfur. For the alkyl derivatives the rates of protonation are dependent on the electronic nature of the R group while the affect of the 4-R′-substituent on the aryl derivatives is small. The overall isotope effects for transfer of the proton from HCl to $[Ni(S_2CR)(triphos)]^+$ {$(K_1^R k_2^R)^H$ / $(K_1^R k_2^R)^D$} are all small (0.94 – 0.25). The protonation of each sulfur in $[Ni(S_2CR)(triphos)]^+$ (R = Me or Ph) has been explored using molecular mechanics calculations (GAUSSIAN09 package, geometries optimized at the B3LYP/Lanl2dz levels of theory). The calculations indicate that the protonation of the sulfur in the equatorial position results in chelate ring-opening, but protonation of the sulfur in the axial position does not. The calculated $pK_a^R$s of the coordinated carboxydithioic acid are rather insensitive to the R-substituent ($pK_a^R$ = 7.2 – 8.3).

The analogous $[Ni(O_2CR)(triphos)]BPh_4$ (R = Et or Ph) have also been prepared and studied. The protonation of these complexes is much more rapid than the dithioate

analogues and so the kinetics of the protonation reactions were studied with the weak acid $lutH^+$ (lut = 2,6-dimethylpyridine). .

The complexes $[Ni(OC_6H_5R\text{-}4)(triphos)]BPh_4$, $[Ni(SePh)(triphos)]BPh_4$ and $[Ni(XR')(triphos)]BPh_4$ (R = H, $CH_3$, Cl or $OCH_3$X = S, R′ = Et, $Bu^t$ or Cy) have been synthesised and characterised. For $[Ni(SeC_6H_5)(triphos)]BPh_4$ and all $[Ni(XR')(triphos)]BPh_4$ the X-ray crystal structures have been determined. The protonation reactions of all these derivatives have been studied using the weak acid $lutH^+$. The kinetics of the protonation reactions is consistent with an equilibrium mechanism in which the acid initially hydrogen bonds to the O or Se site and then undergoes intramolecular proton transfer. In the reaction of $[Ni(SePh)(triphos)]^+$, the hydrogen bonded intermediate accumulates at high concentrations of $lutH^+$, but for the reactions of $[Ni(OC_6H_4R\text{-}4)(triphos)]^+$ the hydrogen bonded intermediate never attains a sufficient concentration to complicate the kinetics. The reason for the slow and similar rates of protonation of $[Ni(XPh)(triphos)]^+$ (X = O, S or Se) have been studied using DFT calculations which indicate that the slow proton transfer is because of steric interactions between $lutH^+$ and the phenyl group on triphos.

$[Ni(SR')_2(dppe)]$ (R′ = Et, $Bu^t$ or Cyh) have been synthesised and characterised using spectroscopy. The kinetics of the protonation reactions of all the derivatives with $lutH^+$ in MeCN is described. The rate law is complicated and the kinetics is consistent with two coupled equilibria where firstly the acid hydrogen bonds to sulfur and this is followed by intramolecular proton transfer to the sulfur.

In the last section of this thesis, the substitution reactions of two types of Fe-S-based clusters $[Fe_4S_4(OR)_4]^{2-}$ and$[\{MoFe_3S_4(OPh)_3\}_2(\mu\text{-}SPh)_3]^{3-}$ have been studied with $PhS^-$ in the presence of $NHEt_3^+$. The clusters were characterised using $^1H$ NMR spectroscopy. The kinetics of the reactions of the clusters with $PhS^-$ is consistent with a mechanism involving an initial rapid protonation step followed by the dissociation of phenoxide in the rate-limiting step. The mechanistic interpretations of these results are discussed in the light of studies on other Fe-S-based clusters and recent DFT calculations which suggest there is an elongation of a Fe-S bond after protonation.

Table of Contents

# Chapter One: Protonation of Coordinated Sulfur Sites Relevant to Metalloenzymes

## 1.1 Proton Transfer to Uncoordinated Sulfur Sites.

There are few studies on proton transfer in molecules or ions that containing sulfur, in comparison with the huge number of studies focused on nitrogen-containing and oxygen-containing molecules. Previous studies [1] show that the proton transfer to sulfur site is slower than the diffusion-controlled limit, in comparison with proton transfer to aryloxide or amines. Thus, deprotonation of acacH (acacH = acetylacetone) by thiolate is 5 times slower than by phenoxide; deprotonation of 4-$NO_2C_6H_4OCH_2CH_2C(O)Me$ by thiolate is 30-50 times slower than with $ArO^-$ and proton transfer between HCN and $HOCH_2CH_2S^-$ is 200 times slower than the reactions with $ArO^-$. It has been suggested that the origin of this behaviour is a consequence of the hydrogen bonding capabilities of the various molecules which occurs prior to electron transfer (Figure 1.1). The sulfur bases are poorer hydrogen bonders than oxygen-based or nitrogen based with a similar p*K*a. Since hydrogen bondig will stabilise the transition state for proton transfer the reactions with the sulfur bases are inherently slower. Comparison of the examples listed above has led to the suggestion that hydrogen bonding is particularly important if the charge on the deprotonated partner is not delocalised. Interestingly, the deprotonation of $ArCH_2NO_2$ is faster than with aryloxide, amines or carboxylates. In these systems the charge is extensively delocalised around the aryl-substituent and nitro-groups. Thus, it is argued, that this extensive delocalisation diminishes the importance of the hydrogen-bonding requirement prior to proton transfer and desolvation of the base becomes the important factor in defining the rates of proton transfer involving $ArCH_2NO_2$. Desolvation of thiolates is favoured over desolvation of the oxygen, and nitrogen-containing bases [2,3].

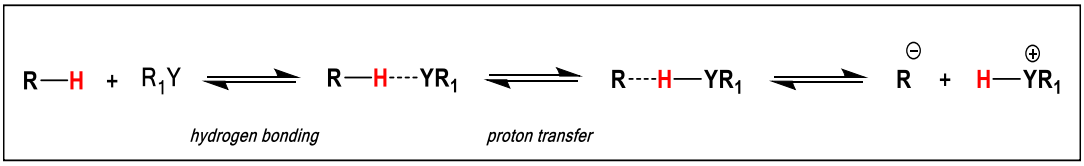


Figure 1.1. General proton transfer mechanism from the acid RH to the base $R_1Y$.

## 1.2 Protonation of coordinated thiolates.

### 1.2.1 Thiolate Ligands in Biology.

The Cysteine and methionine are essential amino acids in biology and cysteinate is a common thiolate ligand in different metalloproteins such as, Cytochromes, Fe-S clusters and Copper Blue proteins (Figure 1.2). Upon the coordination of cysteine the deprotonation reaction will occur. In the same time few examples of thiol complexes have been isolated. The reactions of thiols with metal complexes having a low coordination number produces complexes with thiolate and hydrido ligands or thiolate complexes and release of a proton [4]. Rare examples of thiol complexes have been characterised in the protonation of the binuclear complex $[Ni_2\{(SCH_2CH_2)_2NMe\}_2]$ [5] and the protonation will occur on sulfur site $[Ni_2\{(HSCH_2CH_2)(SCH_2CH_2)NMe\}_2]$ and in the protonation of $[Fe(SPh)(CO)_2\{P(OPh)_3\}_2]^-$. In the latter complex, initial protonation occurs at the metal to form the hydrido species $[FeH(SPh)(CO)_2\{P(OPh)_3\}_2]$. However, a further protonation is observed. It seems unlikely that this protonation is also at the metal and spectroscopic features are not consistent with a dihydrogen complex so it appears that the hydrido thiol complex $[FeH(HSAr)(CO)_2(P(OPh_3)_2]^+$ is produced [6].

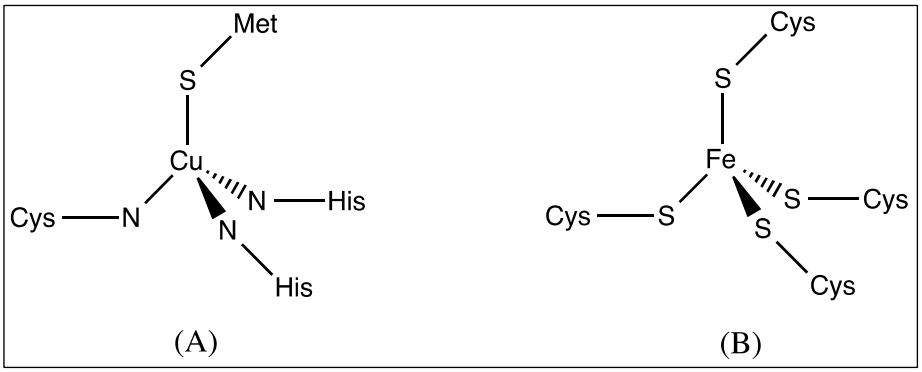


Figure 1.2. The structure of the active site in the (A) copper blue protein;(B) protein rubredoxin

## 1.2.2 Protonation of Thiolate Ligands in Mononuclear Complexes.

There have been only a few kinetic studies on the protonation of coordinated thiolates. Nonetheless, these few studies have revealed a kinetically and mechanistically rich chemistry. The reaction of the square-planar [Ni($SC_6H_4R$-4)$_2$(dppe)] (dppe = $Ph_2PCH_2CH_2PPh_2$) with mixture of $lutH^+$ (lut = 2,6-dimethylpyridine) and lut are equilibrium reaction involving single step protonation of the complex as shown in Figure (1.3) [7].

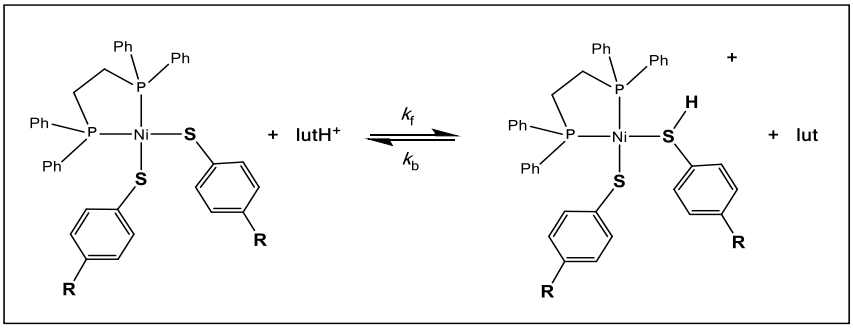


Figure 1.3. Equilibrium reaction between [Ni($SC_6H_4R$-4)$_2$(dppe)] and $lutH^+$.

When the reaction is monitored at a single wavelength using stopped-flow spectrophotometry, the absorbance changes are typical of an equilibrium reaction, thus when the concentration of [lut] is kept constant, the absorbance change increases with increasing concentration of acid. Similarly, when the concentration of $[lutH]^+$ is kept constant, increasing the concentration of [lut] results in a decrease in the absorbance change. Plots of $k_{obs}$/[lut] against [$lutH^+$]/[lut] for the derivatives R = MeO, Me, H or Cl, are linear with a positive intercept. This is consistent with the rate law shown in Equation (1.1), where $k_f$ is the rate constant for protonation of thiolate and $k_b$ is the rate constant for deprotonation of thiol.

$$k_{obs} = k_f[lutH^+] + k_b[lut] \qquad (1.1)$$

Because the p$K_a$ of $lutH^+$ is known in MeCN (15.4) the p$K_a$ of the coordinated thiols can be calculated. The values of p$K_a$ cover the narrow range 15.1 (R = $NO_2$) to 15.8 (R = MeO) in MeCN in comparison with the 2 units difference in the aqueous p$K_a$s of the corresponding free thiols {4.68 (R = $NO_2$), 6.76 (R = MeO)}. It is apparent that the acidity of the free thiol will be effected by coordination to the $\{Ni(dppe)\}^{2+}$ core.

The temperature dependence of the reactions of [Ni($SC_6H_4R$-4)$_2$(dppe)] with mixtures of $lutH^+$ and lut reveals that the values of $\Delta H^{\ddagger}$ and $\Delta S^{\ddagger}$ are dependent on the 4-R substituent,

although, there is no change in the value of $\Delta G^{\ddagger}$ = 13.6 ± 0.3 kcal $mol^{-1}$. As the 4-R substituent becomes more electron donating, the transfer of proton from acid to sulfur in the transition state is more progressed (i.e. transition state becomes more product-like). Interestingly, no detectable kinetic isotope effect was observed in the reactions of $lutD^+$ with any $[Ni(SC_6H_4R\text{-}4)_2(dppe)]$.

The reaction of $[Ni(SC_6H_4NO_2\text{-}4)_2(dppe)]$ with mixtures of $lutH^+$ and lut shows a different kinetic behavior. Plots of $k_{obs}$/[lut] against $[lutH^+]$/[lut] are linear with a positive intercept but only if the concentration of $lutH^+$ is constant. As the concentration of $lutH^+$ is increased the slope of the line decreases but the intercept remains unchanged.

Studies on the reactions of square-planar $[Ni(SC_6H_4R\text{-}4)(triphos)]^+$ [8] (R = MeO, Me, H, Cl or $NO_2$; triphos = $PhP(CH_2CH_2PPh_2)_2$) with mixtures of $[lutH^+]$ and [lut] showed kinetic behaviour similar to that of $[Ni(SC_6H_4NO_2)_2(dppe)]$, described above. The mechanism and the rate law associated with this reaction are shown in Figure (1.4) and Equation (1.2).

The mechanism shown in Figure (1.4) involves two coupled equilibria. In the first step there is rapid formation of a species in which the $lutH^+$ hydrogen-bonds to the sulfur of the thiolate and the second step involves the intramolecular transfer of the proton to the sulfur. It is presumed that the mechanism in Figure (1.4) operates for all the thiolate complexes described above but it is only with $[Ni(SC_6H_4NO_2\text{-}4)_2(dppe)]$ and $[Ni(SC_6H_4R\text{-}4)(triphos)]^+$ that the rate law shown in Equation (1.2) is observed because the hydrogen-bonded precursor is detectable through the kinetics. From the rate law in Equation (1.2), if $K_c[lutH^+] < 1$ the rate law in Equation (1.2) will simplifies to that shown in Equation (1.3), which is in the same form to the rate laws observed for the reactions of $[Ni(SC_6H_4R\text{-}4)_2(dppe)]$ (R = MeO, Me, H or Cl).

$$k_{obs} = K_c k_d[\mathrm{lutH^+}] + k_{-d}[\mathrm{lut}] \qquad (1.2)$$

The reason that the transfer of the proton from acid to sulfur is slow in these systems seems to be a combination of: (i) the effect of the 4-R-substituent on the basicity of the sulfur (weak basicity) (ii) steric effect around the sulfur due to the phenyl-groups on the phosphorus donors in triphos resulting in the lone pairs of electrons on the sulfur being ‘buried’ in the encapsulating phenyl groups.

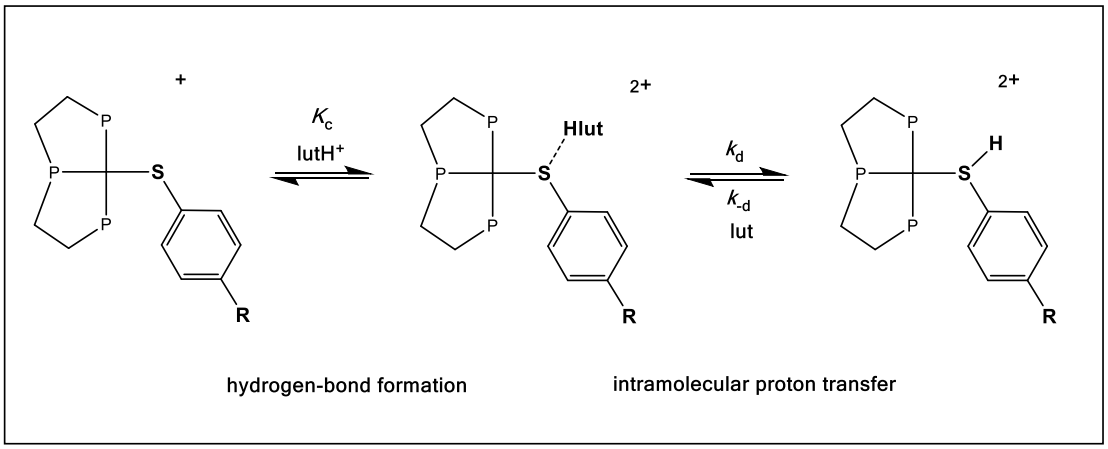


Figure 1.4. Mechanism for the equilibrium reaction between $[Ni(SC_6H_4R\text{-}4)(triphos)]^+$ (phenyl substituents on triphos omitted for clarity) and $lutH^+$ involving initial hydrogen-bonding of the acid to the coordinated thiolate followed by intramolecular proton transfer.

$$k_{obs} = \frac{K_c k_d [\mathrm{lutH^+}]}{1 + K_c[\mathrm{lutH^+}]} + k_{-d}[\mathrm{lut}] \qquad (1.3)$$

Studying the effect of R-substituent on the activation parameters for the intramolecular proton transfer show that with the increasing the electron donation of the R-substituent $\Delta H^{\ddagger}$ becomes smaller and $\Delta S^{\ddagger}$ becomes less positive. The same result shows for $[Ni(SC_6H_4R\text{-}4)_2(dppe)]$.

The isotope effect studies for the reaction of the reaction of $lutD^+$ with $[Ni(SC_6H_4R\text{-}4)(triphos)]^+$ shows there is an isotope effect and its magnitude depends on the nature of the 4-R substituent. For the more electron-withdrawing substituents an inverse isotope effect is observed (R = $NO_2$, $k^H/k^D$ = 0.39; R = Cl, $k^H/k^D$ = 0.88), whilst with the more electron-donating substituents a normal isotope effect is observed (R = Me, $k^H/k^D$ = 1.3; R = MeO, $k^H/k^D$ = 1.2), where inverse isotope effect is observed when the base is weak (electron-withdrawing R substituent) and the transition state is reactant-like, whereas a normal iotope effect is observed when the base is stronger (electron-donating R substituent) and the transition state is reactant-like.

The protonation chemistry of complexes where the protonated ligands can subsequently undergo intramolecular reactions, have been studied using kinetic studies and MSINDO semiempirical and ADF calculations, which help to understand the protonation chemistry

of this type of ligands [9]. The complexes $[Ni(2\text{-}Spy)(triphos)]^+$ (2-Spy = 2-pyridinethiolate) and $[Ni(4\text{-}Spy)(triphos)]^+$ (4-Spy = 4-pyridinethiolate) have been characterized both spectroscopically and by X-ray crystallography. The ligand 4-pyridinethiolate in the complex $[Ni(4\text{-}Spy)(triphos)]^+$ coordinates to nickel through sulfur, and the structure of the complex is a distorted square-planar geometry, while in the complex $[Ni(2\text{-}Spy)(triphos)]^+$, the nickel is five coordinate with the 2-pyridinethiolate ligand acting as a bidentate ligand, coordinating through both the nitrogen and sulfur.

The reaction between $[Ni(4\text{-}Spy)(triphos)]^+$ and mixtures of $lutH^+$ and lut in MeCN is fast (complete within 2 ms) and associated with a small spectroscopic change in the UV-visible spectrum. This behaviour is consistent with rapid protonation of uncoordinated nitrogen atom.

In contrast, the reaction of $[Ni(2\text{-}Spy)(triphos)]^+$ with mixtures of $lutH^+$ and lut is relatively slow and is associated with a significant spectroscopic change. The kinetics of the reaction is different from those observed in the analogous equilibrium protonation reactions of $[Ni(SC_6H_4R\text{-}4)(triphos)]^+$ and $[Ni(SC_6H_4R\text{-}4)_2(dppe)]$. The mechanism is shown in Figure (1.5) and the dependence of $k_{obs}$ on the concentration of $lutH^+$ and lut is shown in Equation (1.4).

The suggested protonation mechanism of $[Ni(2\text{-}Spy)(triphos)]^+$ involves protonation at the sulfur site because the nitrogen is coordinated to nickel and there is no available lone pair of electrons on nitrogen and so protonation cannot occur at the nitrogen. Protonation of sulfur labilises the Ni-N bond, resulting in dissociation of the nitrogen of the bidentate pyridine thiol ligand. The free nitrogen is now more basic than the coordinated sulfur and then the proton will transfer from sulfur to nitrogen site.

$$k_{obs} = \frac{k_e[\mathrm{lutH^+}] + \left(\frac{k_{-e}k_{-g}}{k_g}\right)[\mathrm{lut}]}{1 + \left(\frac{k_{-e}}{k_g}\right)[\mathrm{lutH^+}]} \qquad (1.4)$$

Theoretical calculations predict that the most thermodynamically stable form is that in which the nitrogen is not coordinated.

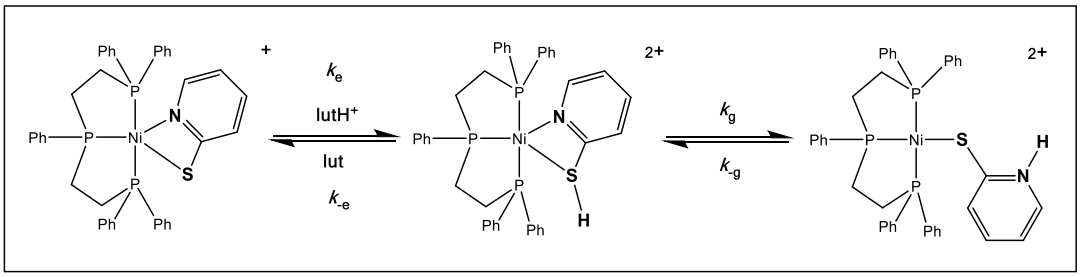


Figure 1.5. Equilibrium reaction between $[Ni(2\text{-}Spy))(triphos)]^+$ and $lutH^+$ involving chelate ring opening of the 2-puridinethiolate ligand and prototropic shift from sulfur to nitrogen.

The protonation reaction on other bidentate pyridinethiolate ligands has been observed. The complexes $[IrH(2\text{-}Spy)(CO)(PPh_3)_2]^+$ and $[OsH(2\text{-}Spy)(CO)(PPh_3)_2]$ have been prepared and characterised using X-ray crystallography and show that the pyridinethiolate coordinate to nickel through sulfur and nitrogen, analogous to that observed in $[Ni(2\text{-}Spy)(triphos)]^+$. However, reaction of the Ir or Os complexes with $HBF_4$ did not result in protonation of the 2-pyridinethiolate ligand and only in the case of $[OsH(2\text{-}Spy)(CO)(PPh_3)_2]$ was the product identified In this case the dihydrogen complex $[Os(\mu^2\text{-}H_2)(2\text{-}Spy)(CO)(PPh_3)_2]^+$ was formed [10].

## 1.3 Protonation of Coordinated Sulfide.

### 1.3.1 Sulfide Ligands in Biology.

The Fe-S clusters are widespread in biology in proteins and enzymes and first isolated and structurally characterised in the 1960s [10]. Most of these Fe-S-based cluster contain sulfide ($S^{2-}$), there are two type of Fe-S based cluster both of them are redox centres and are involved in the transfer of electrons either within the protein (*e.g.* hydrogenases) or as mediators between two other proteins (*e.g.* transfer of electrons between the Fe protein and MoFe-protein of nitrogenase). There are three type of Fe-S based cluster characterised by protein X-ray crystallography as shown in Figure (1.6). In these crystal structures Fe is a tetrahedral centre with one or more Fe-S bond. In the simplest type (rubredoxin), a single Fe is coordinated to the polypeptide by 4 cysteinate residues. In plant ferredoxins, the active site comprises a binuclear unit of 2 tetrahedral Fe atoms, bridged by 2 inorganic sulfurs ($S^{2-}$), and bound to the polypeptide by 2 cysteinates on each Fe. Finally, in bacterial ferredoxins, the active site is a cuboidal cluster containing, at each corner, alternating Fe and sulfur atoms. A cysteinate residue, to the polypeptide, also coordinates each Fe. These Fe-S clusters are redox centres and are involved in the transfer of electrons either within the protein (*e.g.* hydrogenases) or as mediators between two other proteins (*e.g.* transfer of electrons between the Fe protein and MoFe-protein of nitrogenase). Fe-S-based clusters are also found in certain enzymes where they operate either as part of the electron transfer pathway or are part of the active site (the site where substrate is bound and transformed) [11,12]. This class of enzyme contains some of the most economically and environmentally important metalloenzymes including: hydrogenases (catalyse the two electron interconversion of dihydrogen and proton), nitrogenases (catalyse the conversion of dihydrogen and dinitrogen to ammonia) and carbon monoxide dehydrogenase (catalyse the reversible oxidation of CO to $CO_2$). The action of these enzymes involves the transfer of electrons as part of the substrate transformation; in all the Fe-S-based clusters described in this section (whether in proteins or enzymes) the clusters are involved in redox processes. However, the active site in the enzyme aconitase also contains a cuboidal Fe-S cluster despite aconitase being a non-redox enzyme, which equilibrates citric, and isocitric acids [13].

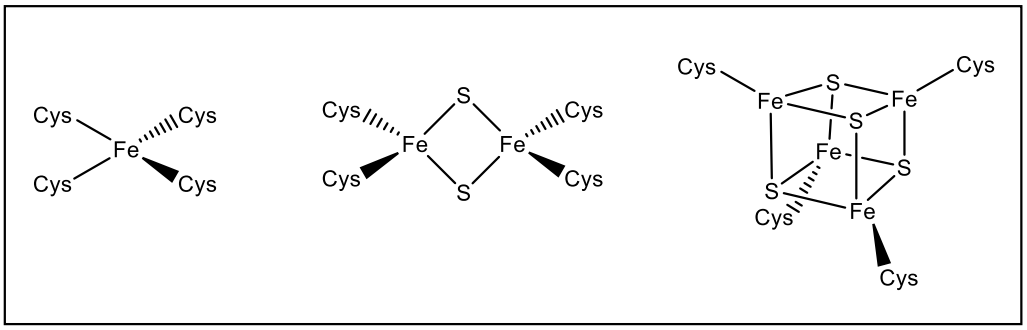


Figure 1.6. The common Fe-S geometries found in biology.

In the enzymes which employ Fe-S-based clusters as the active site, more elaborate structures are observed, with $\{Fe_4S_4\}$ cuboidal clusters ligated to another metal-containing unit via a cysteinate residue (Figure 1.7): siroheme (sulfite reductase); $\{Fe_2(CO)_2(CN)_2(\mu\text{-OH})\}$ (Fe-only hydrogenase) and {Ni(Cys-Gly-Cys)} (CODH A-cluster (synthesis of Acetyl-CoA)). In addition, other elaborate, structurally unique clusters have been identified in: (i) CODH (C-cluster) where it is a $\{Fe_4NiS_5\}$ cluster and (ii) Mo-based nitrogenase, which contains both the $\{Fe_8S_7\}$ P-cluster (electron storage) and the $\{MoFe_7S_9\}$ FeMo-cofactor (active site) (Figure 1.8). From the structures in Figures (1.7) and Figures (1.8), the active side in CODH A cluster, sulfite reductase and Fe-only hydrogenase has two components (one of which is a $\{Fe_4S_4\}$ cuboidal cluster) connected through a cysteinate residue [14].

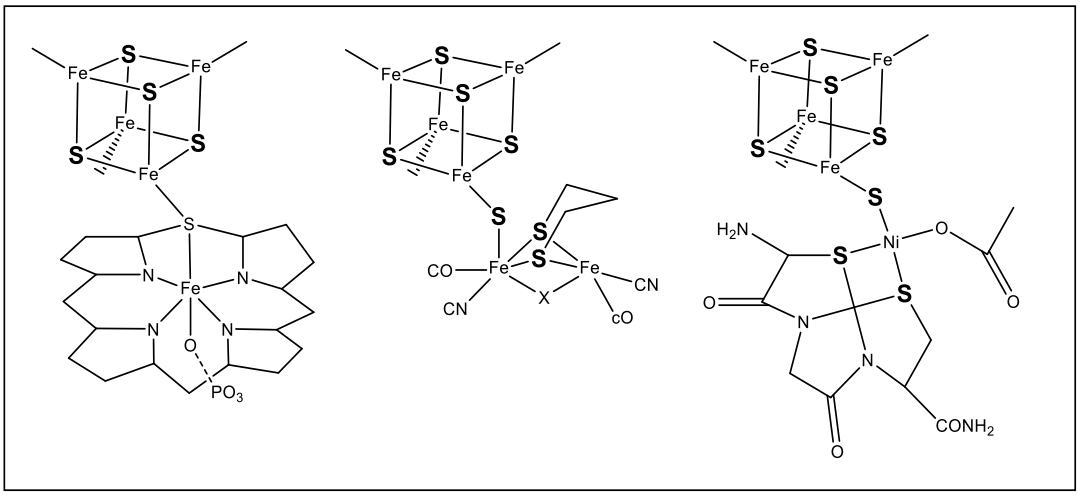


Figure 1.7. Active site structures for (left) sulfite reductase, (centre) Fe-only hydrogenase and (right) CODH A cluster.

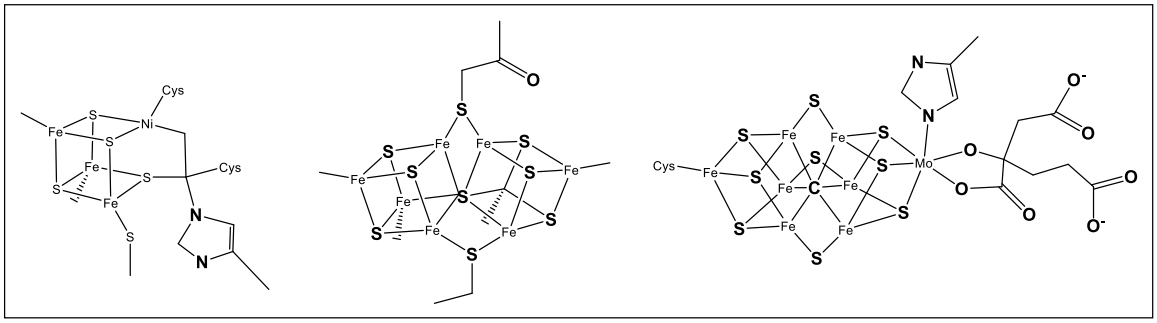


Figure 1.8. Active site structures in (left) CODH C cluster, (centre) P-cluster of nitrogenase and (right) FeMo-cofactor of nitrogenase.

## 1.3.2 Synthetic Fe-S-Based Clusters.

Analogues of all the natural Fe-S centres shown in Figure (1.7) and Figure (1.8) have been prepared and structurally characterised (the first synthetic analogue, $[Fe_4S_4(SCH_2Ph)]^{2-}$ , was accomplished in 1972). This work continues to prepare and study the spectroscopic, electrochemical and reactivity of ever more complex synthetic Fe-S-based clusters in attempts to develop accurate models of the natural clusters. Many synthetic clusters are very close mimics of the natural clusters. The unexpected feature about these synthetic clusters is that their syntheses do not require any exotic or protracted methodology in order to be formed. Rather these structures form in solutions containing the correct proportions of constituent reagents (iron salt, thiolate and elemental sulfur). This has been termed "spontaneous self-assembly" and the term has stuck despite studies which have shown that there is nothing spontaneous about the assembly, and that the cluster formation process involves a series of iron-containing intermediates of various nuclearities [15, 16].

The number of synthetic Fe-S clusters is larger than those found in nature with a wide range of structural types and metal composition having been isolated and characterised: the most well-studied of these being those containing the cuboidal $\{MFe_3S_4\}^{n+}$ (M = V, Nb, Mo, W, Re, Co, Ni) sub-cluster.

### 1.3.3 Protonation of Synthetic Fe-S-Based Clusters.

The first study of the substitution reactions of synthetic Fe-S-based clusters was reported in 1975 by Dukes and Holm [17]. The kinetics of the reaction between the cuboidal $[Fe_4S_4(SBu^t)_4]^{2-}$ and a series of substituted arylthiols ($RC_6H_4SH$) were studied in MeCN as the solvent. The reaction exhibited a first order dependence on the concentrations of both the cluster and the thiol. It was noted that the rate of reaction increases with increasing acidity of the thiols. The suggested mechanism of the reaction is shown in Figure (1.9) and the authors proposed that proton transfer was the slow step. This suggestion needs to be tested because there are lone pairs of electrons on the sulfurs of both the thiolate ligands and the core sulfurs, and protonation at these sites might be expected to be faster than the act of substitution. If proton transfer were slow, it is important to study this fundamental type of reaction to understand the reactions of natural Fe-S-based clusters with protons. The simplest way to do this would be to study the simple proton transfer from an acid to the cluster. The problem is that such a simple reaction is difficult to follow spectroscopically. The clusters are paramagnetic and so their NMR spectra comprise broad and paramagnetically shifted peaks, and EPR spectra are complicated by the multiple spin states associated with the clusters. In addition, there are no diagnostic peaks in the IR spectrum associated with the protonated cluster and the electronic (UV-visible) spectra of the protonated cluster are indistinguishable from that of the parent cluster. An alternative approach to studying protonation of Fe-S-based clusters needed to be developed. The method used was to monitor the effect that acids have on the rates of substitution of the terminal ligands.

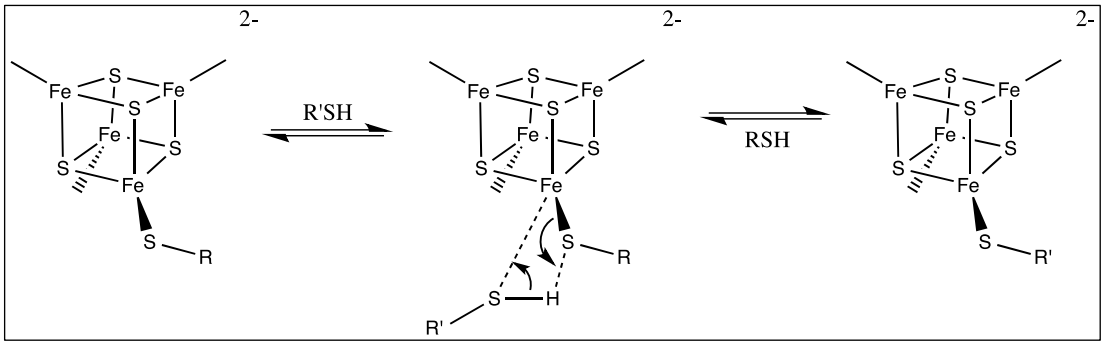


Figure 1.9. Mechanism of the reaction between $[Fe_4S_4(SR)_4]^{2-}$ and RSH proposed by Dukes and Holm 1975.

A system developed by Henderson involves studying the substitution reactions of Fe-S-based clusters in the presence of varying amounts of an acid ($NHEt_3^+$) and conjugate base ($NEt_3$), as shown in Figure (1.10) [18-22]. All reactants are present in a large excess over that of the cluster ([reactant]/[cluster] ≥ 10). The choice of $NHEt_3^+$ is dictated by the p$K_a$ of this acid (p$K_a$ = 18.4 in MeCN) [23] which is sufficiently strong to protonate the cluster but not so strong to decompose the cluster. An important point is that in the substitution of $[Fe_4S_4(SR)_4]^{2-}$ and analogous clusters, the terminal alkylthiolate ligands must be substituted by arylthiolates or terminal arylthiolate ligands by alkylthiolates. Replacement of an alkylthiolate ligand by another alkylthiolate (or arylthiolate by another arylthiolate) is normally associated with little appreciable change in the UV-visible spectra.

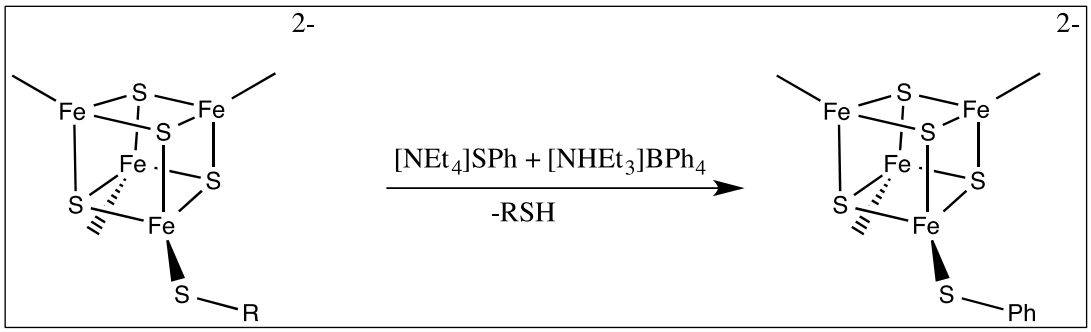


Figure 1.10. Components used to study the acid-catalysed substitution reactions of synthetic Fe-S-based clusters.

In MeCN, a mixture containing $NHEt_3^+$ and $PhS^-$ react rapidly by the protolytic equilibrium shown in Equation (1.5), the concentrations of free $NHEt_3^+$ and $PhS^-$ present in solution containing mixtures $[NHEt_3^+]_0$ and $[PhS^-]_0$ are calculated (provided $[NHEt_3^+]_0 > [PhS^-]_0$) using the expressions: $[NHEt_3^+]_{free} = [NHEt_3^+]_0 - [PhS^-]_0$ and $[PhSH]_{free} = [NEt_3]_{free} = [NHEt_3^+]_0 - [PhS^-]_0$. There is a large difference in p$K_a$s of PhSH (p$K_a$ = 6.2 in $H_2O$) and $NHEt_3^+$ (p$K_a$ = 18.46 in MeCN), so equilibrium constant for Equation (1.5) is very large (ie equilibrium lies to the right hand side). Thus, it is possible to independently control the concentrations of acid, base and nucleophile and hence determine the effect each has on the kinetics of the reaction. In the solution mixture of $NHEt_3^+$ and $PhS^-$, if $[NHEt_3^+]_0 \geq [PhS^-]_0$, PhSH is the nucleophile present since there is no $PhS^-$ present and when $[NHEt_3^+]_0 < [PhS^-]_0$, there are mixtures of both $PhS^-$ and PhSH present.

$$NHEt_3^+ + PhS^- \rightleftharpoons NEt_3 + PhSH \qquad (1.5)$$

Kinetic studies on the reaction of $[Fe_4S_4(SEt)_4]^{2-}$ with PhSH in the presence of $NHEt_3^+$ and $NEt_3$ show the dependence of $k_{obs}$ on the ratio $[NHEt_3^+]/[NEt_3]$ and the rate of the reaction exhibits a non-linear dependence on the ratio $[NHEt_3^+]_{free}/[NEt_3]_{free}$, but does not depend on the absolute concentrations of acid or base. The reaction is independent of the concentration of PhSH and shows that at low values of $[NHEt_3^+]_{free}/[NEt_3]_{free}$, the reaction exhibits a first order dependence on the ratio, and at high value of the ratio of $[NHEt_3^+]_{free}/[NEt_3]_{free}$, the reaction rate is independent of the ratio. The mechanism and associated rate law shown in Figure (1.11) and Equation (1.7).

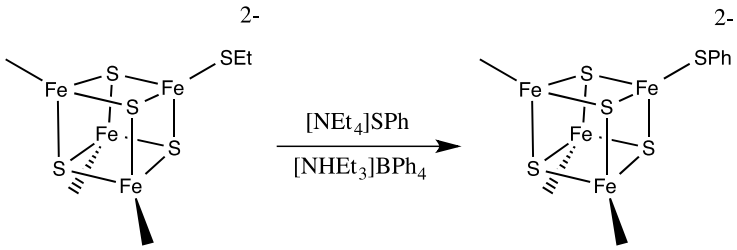


(1.6)

$$\text{Rate} = \left\{\frac{k_0 + K_1 k_2 [\text{NHEt}_3^+]/[\text{NEt}_3]}{1 + K_1 [\text{NHEt}_3^+]/[\text{NEt}_3]}\right\}[\text{cluster}] \qquad (1.7)$$

The mechanism in the Figure (1.11) shows two pathways for the substitution reaction: the simple non-catalysed dissociative pathway and the acid-catalysed dissociative substitution pathway. In the latter pathway, protonation of the cluster apparently makes the ethanethiolate ligand more labile. After dissociation of the ethanthiolate ligand, subsequent attack of the PhSH nucleophile at the vacant site on the Fe completes the substitution. In deriving equation (1.7), the protonation step is a rapidly established pre-equilibrium with the act of substitution being rate-limiting.

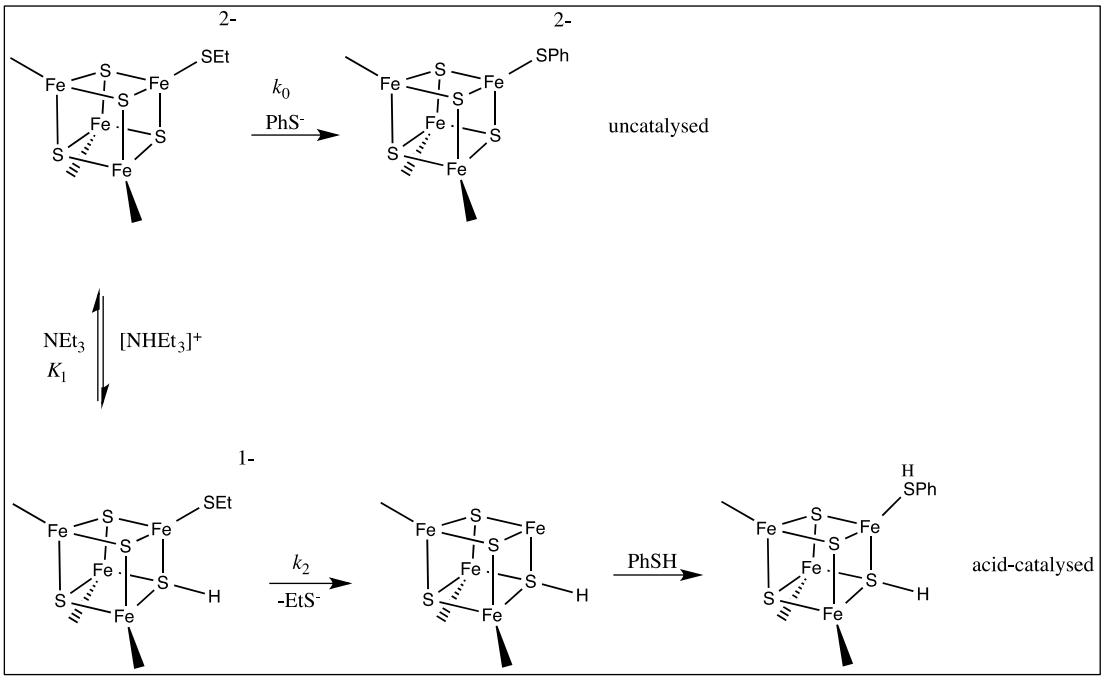


Figure 1.11. Pathways for substitution of terminal EtS ligands on $[Fe_4S_4(SEt)_4]^{2-}$ with PhSH in the presence of $NHEt_3^+$ and $NEt_3$.

## 1.3.4 Characteristics of the Protonation Step.

The kinetic studies of the protonation of Fe-S-based cluster, particularly the dependence on $[NHEt_3^+]_{free}/[NEt_3]_{free}$, indicates that a single proton binds to the cluster and causes the labilisation of the cluster to substitution However, the situation is slightly more complicated. In studies on the substitution reactions of $[FeCl_4]^-$ with $PhS^-$ it is observed that $NHEt_3^+$ can bind to cluster through hydrogen bonding and this interaction will modulate the substitution reaction. In this case the acceleration in the rates of substitution is not due to a protonation, but is formation of the ion-pair $\{[NHEt_3^+].[FeCl_4^-]\}$ which is more active to substitution than the parent $[FeCl_4]^-$. In this ion-pair $\{[NHEt_3^+].[FeCl_4^-]\}$ the proton does not transfer completely but is probably involved in hydrogen bonding between N-H and chloro-ligands. The effect of the formation of an ion-pair on the rate of substitution is less than the effect of protonation [24].

From analysis of the kinetics the values of $K_1$ (protonation equilibrium constant of the cluster) and $k_2$ (rate constant for substitution) can be determined and from the value of $K_1$ and the p$K_a$ of $NHEt_3^+$ in MeCN (p$K_a$ = 18.4) [23], the p$K_a$ of the cluster can be calculated. Further similar studies have been done on other Fe-S-based clusters as shown in Table (1.1). Table (1.1) shows that the value of the calculated p$K_a$ of all the clusters falls in the narrow range 17.9 – 18.9 (in MeCN), in spite of the change in the composition of the

cluster and the terminal ligands. This insensitivity of the p$K_a$ to the composition and structure of the cluster indicates that the site of protonation is not the terminal ligands and suggested the protonation site is bridging core sulfur. Protonation studies for both $[Fe_4S_4(SR)_4]^{2-}$ and $[Fe_4S_4Cl_4]^{2-}$ with same acid shows that the calculated p$K_a$s of these two clusters are very similar, strongly suggesting that the detected protonation is not on the terminal thiolate.

Most synthetic clusters are prepared in MeCN and dissolve in this solvent not in protic solvent. Clearly, for comparison the synthetic cluster with natural Fe-S based clusters it would be advantageous to study the reactions of the synthetic clusters in water. Davies [25] studies the substitution studies of the cluster $[Fe_4S_4(SCH_2CH(OH)Me)_4]^{2-}$ in protic solvent (methanol) and the protonation labilies the terminal substituent by a dissociative mechanism. This behaviour is exactly analogous to that observed for the other synthetic Fe-S-based clusters reacting in MeCN. Analysis of the kinetic data in methanol yields p$K_a$ = 8.5 for $[Fe_4S_4(SCH_2CH(OH)Me)_4]^{2-}$. Other studies on $[Fe_4S_4(SCH_2CH_2CO_2)_4]^{6-}$ indicate p$K_a$ = 7.4 for this cluster in water [26].

| | Cluster | p$K_a$ |
|---|---|---|
| Fe-Cl cluster: | $[Cl_2FeS_2VS_2FeCl_2]^{3-}$ | 17.9 |
| | $[S_2MoS_2FeCl_2]^{2-}$ | 17.9 |
| | $[Fe_4S_4Cl_4]^{2-}$ | 18.8 |
| | $[\{MoFe_3S_4Cl_3\}_2(\mu\text{-}SEt)_3]^{3-}$ | 18.6 |
| | $[\{WFe_3S_4Cl_3\}_2(\mu\text{-}SEt)_3]^{3-}$ | 18.2 |
| | $[\{WFe_3S_4Cl_3\}_2(\mu\text{-}OMe)_3]^{3-}$ | 18.4 |
| | $[Fe_2S_2Cl_3(NCMe)]^{-}$ | 18.1 |
| Fe-SR clusters: | $[Fe_4S_4(SPh)_4]^{2-}$ | 18.6 |
| | $[Fe_4S_4(SEt)_4]^{2-}$ | 18.0 |
| | $[\{MoFe_3S_4(SEt)_3\}_2(\mu\text{-}SEt)_3]^{3-}$ | 18.1 |
| | $[\{WFe_3S_4(SEt)_3\}_2(\mu\text{-}SEt)_3]^{3-}$ | 18.3 |
| | $[Fe_6S_9(SEt)_2]^{4-}$ | 17.9 |

Table 1.1: The p$K_a$s of synthetic Fe-S-based clusters determined from the kinetics of the acid-catalysed substitution reactions in MeCN [44].

There are several protonation sites on cuboidal $\{Fe_4S_4\}^{2+}$ and $\{MFe_3S_4\}^{n+}$ clusters, and the kinetic studies indicated that the protonation will be on bridging sulfur and this seems reasonable based on the expected relative basicities of the cluster components. Indication that protons could bind to the cluster in a multi-site interaction comes from studies measuring the binding affinities of 4-$YC_6H_4COCl$ (Y = MeO, H or Cl) to $[Fe_4S_4(SR)_4]^{2-}$ (R = Ph, Et or $Bu^t$) [27,28].

In these studies it was observed that maximum binding affinity of the acid chloride to the cluster is observed when the acid chloride contained the most electron-withdrawing 4-Y-substituents. This observation is consistent with the acid chlorides binding to the cluster as shown in Figure (1.13) with both the acyl oxygen binding to the Fe and the carbonyl carbon interacting with the sulfur of the terminal thiolate.

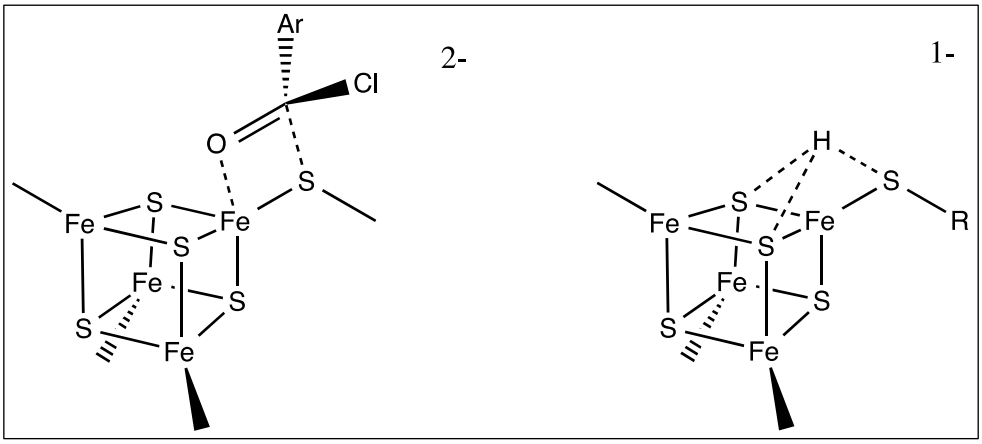


Figure 1.13. Proposed binding of acid chloride to $[Fe_4S_4(SR)_4]^{2-}$ (left) showing involvement of terminal thiolate ligand. On the right is a possible structure for proton binding to the cluster involving a similar interaction with the terminal thiolate and core sulfides.

Henderson [29] studies on the acid-catalysed substitution reactions led to consideration of the stereochemical relationship between the site of protonation and the site of substitution. Studies on $[Cl_2FeS_2VS_2FeCl_2]^{3-}$ indicate that maximum labilisation is attained only when the proton binds to a sulfur adjacent to the nucleophile-binding site.

In most Fe-S-based clusters the metal sites are magnetically coupled and hence communicate with one another. However, in the linear trinuclear cluster $[Cl_2FeS_2VS_2FeCl_2]^{3-}$ the two Fe sites are chemically equivalent and the two Fe atoms are magnetically isolated by the central V atom [30]. In $[Cl_2FeS_2VS_2FeCl_2]^{3-}$, the Fe sites undergo both uncatalysed and acid-catalysed substitution reactions with PhSH in the presence of $NHEt_3^+$ and $NEt_3$. The rapid acid-catalysed substitution reaction exhibits a first order dependence on the concentration of PhSH indicating the substitution reaction of the cluster is associative. There are two possible pathways for the acid catalysed substitution reaction of $[Cl_2FeS_2VS_2FeCl_2]^{3-}$. Protonation of $[Cl_2FeS_2VS_2FeCl_2]^{3-}$ will produce $[Cl_2FeS_2VS(SH)FeCl_2]^{2-}$ and the substitution reaction can occur either on the close Fe atom and in this case the protonation will labilise the Fe centre, or the protonation will occur on the far Fe centre and the V atom will shield the labilising effect of the proton on

the substitution by PhSH and therefore the reaction will be slow as shown in Figure (1.14).

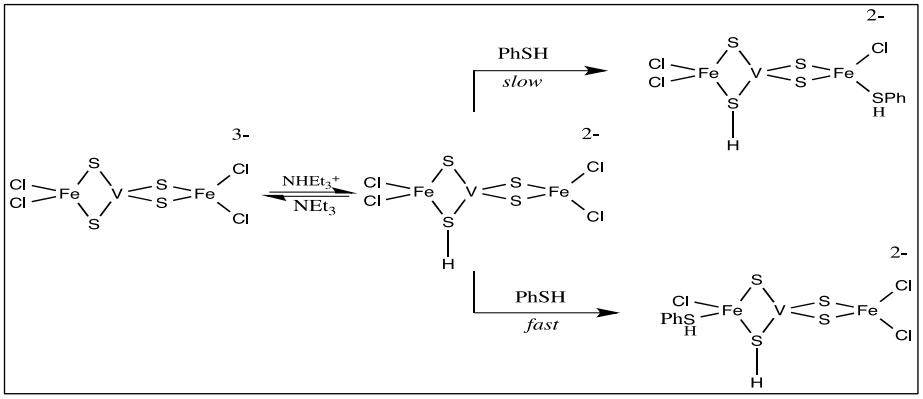


Figure 1.14. Alternative pathways for the acid-catalysed substitution reaction of $[Cl_2FeS_2VS_2FeCl_2]^{3-}$. Top pathway involves protonation and substitution at sites remote from one another whilst the bottom pathway involves protonation and substitution at adjacent sites.

If the protonation site and nucleophile-binding site must always be adjacent in the acid-catalysed substitution reactions of Fe-S-based clusters it is worth considering the corresponding reactions of cuboidal clusters as shown in Figure (1.15).

In cuboidal $[Fe_4S_4X_4]^{2-}$ clusters all Fe atoms are equivalent and three of these Fe atoms are adjacent to protonated sulfur whilst one Fe is remote from the protonated site. So, based on the studies with $[Cl_2FeS_2VS_2FeCl_2]^{3-}$, the substitution reaction on these three Fe atoms could be faster than protonation at the single remote Fe. In the structure of cuboidal $[MFe_3S_4X_3]^{n-}$ (M = Mo, W, Re, V or Nb) [31] all Fe sites are equivalent but three of the four sulfurs are bound to M and the fourth sulfur is bound only to Fe sites. Furthermore, in $[MFe_3S_4X_3]^{n-}$ all Fe sites are equivalent If protonation occurs at any of the $\mu_3$-S sites bound to M then only two Fe sites are adjacent and hence substitution is facilitated at these sites. In contrast, if protonation occurs at the unique $\mu_3$-S, then all three Fe sites are labilised as shown in Figure (1.15).

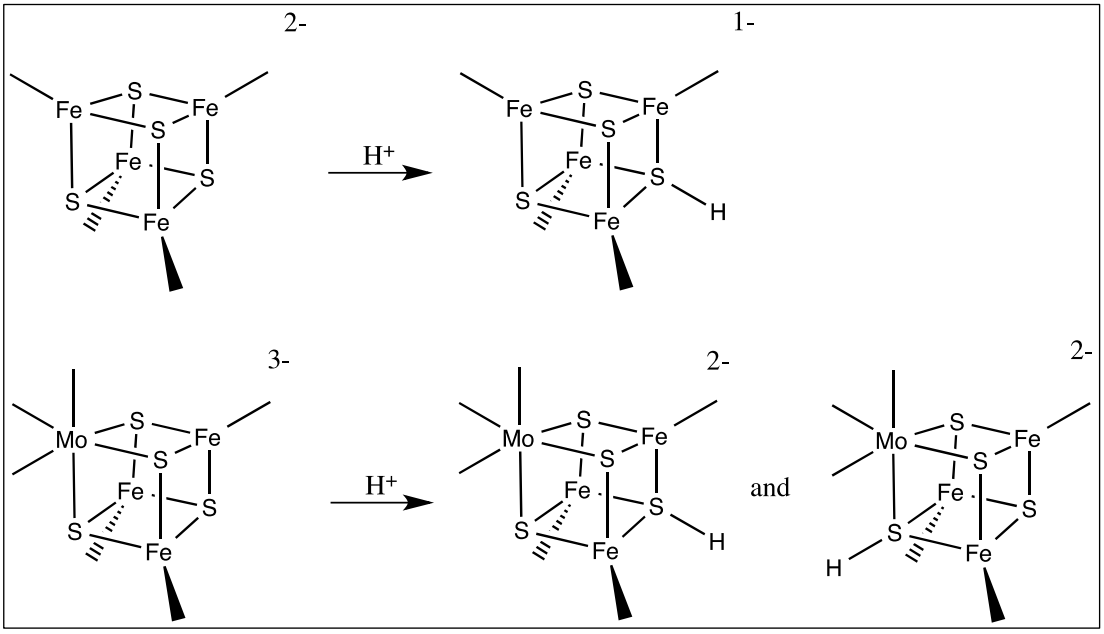


Figure 1.15. Fe site discrimination in cuboidal Fe-S-based clusters after protonation of core S.

We will now consider the electronic factors that could occur upon protonation. Protonation would be expected to result in a change in the electron density distribution within the cluster and the electron density will be pulled towards the protonation site and decrease the electron density from site of substitution (Fe sites adjacent to the protonated sulfur). Therefore the protonation could facilitate attack of the nucleophile in an associative substitution step [32]. The electronic effects on the lability of the cluster have been studied, and specifically the rate of dissociation of the terminal chloro-ligands in the reactions of $[Fe_4S_4Cl_4]^{2-}$ with a series of 4-$RC_6H_4S^-$ (R = MeO, Me, H, Cl or $CF_3$). The uncatalysed substitution reactions of $[Fe_4S_4Cl_4]^{2-}$ with 4-$RC_6H_4S^-$ to form $[Fe_4S_4(SC_6H_4R\text{-}4)Cl_3]^{2-}$, occur by an associative mechanism with the thiolate ion binding to the cluster prior to dissociation of the chloro-group. The effect of the 4-R substituent on the lability of the Fe-Cl bond can be monitored by analysis of the kinetic data for dissociation of the chloro-ligand from $[Fe_4S_4(SC_6H_4R\text{-}4)Cl_4]^{3-}$, The surprising observation is that as the 4-R-substituent becomes more electron-withdrawing the lability of the chloro-group increases. From the mechanism, it might be expected that electron-withdrawing substituents would decrease Fe-Cl dissociation. Clearly, other factors must be important in labilising anions from these clusters. It is suggested that the electron-withdrawing substituents diminish the anion-anion repulsion felt as the thiolate approaches the cluster and this facilitates the reaction.

### 1.3.5 Rates of Proton Transfer to Fe-S-Based Clusters.

The protonation of Fe-S-based clusters (by $NHEt_3^+$) occurs prior to the act of substitution and is rapid compared to the act of substitution. Consequently the analysis of the kinetics in these systems does not allow us to determine how rapidly protons are transferred to the clusters. The proton transfer from $NHEt_3^+$ to cluster is complete within the dead time of the stopped-flow apparatus, 1-2 ms, even when [$NHEt_3^+$] = 1.0 mM) [33]. To measure the rates of proton transfer, a much weaker acid than $NHEt_3^+$ was used, such as, a pyrrolidinium ion ($pyrrH^+$, p$K_a$ = 21.5 in MeCN). Since the p$K_a$ of all synthetic Fe-S-based clusters fall in the range 17.9 – 18.9, protonation of a cluster by $pyrrH^+$ is thermodynamically unfavourable with the associated equilibrium constants calculated to be in the range, $K_H \sim 10^{-3} - 10^{-4}$. Consequently, when using $pyrrH^+$ the rates of proton transfer are slower than those with $NHEt_3^+$. In reactions of a Fe-S-based cluster with $PhS^-$ in the presence of $pyrrH^+$ there are, as with $NHEt_3^+$, two steps (protonation and substitution). The rate-limiting step will depend on the concentration of the acid or the nucleophile [34]. $PyrrH^+$ is too weak an acid to protonate free $PhS^-$ and so no free PhSH is generated in mixtures containing $pyrrH^+$ and $PhS^-$. Consequently, the nucleophile is always $PhS^-$. Therefore the substitution reaction with $pyrrH^+$ will consider the two limiting cases, the binding of nucleophile before the proton transfer and the binding of nucleophile after the proton transfer.

### 1.3.6 Kinetics when Nucleophile Binds Before Proton Transfer.

In the reactions of $[Fe_4S_4Cl_4]^{2-}$ with $pyrrH^+$ and $PhS^-$, the $PhS^-$ binds rapidly to the cluster and so in this case the nucleophile binding to cluster before the proton transfer. The kinetics of the reaction between $[Fe_4S_4Cl_4]^{2-}$ and $PhS^-$ in the presence of $pyrrH^+$ exhibits a first order dependence on the concentration of the nucleophile ($PhS^-$), but a non-linear dependence on the concentration of $pyrrH^+$. These kinetics are consistent with the mechanism shown in Figure (1.16) in which initially $PhS^-$ binds to the cluster to form $[Fe_4S_4Cl_4(SPh)]^{3-}$ then this intermediate can convert to the product by dissociation of a chloro-ligand. This is the dominant pathway that operates at low concentration of $pyrrH^+$ and is the normal associative substitution mechanism between $[Fe_4S_4Cl_4]^{2-}$ and $PhS^-$. At higher concentrations of $pyrrH^+$, the rate of protonation of $[Fe_4S_4Cl_4(SPh)]^{3-}$ by $pyrrH^+$ exceeds the rate of dissociation of the chloro-ligand from $[Fe_4S_4Cl_4(SPh)]^{3-}$, and in this case the mechanism which involves protonation of $[Fe_4S_4Cl_4(SPh)]^{3-}$ is the dominant

pathway. The analysis of the kinetic data for both, the reaction of $[Fe_4S_4Cl_4]^{2-}$ and $PhS^-$ in the presence of $pyrrH^+$, and the reaction of $[Fe_4S_4Cl_4]^{2-}$ and $PhS^-$ without $pyrrH^+$ allow calculation of the rate constants ($k_3$, $k_{-3}$, $k_4^{PhS}$ and $k_5$) shown in the rate law in Equation (1.8) [33-35].

$$\frac{-d[\text{cluster}]}{dt} = \frac{(k_3k_5 + k_3k_4^{\text{PhS}}[\text{pyrrH}^+])[\text{PhS}^-][\text{cluster}]}{k_{-3} + k_5 + k_4^{\text{PhS}}[\text{pyrrH}^+]} \qquad (1.8)$$

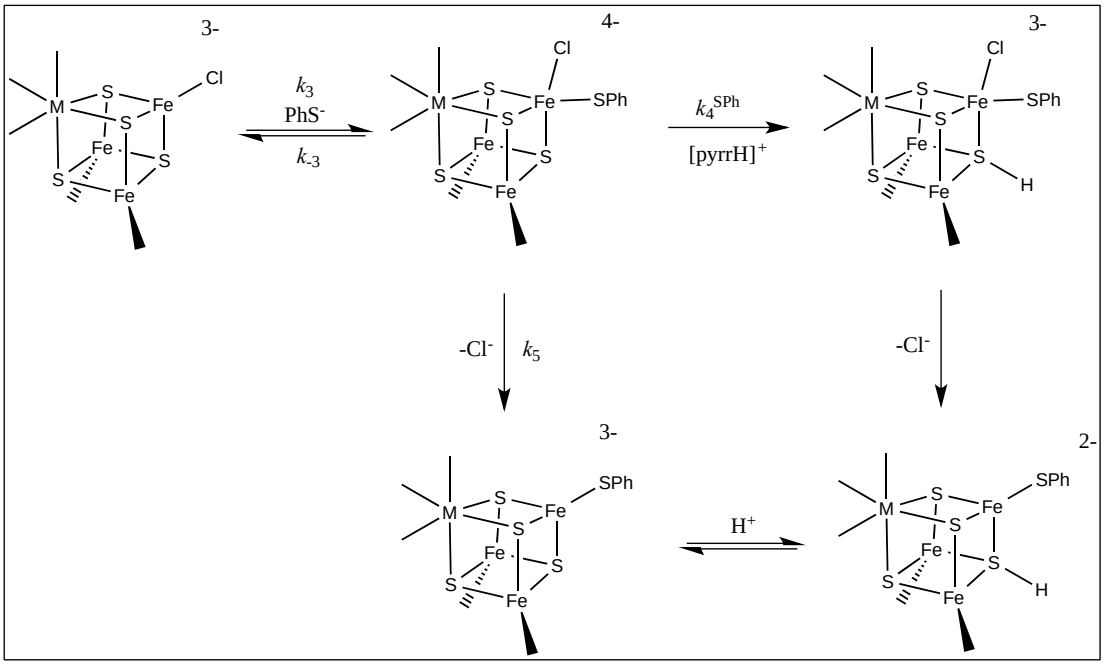


Figure 1.16. Mechanism for the reaction between Fe-S-based clusters and $PhS^-$ in the presence of $pyrrH^+$ where the nucleophile binds before the protonation.

## 1.3.7 Kinetics when Nucleophile Binds after Proton Transfer.

If the nucleophile is weak (binds slowly to the cluster) then proton transfer can occur before the nucleophile binds to the cluster. Such behavior is observed when the nucleophile is a halide ($Br^-$ or $I^-$) [35]. The reaction of $[Fe_4S_4Cl_4]^{2-}$ and $Br^-$ in the presence of $pyrrH^+$ exhibits first order dependences on the concentrations of cluster and $pyrrH^+$, but is independent of the concentration of nucleophile. The mechanism shown in Figure (1.17) in which initial protonation of the cluster by $pyrrH^+$ is followed by substitution, which can be dissociative or associative, and the rate law associated with this mechanism shown in Equation (1.9).

$$\text{Rate} = k_6[\text{pyrrH}^+][\text{cluster}] \qquad (1.9)$$

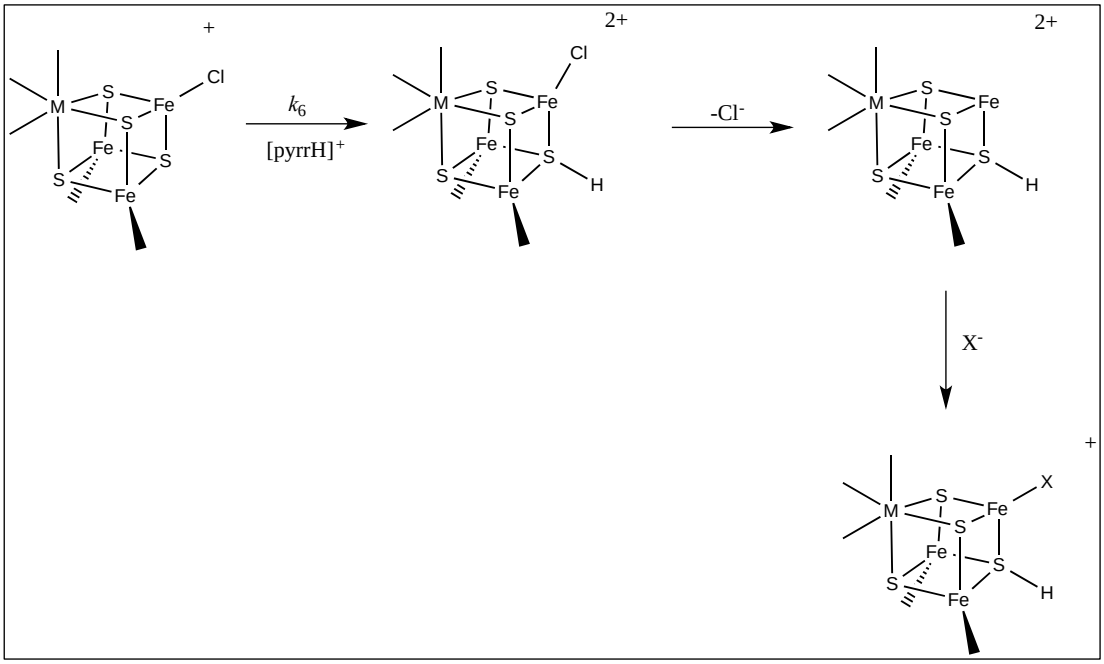


Figure 1.17. Mechanism for the reaction between Fe-S-based clusters and $X^-$ (X = halide) in the presence of $pyrrH^+$ where the nucleophile binds after the protonation.

## 1.3.8 Rate Constants for Proton Transfer to Fe-S-Based Clusters.

By analysis of the results of the protonation reactions for both cases described above it is possible to determine the rate constants for proton transfer from $pyrrH^+$ to synthetic Fe-S-based clusters before and after binding $PhS^-$ [33-35]. The rate constants are shown in Table (1.2).

| Rate Constant for proton transfer | | | |
|---|---|---|---|
| cluster | $\Delta pK_a$ | $k_6$ / $dm^3\ mol^{-1}\ s^{-1}$ | $k_4^{SPh}$ / $dm^3\ mol^{-1}\ s^{-1}$ |
| $[Fe_4S_4Cl_4]^{2-}$ | 2.7 | $2.4 \times 10^4$ | $1.8 \times 10^6$ |
| $[\{MoFe_3S_4Cl_3\}_2(\mu\text{-}SEt)_3]^{3-}$ | 2.9 | $2.5 \times 10^2$ | $6.0 \times 10^6$ |
| $[\{MoFe_3S_4Cl_3\}_2(\mu\text{-}SPh)_3]^{3-}$ | | $5.0 \times 10^2$ | $1.6 \times 10^6$ |
| $[\{WFe_3S_4Cl_3\}_2(\mu\text{-}SEt)_3]^{3-}$ | 3.3 | $8.5 \times 10^2$ | $2.5 \times 10^3$ |
| $[\{WFe_3S_4Cl_3\}_2(\mu\text{-}OMe)_3]^{3-}$ | 3.1 | | $7.5 \times 10^3$ |
| $[Fe_2S_2Cl_4]^{2-}$ | 3.4 | $1.9 \times 10^3$ | $8.8 \times 10^3$ |
| $[S_2MoS_2FeCl_2]^{2-}$ | 3.6 | $1.0 \times 10^5$ | |
| $[S_2WS_2FeCl_2]^{2-}$ | 3.4 | $2.0 \times 10^5$ | |

Table 1.2. Summary of the rate constants for proton transfer to synthetic Fe-S-based clusters ($k_6$) and the same clusters containing an additional bound $PhS^-$ ($k_4^{PhS}$).

It is evident from the data in Table (1.2) that the rate constants for proton transfer are variable and depend on the following factors. (i) The metal composition of the cluster; in the cuboidal clusters, the $\{Fe_4S_4\}^{2+}$ cluster protonates about 100 times faster than either $\{MoFe_3S_4\}$ or $\{WFe_3S_4\}$. (ii) For the binuclear clusters of core composition $\{MS_2Fe\}^{n+}$, the rate of protonation of $\{FeS_2Fe\}^{2+}$ is 100 times slower than either $\{MoS_2Fe\}^{4+}$ or $\{WS_2Fe\}^{4+}$. (iii) The initial binding of $PhS^-$ to the cluster has a significant effect on the rate of the proton transfer. In addition, comparison of the rates of proton transfer to $[\{WFe_3S_4Cl_3\}_2(\mu\text{-}L)_3]^{3-}$ (L = SEt or OMe) indicates that the change of the bridging ligands have small effect on the rate of proton transfer.

Another feature of the data in Table (1.2) is that the rates of proton transfer to the parent clusters do not correlate with the thermodynamic driving force of the reactions. Because of the change in the p$K_a$s associated with change in the composition of Fe-S-based clusters is a narrow range, the differences in the thermodynamic driving forces for the reactions ($\Delta pK_a = pK_a^{pyrrH} - pK_a^{cluster}$) are small. It is clear from the Table (1.2) that the thermodynamic driving force is not the key factor controlling the rates of proton transfer and depends on the following observations (i) For the cuboidal clusters, the rate of proton transfer from $pyrrH^+$ to $[Fe_4S_4Cl_4]^{2-}$ ($\Delta pK_a = 2.7$) is $k = 2.4 \times 10^4$ dm$^3$ mol$^{-1}$ s$^{-1}$, whilst the rate of proton transfer from $pyrrH^+$ to $[\{WFe_3S_4Cl_3\}_2(\mu\text{-}SEt)_3]^{3-}$ ($\Delta pK_a = 3.3$) is $k = 8.5 \times 10^2$ dm$^3$ mol$^{-1}$ s$^{-1}$. (ii) For the reactions of both $[Fe_2S_2Cl_4]^{2-}$ and $[S_2WS_2FeCl_2]^{2-}$ with $pyrrH^+$ the thermodynamic driving force is the same ($\Delta pK_a = 3.3$) but the rates of proton transfer are markedly different (for $[Fe_2S_2Cl_4]^{2-}$, $k = 1.9 \times 10^3$ dm$^3$ mol$^{-1}$ s$^{-1}$ and for $[S_2WS_2FeCl_2]^{2-}$, $k = 2.0 \times 10^5$ dm$^3$ mol$^{-1}$ s$^{-1}$).

### 1.3.9 Proton Transfer and Bond Reorganisation in Fe-S-Based Clusters.

It has been suggested that the slow rates of proton transfer involving Fe-S-based clusters and the effects of cluster composition, nuclearity and thermodynamic driving force on the rates of proton transfer is because bond length and angle reorganisation is the predominant factor controlling the rates of proton transfer in Fe-S-based clusters. An interesting observation in these protonation reactions is that the reactions of clusters with $pyrrD^+$ show no significant primary isotope effect [36]. This behaviour is also consistent with reorganisation of the cluster being a significant barrier to proton transfer.

How electronic factors affect the rates of proton transfer has been investigated in the reactions of $[Fe_4S_4Cl_4]^{2-}$ with 4-$RC_6H_4S^-$ in the presence of $pyrrH^+$ [32].The reaction occurs

by the mechanism shown in Figure (1.18) in which proton transfer occurs after the binding of the thiolate. The rate constant for proton transfer ($k_4^R$) increases, as the 4-R-substituent becomes more electron-withdrawing as indicated in the data in Figure (1.18). This observation is understandable if the effect of the 4-R-substituent is to moderate the bond dimensions within the cluster. Electron-withdrawing 4-R-substituents will shorten the bond lengths around the protonation site, which is what is required when the proton is transferred. Thus, when the proton transfers, the energetics associated with bond reorganisation have been met.

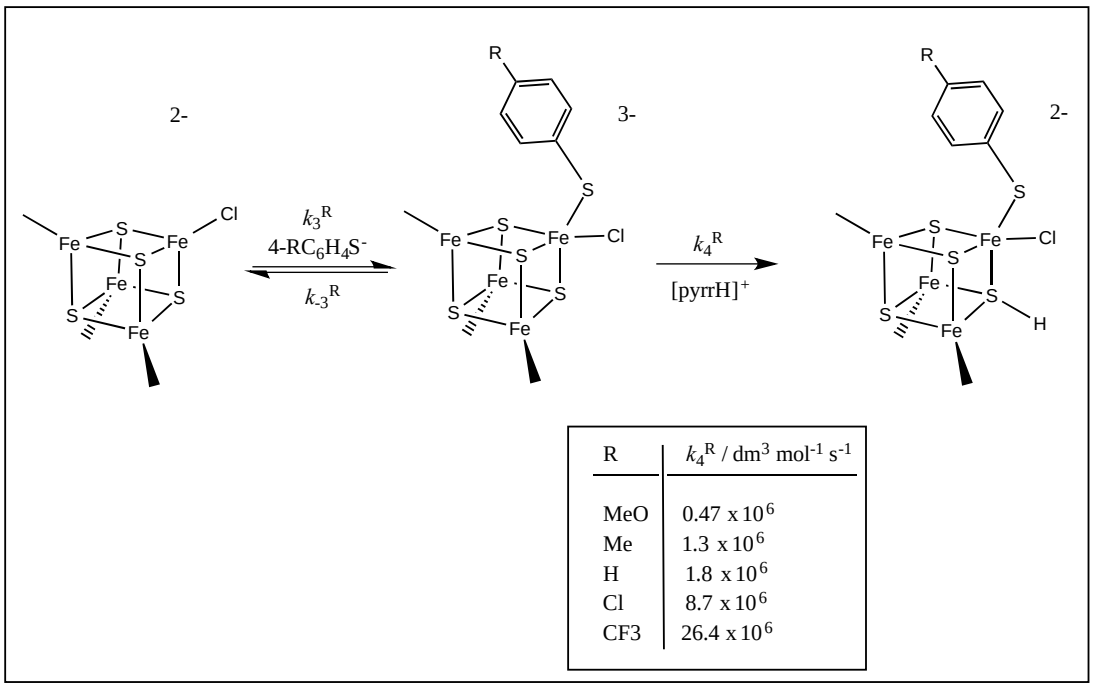


| R | $k_4^R$ / dm$^3$ mol$^{-1}$ s$^{-1}$ |
|---|---|
| MeO | 0.47 x 10$^6$ |
| Me | 1.3 x 10$^6$ |
| H | 1.8 x 10$^6$ |
| Cl | 8.7 x 10$^6$ |
| CF3 | 26.4 x 10$^6$ |

Figure 1.18. Effect of 4-R-substituent in $[Fe_4S_4Cl_4(SC_6H_4R\text{-}4)]^{3-}$ on the rate of proton transfer from pyrr$H^+$.

The extensive range of dicuboidal clusters of the type $[\{MFe_3S_4Cl_3\}_2(\mu\text{-}L)_3]^{3-}$ (M = Mo, W, Nb, Ta, Re or V; L = thiolate or alkoxide) are isostructural [11,12,14] and comparison of their reactivities allows delineation of the effect of changing one of the metals (M) in the cluster core and also the effect of changing the bridging ligands (L) which are bonded to M and hence remote from the substitution sites (on the Fe). The isostructural clusters $[\{MFe_3S_4Cl_3\}_2(\mu\text{-}SEt)_3]^{3-}$ (M = Mo or W) have been prepared and their protonation chemistry studied with both $NHEt_3^+$ and pyrr$H^+$. The substitution studies of these clusters using $NHEt_3^+$ show that the substitution step is facilitated by protonation and, in both clusters (M = Mo or W), the mechanism occurs in an associative pathway. Analysis of the kinetic data indicated that the p$K_a$s of both clusters fall in the normal range (17.9 – 18.9). Analysis of the kinetics of the substitution reactions of both clusters with $PhS^-$ in the

presence of $pyrrH^+$ are consistent with the mechanism in Figure (1.16). Comparison of the results allows us to measure the effect that changing M from Mo to W has on the rate of proton transfer and rate of binding of $PhS^-$, as shown in Table (1.3) [24,34,37].

| Effect of the metal composition | | |
|---|---|---|
| Cluster | $k_3$ / $dm^3\ mol^{-1}\ s^{-1}$ | $k_4^{SPh}$ / $dm^3\ mol^{-1}\ s^{-1}$ |
| $[\{MoFe_3S_4Cl_3\}_2(\mu\text{-}SEt)_3]^{3-}$ | $3.3 \times 10^5$ | $6.0 \times 10^6$ |
| $[\{WFe_3S_4Cl_3\}_2(\mu\text{-}SEt)_3]^{3-}$ | $1.0 \times 10^3$ | $2.5 \times 10^3$ |
| | | |
| Effect of Non-Participating ligands | | |
| Cluster | $k_3$ / $dm^3\ mol^{-1}\ s^{-1}$ | $k_4^{SPh}$ / $dm^3\ mol^{-1}\ s^{-1}$ |
| $[\{WFe_3S_4Cl_3\}_2(\mu\text{-}SEt)_3]^{3-}$ | $1.0 \times 10^3$ | $2.5 \times 10^3$ |
| $[\{WFe_3S_4Cl_3\}_2(\mu\text{-}OMe)_3]^{3-}$ | $3.0 \times 10^3$ | $7.2 \times 10^3$ |

Table 1.3. The effect of changing bridging ligands (L) and metal composition (M) on the rates of proton transfer from $pyrrH^+$.

The studies indicated that the rates of protonation and substitution for the W-containing cluster are slower than for the Mo-containing cluster. That both substitution and protonation are both faster for the Mo cluster cannot be an electronic effect since electronic factors, which facilitate binding of anions, would disfavour binding of cations. It has been suggested that this is further evidence that the bond reorganization is a key factor affecting the rate.

The isostructural clusters $[\{WFe_3S_4Cl_3\}_2(\mu\text{-}L)_3]^{3-}$ (L = SEt or OMe) have also been prepared and studied using stopped-flow spectrophotometry. Studies on these clusters allow investigation of the effect of changing the bridging ligands on the reactivity of the Fe-Cl groups [24,34]. In the reactions of $[\{WFe_3S_4Cl_3\}_2(\mu\text{-}L)_3]^{3-}$ with $PhS^-$ in the presence of $pyrrH^+$, both the rate of thiolate binding and the rate of proton transfer are faster with the L = OMe derivative. Again, this is inconsistent with the effect of the bridging ligands on reactivity being an electronic effect. That both the binding of anions and cations are facilitated by the same change in the cluster indicates that bond reorganisation is the dominant barrier to both processes. It is worth mentioning that the effect of the bridging L ligands is smaller than the effect of changing the metal content of the cluster core. This is because the Mo or W is part of the cluster core.

## 1.4 Protonation Involving Natural Fe-S-Based Clusters.

The Fe-S-based cluster is the catalytic site in metalloenzyme and the studies on nitrogenase led to understand the composition, structural and characteristics of the component Fe-S clusters. The nitrogenases are a family of metalloenzymes, which convert dinitrogen into ammonia. Biochemical/genetical studies have shown that there are three types of nitrogenases. Mo-nitrogenase, V-nitrogenase and Fe-only-nitrogenase [38]. All three nitrogenases comprise two essential proteins: the Fe-protein and the MFe-protein (M = Mo, V or Fe). The Fe-protein is the smaller of the two proteins and contains a single $\{Fe_4S_4\}$ cuboidal cluster, which mediates electron transfer from the external reductant (flavodoxin or ferredoxin) to the larger MFe-protein. The MFe-protein contains two unique Fe-S-based clusters: P-clusters which have a $\{Fe_8S_7\}$ core and FeM-cofactor which have a $\{MFe_7S_9\}$ (M = Mo, V or Fe) core, as shown in Figure (1.19), The P-cluster is believed to be effectively a capacitor which subsequently transfers electrons to the active site (FeM-cofactor) where the dinitrogen is bound and transformed into ammonia. The studies to date have focused on the nitrogenase, which contains Mo, Fe and S (the Mo-nitrogenase). In this enzyme the active site has been structurally characterised by X-ray crystallography [39,40]. A feature of these structures is the extensive hydrogen bonding between the cluster and polypeptide as shown in Figure (1.19), The active site of the Mo-nitrogenase (FeMo-cofactor) is a cluster $Fe_7S_9MoC$ shown in Figures (1.19).

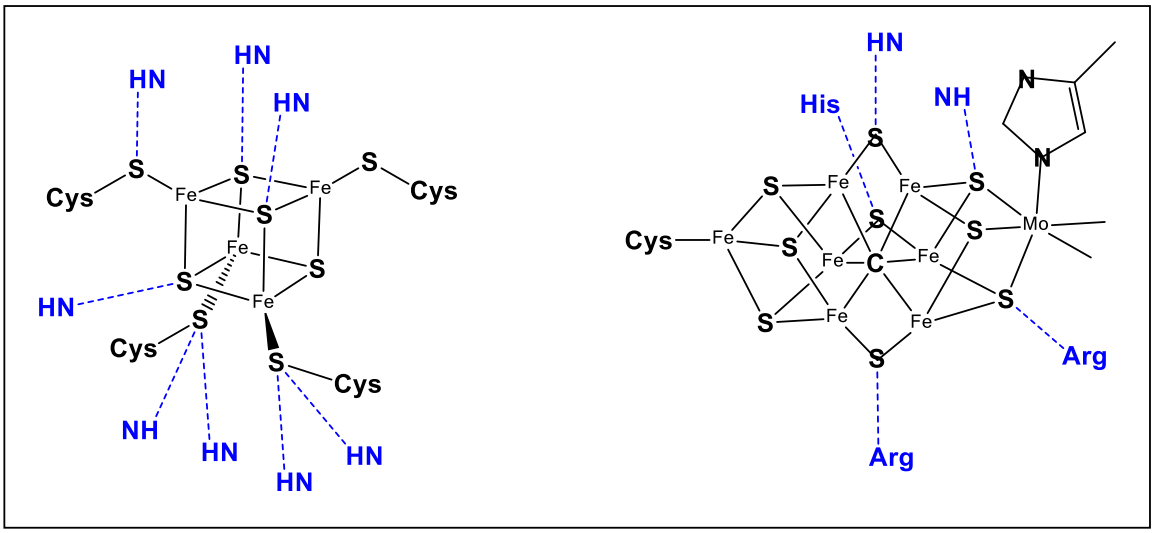


Figure 1.19. Hydrogen bonding from polypeptide to (left) $\{Fe_4S_4\}$ ferredoxin cuboidal cluster in Peptococcus aerogenes and (right) FeMo-cofactor in nitrogenase.

The active site is bonded to the polypeptide through two positions: a histidine residue coordinated to the Mo and a cysteinate residue coordinated to the terminal Fe. As shown in Figure (1.19), all Fe sites are tetrahedral whilst the Mo is octahedral with the coordination sphere occupied by 3 cluster sulfides, the imidazole of a histidine, and homocitrate coordinated as a bidentate ligand to Mo, through the alkoxy and a carboxylate group. Recent experimental [41] and computational studies [42,43] have focussed on the portion of the FeMo-cofactor shown in Figure (1.20) and the sequence of proton and electron transfer reactions produce a state of the enzyme, which is capable of binding and transforming dinitrogen.

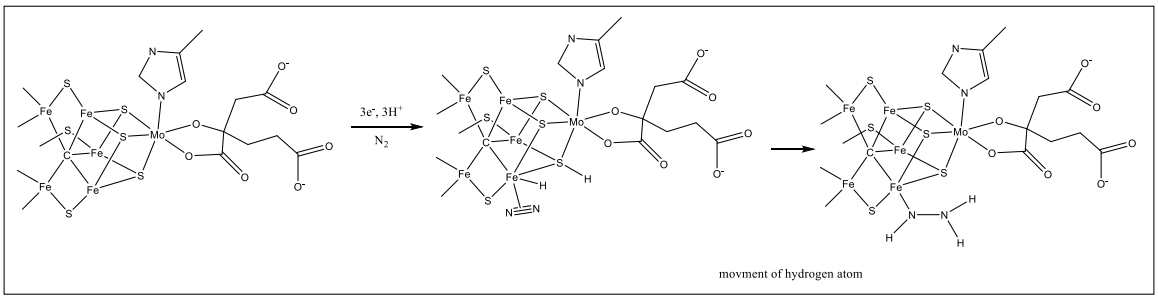


Figure 1.20. Mechanism proposed [41] for the initial stages in the binding and transformation of dinitrogen at the FeMo-cofactor.

The main difference between them the efficiency in reducing nitrogen to ammonia as shown in Equations (1.10 - 1.12) where the Mo derivative is the best because the Mo atoms slow the protonation of the cluster, Because the conversion of dinitrogen into ammonia necessarily requires the presence of protons, and the transformation occurs at a highly reduced Fe-S-based cluster (3 electrons reduced from the resting state as indicated in Figure (1.20), protons can bind to the cluster and be reduced to dihydrogen which is released in an energy, non-productive side reaction which competes with the binding and reduction of dinitrogen. This dihydrogen production is prevalent and no nitrogenase can avoid it. Consequently, some dihydrogen is always produced together with the ammonia.

$$N_2 + 8H^+ + 8e \longrightarrow 2NH_3 + H_2 \qquad \text{(Mo)} \qquad (1.10)$$

$$N_2 + 12H^+ + 12e \longrightarrow 2NH_3 + 3H_2 \qquad \text{(V)} \qquad (1.11)$$

$$N_2 + 21H^+ + 21e \longrightarrow 2NH_3 + 7.5H_2 \qquad \text{(Fe)} \qquad (1.12)$$

Studies on the substrate binding affinities and rates of protonation of the cluster in synthetic cuboidal Fe-S-based clusters containing the $\{MFe_3S_4\}^{n+}$ (M = Fe, Mo or W)

core {Figure (1.21)} have shown that changing a single metal in the cluster affects the substrate binding affinity and rates of protonation differently [18-20,22]. As shown by the data in Table (1.4) the substrate binding affinities for $\{MFe_3S_4\}$ follow the order M = Mo > Fe whereas the rates of protonation follow the order Fe > W ~ Mo.

The difference in efficiencies of the Fe-S-based cluster depend on their structure [35] and to increase the ability to nitrogen fixation, the active site should minimise the production of dihydrogen and maximise the production of ammonia. There are several ways this could be accomplished: (i) the rate of binding and transforming dinitrogen could be much faster than the rate of protonation and dihydrogen production (*i.e.* total kinetic control); (ii) the affinity of the cluster for dinitrogen could be much higher than its affinity for protons (*i.e.* total thermodynamic control) or (iii) a mixture of kinetic and thermodynamic control which is what appears to operate in the synthetic Fe-S-based clusters, where the presence of Mo (or W) in the cluster suppresses the rate of protonation but favours the affinity of the cluster to bind small molecules and ions.

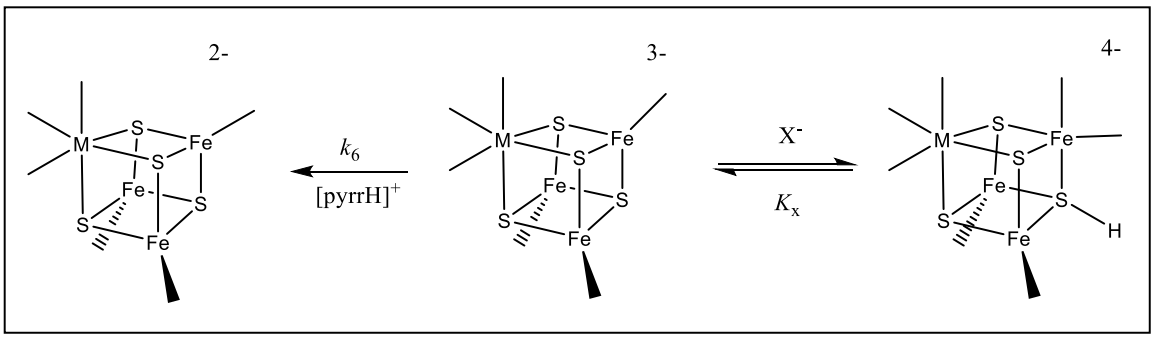


Figure 1.21. Suggested competing pathways for substrate binding and transformation (right) and protonation and dihydrogen production (left) in the reactions of both synthetic clusters and FeMo-cofactor.

| | $K_x$ / $dm^3$ $mol^{-1}$ | |
|---|---|---|
| X | M = Fe | M = Mo |
| $Cl^-$ | 202 | 1550 |
| $Br^-$ | 96 | 850 |
| $PhS^-$ | 68 | 129 |
| CO | -300 | -800 |
| $N_2O$ | -300 | -1030 |
| $Bu^tNc$ | >2000 | |

| M | $k_6$ / $dm^3$ $mol^{-1}s^{-1}$ |
|---|---|
| M = Fe | $2.4 \times 10^4$ |
| M = Mo | $2.5 \times 10^2$ |
| M = W | $8.5 \times 10^2$ |

Table 1.4: How the metal composition of the synthetic clusters in Figure (1.21) affects the two competing pathways.

## References.


1 M. Eigen, *Angewandte Chemie, Int Ed.* **1964**, *3*, 1.

2 C. F. Bernasconi and R. L. Montañez, *J. Org. Chem.* **1997**, *62*, 8162.

3 C. F. Bernasconi, D. M. Wiersema and W. Stronach, *J. Org. Chem.* **1993**, *58*, 217.

4 R. A. Henderson, D. L. Hughes, R. L. Richards and C. Shortman, *J. Chem. Soc., Dalton Trans*. **1987**, 1115.

5 C. B. Allan, G. Davidson, S. B. Choudhury, GZ. U, K. Bose, R. O. Day and M. J. Maroney, *Inorg. Chem*. **1998**, *37*, 4166.

6 S. A. Wender, J. H. Reibenspies, J. S. Kim and M. Y. Darensbourg, *Inorg. Chem*. **1994**, *33*, 1421.

7 V. Autissier, W. Clegg, R. W. Harrington and R. A. Henderson, *Inorg. Chem*. **2004**, *43*, 3098.

8 V. Autissier, P. M. Zarza, A. Petrou, W. Clegg, R. W. Harrington and R. A. Henderson, *Inorg. Chem.* **2004**, *43*, 3106.

9 A. L. Petrou, A. D. Koutselos, H. S. Wahab, W. Clegg, R. W. Harrington and R. A. Henderson, *Inorg. Chem*. **2011**, *50*, 847.

10 L. Dahlenburg and M. Kühnlein, *Eur. J. Inorg. Chem*. **2000**, *9*, 2117.

11 R. H. Holm, P. Kennepohl and E. I. Solomon, *Chem. Rev*. **1996**, *96*, 2239.

12 S. C. Lee and R. H. Holm, *Chem Rev*. **2004**, *104*, 1135.

13 H. Beinert, M. C. Kennedy and C. D. Stout, *Chem. Rev*. **1996**, *96*, 2335.

14 P. Venkateswara and R. H. Holm, *Chem. Rev.* **2004**, *104*, 527.

15 K. S. Hagen, J. G. Reynolds and R. H. Holm, *J. Am. Chem. Soc*. **1981**, *103*, 4054.

16 Z. Cui and R. A. Henderson, *Trans. Met. Chem.* **2006**, *31*, 530.

17 G. R. Dukes R. H. Holm, *J. Am. Chem. Soc*. **1975**, *97*, 528.

18 R. A. Henderson and K. E. Oglieve, *J. Chem. Soc., Dalton Trans*. **1993**, 1467.

19 R. A. Henderson and K. E. Oglieve, *J. Chem. Soc., Dalton Trans*. **1993**, 1473.

20 R. A. Henderson and K. E. Oglieve, *J. Chem. Soc., Chem. Commun*. **1994**, 377.

21 R. A. Henderson and K. E. Oglieve, *J. Chem. Soc., Dalton Trans*. **1998**, 1731.

22 A. J. Dunford and R. A. Henderson, *J. Coord Chem*. **2010**, *63*, 2507.

23 K. Izutsu, "*Acid-Base Dissociation Constants in Dipolar Aprotic Solvents"*, Blackwell Scientific, Oxford, UK, **1990**.

24 B. Garrett and R. A. Henderson, *J. Chem. Soc., Dalton Trans*. **2005**, 2395.

25 S. C. Davies, D. J. Evans, R. A. Henderson, D. L. Hughes and S. Longhurst, *J. Chem. Soc., Dalton Trans*. **2001**, 3470.

26 Job R. C.; Bruice, T. C.; *Proc. Natl. Acad. Sci*. **1975**, *72*, 2478.

27 K. Bates and R. A. Henderson, *Inorg. Chem*. **2008**, *47*, 5850.

28 K. Bates, L. Johnson and R. A. Henderson, *Inorg. Chem*. **2006**, *45*, 9423.

29 K. L. C. Grönberg, and R. A. Henderson, *J. Chem. Soc., Dalton Trans*. **1996**, 3667.

30 V. Do, E. D. Simhon and R. H. Holm, *Inorg. Chem*. **1985**, *24*, 4635.

31 R. A. Henderson, *Chem. Rev*., **2005**, 105, 2365

32 A. J. Dunford and R. A. Henderson, *Chem. Commun*. **2002**, 360.

33 R. A. Henderson and K. E. Oglieve, *J. Chem. Soc., Dalton Trans*. **1999**, 3927.

34 K. Bates, B. Garrett, R. A. Henderson, *Inorg. Chem*. **2007**, *46*, 11145.

35 J. Bell, A. J. Dunford, E. Hollis and R. A. Henderson, *Angew. Chem. Int. Ed*. **2003**, *42*, 1149.

36 A. J. Dunford and R. A. Henderson, *J. Chem. Soc., Dalton Trans*. **2002**, 2837.

37 B. Garrett and R. A. Henderson, *J. Chem. Soc., Dalton Trans*. **2010,** 4586**.**

38 R. R. Eady, *Chem. Rev*. **1996**, *96*, 3013.

39 B. Burgess and D. J. Lowe, *Chem. Rev*. **1996**, *96*, 2983.

40 J. B. Howard and D. C. Rees, *Chem. Rev.* **1996**, *96*, 2965.

41 B. M. Hoffman, D. R. Dean and L. C. Seefeldt, *Accounts Chem. Res*. **2009**, *42*, 609.

42 I. Dance, *Dalton Trans.* **2008**, 5977.

43 I. Dance, *Dalton Trans*. **2010**, 2972.

R. A. Henderson, *BioInorg React Mech*. **2012**, *8*, 11.

# Chapter Two: Synthesis and Protonation Studies on $[Ni(Y_2CR)(triphos)\}]^+$

**(triphos = $PhP(CH_2CH_2PPh_2)_2$, Y = S, R = Me, Et, $Bu^n$, $C_6H_5$, $C_6H_4Me$-4, $C_6H_4Cl$-4, $C_6H_4OMe$-4; Y = O, R = Et, $C_6H_5$)**

## 2.1 Introduction.

Understanding the factors that control the proton transfer to sites coordinated to metals is important in protonation reactions [1]. There are many studies on the rate of proton transfer to oxygen sites in comparson to sulfur sites [2,3]. The protonation of coordinated sulfur site is essential in metalloenzyme (such as as nitrogenases and hydrogenases), in this type of the reaction the proton bonds to cysteinate sulfur ligated to metal site [4]. The protonation of non-coordinated oxygen sites are diffusion controlled in comparison with analogous sulfur sites, which is slower by up to a factor (ca. 30 – 40). The difference between the oxygen and sulfur compounds coming from the difference in the basicity of the oxygen and sulfur and therefore the ability to make hydrogen bonding, which happens prior to proton transfer and this will stabilise the transition state for proton transfer. Previous stopped-flow studies on the protonation of the coordinated thiolate in $[Ni(thiolate)(triphos)]^+$ (triphos = $PhP\text{-}(CH_2CH_2PPh_2)_2$) give information about both the initial hydrogen-bonded intermediate and the subsequent intramolecular transfer of the proton [5].

Furthermore, in a recent study on the isostructural series $[Ni(XPh)(triphos)]^+$ (X = O, S or Se), that the rates of proton transfer from the weak acid, $lutH^+$ (lut = 2,6-dimethylpyridine; $pK_a$ = 14.1 in MeCN) [6], and deprotonation of the complex conjugate acid by lut, are all slow and essentially independent of the donor atom, X [7]. This is because of the seric effect of the phenyl substituent on triphos, which limits the access of the $lutH^+$ to the donor atom.

In this chapter described the synthesis and X-ray crystal structures of $[Ni(S_2CR)(triphos)]^+$ (R = Me, Et, $Bu^n$ or Ph; $RCS_2^-$ = carboxydithioate; triphos = $PhP\{CH_2CH_2PPh_2\}_2$). Stopped-flow kinetic studies show that the reactions of these complexes with anhydrous HCl in MeCN involve an equilibrium protonation of the complex and subsequent interconversion of the bidentate to monodentate alkyl- or arylcarboxydithioic acid as shown in Figure (2.1). In all cases proton transfer is slow and the kinetics reveal that proton transfer is preceded by the formation of a detectable hydrogen bonded intermediate. The measured kinetic isotope effects associated with the transfer of proton from HCl to complex are small ($k_H/k_D$ = 0.9 – 1.14) and detailed studies show that this is because formation of the hydrogen bonded intermediate is associated with an inverse equilibrium isotope effect ($K_H/K_D$ = 0.44 – 0.85) but the intramolecular proton transfer step is associated with a normal isotope rate effect ($k_H/k_D$ = 1.3 – 2.0).

DFT calculation using Gaussian have been used to further explore the reaction mechanism.

The carboxylate analogues, $[Ni(O_2CR)(triphos)]^+$ (R = Et or Ph), have also been prepared allowing comparison of the reactions of carboxylate and carboxydithioate complexes with acid. Reactions of $[Ni(O_2CR)(triphos)]^+$ with anhydrous HCl are complete within the dead-time of the stopped-flow apparatus (~ 2 ms) but studies with mixtures of $lutH^+$ and lut (lut = 2,6-dimethylpyridine) slow proton transfer occurs in these systems. Comparison of the data for the analogous $[Ni(X_2CPh)(triphos)]^+$ shows that when X = O, $pK_a^O$ = 13.7 and when X = S, $pK_a^S$ = 7.2, and that the carboxylate protonates at least 100 times faster than the dithionate.

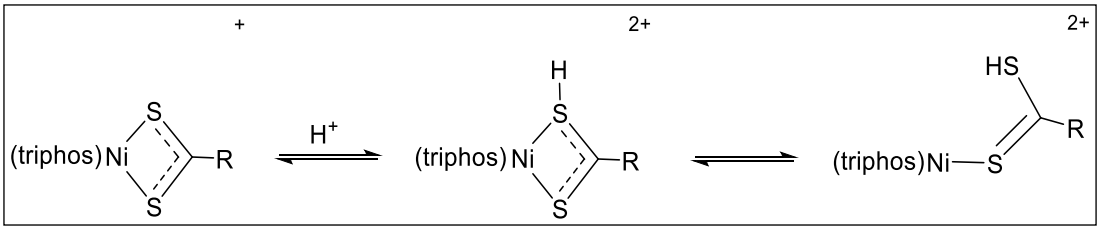


Figure 2.1. Protonation of $[Ni(S_2CR)(triphos)]^+$

## 2.2 Experimental and Methods

### 2.2.1 General Experimental

All preparations and manipulations were routinely performed under oxygen-free atmosphere using Schlenk or syringe techniques as appropriate.

#### 2.2.1.1 Solvents

All solvents were dried and distilled under dinitrogen immediately prior to use. Toluene and hexane were used as received without any further purfications. Acetonitrile was distilled from calcium hydride and methanol from $Mg(OMe)_2$ (generated *in situ*). Tetrahydrofuran (THF) and diethyl ether (ether) were distilled from sodium.

#### 2.2.1.2 Proton Nuclear Magnetic Resonance Spectroscopy ($^1$H NMR Spectroscopy).

$^1$H NMR spectra and $^{31}P\{^1H\}$ NMR were recorded on a 400 MHz Jeol spectrometer. Samples were made up in dry, degassed $CD_3CN$ under an atmosphere of dinitrogen and chemical shifts are quoted relative to tetramethylsilane (TMS).

#### 2.2.1.3 Preparation of Compounds.

The following chemicals were purchased from Sigma-Aldrich and used as received without any further purfications: $NiCl_2.6H_2O$, benzyltrimethylammonium hydroxide, bis(2-diphenylphosphinoethyl)phenylphosphine = triphos, sodium tetraphenylborate, carbon disulphide. The deuterated solvents, methanol-$d_1$ and $D_2O$ were purchased from Sigma-Aldrich and used as received and $CD_3CN$ was purchased from Goss Scientific and used as received.

### 2.2.1.3.1 Synthesis of $[BzMe_3N]S_2CR$ (Bz = $CH_2Ph$, R = Me, Et, $Bu^n$, $C_6H_4Me$-4, $C_6H_5$, $C_6H_4Cl$-4, $C_6H_4OMe$-4) [8].

$$RMgBr + CS_2 \longrightarrow RCS_2MgBr \xrightarrow{HCl} RCS_2H \xrightarrow{[BzN(CH_3)_3]OH} [BzN(CH_3)_3]S_2CR \qquad (2.1)$$

All manipulation was performed in a fume cupboard. Carbon disulfide (0.78 g, 0.01 mol) in anhydrous THF (20 ml) was slowly added to the Grignard reagent (10 ml, 0.01 mol). Cooling with a water bath may be necessary. The mixture was allowed to react for 1.5 h. About 20 ml of the solvent was removed by a rotatory evaporator without warming (keeping the temperature below 25 $^{O}C$). The residue was poured into a mixture of ice (10 g), 10 M hydrochloric acid (5 ml), and hexane (8 ml). The free dithioacid was extracted with hexane (2 x 5 ml) and the collected organic phases were dried over anhydrous magnesium sulfate. After filtration, benzyltrimethyl ammonium hydroxide (3.5 g of a 40 wt% solution in methanol) was added to the carboxydithioic acid solution. The mixture was then evaporated to dryness *in vacuo*. The deep purple or violet crystals of the ammonium carboxydithioate salt were washed with cold hexane and dried at room temperature.

### 2.2.1.3.2 Synthesis of DCl [9].

DCl was prepared *in situ* by addition of $Me_3SiCl$ (3.17 ml, 25 mmol) dropwise to a solution of MeOD (1.0 ml, 25 mmol) in 25 ml of $CH_3CN$ the resulting solution contain 25 mmol DCl and $(CH_3)_3SiOCH_3$. $(CH_3)_3SiOCH_3$ is inert and doesn't react with $[Ni(Y_2CR)(triphos)]^+$.

$$CH_3OD + (CH_3)_3SiCl \xrightarrow{CH_3CN} DCl + (CH_3)_3SiOCH_3 \qquad (2.2)$$

### 2.2.1.4 Synthesis of Nickel Complexes.

### 2.2.1.4.1 Synthesis of [NiCl(triphos)]$BPh_4$ [10].

$$NiCl_2.6H_2O + \text{triphos} \longrightarrow [NiCl(\text{triphos})]Cl + 6H_2O \quad (2.3)$$

$$[NiCl(\text{triphos})]Cl + Na[BPh_4] \longrightarrow [NiCl(\text{triphos})]BPh_4 + NaCl \quad (2.4)$$

To a solution of $NiCl_2.6H_2O$ (1.6 g; 6.7 mmol) in MeOH (ca. 20 ml) was added a solution of triphos (3.5 g; 6.7 mmol) in a 50:50 toluene/MeOH mixture, and the resulting red solution was stirred at room temperature. After allowing all the solid to dissolve (*ca.* 1 h), the volume was reduced *in vacuo* and then a solution containing 1 mol equiv of $NaBPh_4$ in MeOH was added dropwise to produce a bright yellow solid of [NiCl(triphos)]$BPh_4$. The product was removed by filtration and washed with methanol then dried in air (yield 82%). the solid was dissolved in (10 ml) THF (10 ml) and then a large excess of MeOH was added to complete the recrystallization of [NiCl(triphos)]$BPh_4$. Leaving the solution undisturbed at room temperature for 48 h produced well-formed yellow crystal. These crystals were removed by filtration, washed with MeOH, and dried *in vacuo.*

The identity and purity of the product was confirmed by $^1$H NMR and $^{31}P\{^1H\}$ NMR spectroscopy.

$^1$H NMR (400 MHz, Acetonitrile-$d_3$) δ 8.65 – 6.44 (m, 45H *Ph*P), 3.24 – 2.1 (broad, 4H, $CH_2$).

$^{31}P\{^1H\}$ NMR (162 MHz, Acetonitrile-$d_3$) δ 47.48 (d, $J_{pp}$ = 50.7 Hz), 115.50 (t, $J_{pp}$ = 50 Hz).

### 2.2.1.4.2 Synthesis of [Ni($S_2$CMe)(triphos)]$BPh_4$.

$$[NiCl(triphos)]BPh_4 \xrightarrow{[BzN(CH_3)_3]S_2CMe} [Ni(S_2CMe)(triphos)]BPh_4 + [PhCH_2N(CH_3)_3]Cl \quad (2.5)$$

To a suspension of [NiCl(triphos)]$BPh_4$ (0.5 g; 0.53 mmol) in THF (*ca.* 20 ml) was added [$PhCH_2N(CH_3)_3$]$S_2$CMe (0.2520 g; 0.75 mmol). The color changed rapidly from bright yellow to dark red, and the mixture became homogeneous. After the solution was stirred for *ca.* 2 hrs, the mixture was filtered and the filtrate was reduce *in vacuo* to ca. 10 ml. Addition of an excess of hexane (50 ml) produced a dark red microcrystalline solid. Dissolving the solid in the minimum amount of THF and then adding a large excess of hexane achieved recrystallization of the complex. Leaving the solution undisturbed at room temperature for 48 h produced red crystals which were dried *in vacuo* (yield *ca.* 60%). The identity and purity of the product were confirmed by $^1$H NMR and $^{31}$P{$^1$H} NMR spectroscopy.

$^1$H NMR (400 MHz, acetonitrile-$d_3$) δ 8.45 – 6.75 (m, 45H *Ph*P), 3.5 – 2.23 (broad, 8H, $CH_2$), 1.36 (s, 3H, $CH_3$).

$^{31}$P{$^1$H} NMR (162 MHz, acetonitrile-$d_3$) δ 47.84 – 47.53 (d, $J_{PP}$ = 50.7 Hz), 111.90 - 111.28 (t, $J_{PP}$ = 50 Hz).

### 2.2.1.4.3 Synthesis of [Ni($S_2$CEt)(triphos)]$BPh_4$.

This complex was prepared in a similar manner to that described above for [Ni($S_2$CMe)(triphos)]$BPh_4$. The purity and the identification of the product was confirmed by the $^1$H NMR and $^{31}$P{$^1$H} NMR spectra and X-Ray crystallography. $^1$H NMR (400 MHz, acetonitrile-$d_3$) δ 8.2 - 6.4 (m, 45H, *Ph*P), 3.2 – 2.17 (broad, 8H, $CH_2$), 3.08 – 3.00 (q, 2H, $CH_2$, $J_{PP}$ = 7.23 Hz), 1.0 – 0.6 (t, 3H, $CH_3$, $J_{PP}$ = 7.25 Hz).

$^{31}$P{$^1$H} NMR (162 MHz, acetonitrile-$d_3$) δ 53.0 – 51.9 (d, $J_{PP}$ =32.3 Hz), 113.86 - 113.46 (t, $J_{PP}$ = 32.1 Hz).

### 2.2.1.4.4 Synthesis of [Ni($S_2CBu^n$)(triphos)]$BPh_4$.

This complex was prepared in a similar manner to that described above for [Ni($S_2$CMe)(triphos)]$BPh_4$. The purity and the identification of the product were confirmed by the $^1$H NMR and $^{31}$P{$^1$H} NMR spectra.

$^1$H NMR (400 MHz, acetonitrile-$d_3$) δ 9.1 – 6.79 (m, 45H, *Ph*P), 3.4 – 2.5 (broad, 8H, $CH_2$), 3.72 – 3.61 (t, 2H, $J_{PP}$ = 7.83Hz, $CH_2$), 1.3 – 1.01 (m, 4H, $CH_2$), 0.9 – 0.6 (t, 3H $J_{PP}$ = 7.12Hz, $CH_3$).

$^{31}$P{$^1$H} NMR (162 MHz, acetonitrile-$d_3$) δ 5.78 – 51.58 (d, $J_{PP}$ =32 Hz), 114.14 -113.75 (t, $J_{PP}$ = 32 Hz).

### 2.2.1.4.5 Synthesis of [Ni($S_2$CPh)(triphos)]$BPh_4$.

This complex was prepared in a similar manner to that described above for [Ni($S_2$CMe)(triphos)]$BPh_4$. The purity and the identification of the product were confirmed by the $^1$H NMR and $^{31}$P{$^1$H} NMR spectra and X-Ray crystallography.

$^1$H NMR (400 MHz, acetonitrile-$d_3$) δ 8.25 – 6.76 (m, 50H, *Ph*P), 3.24 – 2.1 (broad, 8H, $CH_2$).

$^{31}$P{$^1$H} NMR (162 MHz, acetonitrile-$d_3$) δ 52.88-52.69 (d, $J_{PP}$ =31.2 Hz), 113.22-112.82 (t, $J_{PP}$ = 31.7 Hz).

### 2.2.1.4.6 Synthesis of [Ni($S_2CC_6H_4$Me-4)(triphos)]$BPh_4$.

This complexes was prepared in a similar manner to that described above for [Ni($S_2$CMe)(triphos)]$BPh_4$. The purity and the identification of the product were confirmed by the $^1$H NMR and $^{31}$P{$^1$H} NMR spectra and X-Ray crystallography.

$^1$H NMR (400 MHz, acetonitrile-$d_3$) δ 8.24 – 6.75 (m, 49H, *Ph*P), 3.08 – 2.07 (broad, 8H, $CH_2$) 2.3(s, 3H, -$CH_3$).

$^{31}$P{$^1$H} NMR (162 MHz, acetonitrile-$d_3$) δ 50.61 – 50.32 (d, $J_{PP}$ =30.1Hz), 109.52 - 109.14 (t, $J_{PP}$ = 30.6 Hz).

### 2.2.1.4.7 Synthesis of $[Ni(S_2CC_6H_4Cl\text{-}4)(triphos)]BPh_4$.

This complexes was prepared in a similar manner to that described above for $[Ni(S_2CMe)(triphos)]BPh_4$. The purity and the identification of the product were confirmed by the $^1H$ NMR and $^{31}P\{^1H\}$ NMR spectra and X-Ray crystallography.

$^1H$ NMR (400 MHz, acetonitrile-$d_3$) δ 8.30 – 6.79 (m, 49H, *Ph*P), 3.1 – 2.02 (broad, 8H, $CH_2$).

$^{31}P\{^1H\}$ NMR (162 MHz, acetonitrile-$d_3$) δ 53.73 – 53.54 (d, $J_{PP}$ =31.05 Hz), 113.61 - 113.22 (t, $J_{PP}$ = 31.05 Hz).

### 2.2.1.4.8 Synthesis of $[Ni(S_2CC_6H_4OMe\text{-}4)(triphos)]BPh_4$.

This complexes was prepared in a similar manner to that described above for $[Ni(S_2CMe)(triphos)]BPh_4$. The purity and the identification of the product were confirmed by the $^1H$ NMR and $^{31}P\{^1H\}$ NMR spectra and X-Ray crystallography.

$^1H$ NMR (400 MHz, Acetonitrile-$d_3$) δ 8.26 – 6.69 (m,49H, *Ph*P), 3.79 (s, 3H, O$CH_3$), 3.05– 2.3 (broad, 8H, $CH_2$),

$^{31}P\{^1H\}$ NMR (162 MHz, Acetonitrile-$d_3$) δ 51.22–51.03 (d, $J_{PP}$ =31.1 Hz), 112.52-112.3 (t, $J_{PP}$ = 31 Hz).

### 2.2.1.4.9 Synthesis of $[Ni(O_2CC_6H_5)(triphos)]BPh_4$.

$[NiCl(triphos)]BPh_4$ (0.568 g, 0.6 mmol) was dissolved in 15-20 ml of dry THF, and then a solution of sodium benzoate (0.864 g, 6 mmol) in methanol was added. The solution changed rapidly from yellow to red and was stirred overnight. All volatiles were removed *in vacuo*, to produce a red microcrystalline solid. The dry solid was extracted with the minimum amount of $CH_2Cl_2$ to form a red solution and a white solid (presumably sodium chloride). The sodium salts were removed by filtration and washed with $CH_2Cl_2$ to ensure complete extraction of the desired red product. Layering EtOH on the red solution produced (after several days of slow diffusion) red product, $[Ni(O_2CC_6H_5)(triphos)]BPh_4$. The purity and the identification of the product were confirmed by $^1H$ NMR and $^{31}P\{^1H\}$ NMR spectrascopy.

$^1H$ NMR (400 MHz, acetonitrile-$d_3$) δ 8.82 – 6.63 (m, 50H, *Ph*P), 3.2 – 2.23 (broad, 8H, $CH_2$).

$^{31}P\{^{1}H\}$ NMR (162 MHz, acetonitrile-$d_3$) δ 102.5 - 101.2 (t, $J_{PP}$=55.7 Hz), 46.5 – 44.6 (d, $J_{PP}$ = 55.7 Hz).

### 2.2.1.4.10 Synthesis of $[Ni(O_2CEt)(triphos)]BPh_4$.

This complexes was prepared in a similar manner to that described for $[Ni(O_2CC_6H_5)(triphos)]BPh_4$. The purity and the identification of the product were confirmed by $^{1}H$ NMR and $^{31}P\{^{1}H\}$ NMR spectroscopy.

$^{1}H$ NMR (400 MHz, Acetonitrile-$d_3$) δ 8.88 – 6.63 (m, 45H, *Ph*P), 3.19 – 2.42 (broad, 8H, $CH_2$), 1.51 (q, 2H, $J_{PP}$ = 7.2 Hz, $CH_2$-$CH_3$), 2.2 – 2.1 (t, 3H, $J_{PP}$ = 7.5 Hz, $CH_3$).

$^{31}P\{^{1}H\}$ NMR (162 MHz, Acetonitrile-$d_3$) δ 111.7 (t, $J_{PP}$ = 50.6 Hz), 47.2 (d, $J_{PP}$ = 50.6 Hz).

### 2.2.1.4.11 DFT Calculation

The geometry optimization of the complexes was achieved by performing DFT calculation using Gaussian 09 package [11], at the B3LYP/Lanl2dz levels of theory used for the optimization for H, C, N, S, P and Ni, with the terminal condition being a root mean sequare (RMS) < 0.001 kcal $mol^{-1}$. The experimental studies has been done in acetonitrile solvent, so we have considered the solvent effect in the geometry optimization by means of the well- known polarized continuum model (IEFPCM) [12] with the default parameters embedded in Gaussian 09 to obtain a valid approximation of chemical environment.

## 2.3 Result and Discussion.

## 2.3.1 Characterization of Complexes.

### 2.3.1.1 NMR Spectroscopy.

The $^{1}H$ and $^{31}P\{^{1}H\}$ NMR spectra for all the complexes $[Ni(S_2CR)(triphos)]BPh_4$ ( R = Me, Et or $Bu^n$) and $[Ni(S_2CC_6H_4R'\text{-}4)(triphos)]BPh_4$ (R′ = H, Me, Cl or OMe) were recorded in $CD_3CN$.

In the $^{1}H$ NMR spectra, the $CH_2$ groups of the triphos in both the carboxydithioate and carboxylate complexes appear as broad peaks in the region of δ = 2 - 3.5 ppm. The broadness is attributed to the $CH_2$ groups of the phosphine ligand, which is flipping up and down in the molecule and resulting in the conformational equilibrium shown in Figure (2.2) [13].

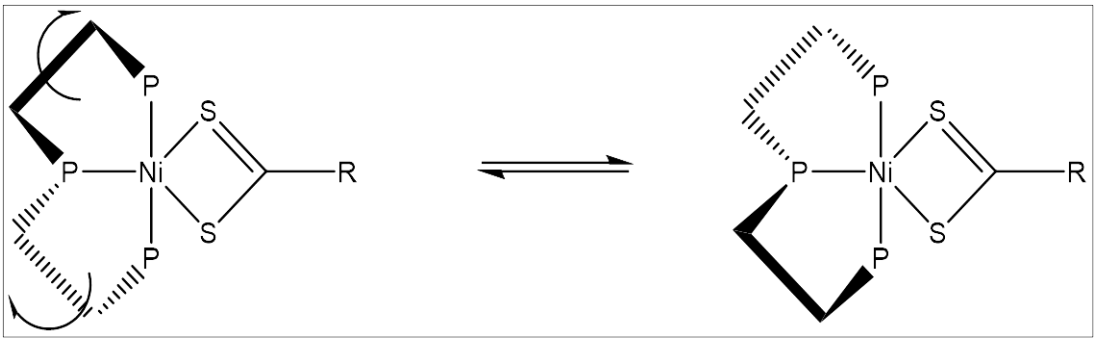


Figure 2.2. Conformational equilibrium of the flipping of the $CH_2$ groups in the triphos ligand. The phenyl groups on the phosphine are omitted for clarity.

The phenyl groups in the tetraphenyl borate, triphos, dithiolate and dicarboxylate ligands all show peaks in the region δ = 6 - 8 ppm as shown in Figure (2.3). Detailed assignment of the peaks is not possible due to the presence of so many overlapping peaks in this region. The peaks of the alkyl substituents on the dithiolate ligands appeared in the region δ = 0.5 – 3.6 ppm. Using the $^{1}H$ NMR spectra are not a sufficiently good tool for checking the purity of our complexes there are two type of possible impurities that would be expected in the products, the sodium thiolate salts and $[NiCl(triphos)]BPh_4$ which have $^{1}H$ NMR spectra very similar to the products.

$^{31}P\{^{1}H\}$ NMR spectra for the complexes consist of two sets of peaks. The two terminal phosphorus atoms ($PPh_2$) of the triphos give doublet peak in the region δ = 47-54 ppm which is attributed to the coupling of terminal phosphorus atoms ($PPh_2$) with the single phosphorus atom (PPh) in the centre of the triphos ligand ($J_{PP}$ = 32 Hz). The central phosphorus atom couples with the two terminal phosphorus and shows a triplet signal in the range δ = 104 - 114 ppm ($J_{PP}$ = 32 Hz) as shown in Figure (2.4).

The best way to detect the presence of any unreacted [NiCl(triphos)]$BPh_4$ is using $^{31}P\{^{1}H\}$ NMR spectroscopy. The $^{31}P\{^{1}H\}$ NMR spectrum of [NiCl(triphos)]$BPh_4$ in $CD_3CN$ shows two sets of peaks. A doublet at (δ = 48.6 - 46.6 ppm) and a triplet at (δ = 112.5 – 110.6 ppm). Consequently contamination of the product with [NiCl(triphos)]$BPh_4$ can easily be detected with $^{31}P\{^{1}H\}$ NMR spectroscopy.

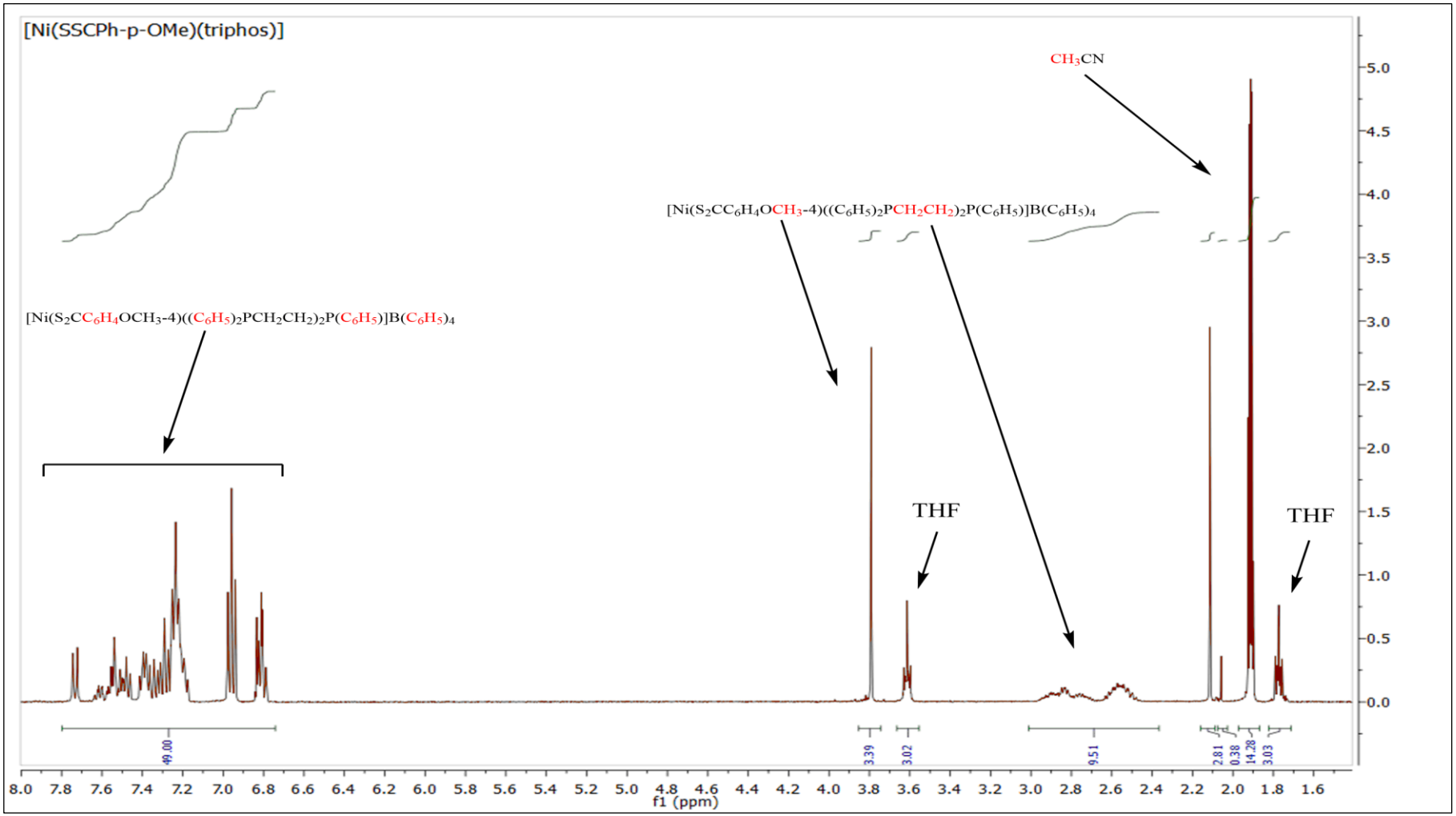


**Figure 2.3. $^{1}$H NMR spectrum of [Ni($S_2CC_6H_4OMe$-4)(triphos)]$BPh_4$ in acetonitrile. The THF molecule included in the crystal structure.**

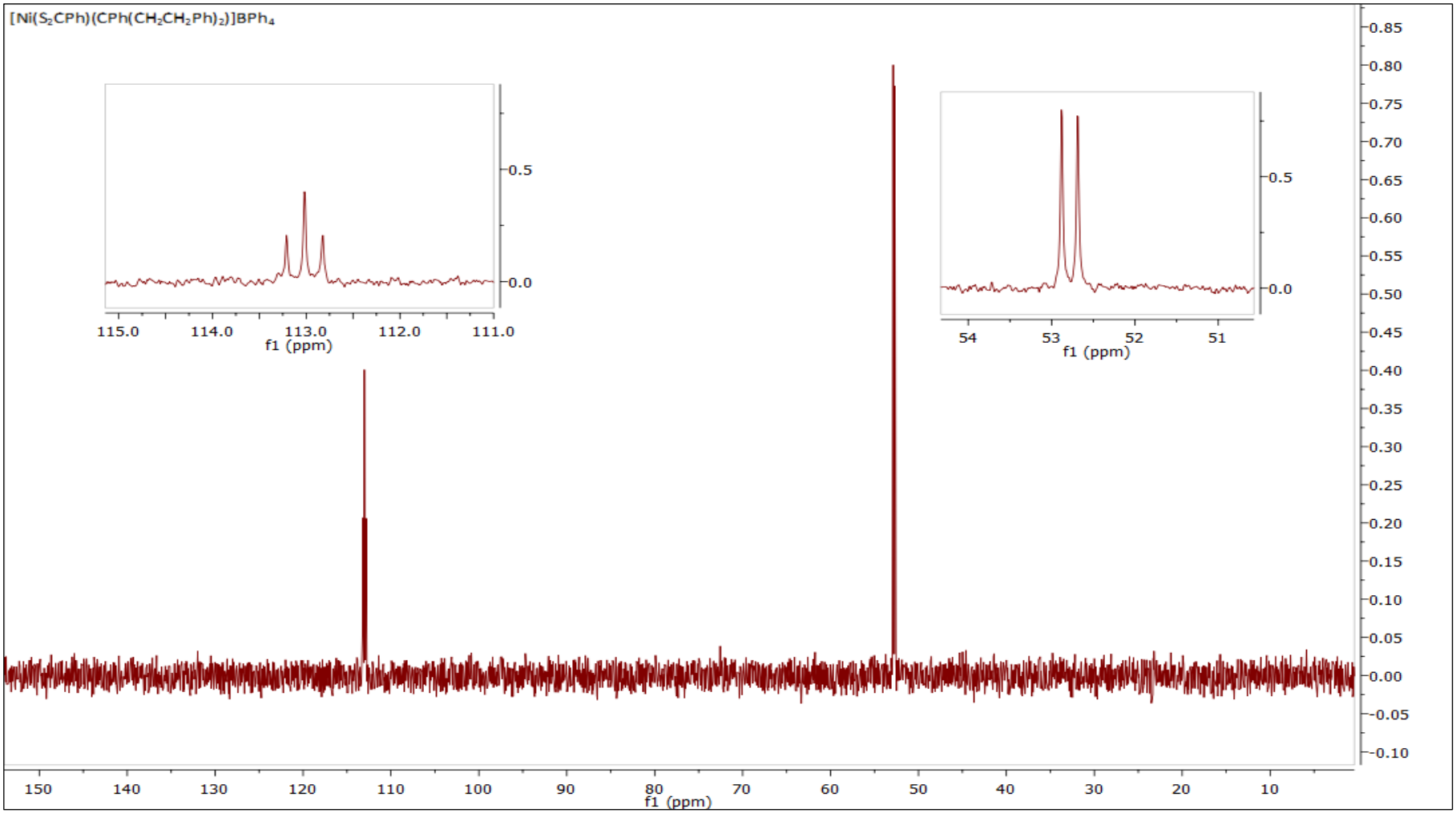


**Figure 2.4. $^{1}$H NMR spectrum of [Ni($S_2CC_6H_4OMe$-4)(triphos)]$BPh_4$ in acetonitrile.**

### 2.3.1.2 Elemental Analysis.

Elemental analysis have been determined for some complexes to check if the complexes are free from the byproduct and other unreacted starting materials (Table 2.1). The difference between the theortical and the experimental value does not exceed 0.7%, which shows a reasonable purity considering an error from the analyser of 0.3% (Table 2.1)

| R-substituent | %C (theoretical value) | %H (theoretical value) |
|---|---|---|
| Me | 71.1(71.8) | 6.0(5.62) |
| Et | 71.23(71.99) | 6.0(5.74) |
| $Bu^n$ | 71.9(72.36) | 6.0(5.62) |
| $C_6H_4OCH_3$-4 | 71.5(71.9) | 5.9(5.8) |

Table 2.1. CH analysis of $[Ni(S_2CR)(triphos)]BPh_4$ (R = Me, Et, $Bu^n$) and $[Ni(S_2CC_6H_4R'\text{-}4)(triphos)]BPh_4$ (R = H, Me, Cl, OMe)

### 2.3.1.3 X-ray Crystallography

The X-ray crystal structures of the complexes [Ni($S_2CC_6H_4$R-4)(triphos)]$BPh_4$ (R = H, Me, Cl and OMe) and [Ni($S_2$CEt)(triphos)]$BPh_4$ have been determined and the structure of the cations are shown in Figure (2.5). The nickel is 5-coordinate with the coordination sphere made up of the three phosphorus donors of the triphos and the carboxydithioate ligand acting as a bidentate ligand. The structure of the cation is best described as a trigonal bipyramid.

Addison [14], has defined the angular structural parameter, $\tau = (\beta - \alpha)/60$ (where $\alpha$ = smaller of basal angles and $\beta$ = larger of basal angles). The parameter $\tau$ is an index of trigonality in 5-coordinate complexes. For a perfect square-based pyramid, $\tau = 0$ and for a perfect trigonal bipyramid $\tau = 1.0$. For the complexes described herein $\beta$ = the angle $P_2NiS_1$ and $\alpha$ = the angle $P_1NiS_2$. Hence, R = Et, $\tau = 0.84$; R = Ph, $\tau = 1.15$; R = $C_6H_4$OMe-4, $\tau = 1.01$; R = $C_6H_4$Cl-4, $\tau = 0.96$. Indicating in all cases that the complexes are trigonal bipyramids. The trigonal plane comprises the two terminal phosphorus atoms of the triphos ligand and a sulfur from the dithioate ligand {$P_{t1}$-Ni-$S_2$ = 107.41°(2) - 125.86°(4), $P_{t1}$-Ni-$P_{t2}$ = 118.98(2)° - 131.15(4)°, $P_{t2}$-Ni-$S_2$ = 102.95(4)° - 130.66(3)°}. The axial positions are occupied by the central phosphorus of the triphos ligand and the other sulfur of the dithioate ligand. In the dithioate ligand, $S_1$-C-$S_2$ = 109.71(11)°-113.7(2)°. Selected bond lengths associated with the nickel and its ligands are presented in the legend to Figure (2.5) and Table (2.2) and Table (2.3).

Henderson [15] previously described the X-ray crystal structure of [Ni(2-Spy)(triphos)]$^+$ (2-Spy = 2-thiopyridine), in which the nickel is also five-coordinate and the 2-Spy ligand is a bidentate (The structure is a distorted trigonal bipyramid with the trigonal plane including the two terminal phosphorus atoms of the triphos ligand and the nitrogen of the 2-Spy ligand. The two axial positions are occupied by the central phosphorus of the triphos ligand and the sulfur). The structures of [Ni($S_2CC_6H_4$R-4)(triphos)]$BPh_4$ (R = H, Me, Cl and OMe) and [Ni($S_2$CEt)(triphos)]$BPh_4$ and the previously reported complex [Ni(2-Spy)(triphos)]$^+$ are very similar. Thus, in [Ni(2-Spy)(triphos)]$^+$ the structure is also best described as a distorted trigonal bipyramid. Table (2.2) and Table (2.3) show the bond angles and the bond lengths for [Ni($S_2CC_6H_4$R-4)(triphos)]$BPh_4$ (R = H, Me, Cl and OMe) and [Ni($S_2$CEt)(triphos)]$BPh_4$ and [Ni(2-Spy)(triphos)]$^+$.

$[Ni(S_2CEt)(triphos)]^+$

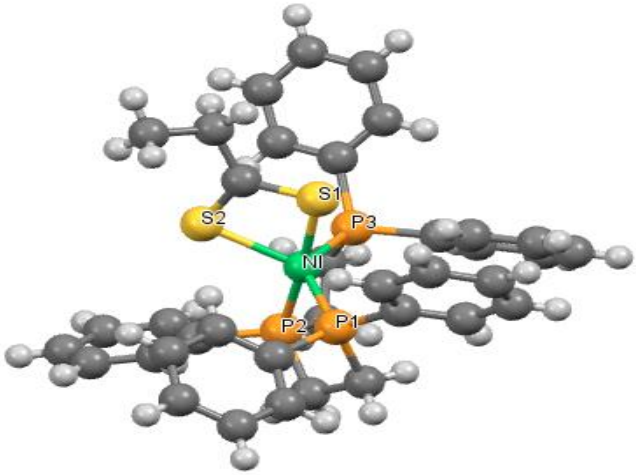


$[Ni(S_2CC_6H_5)(triphos)]^+$

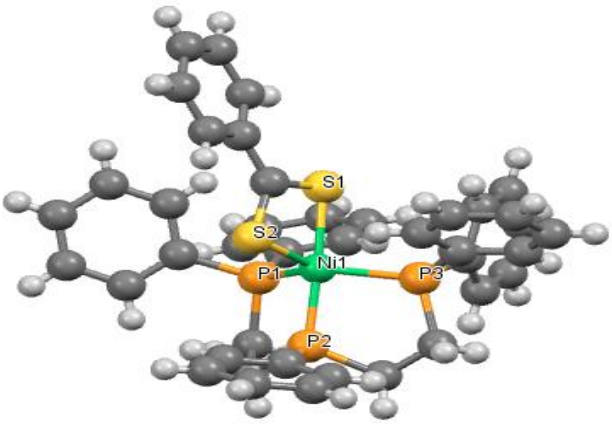


$[Ni(S_2CC_6H_4Cl\text{-}4)(triphos)]^+$

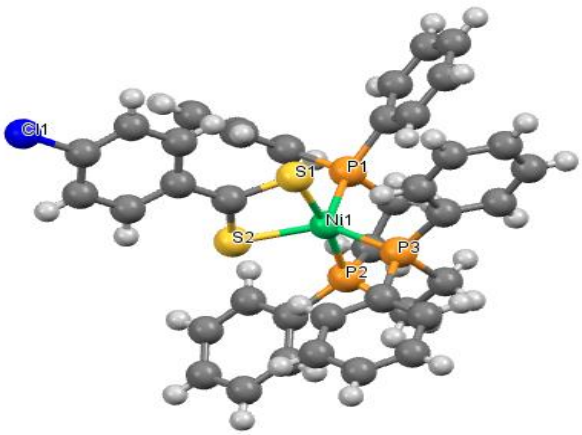

$[Ni(S_2CC_6H_4Me\text{-}4)(triphos)]^+$

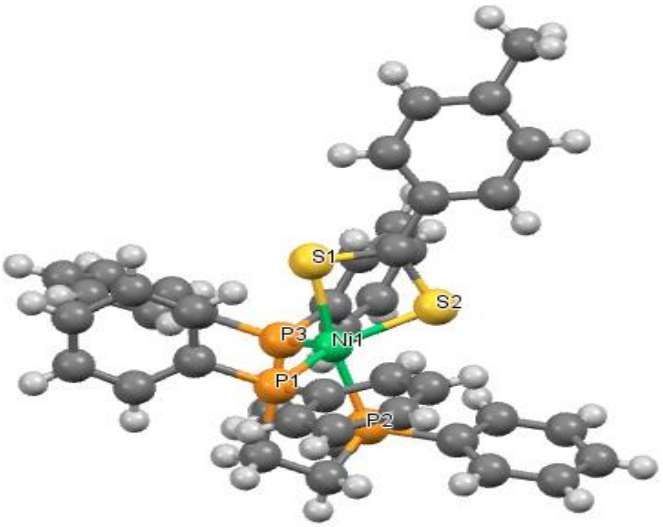


$[Ni(S_2CC_6H_4OMe\text{-}4)(triphos)]^+$

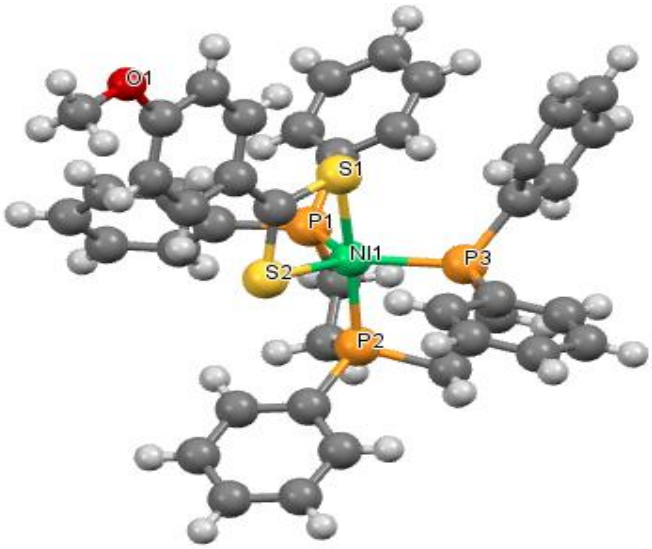


Figure 2.5. Structure of the cation in $[Ni(S_2CC_6H_4R\text{-}4)(triphos)]BPh_4$. (R = H, $CH_3$, $OCH_3$, Cl) and $[Ni(S_2CEt)(triphos)]BPh_4$, where (green = Nickel, orange = Phosphorous, yellow = Sulfur, red = Oxygen and blue = Chloride )

| $[Ni(S_2CR)(triphos)]^+$ | R = $C_6H_5$ | R = $C_6H_4OMe$-4 | R=$C_6H_4Cl$-4 | R = $C_6H_4Me$-4 | R = Et | $[Ni(2\text{-}Spy)(triphos)]^+$ |
|---|---|---|---|---|---|---|
| Bond Angle | | | | | | |
| $P_{t1}$-Ni- $S_1$ | 92.70(3) | 96.86(2) | 96.86(2) | 76.21(3) | 95.75(4) | 92.08(3) |
| $P_{t1}$-Ni-$S_2$ | 107.41(3) | 112.90(2) | 114.67(2) | 76.21(3) | 125.86(4) | |
| $P_c$ -Ni-$S_1$ | 176.60(3) | 173.69(2) | 172.38(2) | 76.21(3) | 176.27(4) | 178.98(4) |
| $P_c$ -Ni-$S_2$ | 100.50(3) | 97.99(2) | 96.423(19) | 76.21(3) | 100.73(4) | |
| $P_{t2}$-Ni-$S_1$ | 94.90(3) | 94.70(2) | 96.08(2) | 76.21(3) | 94.35(4) | 93.93(3) |
| $P_{t2}$-Ni-$S_2$ | 121.76(3) | 128.05(2) | 129.42(2) | 76.21(3) | 102.95(4) | |
| $P_c$ -Ni- $P_{t1}$ | 87.70(3) | 87.72(2) | 87.936(19) | 76.21(3) | 85.88(4) | 87.08(3) |
| $P_c$ -Ni- $P_{t2}$ | 87.39(3) | 86.82(2) | 87.08(2) | 76.21(3) | 87.06(4) | 87.08(3) |
| $P_{t1}$-Ni-$P_{t2}$ | 130.66(3) | 118.98(2) | 115.87(2) | 76.21(3) | 131.15(4) | 146.34(3) |
| $S_1$-Ni-$S_2$ | 76.16(2) | 76.25(2) | 76.211(18) | 76.21(3) | 75.60(4) | |
| $P_{t1}$-Ni-N | | | | | | 119.08(7) |
| $P_c$ -Ni-N | | | | | | 119.08(7) |
| $P_{t2}$-Ni-N | | | | | | 94.11(7) |
| N-Ni-S | | | | | | 70.81(6) |

Table 2.2. Selected bond angles for the cations in $[Ni(S_2CC_6H_4R\text{-}4)(triphos)]BPh_4$. (R = H, $CH_3$, $OCH_3$, Cl) and $[Ni(S_2CEt)(triphos)]BPh_4$.

| $[Ni(S_2CR)(triphos)]^+$ | R = $C_6H_5$ | R = $C_6H_4OMe$-4 | R=$C_6H_4Cl$-4 | R = $C_6H_4Me$-4 | R = Et | $[Ni(2\text{-}Spy)(triphos)]^+$ |
|---|---|---|---|---|---|---|
| Ni-S1 | 2.2321(7) | 2.2206(6) | 2.2296(5) | 2.2327(8) | 2.2342(11) | 2.2644(8) |
| Ni-$S_2$ | 2.3179(7) | 2.2683(6) | 2.2559(5) | 2.2599(8) | 2.3448(10) | |
| Ni-$P_{t1}$ | 2.2227(7) | 2.2367(6) | 2.2315(5) | 2.2204(8) | 2.1733(10) | 2.1637(9) |
| Ni-$P_c$ | 2.1484(7) | 2.1712(6) | 2.1739(5) | 2.1757(8) | 2.1516(11) | 2.1310(8) |
| Ni-$P_{t2}$ | 2.2066(7) | 2.2074(6) | 2.2144(6) | 2.2315(8) | 2.2174(11) | 2.1966(9) |
| Ni-N | | | | | | 2.164(2) |

Table 2.3. Selected bond lengths for the cations in $[Ni(S_2CC_6H_4R\text{-}4)(triphos)]BPh_4$. (R = H, Me, OMe, Cl) and $[Ni(S_2CEt)(triphos)]BPh_4$.

## 2.4 Kinetic studies Using Stopped-Flow Spectrophotometry.

All kinetic studies were performed using an Applied Photophysics SX.18 MV stopped-flow spectrophotometer. The temperature was maintained at 25.0 ± 0.1 ºC using a Grant LTD 6G thermostat tank with combined re-circulating pump. The solutions of cluster and reactants were prepared under an atmosphere of dinitrogen and transferred to the spectrophotometer using all glass syringes. Solutions of reagents were prepared by dilution from freshly made stock solutions in MeCN and used within 1 hr.

The kinetics of the reaction between $[Ni(S_2CR)(triphos)]BPh_4$ (R = Me, Et, $Bu^n$), **[**$Ni(S_2CC_6H_5R\text{-}4)(triphos)]BPh_4$ (R = Me, H, Cl, OMe) with a mixture of anhydrous HCl and $Cl^-$ has been measured using a stopped-flow spectrophotometer in MeCN at 25.0 $^{\circ}$C. The kinetic studies were performed under pseudo first order conditions, with concentrations of acid and base in at least a 10-fold excess over the concentration of the complex (0.5 mmol $dm^{-3}$). The stock solutions of the acid and the base were used to prepare the more dilute mixtures, and all solutions were used within one hour of preparation. The concentration used for all complexes $[Ni(S_2CR)(triphos)]BPh_4$ (R = Me, Et, $Bu^n$) and **[**$Ni(S_2CC_6H_5R\text{-}4)(triphos)]BPh_4$ (R = H, Me, Cl, OMe) are as shown in the Table (2.4).

| Complex | [Ni] mmol $dm^{-3}$ | [HCl] mmol $dm^{-3}$ | [$Cl^-$] mmol $dm^{-3}$ |
|---|---|---|---|
| $[Ni(S_2CMe)(triphos)]^+$ | 0.5 | 50.0<br>100.0 | 2.5 – 50.0<br>2.5 – 50.0 |
| $[Ni(S_2CEt)(triphos)]^+$ | 0.5 | 25.0<br>50.0<br>100.0 | 1.0 – 10.0<br>2.5 –30.0<br>2.5 –30.0 |
| $[Ni(S_2CBu^n)(triphos)]^+$ | 0.5 | 100.0<br>200.0 | 5.0 – 100.0<br>5.0 – 100.0 |
| **[**$Ni(S_2CC_6H_6)(triphos)]^+$ | 0.5 | 100.0<br>150.0 | 1.0 – 15.0<br>1.0 – 15.0 |
| **[**$Ni(S_2CC_6H_5Me\text{-}4)(triphos)]^+$ | 0.5 | 200.0<br>300.0 | 0.0 – 10.0<br>0.0 – 10.0 |
| **[**$Ni(S_2CC_6H_5OMe\text{-}4)(triphos)]^+$ | 0.5 | 200.0<br>300.0 | 0.0 – 10.0<br>0.0 – 10.0 |
| **[**$Ni(S_2CC_6H_5Cl\text{-}4)(triphos)]^+$ | 0.5 | 200.0<br>300.0 | 0.0 – 10.0<br>0.0 – 10.0 |

Table 2.4. Shows the concentration used for all complexes, HCl and $Cl^-$.

The wavelength used was 420 nm for all the complexes. Typical absorbance/time curve obtained for all [Ni($S_2$CR)(triphos)]$BPh_4$ (R = Me, Et, $Bu^n$) and [Ni($S_2CC_6H_5$R-4)(triphos)]$BPh_4$ (R = H, Me, Cl, OMe) complexes is shown in Figure (2.6). All curves fitted to the equation: $A_t = A_f + \Delta A.\, e^{-k_{obs}.t}$ (where $A_t$ = the absorbance at any time, $A_f$ = final absorbance, $\Delta A = A_i - A_f$, $A_i$ = initial absorbance. At this wavelength only the nickel complexes will absorb, so the absorbance belongs to the concentration of the complex. Consequently, the shapes of the absorbance changes indicate the kinetic order with respect to the complex.

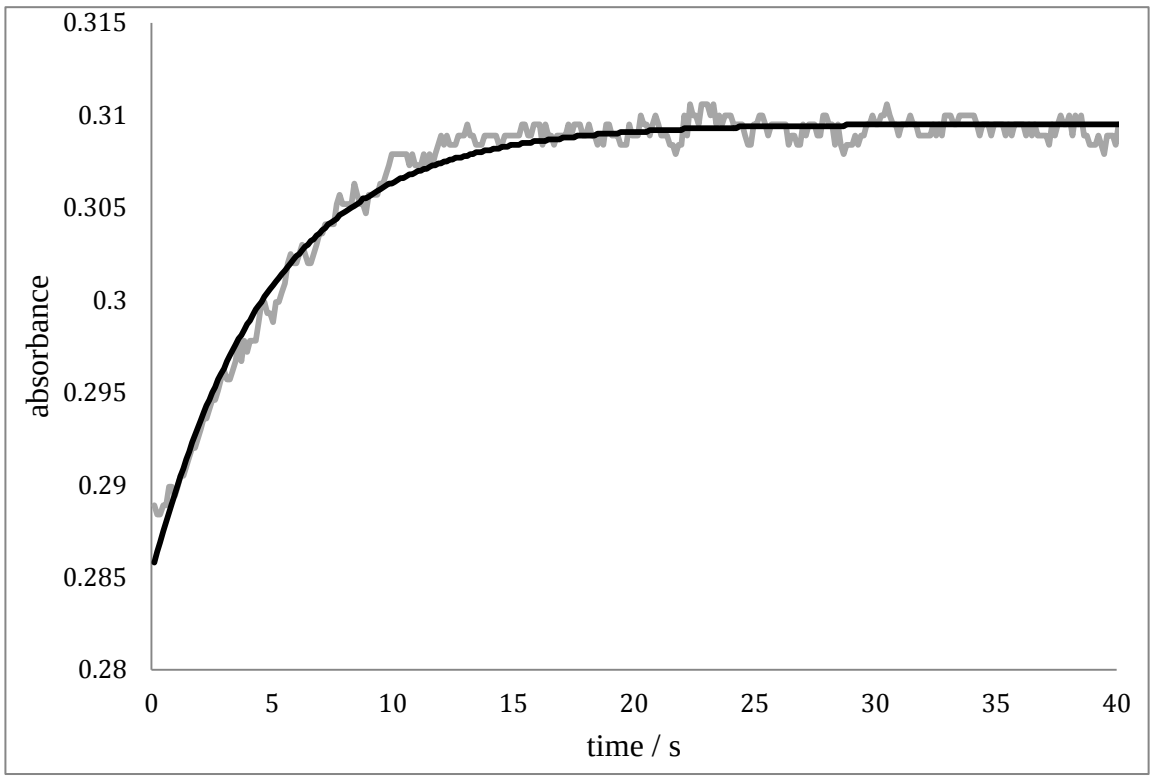


Figure 2.6. Stopped-flow absorbance-time curve for the reaction of [Ni($S_2$CEt)(triphos)]+ (0.5 mmol $dm^{-3}$) with HCl (40 mmol $dm^{-3}$) in MeCN at 25.0 $^oC$ ($\lambda$ = 420 nm). The experimental trace is shown in black and the exponential curve fit is shown in grey. The curve fit is defined by the equation $A_t = 0.325 - 0.042e^{-0.35t}$.

## 2.4.1 Kinetics of the reaction between $[Ni(S_2CR)(triphos)]^+$ (R = Me, Et or $Bu^n$) and HCl in the presence of $[Cl^-]$.

### 2.4.1.1 Protonation Reaction with HCl.

In studies on the reactions of $[Ni(S_2CR)(triphos)]^+$ (R = Me, Et or $Bu^n$) and HCl, The dependence on the concentration of HCl is complicated as shown in Figure (2.8), and involves a change in the kinetic order over the concentration range of HCl studied. At low concentrations of HCl the reaction exhibits a first order dependence on [HCl] but at high concentrations of HCl the rate of the reaction is independent of [HCl]. The data was analysed by the usual plot of $1/k_{obs}$ versus 1/[HCl] [16], which yields a straight line as shown in Figure (2.9) and allows derivation of the rate law shown in Equation (2.5). When R = Me, a = 4.69 x $10^3$ $dm^3$ $mol^{-1}$ $s^{-1}$, b = 67.0 $dm^3$ $mol^{-1}$; R = Et: a = 39.5 $dm^3$ $mol^{-1}$ $s^{-1}$, b = 84.0 $dm^3$ $mol^{-1}$; R= $Bu^n$: a = 19.9 $dm^3$ $mol^{-1}$ $s^{-1}$, b = 71.0 $dm^3$ $mol^{-1}$ as shown in Table (5). The proposed mechanism of the reactions between $[Ni(S_2CR)(triphos)]^+$ and HCl in MeCN (R = Me, Et , $Bu^n$) is shown in Figure (2.7).

$$\text{Rate} = \frac{a\ [HCl\,][Ni(S_2CR)(triphos)^+]}{1 + b\,[HCl]} \qquad (2.5)$$

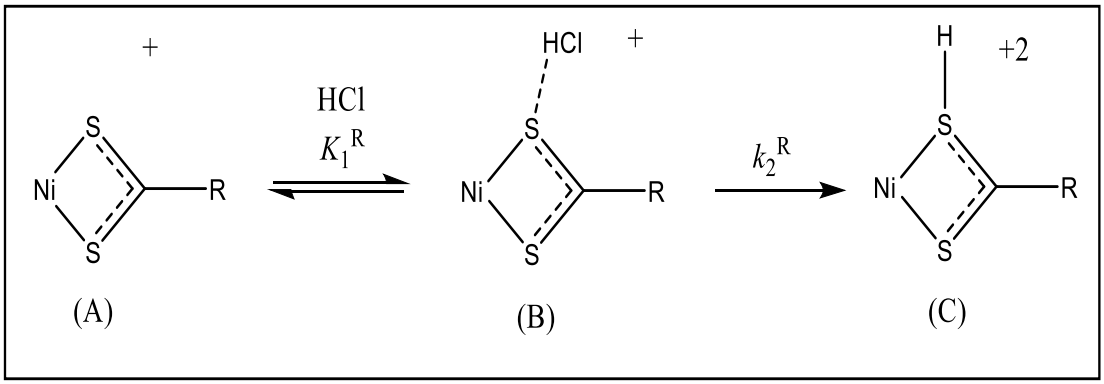


Figure 2.7. Mechanisms of protonation of $[Ni(S_2CR)(triphos)]^+$ (R = Me, Et , $Bu^n$). triphos ligand omitted for clarity.

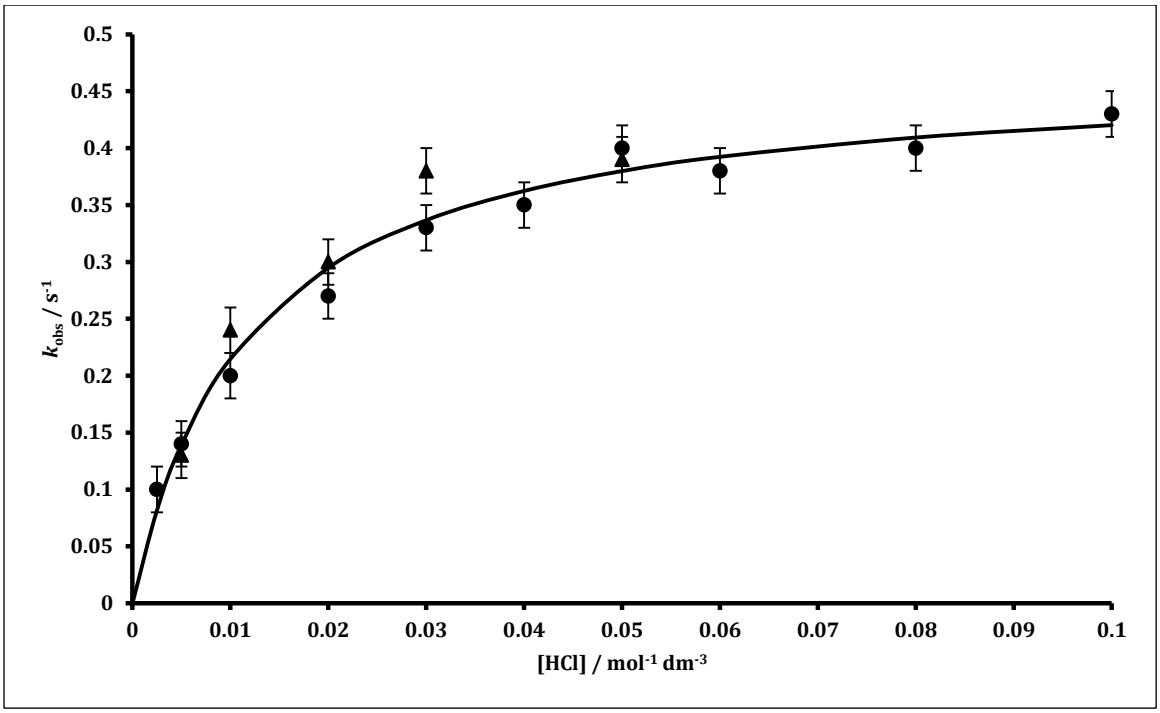


Figure 2.8. Kinetic data for the reaction of $[Ni(S_2CEt)(triphos)]^+$ ([Ni] = 0.5 mmol $dm^{-3}$) with HCl in MeCN at 25.0 $^oC$. Data points corresponded to: HCl = 2.5 – 100 mmol $dm^{-3}$ and the error bar corresponding to 5%.

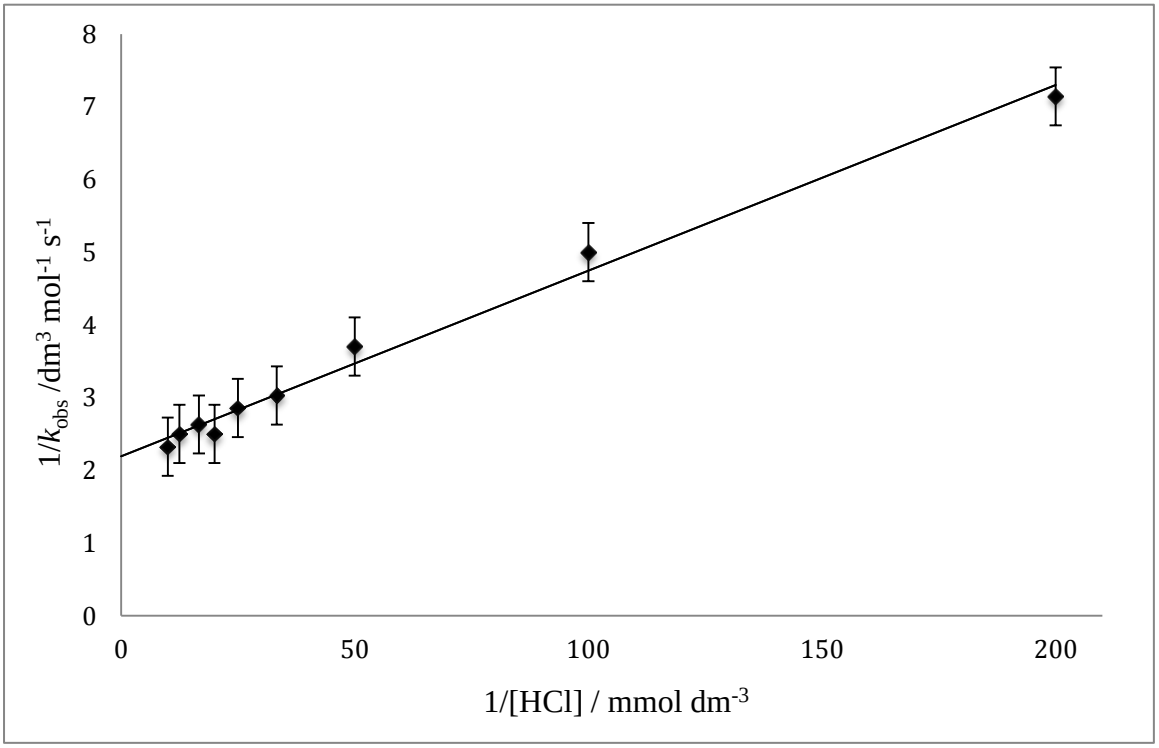


Figure 2.9. Plot of $1/k_{obs}$ versus 1/[HCl] $[Ni(S_2CEt)(triphos)]^+$ ([Ni] = 0.5 mmol $dm^{-3}$) with HCl in MeCN at 25.0 $^oC$. Data points corresponded to: HCl = 2.5 – 100 mmol $dm^{-3}$ and the error bar corresponding to 5%.

From the mechanism in Figure (2.7), we can derive the rate law associated with this reaction. The rate law is derived as follow:

$$\text{Rate} = k_2^{\text{R}}[\text{B}]_{\text{e}} \qquad \text{(e = equilibrium concentration)} \tag{2.6}$$

Since

$$K_1^{\text{R}} = \frac{[\text{B}]\text{e}}{[\text{A}]\text{e}\ [\text{HCl}]} \tag{2.7}$$

$$\text{Rate} = K_1^{\text{R}} k_2^{\text{R}}[\text{A}]_{\text{e}}[\text{HCl}] \tag{2.8}$$

Because there must be mass balance for A:

$[\text{A}]_{\text{Tot}} = [\text{A}]_{\text{e}} + [\text{B}]_{\text{e}}$ (Tot = total concentration)

$[\text{A}]_{\text{Tot}} = [\text{A}]_{\text{e}} + K_1^{\text{R}}[\text{A}]_{\text{e}}\ [\text{HCl}]$

$$[\text{A}]_{\text{Tot}} = \{1 + K_1^{\text{R}}[\text{HCl}]\}[\text{A}]_{\text{e}} \tag{2.9}$$

Substituting equation (2.9) into equation (2.8) we obtain equation (2.10).

$$\text{Rate} = \frac{K_1^{\text{R}} k_2^{\text{R}}\ [\text{HCl}][\text{A}]_{\text{Tot}}}{1\ +\ K_1^{\text{R}}\ [\text{HCl}]} \tag{2.10}$$

$$\text{Rate}\ = \frac{K_1^{\text{R}} k_2^{\text{R}}\ [\text{HCl}\ ][\text{Ni}(\text{S}_2\text{CR})(\text{triphos})^{+}]}{1\ +\ K_1^{\text{R}}\ [\text{HCl}]}$$

$$k_{\text{obs}} = \frac{K_1^{\text{R}} k_2^{\text{R}}\ [\text{HCl}]}{1\ +\ K_1^{\text{R}}\ [\text{HCl}]} \tag{2.11}$$

Rearrangement of equation (2.11) gives equation (2.12).

$$\frac{1}{k_{\text{obs}}} = \frac{1}{K_1^{\text{R}} k_2^{\text{R}}\ [\text{HCl}]} + \frac{1}{k_2^{\text{R}}} \tag{2.12}$$

Plotting $(1/k_{obs})$ versus $(1/[HCl])$ will give straight line with intercept corresponding to $(1/k_2^R)$ and the gradient corresponds to $(1/K_1^R k_2^R)$ [16] and the rate constants from the plots shows in Table (2.5).

| R | $K_1^R$ / $dm^3\ mol^{-1}$ | $k_2^R$ / $s^{-1}$ | $K_1^R k_2^R$ / $dm^3\ mol^{-1}\ s^{-1}$ |
|---|---|---|---|
| Me | 67 | 70 | 4690 |
| Et | 84 | 0.47 | 39.5 |
| $Bu^n$ | 71 | 0.28 | 19.9 |

Table 2.5. Summary of elementary rate and equilibrium constants for the reactions of $[Ni(S_2CR)(triphos)]BPh_4$ (R = Me, Et, $Bu^n$) with HCl in MeCN at 25.0 $^oC$.

### 2.4.1.2 Protonation Reaction with HCl in the presence of $Cl^-$.

In further kinetic studies, the effect of $Cl^-$ on the rates of the reactions was investigated. The effect of $Cl^-$ on the reactions of HCl with $[Ni(S_2CEt)(triphos)]^+$ or $[Ni(S_2CBu^n)(triphos)]^+$ is different than the effect $Cl^-$ has on the reaction between HCl and $[Ni(S_2CMe)(triphos)]^+$. For the reactions of $[Ni(S_2CEt)(triphos)]^+$ or $[Ni(S_2CBu^n)(triphos)]^+$, $Cl^-$ accelerates the rate of the reaction, whereas for the reaction with $[Ni(S_2CMe)(triphos)]^+$, $Cl^-$ inhibits the reaction.

As the solvent is MeCN, HCl will be a weak acid and the concentration of HCl will change after the addition of $Cl^-$ as shown in Equation (2.13) [17].

$$HCl + Cl^- \xrightarrow{K_H} HCl_2^- \qquad \text{(homoconjugation equilibrium)} \qquad (2.13)$$

The concentrations of HCl, $Cl^-$ and $HCl_2^-$ formed at equilibrium ($[HCl]_e$ and $[Cl^-]_e$) were calculated according to Equation (2.13) in the following way and the values are presented in the appendix 1.

$$HCl + Cl^- \xrightarrow{K_H} HCl_2^-$$

| | | | |
|---|---|---|---|
| Initial conc = | 0 | 0 | 0 |
| Equilibrium = | a-x | b-x | x |

$$K_H = \frac{x}{(a-x)(b-x)}$$

$$x^2 - (a+b)x + ab = (\frac{1}{K_H})x$$

$$x^2 - \left(a + b + \frac{1}{K_H}\right)x + ab = 0$$

To solve the general quadratic equation.

$$Ax^2 + Bx + C = 0 \qquad (2.14)$$

$$x = \frac{-B \pm \sqrt{B^2 - 4AC}}{2A}$$

Applying this to equation (2.14)

$$x = \frac{(a + b + \frac{1}{K_H}) \pm \sqrt{(a + b + \frac{1}{K_H})^2 - 4ab}}{2}$$

$[HCl]_e$ = a-x

$[Cl]_e$ = b-x

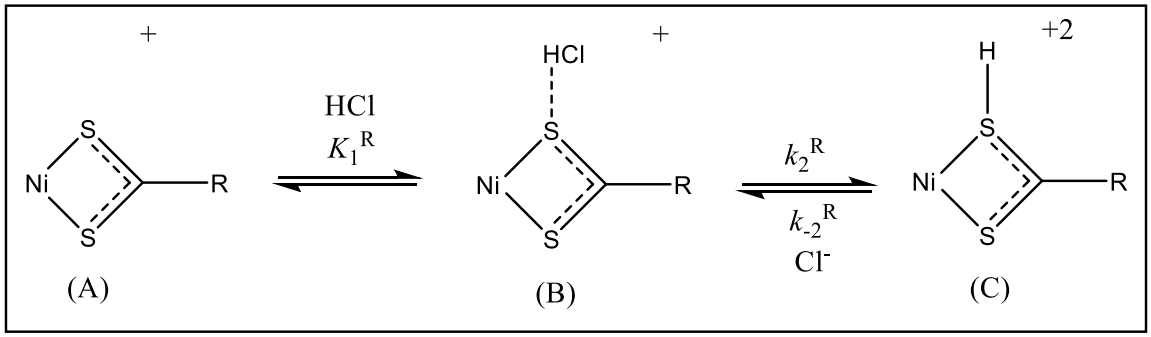


Figure 2.10. Mechanisms of protonation of $[Ni(S_2CR)(triphos)]^+$ (R = Et or $Bu^n$).

Figure (2.10) illustrated the reactions of HCl with $[Ni(S_2CEt)(triphos)]^+$ or $[Ni(S_2CBu^n)(triphos)]^+$ in the presence of $Cl^-$. This mechanism is the same as presented in Figure 9 but shows the reverse (deprotonation) step, $k_{-2}^R$, which is dependent on the concentration of $Cl^-$. The rate law associated with this mechanism is derived as follows. Since the reaction is an overall equilibrium process, it follows that:

$$\text{Rate} = k_2^R [B]_e - k_{-2}^R [Cl^-]_e [C]_e \quad (2.14)$$

Since

$$K_1^R = \frac{[B]_e}{[A]_e[HCl]_e} \quad (2.15)$$

$$[B]_e = K_1^R [A]_e[HCl]_e \quad (2.16)$$

Substituting Equation (2.16) into Equation (2.14) gives:

$$\text{Rate} = k_2^R K_1^R [A]_e[HCl]_e - k_{-2}^R [Cl^-]_e [C]_e \quad (2.17)$$

The concentration of $[A]_e$ and $[B]_e$ are unknown.

$[A]_{Tot} = [A]_e + [B]_e$

$[A]_{Tot} = [A]_e + K_1^R [A]_e[HCl]_e$

$$[A]_{Tot} = \{1 + K_1^R[HCl]_e\}[A]_e \quad (2.18)$$

$$[A]_e = [A]_{Tot} /(1 + K_1^R [HCl]_e) \quad (2.19)$$

Substituting Equation (2.19) into Equation (2.17) gives.

$$\text{Rate} = \frac{K_1^R k_2^R [HCl]_e [A]_T}{1 + K_1^R [HCl]_e} - k_{-2}^R [Cl^-]_e [C]_e \quad (2.20)$$

$$\text{Rate} = \{\frac{K_1^R k_2^R [HCl]_e}{1 + K_1^R [HCl]_e} + k_{-2}^R [Cl^-]_e\}[A]_T \quad (2.21)$$

For the reactions with $[Ni(S_2CEt)(triphos)]^+$ or $[Ni(S_2CBu^n)(triphos)]^+$, the plots of $\{k_{obs} - (a[HCl]_e/(1 + b[HCl]_e))\}$ versus $[Cl^-]_e$ are a straight line going through the origin as shown in Figure (1.11). Thus for these complexes the rate law is that shown in Equation (2.22), where. $k_{-2}^{Et}$ = 380 dm$^3$ mol$^{-1}$ s$^{-1}$ and $k_{-2}^{Bu^n}$ = 74 dm$^3$ mol$^{-1}$ s$^{-1}$.

$$\text{Rate} = \{\frac{K_1^R k_2^R [HCl]_e}{1 + K_1^R [HCl]_e} + k_{-2}^R [Cl^-]_e\}[A]_T \qquad (2.22)$$

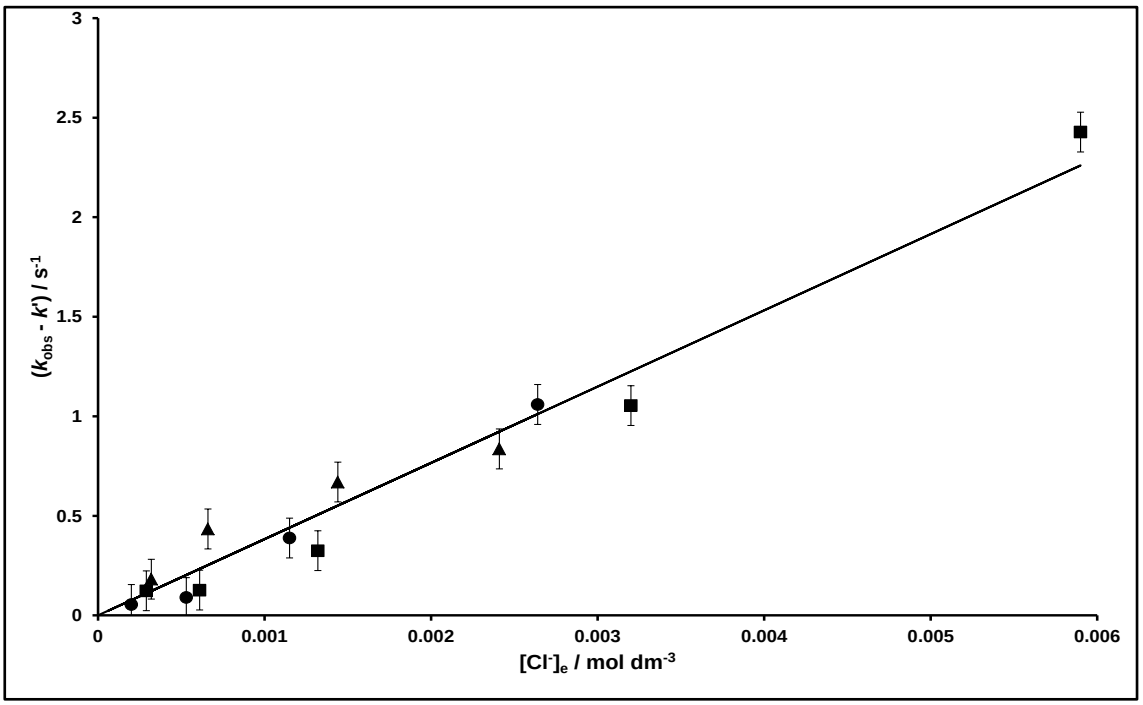


Figure 2.11. Kinetic data for the reaction of $Ni(S_2CEt)(triphos)]^+$ (0.5 mmol dm$^{-3}$) with HCl in the presence of $Cl^-$ in MeCN at 25.0 $^o$C. Graph of ($k_{obs} - k'$) versus $[Cl^-]_e$, where $k'$ = $a[HCl]_e/(1 + b[HCl]_e$. Data points correspond to: [HCl] = 25.0 mmol dm$^{-3}$, [$Cl^-$] = 1.0 – 10.0 mmol dm$^{-3}$ (●); [HCl] = 50.0 mmol dm$^{-3}$, [$Cl^-$] = 2.5 – 30.0 mmol dm$^{-3}$ (■); [HCl] = 100.0 mmol dm$^{-3}$, [$Cl^-$] = 2.5 – 30.0 mmol dm$^{-3}$ (▲). The error bar corresponding to 5%.

The reaction of $[Ni(S_2CMe)(triphos)]^+$ with HCl in the presence of $Cl^-$ is complicated and the data shows that the addition of $Cl^-$ will decrease the $k_{obs}$ and at high concentration of $Cl^-$ the reaction rate is not zero, but levels off at ~ 18 s$^{-1}$. The reactions will follow the mechanism shows in Figure (2.12).

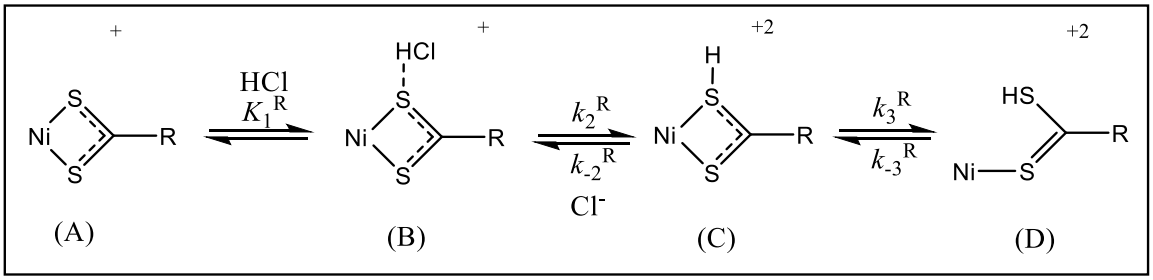


Figure 2.12. The mechanism of the reaction of $[Ni(S_2CMe)(triphos)]^+$ with HCl in the presence of $Cl^-$.

The derivation of the rate law associated with the mechanism in Figure (2.14) is as follow.

Rate = $k_3^R[C]_e - k_{-3}^R [D]_e$ (2.23)

$[C]_e$ is steady state.

$k_2^R [B]_e = k_3^R [C]_e + k_{-2}^R [C]_e [Cl^-]_e$

$[C]_e = k_2^R [B]_e / k_3^R + k_{-2}^R[Cl^-]_e$ (2.24)

B formed from in equilibrium reaction from A.

$K_1^R = [B]_e /[A]_e[HCl]_e$

$[B]_e = K_1^R[A]_e[HCl]_e$ (2.25)

Addition equation 2.25 to 2.24 gives equation 2.26.

$[C]_e= k_2^R K_1[A]_e[HCl]_e/(k_3^R + k_{-2}^R [Cl^-]_e)$

$$[C]_e = \frac{K_1^R k_2^R [A]_e [HCl]_e}{(k_3^R + k_{-2}^R [Cl^-]_e)} \quad (2.26)$$

$[A]_T = [A]_e + [B]_e$

$[A]_T = [A]_e + K_1^R [A]_e[HCl_e]$

$[A]_T = [A]_e\,(1 + K_1^R\,[HCl]_e)$

$$[A]_e = [A]_T / (1 + K_1^R\,[HCl]_e) \qquad (2.27)$$

Addition of Equation (2.27) to 2.26 gives 2.28.

$$[C]_e = \frac{K_1^R k_2^R [HCl]_e [A]_T}{(1 + K_1^R\,[HCl]_e)(k_3^R + k_{-2}^R [Cl^-]_e)} \qquad (2.28)$$

Addition of equation 2.28 to 2.23 gives 2.29

$$\text{Rate} = \frac{K_1^R k_2^R k_3^R\,[HCl]_e [A]_T}{(1 + K_1^R\,[HCl]_e)(k_3^R + k_{-2}^R [Cl^-]_e)} - k_{-3}^R\,[D]_e \qquad (2.29)$$

Rearrangement equation 2.29 gives:

$$\text{Rate} = \left\{ \frac{K_1^R k_2^R [HCl]_e}{(1 + K_1^R [HCl]_e)\left(1 + \frac{k_{-2}^R}{k_3^R}[Cl^-]_e\right)} + k_{-3}^R \right\} [Ni(S_2CMe)(triphos)^+] \qquad (2.30)$$

To analyse the data, the value of $k_{obs}$ were corrected for both the effect of changes of the concentration of HCl, as described in Equation (2.22) and given by $k'$ = 4.69 x $10^3[HCl]_e/(1 + 67.0[HCl]_e)$ and the limiting rate constant at high concentrations of $Cl^-$ ($k_{obs}$ = 18 $s^{-1}$), thus plot of ($k_{obs}$ - 18) / $k$' against concentration of $[Cl^-]_e$ gives the curve as shown in Figure (2.13). The rate law for the reaction of $[Ni(S_2CMe)(triphos)]^+$ with HCl in the presence of $Cl^-$ is that shown in Equation (2.30).

Figure (2.14), shows the mechanism of the reaction of $[Ni(S_2CMe)(triphos)]^+$ with HCl in the presence of $Cl^-$. ; ($k_{-2}^R/k_3^R$) = 250.0 and $k_{-3}^R$ = 18.0 $s^{-1}$.

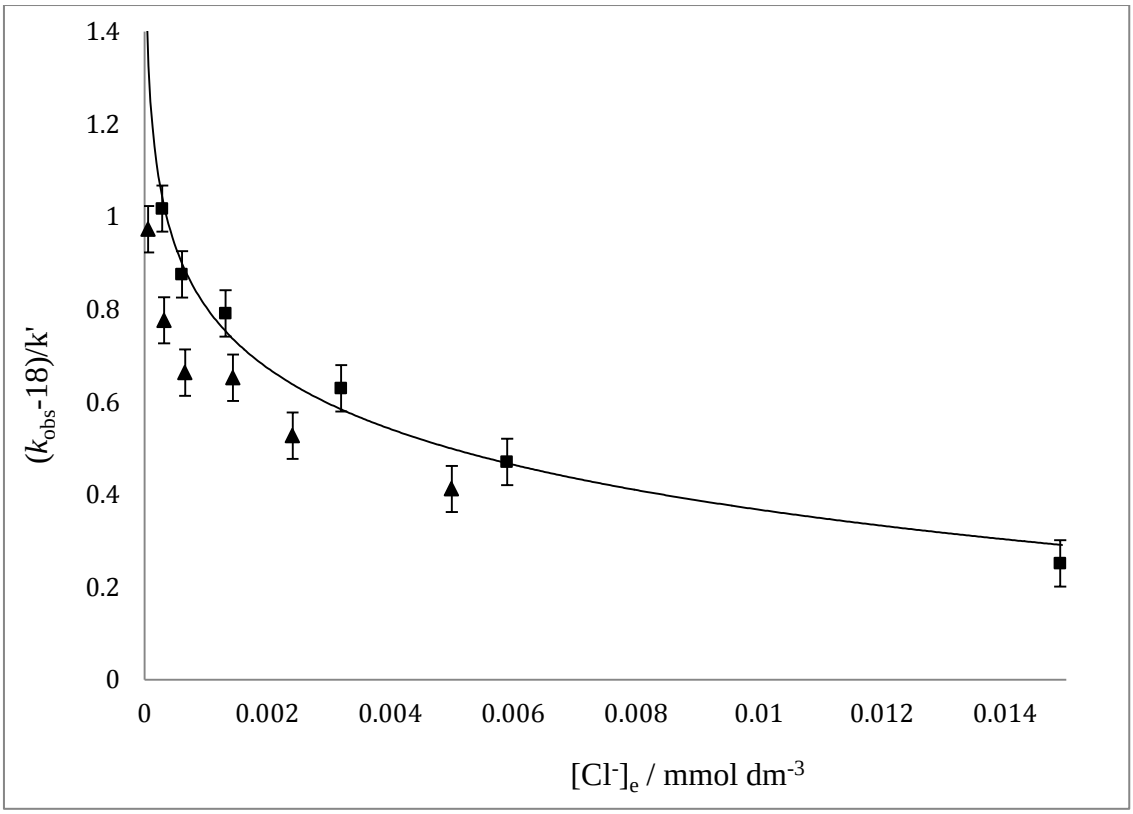


Figure 2.13. Kinetic data for the reaction of $[Ni(S_2CMe)(triphos)]^+$ ([Ni] = 0.5 mmol dm$^{-3}$) with mixture of HCl and $Cl^-$ in MeCN at 25.0 $^oC$. Data points correspond to: [HCl] = 50.0 mmol dm$^{-3}$, [$Cl^-$] = 2.5 – 50.0 mmol dm$^{-3}$ (■); [HCl] = 100.0 mmol dm$^{-3}$, [$Cl^-$] = 2.5 – 50.0 mmol dm$^{-3}$ (▲). The error bar corresponding to 5%.

$$\text{Rate} = \left\{ \frac{K_1^{\mathrm{R}} k_2^{\mathrm{R}} [\mathrm{HCl}]_{\mathrm{e}}}{(1 + K_1^R [\mathrm{HCl}]_{\mathrm{e}}) \left(1 + \frac{k_{-2}^{\mathrm{R}}}{k_3^{\mathrm{R}}} [\mathrm{Cl}^-]_{\mathrm{e}}\right)} + k_{-3}^{\mathrm{R}} \right\} [\mathrm{Ni}(\mathrm{S_2CMe})(\mathrm{triphos})^+] \qquad (2.31)$$

$$\text{Rate} = \{ \frac{\mathrm{a}[\mathrm{HCl}]_{\mathrm{e}}}{(1 + \mathrm{b})(1 + \mathrm{d}[\mathrm{Cl}^-]_{\mathrm{e}})} + \mathrm{e} \} [\mathrm{Ni}(\mathrm{S_2CMe})(\mathrm{triphos})^+] \qquad (2.32)$$

The rate law shown in Equation (2.31) is consistent with the mechanism involving two coupled equilibria, shown in Figure (2.12). However, the kinetics are also consistent with the mechanism shown in Figure (2.14). The mechanism in Figure (2.14), involves initial ring-opening of the dithioate ligand ($k_{\mathrm{a}}^{\mathrm{R}}$) which is then protonated in the subsequent step ($k_{\mathrm{b}}^{\mathrm{R}}$). Assuming that the ring-opened intermediate is a steady state species, the rate law

associated with mechanism in Figure (2.14) is that shown in Equation (2.30). Which is derived below.

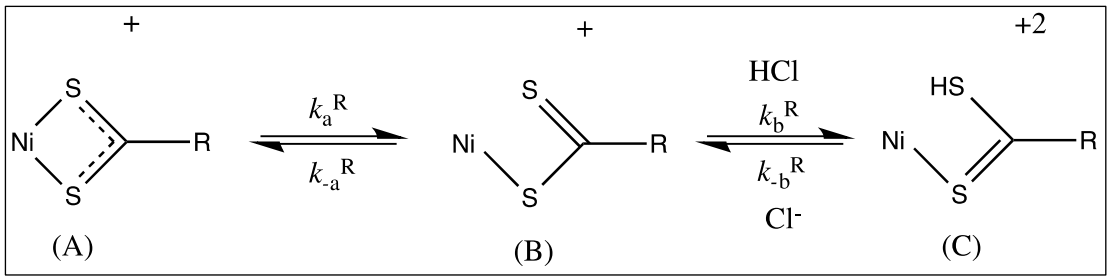


Figure 2.14. Shows the mechanism of the reaction of $[Ni(S_2CR)(triphos)]^+$ with HCl in the presence of $Cl^-$.

The rate law associated with the mechanism shown in Figure (2.14) is derived below.

$$\text{Rate} = k_b^R[B][HCl]_e - k_{-b}^R[C][Cl^-]_e \quad (2.33)$$

If [B] is steady state intermediate:

$$k_a^R[A] = k_{-a}^R[B] + k_b^R[B][HCl]_e$$

$$[B] = \frac{k_a^R[A]}{k_{-a}^R + k_b^R[HCl]_e}$$

$$\text{Rate} = \frac{k_b^R k_a^R[A][HCl]_e}{k_{-a}^R + k_b^R[HCl]_e} - k_{-b}^R[Cl^-]_e[C] \quad (2.34)$$

$$\text{Rate} = \left\{ \frac{k_b^R \frac{k_a^R}{k_{-a}^R}[HCl]_e}{1 + \frac{k_b^R}{k_{-a}^R}[HCl]_e} + k_{-b}^R[Cl^-]_e \right\} [Ni(S_2CR)(triphos)^+] \quad (2.35)$$

Although this rate law is of the same form as observed experimentally {Equation (2.22)}, this is not the favoured mechanism for the following reasons. (1) There is no evidence (eg from NMR spectroscopy) that any $[Ni(S_2CR)(triphos)]^+$ is undergoing rapid chelate ring-opening and closure in the absence of acid. (2) Using this mechanism it is difficult to rationalise the inhibiting effect of $Cl^-$ on the reaction between $[Ni(S_2CMe)(triphos)]^+$ and

HCl Equation (2.35). (3) Studies with DCl (*vide infra*) show that both steps in the mechanism equilibria are associated with isotope effects. Clearly, the mechanism in Figure (2.14), the chelate ring opening is not dependent on the acid and thus $k_a^R$ cannot show an isotope effect. Mechanism in Figure (2.12) is consistent with all the kinetic data for the R = Me, Et and $Bu^n$ complexes. In the mechanism in Figure (2.12) this mechanism there are three coupled equilibria. The first two equilibria are associated with protonation of the coordinated bidentate dithioate ligand, and the final equilibrium corresponds to the chelate ring-opening step. The protonation of the dithioate occurs in two steps: an initial formation of a hydrogen bonded precursor followed by intramolecular proton transfer from Cl to S. There is nothing unusual about this mechanism for proton transfer. It seems likely that, in general, any proton transfer reactions will involve the formation of a hydrogen bonded precursor, it is just that in this system (because proton transfer is slow) that the precursor accumulates. Similar kinetics have been observed in the protonation reactions of other ligands bound to the $\{Ni(triphos)\}^{2+}$ site [18].

In deriving the rate law associated with this mechanism it is assumed that formation of the hydrogen-bonding precursor is a rapidly established equilibrium. The rate law will then depend on whether proton transfer ($k_2^R$) or the chelate ring-opening ($k_3^R$) is rate-limiting. If proton transfer is rate limiting ($k_3^R$ is fast) the rate law associated with mechanism in Figure (2.14), is that shown in Equation (2.22). However, if chelate ring-opening is rate-limiting, then the rate law is that shown in Equation (2.30).

The values of the elementary rate and equilibrium constants for the reactions of $[Ni(S_2CR)(triphos)]^+$ with mixtures of HCl and $Cl^-$ are summarised in Table (2.6).

| R | $K_1^R$ /$dm^3$ $mol^{-1}$ | $k_2^R$ /$s^{-1}$ | $K_1^R k_2^R$ /$dm^3$ $mol^{-1}$ $s^{-1}$ | $k_{-2}^R$ /$dm^3$ $mol^{-1}$ $s^{-1}$ | $k_{-2}^R/k_3^R$ | $k_{-3}^R$ /$s^{-1}$ | $K_1^R K_2^R$ |
|---|---|---|---|---|---|---|---|
| Me | 67 | 70 | 4690 | | 250 | 18 | |
| Et | 84 | 0.47 | 39.5 | 380 | | | 0.10 |
| $Bu^n$ | 71 | 0.28 | 19.9 | 74 | | | 0.27 |
| Ph | | | 2.18 | 200 | | | 0.011 |

Table 2.6. Summary of elementary rate and equilibrium constants for the reactions of $[Ni(S_2CR)(triphos)]^+$ with mixtures of HCl and $Cl^-$ in MeCN at 25.0 $^oC$.

The protonation of $[Ni(S_2CMe)(triphos)]^+$ is appreciably faster than that of $[Ni(S_2CEt)(triphos)]^+$ or $[Ni(S_2CBu^n)(triphos)]^+$ ($k^{Me} : k^{Et} : k^{Bu}$ = 236 : 2 : 1). This is

presumably because of the strongly electron-releasing ability of the methyl substituent, because protonation so fast for $[Ni(S_2CMe)(triphos)]^+$, for this complex, the chelate ring-opening step becomes rate-limiting. In contrast, for $[Ni(S_2CEt)(triphos)]^+$ or $[Ni(S_2CBu^n)(triphos)]^+$ proton transfer is rate-limiting and chelate ring-opening is relatively fast.

It is pertinent to note that for the complexes $[Ni(S_2CR)(triphos)]^+$ (R = Et, $Bu^n$ or Ph *vide infra*) the observed rate laws are only consistent with the equilibrium protonation of these complexes and there is no evidence for the chelate ring opening step. This is because in these systems proton transfer is rate-limiting. It is only in the reaction of $[Ni(S_2CMe)(triphos)]^+$ with HCl that the kinetics indicate the chelate ring-opening step. Nonetheless, it seems likely that because the complexes are all so similar that the chelate ring-opening occurs after protonation in all of them.

### 2.4.2 Kinetics of the reaction between $[Ni(S_2CPh)(triphos)]^+$ and HCl in the Presence of $Cl^-$.

The kinetics of the reactions between all $[Ni(S_2CPh)(triphos)]^+$ and HCl in the presence of $Cl^-$ in MeCN were studied under pseudo-first order conditions ([HCl]/[Ni] ≥ 10) using stopped-flow spectrophotometry and the reaction exhibits a first order dependence on the concentration of complex. The absorbance-time traces are excellent fits to a single exponential consistent with the reaction exhibiting a first order dependence on the concentration of $[Ni(S_2CPh)(triphos)]^+$. The dependence of the rate of the reaction on the concentrations of HCl and $Cl^-$ were obtained from a plot of $k_{obs}/[Cl^-]_e$ versus $[HCl]_e/[Cl^-]_e$ which is a straight line with an intercept as shown in Figure (2.15). The rate law associated with this reaction is shown in Equation (2.36), and is that of an equilibrium protonation reaction.

$$\text{Rate} = \{2.18[HCl]_e + 200[Cl^-]_e\}[Ni(S_2CPh)(triphos)^+] \qquad (2.36)$$

This rate law is also consistent with the mechanism in Figure (2.12) assuming that $K_1^{Ph}$ is a rapidly established equilibrium and that proton transfer ($k_2^{Ph}$) is rate-limiting, gives the rate law shown in Equation (2.37), but when $K_1^{Ph}$ $[HCl]_e$ < 1 then Equation (2.37)

simplifies to Equation (2.38). The values of the elementary rate constants are shown in Table (2.7).

$$\text{Rate} = \frac{K_1^{\text{Ph}} k_2^{\text{Ph}} [\text{HCl}]_e}{1 + K_1^{\text{Ph}} [\text{HCl}]_e} + k_{-2}^{\text{R}} [\text{Cl}]_e^- [\text{Ni}(\text{S}_2\text{CPh})(\text{triphos})^+] \quad (2.37)$$

$$\text{Rate} = \{K_1^{\text{Ph}} k_2^{\text{Ph}} [\text{HCl}]_e + k_{-2}^{\text{Ph}} [\text{Cl}^-]_e\} [\text{Ni}(\text{S}_2\text{CPh})(\text{triphos})^+] \quad (2.38)$$

Comparison of the data in Table (2.6) and Table (2.7) shows that proton transfer to $[Ni(S_2CPh)(triphos)]^+$ is slower than to alkyl dithioate complexes and this is due to the much lower value of $K_1^{Ph}$. It seems likely that the strength of the hydrogen bonding of HCl to $[Ni(S_2CR)(triphos)]^+$ is controlled by the basicity of the dithioate ligand.

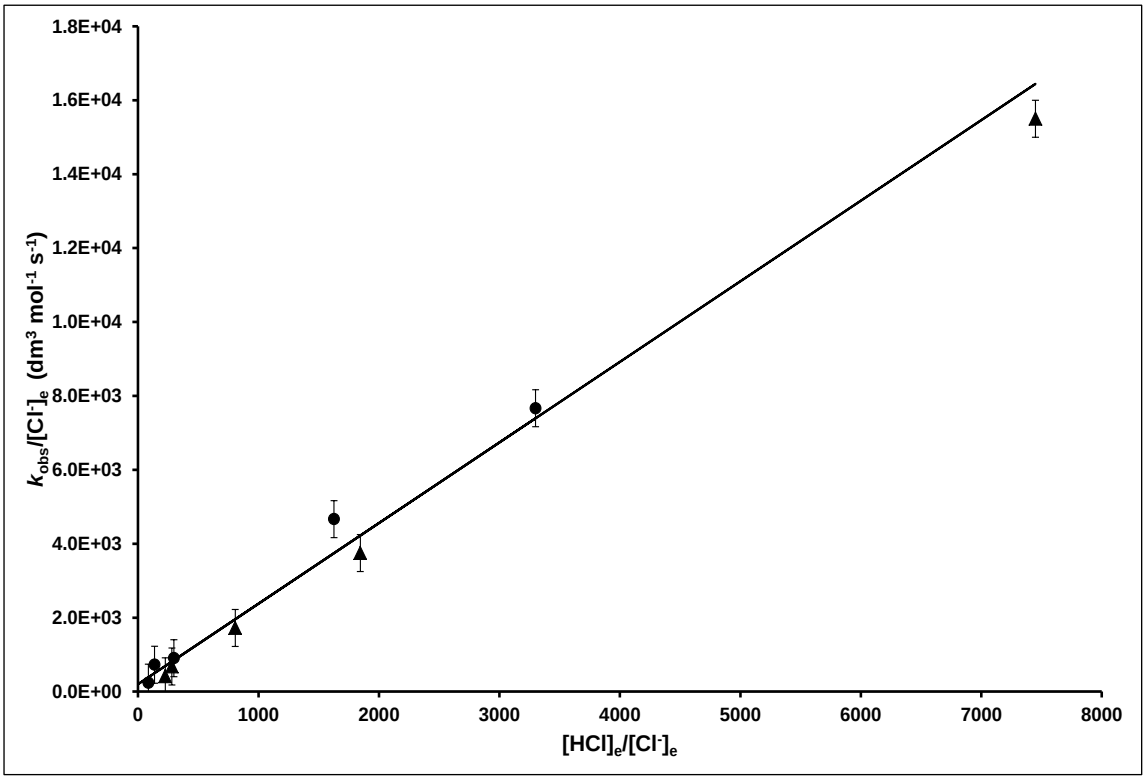


Figure 2.15. Kinetic data for the reaction of $[Ni(S_2CPh)(triphos)]^+$ (0.5 mmol dm$^{-3}$) with HCl in the presence of $Cl^-$ in MeCN at 25.0 $^oC$. Graph of $k_{obs}/[Cl^-]_e$ versus $[HCl]_e/[Cl^-]_e$ : [HCl]= 100.0 mmol dm$^{-3}$, [$Cl^-$] = 1.0 – 15.0 mmol dm$^{-3}$ (●); [HCl] = 150.0 mmol dm$^{-3}$, [$Cl^-$] = 1.0 – 15.0 mmol dm$^{-3}$ (▲). The error bar correspond to 5% error.

| R | $K_1^R k_2^R$ /dm$^3$ mol$^{-1}$ s$^{-1}$ | $k_{-2}^R$ /dm$^3$ mol$^{-1}$ s$^{-1}$ | $K_1^R K_2^R$ |
|---|---|---|---|
| $C_6H_5$ | 2.18 | 200 | 0.011 |
| $C_6H_4$Me-R | 1.17 | 223 | 0.0052 |
| $C_6H_4$Cl-R | 1.617 | 225 | 0.0051 |
| $C_6H_4$OMe-R | 0.684 | 248 | 0.0027 |

Table 2.7. Summary of elementary rate and equilibrium constants for the reactions of $[Ni(S_2CR)(triphos)]^+$ with mixtures of HCl and $Cl^-$ in MeCN at 25.0 $^oC$.

### 2.4.3 Isotope Effects for the reaction of $[Ni(S_2CR)(triphos)]^+$ with DCl (Where R = Me, Et or $Bu^n$).

Kinetic isotope effect refers to the change in the rate of a chemical reaction upon substitution of an atom in the reactant with one of its isotopes. Formally, it is defined as the ratio between the rate constants of the reactants involving the light atom ($k_L$) and the heavy atom ($k_H$) [19].

Since the effect of the isotope is related to vibrational frequencies of the affected bonds, the best change in the isotopic rate can be found when the relative mass change is greatest. For instance, changing a hydrogen atom to deuterium represents a 100% increase in mass, while replacing carbon-12 with carbon-13, the mass increases by only 8%. The rate of a reaction involving a C–H bond is typically 6–10 times faster than the corresponding C–D bond, while a $^{12}C$ reaction is only ~1.04 times faster than the corresponding $^{13}C$ reaction.

The rate of reactions can be affected in a variety ways as a consequence of isotope substitution. In many cases, by noting the change of the mass of an atom and then the effects on the vibration frequency of the chemical bond that it forms, the rate difference can be rationalized. Changing the isotope of an atom whose movement is involved in the transition state will affect the rate of the reaction; mathematically this can be expressed as shown in Equation (2.39), which shows the kinetic isotope effect, in terms of difference of energy between the two isotopic reactions ($E_H$ and $E_D$ the activation energy for the reaction with hydrogen and deuterium respectively) [19]:

$$\frac{k_{\mathrm{H}}}{k_{\mathrm{D}}} = \frac{\mathrm{e}^{-(\mathrm{E_H/RT})}}{\mathrm{e}^{-(\mathrm{E_D/RT})}} \qquad (2.39)$$

1- If $k^{\mathrm{H}} > k^{\mathrm{D}}$ ($k^{\mathrm{H}} / k^{\mathrm{D}} > 1$). This is known as a normal isotopic effect where the lighter mass species reacts faster than the heavier one.
2- If $k^{\mathrm{H}} = k^{\mathrm{D}}$. The change of isotope does not influences the reaction.
3- If $k^{\mathrm{H}} < k^{\mathrm{D}}$ ($k^{\mathrm{H}} / k^{\mathrm{D}} <$ I). This is known as an inverse isotopic effect where the heavier mass species reacts more rapidly than the lighter one.

As the reactions between HCl and $[Ni(S_2CR)(triphos)]^+$ involve slow proton transfer steps the effects of using DCl have been investigated. In particular, because the proton transfer to $[Ni(S_2CR)(triphos)]^+$ (R = Me, Et or $Bu^n$) involves initial formation of the hydrogen bonded species $K_1^R$ followed by intramolecular proton transfer ($k_2^R$) and that both these steps are distinguishable in the kinetics, it is of interest to see how the isotopic change in the acid affects $K_1^R$ and $k_2^R$ separately. In principle, the isotope effect for the reaction of $[Ni(S_2CPh)(triphos)]^+$ could be measured, however, there is a problem of analysing the data. The same problem is encountered in attempting to measure the isotope effect of the reaction between DCl and $[Ni(S_2CR)(triphos)]^+$ (R = Me, Et or $Bu^n$) in the presence of $Cl^-$. As indicated above, mixtures of HCl and $Cl^-$ are involved in the homoconjugation equilibrium reaction as shown in Equation 2.13, and the concentrations of $[HCl]_e$ and $[Cl^-]_e$ in such mixtures can be calculated using the homoconjugation equilibrium constant ($K_{\mathrm{H}}$). Unfortunately, the homoconjugation equilibrium constant for mixtures of DCl and $Cl^-$ is unknown and would be expected to be different to $K_{\mathrm{H}}$. Consequently, only the kinetics of the reactions of $[Ni(S_2CR)(triphos)]^+$ (R = Me, Et or $Bu^n$) with DCl alone have been measured, Figure (2.16) shows the effect of changing HCl for DCl on the rate of the reaction with $[Ni(S_2CEt)(triphos)]^+$.

The kinetics of the reactions between $[Ni(S_2CR)(triphos)]^+$ (R = Me, Et or $Bu^n$) and DCl in MeCN follow the same behaviour as the analogous reactions with HCl. Thus, from the absorbance-time trace the reactions exhibit a first order dependence on the concentration of complex and a non-linear dependence on the concentration of DCl. Analysis of the dependence of the reaction rate on the concentration of DCl (using plots of $1/k_{\mathrm{obs}}$ versus 1/[DCl]), yields the values of $(K_1^R)^{\mathrm{D}}$ and $(k_2^R)^{\mathrm{D}}$ shown in Table (2.8).

The first point to note about these data is that the overall isotope effects for transfer of the proton from HCl to $[Ni(S_2CR)(triphos)]^+$ $\{(K_1^R k_2^R)^{\mathrm{H}} / (K_1^R k_2^R)^{\mathrm{D}}\}$ are all small (0.94 – 0.25). Inspection of the individual isotope effects for $K_1^R$ and $k_2^R$ reveals that the small overall isotope effects for $(K_1^R k_2^R)^{\mathrm{H}} / (K_1^R k_2^R)^{\mathrm{D}}$ is a consequence of much larger, but

opposing, isotope effects for the individual components ($K_1^R$ and $k_2^R$). Thus, for all these complexes, the hydrogen bonding step is associated with an inverse equilibrium isotope effect {( $K_1^R$)$^H$ / ($K_1^R$)$^D$ = 0.44 – 0.85} and the intramolecular proton transfer step are associated with a normal primary isotope effect {($k_2^R$)$^H$ / ($k_2^R$)$^D$ = 1.3 – 2.0). These isotope effects are consistent with the mechanism. As discussed above, comparison of the kinetic parameters for [Ni($S_2$CR)(triphos)]$^+$ and [Ni($S_2$CPh)(triphos)]$^+$ indicate that the equilibrium constant for the formation of the hydrogen bonded species ($K_1^R$) is affected by the basicity of the dithioate ligand. It is to be anticipated that DCl will be a slightly stronger acid than HCl and this is reflected in the values of ($K_1^R$)$^H$ / ($K_1^R$)$^D$. The normal kinetic isotope effects for ($k_2^R$)$^H$ / ($k_2^R$)$^D$ are consistent with this step involving the intramolecular transfer of a proton [20].

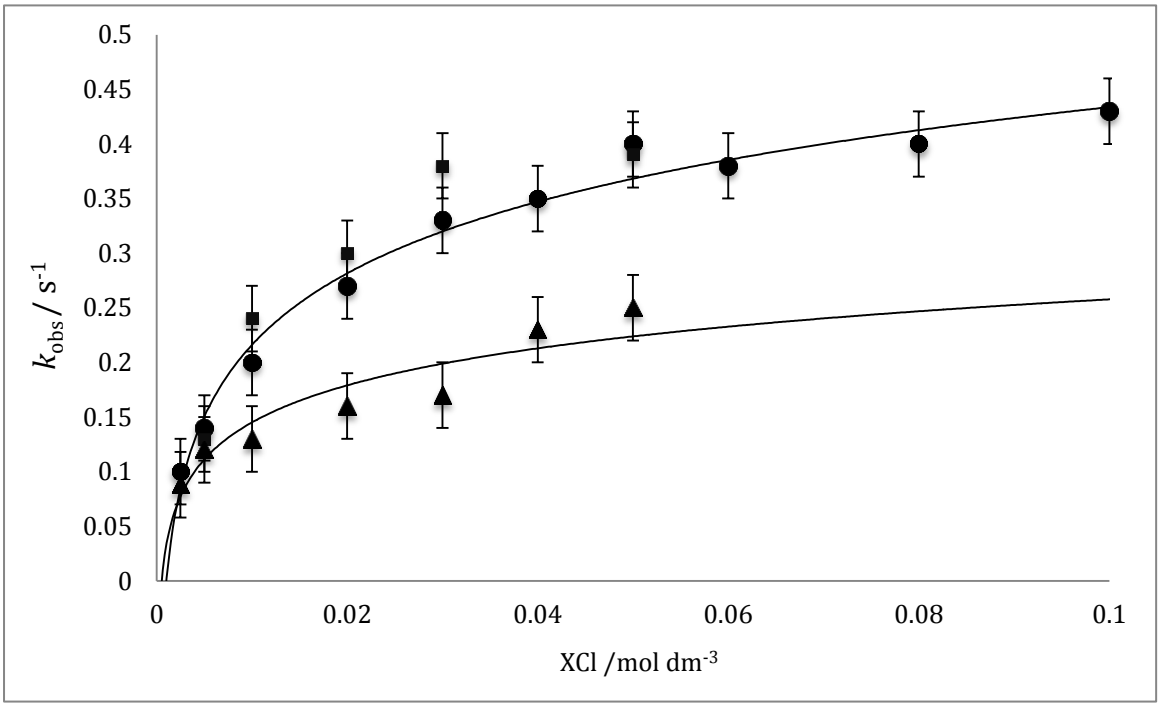


Figure 2.16. Kinetic data showing the normal isotope effect for the reaction of [Ni($S_2$CEt)(triphos)]$^+$ (0.5 mmol dm$^{-3}$) with XCl (X= H (● and ■); X= D(▲)) in MeCN at 25.0 $^o$C.

| R | $K_1^R$ /dm$^3$ mol$^{-1}$ | $K_1^R k_2^R$ /dm$^3$ mol$^{-1}$ s$^{-1}$ | $(K_1^R)^H$ /dm$^3$ mol$^{-1}$ | $(K_1^R k_2^R)^D$/ dm$^3$ mol$^{-1}$ s$^{-1}$ | $(K_1^R k_2^R)^H$/ $(K_1^R k_2^R)^D$ | $(k_2^R)^H$/ $(k_2^R)^D$ |
|---|---|---|---|---|---|---|
| Me | 67 | 4690 | 106 | 5000 | 0.938 | 0.63 |
| Et | 84 | 39.5 | 274 | 57 | 0.69 | 0.30 |
| Bu$^n$ | 71 | 19.9 | 370 | 80 | 0.248 | 0.88 |

Table 2.8. Summary of elementary rate and equilibrium constants for the reactions of [Ni($S_2$CR)(triphos)]$^+$ with mixtures of DCl in MeCN at 25.0 $^o$C.

### 2.4.4 Kinetics of the reaction between $[Ni(O_2CR)(triphos)]^+$ (R = Et or Ph) and $lutH^+$ in the presence of lut(lut = 2,6-dimethylpyridine).

We have also prepared the analogous $[Ni(O_2CR)(triphos)]^+$ (R = Et or Ph) and studied the protonation of these complexes. In reactions between anhydrous HCl and $[Ni(O_2CR)(triphos)]^+$ in the presene of $Cl^-$ in MeCN the reactions are complete within the dead-time (the time for the solutions to mix and then stop) of the stopped-flow apparatus (*ca* 2 ms). This was anticipated because usually the rates of proton transfer to oxygen sites are appreciably faster than proton transfer to the analogous sulfur sites [4.3]. However, the reactions of $[Ni(O_2CR)(triphos)]^+$ with mixtures of $lutH^+$ (the preparation of $lutH^+$ in section 3.2.1.4) and lut (lut = 2,6-dimethylpyridine) were sufficiently slow to be studied by stopped-flow spectrophotometry because $lutH^+$ is much weaker acid in MeCN than HCl ($pK_a$ (HCl) = 8.9, $pK_a$ ($lutH^+$) = 14.1) [21]. There is no detectable reaction of $lutH^+$ with any $[Ni(S_2CR)(triphos)]^+$. These observations show qualitatively that the rates of proton transfer to the analogous oxygen and sulfur sites are appreciably different.

When monitored on a stopped-flow apparatus the reactions of $[Ni(O_2CR)(triphos)]^+$ with mixtures of $lutH^+$ and lut exhibit absorbance-time curves which are excellent fits to a single exponential, consistent with the reaction exhibiting a first-order dependence on the concentration of complex. The dependences on the concentrations of $lutH^+$ and lut were established by plots of $k_{obs}$/[lut] versus $[lutH^+]$/[lut] as shown in Figure (2.18). The plots are straight lines with an intercept. Consequently, the rate law for the reaction is that shown in Equation (2.40). When R = Et, f = 2.64 x $10^4$ $dm^3$ $mol^{-1}$ $s^{-1}$ and g = 6 x $10^4$ $dm^3$ $mol^{-1}$ $s^{-1}$; when R = Ph, f = 1.93 x $10^4$ $dm^3$ $mol^{-1}$ $s^{-1}$ and g = 5 x $10^4$ $dm^3$ $mol^{-1}$ $s^{-1}$. It should be noted that the homoconjugation equilibrium constant involving $lutH^+$ and lut is very small and cannot be measured. Consequently, no correction to the concentrations of $lutH^+$ and lut need to be made.

$$\text{Rate} = \{f\,[lutH^+] + g[lut]\}[Ni(O_2CR)(triphos)^+] \qquad (2.40)$$

This rate law is consistent with the mechanism shown in Figure (2.18), which is analogous to that described for the reactions of $[Ni(S_2CR)(triphos)]^+$ with HCl in the presence of $Cl^-$ (shown in Figure (2.12)), when the intramolecular proton transfer step is rate-limiting. Assuming that formation of the hydrogen bonded intermediate ($K_4^R$) is a rapidly established equilibrium, but that $K_4^R[lutH^+] < 1$, the rate law associated with the

mechanism in Figure (2.18) is Equation (2.41). Comparison of Equations (2.49) and Equations (2.50), gives the values of the elementary rate and equilibrium constants for the reactions of $[Ni(O_2CR)(triphos)]^+$ with mixtures of $lutH^+$ and lut summarised in Table (2.9).

$$\text{Rate} = \{K_4^R k_5^R\ [lutH^+] + k_{-5}^R[lut]\}[Ni(O_2CPh)(triphos)^+] \qquad (2.41)$$

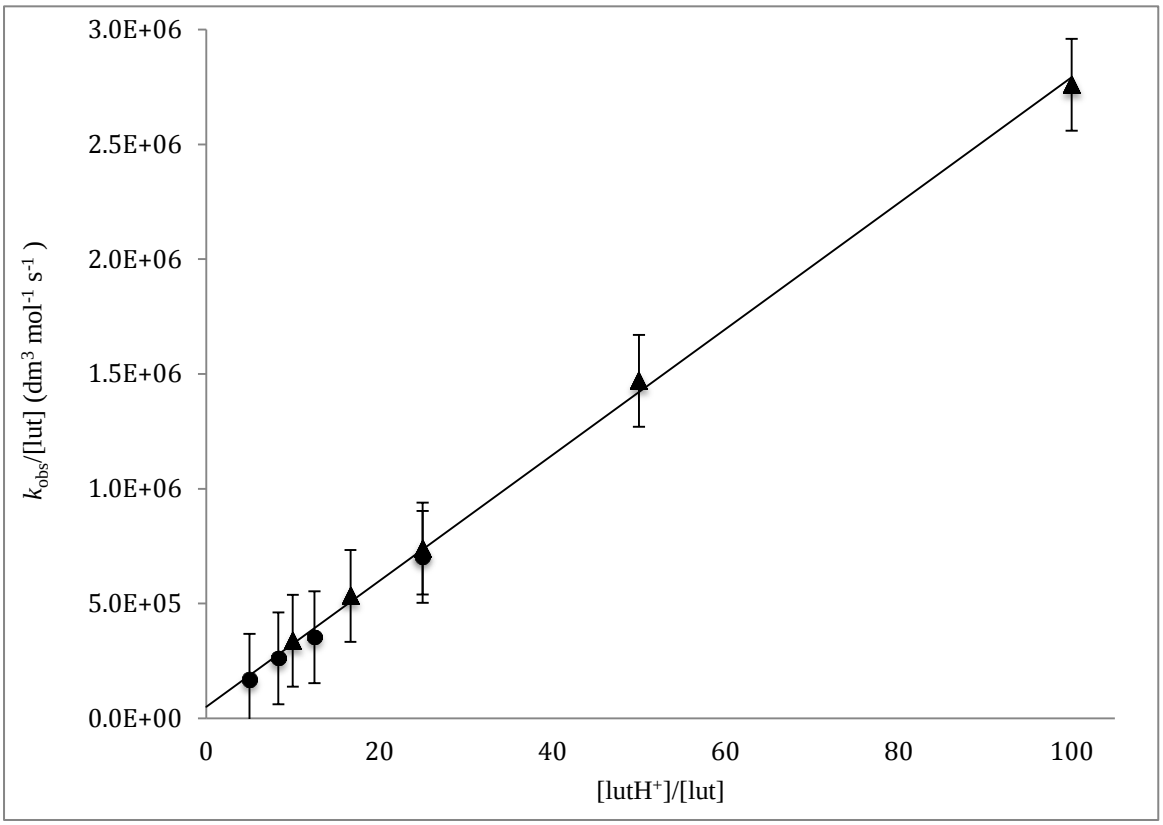


Figure 2.17. Kinetic data plot of $k_{obs}$/[lut] versus [lutH$^+$]/[lut] for the reaction of $Ni(O_2CEt)(triphos)]^+$ (0.25 mmol dm$^{-3}$) with $lutH^+$ in the presence of lut in MeCN at 25.0 $^oC$. plot of $k_{obs}$/[lut] versus [lutH$^+$]/[lut]. Data points correspond to: [lutH$^+$] = 2.5 mmol dm$^{-3}$, [lut] = 0.05 – 0.50 mmol dm$^{-3}$ (●); [lutH+] = 5.0 mmol dm$^{-3}$, [lut] = 0.05 – 0.5 mmol dm$^{-3}$ (▲). The error bar corresponded to 5% error.

| R | $K_4^R k_5^R$ /dm$^3$ mol$^{-1}$ s$^{-1}$ | $k_{-5}^R$ /dm$^3$ mol$^{-1}$ s$^{-1}$ | $K_4^R K_5^R$ |
|---|---|---|---|
| Et | 2.64 x 10$^4$ | 6.0 x 10$^4$ | 0.44 |
| Ph | 1.90 x 10$^4$ | 5.0 x 10$^4$ | 0.38 |

Table 2.9. Summary of elementary rate and equilibrium constants for the reactions of $[Ni(O_2CR)(triphos)]^+$ with mixtures of $lutH^+$ and lut in MeCN at 25.0 $^oC$.

For both the dithioate and carboxylate complexes the trend in the rate constants are the same: (i) for protonation, $(K_4^{Et}k_5^{Et})^{Y} \sim (K_4^{Ph}k_5^{Ph})^{Y}$ and for deprotonation, $(k_{-5}^{Et})^{Y} \sim (k_{-5}^{Ph})^{Y}$. However, for the protonation step it is evident that the rates of proton transfer to O $\{(K_4^{Et}k_5^{Et})^{O}/(K_4^{Ph}k_5^{Ph})^{O} = 1.4\}$ are slightly less sensitive to the R-substituent than the rates of proton transfer to S $\{(K_4^{Et}k_5^{Et})^{S}/((K_4^{Ph}k_5^{Ph}))^{S} = 18\}$.

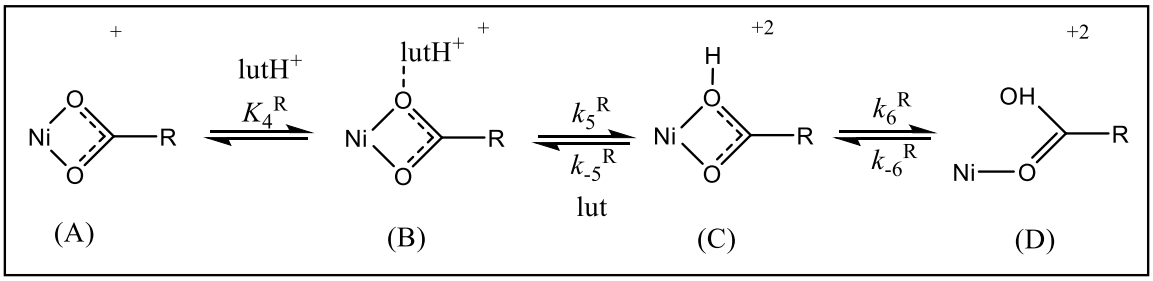


Figure (2.18). Mechanism of protonation and Ni-O cleavage for $[Ni(O_2CR)(triphos)]^{+}$.

## 2.4.5 Computational studies on the protonation site.

The X-ray crystallography shows that the structures of $[Ni(S_2CR)(triphos)]^+$ are trigonal bipyramidal and from the structure there are two sulfur sites for protonation the equatorial and axial sites. The kinetic studies indicate a single protonation but cannot distinguish between both sites being protonatable or protonation being restricted to single sulfur.

The protonation of each sulfur in $[Ni(S_2CR)(triphos)]^+$ (R = Me or Ph) has been explored using DFT (GAUSSIAN09 package, [11] geometries optimized at the B3LYP/Lanl2dz levels of theory), the calculations indicate that the protonation of the equatorial position ($S_2$) results in chelate ring-opening to form species A as shown in Figure (2.19).

The calculated bond angles for A are consistent with the Ni having a square-planar geometry as shown in Figure (2.21) and Table (2.10). This result is consistent with the kinetic result in Equation (2.39) and Equation (2.40), also the calculation predict that the protonation of axial sulfur ($S_1$) in $[Ni(S_2CR)(triphos)]^+$ can occur without ring-opening.

From the structural data in Table (2.10) for the products A and B and the dimension of the complex $[Ni(S_2CPh)(triphos)]^+$ from the X-ray crystallographic data, it is clear that protonation at $S_2$ followed by dissociation of the Ni-$S_2$H bond readily forms the square-planar product after relatively minor intramolecular movement of $P_1$ and $P_3$. In contrast, protonation of S1 followed by dissociation of Ni-$S_1$H could only produce a square-planar product after significant movement of the Ni-$S_2$ bond and the minor movement of $P_1$ and $P_3$.

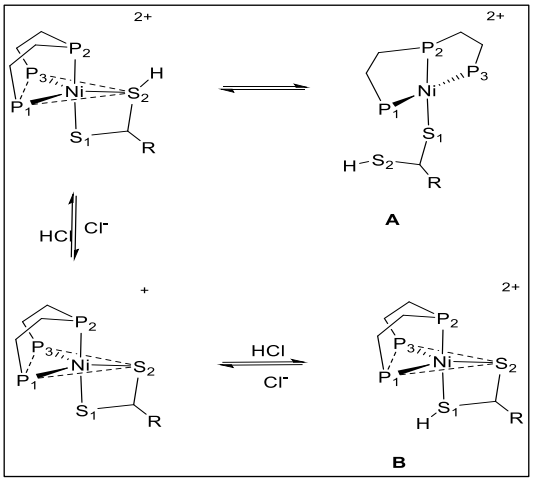


Figure 2.19. Consequences of protonation at axial ($S_1$) and equatorial ($S_2$) sulfur of $[Ni(S_2CR)(triphos)]^+$ (R = Me or Ph).

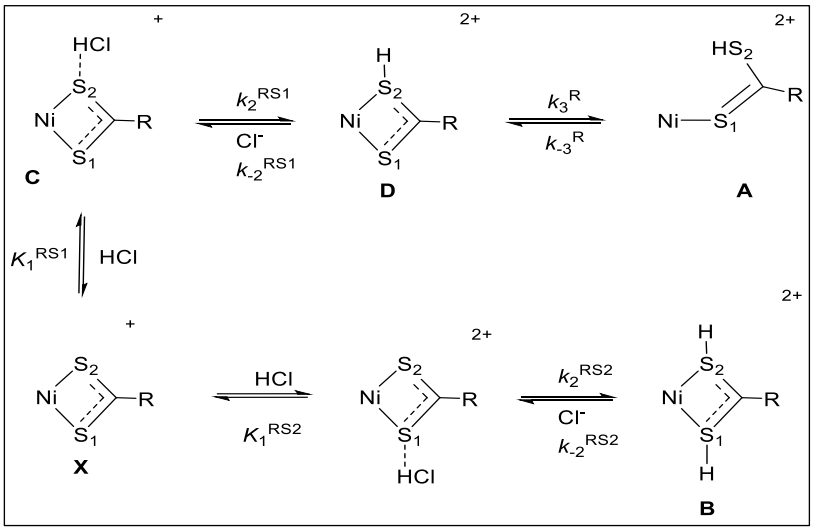


Figure 2.20. Mechanism for the reactions of $[Ni(S_2CR)(triphos)]^+$ with HCl in the presence of $Cl^-$, accomodating the results of the DFT calculations which indicate that protonation can occur at both sulfurs but with different structural consequences .

It seems likely that chelate ring-opening is energetically less demanding after $S_2$ is protonated than after protonation of $S_1$.

| | Complex A | Complex B |
|---|---|---|
| *bond lengths* | | |
| Ni-$P_1$ | 2.2665 | 2.2665 |
| Ni-$P_2$ | 2.2176 | 2.2630 |
| Ni-$P_3$ | 2.2630 | 2.2176 |
| Ni-$S_1$ | 2.2865 | 2.0423 |
| Ni-$S_2$ | 3.5122 | 2.4400 |
| *bond angles* | | |
| $P_1$-Ni-$P_2$ | 85.90 | 85.90 |
| $P_1$-Ni-$P_3$ | 152.31 | 152.31 |
| $P_1$-Ni-$S_1$ | 94.17 | 90.91 |
| $P_1$-Ni-$S_2$ | | 104.47 |
| $P_2$-Ni-$P_3$ | 85.25 | 85.25 |
| $P_2$-Ni-$S_1$ | 179.93 | 167.33 |
| $P_2$-Ni-$S_2$ | | 123.24 |
| $P_3$-Ni-$S_1$ | 94.69 | 92.04 |
| $P_3$-Ni-$S_2$ | | 102.33 |

Table 2.10. Selected bond lengths and bond angles of $Ni(S(SH)CPh)(triphos)]^{2+}$ from DFT calculations

The results of these theoretical calculations indicate that the mechanism presented in Figure (2.14) may need to be modified to accommodate protonation at either sulfur and

the different consequences for chelate ring opening. This modified mechanism is shown in Figure (2.20) and the rate law associated with this mechanism is shown in Equation (2.42).

$$R = \left\{ \frac{(K_1^{RS_1} k_2^{RS_1} + K_1^{RS_2} k_2^{RS_2})[HCl]_e}{1 + (K_1^{RS_1} + K_1^{RS_2})[HCl]_e} + (k_{-2}^{RS_1} + k_{-2}^{RS_2})[Cl^-]_e \right\} [Ni(S_2CR)(triphos)^+] \quad (2.42)$$

The calculations do not indicate the relative rates of protonation of $S_1$ and $S_2$. If the rate of protonation on both $S_1$ and $S_2$ are similar then the Equation (2.58) is the accurate description of the kinetics. However, if protonation at one sulfur is much faster than protonation at the other then the equations presented earlier in this chapter are more appropriate.

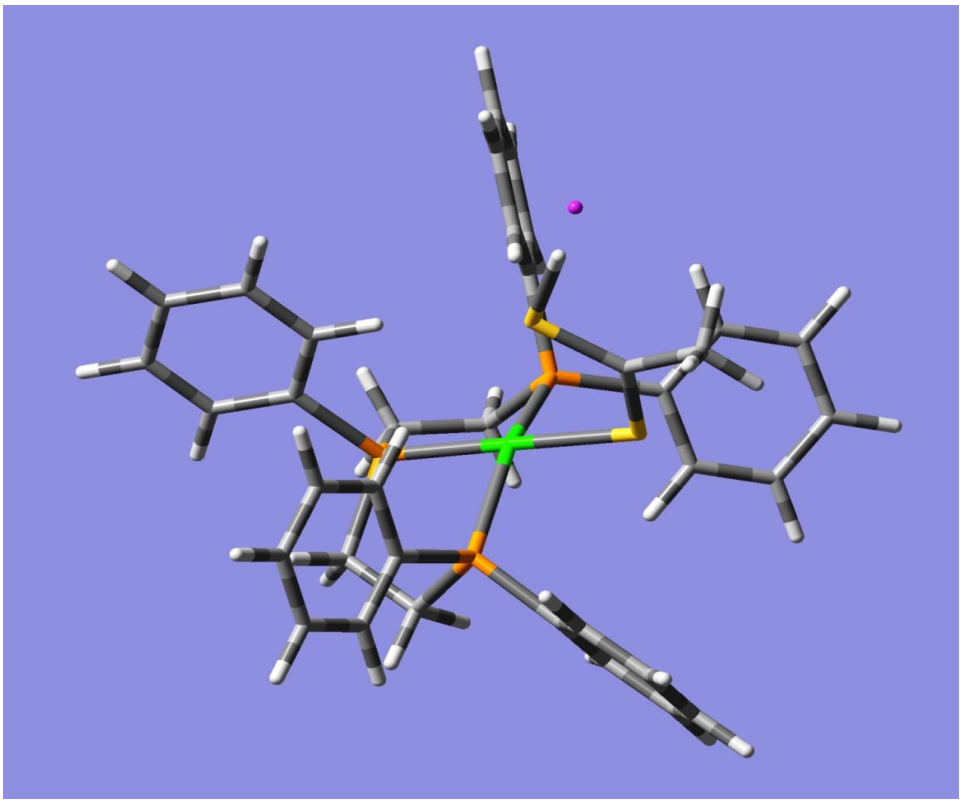

Figure 2.21. Picture of the optimised structure of $[Ni(HS2CMe)(triphos)]^{2+}$ (EMe) showing the protonated carboxydithioate ligand has undergone chelate ring opening. Key: Ni = green; P = orange; S = yellow; H = white, C = grey and Cl = magenta.

## 2.4.6 Comparison of the basicities of $[Ni(X_2CR)(triphos)]^+$ (X = O or S).

The elementary rate and equilibrium constants determined from analysis of the kinetics of the reactions of HCl with $[Ni(S_2CR)(triphos)]^+$ (R = Et, $Bu^n$ or Ph) and $lutH^+$ with $[Ni(O_2CR)(triphos)]^+$ (R = Et or Ph) allow us to calculate the p$K_a$s of the protonated coordinated carboxydithioate and carboxylate analogues when coordinated to the $\{Ni(triphos)\}^{2+}$ site. $K_1^R K_2^R$

The equilibrium constant for the protonation of $[Ni(S_2CR)(triphos)]^+$ is $K_1^R K_2^R = K_1^R k_2^R / k_{-2}^R$ These values are presented in Table (2.6). The p$K_a$ of HCl in MeCN is 8.9 [21]. Using this value and the values of $K_1^R K_2^R$ the p$K_a$s of $[Ni(S_2CR)(triphos)]^+$ in MeCN can be calculated (using equation 2.51, which is derived below), and are shown in Table (2.6). The most notable feature is that for $[Ni(S_2CR)(triphos)]^+$, the p$K_a^R$ is rather insensitive to the R-substituent (p$K_a^R$ = 7.2 – 8.3). Using the kinetic data for the reaction of $lutH^+$ with $[Ni(O_2CR)(triphos)]^+$ to calculate $(K_1^R K_2^R)^O$ and the literature value of the p$K_a$ = 14.1 for $lutH^+$ [21], the values $(pK_a^{Et})^O$ = 13.7 and $(pK_a^{Ph})^O$ = 13.7 can be calculated. The different kinetics for the reaction of HCl with $[Ni(S_2CMe)(triphos)]^+$ means that we cannot calculate the equilibrium constant $(K_1^R K_2^R)^S$ for the protonation reaction of this complex.

Comparison with the values of $(pK_a^R)^S$ for $[Ni(S_2CR)(triphos)]^+$ indicates that: (i) for both dithioate and carboxylate complexes the Et and Ph derivatives have effectively the same p$K_a$ and (ii) in analogous complexes the coordinated carboxylate is *ca* 3.2 x $10^6$ (R = Ph) and *ca* 0.6 x $10^6$ (R = Et) times more basic than coordinated dithioate. The small distinction between the R = Ph and R = Et values is a consequence of the marginally greater sensitivity of the p$K_a$s for the R-substituents for dithioates compared to carboxylates.

The p$K_a$ calculated using the rates of protonation and deprotonation of $[Ni(O_2CPh)(triphos)]^+$ with $lutH^+$ may not reflect the true basicity of the ligand, but rather the access that $lutH^+$ has to this basic site. On the other hand, HCl is clearly much less sterically demanding than $lutH^+$ and the p$K_a$ determined from the kinetics is more likely to accurately reflect the basicity of the coordinated dithioate.

$$[Ni(S_2CR)(triphos)]^+ + [lutH]^+ \underset{}{\overset{K_1}{\rightleftharpoons}} [Ni(HS_2CR)(triphos)]^+ + [lut]$$

$$lutH^+ \overset{K_a}{\rightleftharpoons} lut + H^+$$

$$K_1K_2 = \frac{\mathrm{Ni(HS_2CR)(triphos)]^{2+}[lut]}}{\mathrm{[Ni(S_2CR)(triphos)]^{+}\ \ [lutH^{+}]}} \tag{2.51}$$

$$K_1K_2 = \frac{\mathrm{Ni(HS_2CR)(triphos)]^{2+}[lut][H^{+}]}}{\mathrm{[Ni(S_2CR)(triphos)]^{+}\ \ [lutH^{+}][H^{+}]}} \tag{2.53}$$

$$K_1K_2 = \frac{\mathrm{Ni(HS_2CR)(triphos)]^{2+}}}{\mathrm{[Ni(S_2CR)(triphos)]^{+}\ [H^{+}]}} \frac{\mathrm{[lut][H^{+}]}}{\mathrm{[lutH^{+}]}} \tag{2.54}$$

$$K_{\mathrm{a}}^{\mathrm{lutH^{+}}} = \frac{\mathrm{[lut][H^{+}]}}{\mathrm{[lutH^{+}]}} \tag{2.55}$$

$$K_1K_2 = \frac{\mathrm{Ni(HS_2CR)(triphos)]^{2+}}}{\mathrm{[Ni(S_2CR)(triphos)]^{+}\ [H^{+}]}} K_{\mathrm{a}}^{\mathrm{lutH^{+}}} \tag{2.56}$$

$$K_1K_2 = \frac{K_{\mathrm{a}}^{\mathrm{lutH^{+}}}}{K_{\mathrm{a}}^{\mathrm{[Ni(HS_2CR)(triphos)]^{2+}}}} \tag{2.57}$$

## 2.5 Conclusions.

The studies reported herein show that the rates of protonation of coordinated carboxydithioates are significantly slower than the diffusion-controlled limit ($k_{diff} \sim 3.7 \times 10^{10}$ $dm^3$ $mol^{-1}$ $s^{-1}$ in MeCN) [22]. The rates of proton transfer are ca. $10^7$ - $10^{10}$ slower than the diffusion-controlled limit and the reason for this slowness is because the reactions are thermodynamically unfavourable and the steric factors contribute to the slowness of the reactions [23], as suggested for the protonation reactions of $[Ni(XPh)(triphos)]^+$ (X = O, S or Se).

The kinetics for the protonation of $[Ni(S_2CR)(triphos)]^+$ (R = alkyl) with HCl indicate a two-step equilibrium mechanism. The initial step involves the rapid formation of a hydrogen-bonded precursor ($K^R$) and this is followed by intramolecular proton transfer ($k_2^R$) to form the coordinated carboxydithioic acid. For the R = Me derivative the kinetics also indicate that the coordinated carboxydithioic acid undergoes chelate ring-opening. It seems likely that for all $[Ni(S_2CR)(triphos)]^+$ (R = alkyl or aryl) the same mechanism operates. The measured kinetic isotope effects for the complete transfer of a proton from HCl to $[Ni(S_2CR)(triphos)]^+$ (R = Me, Et or $Bu^n$) are small $\{(K_1^R K_2^R)^H / (K_1^R K_2^R)^D = 0.79 – 1.14\}$. This is the result of a small inverse equilibrium isotope effect for the formation of the precursor hydrogen-bonded adduct $\{(K_1^R)^H / (K_1^R)^D = 0.44–0.85\}$ and a significant kinetic primary isotope effect for the intramolecular proton transfer step $\{(k_2^R)^H / (k_2^R)^D = 1.33 – 1.81\}$. Finally, DFT calculations indicate that protonation can occur at either the equatorial or the axial sulfur sites, but that chelate ring-opening of the carboxydithionic acid occurs only after protonation of the equatorial sulfur.

## 2.6 References.


1. R. A. Henderson, *Angew. Chem., Int. Ed. Engl.*, **1996**, 35, 946.
2. M. Eigen, *Angew. Chem., Int. Ed. Engl.* **1964**, 3, 1.
3. (a) C. F. Bernasconi and R. L. Montañez, *J. Org. Chem.* **1997**, *62*, 8162. (b) C. F. Bernasconi, D. Wiersema and M. W. Stronach, *J. Org. Chem.* **1993**, *58*, 217.
4. R. H. Holm and E. I. Solomon, *Chem. Rev*., **1996**, 96, 2239
5. V. Autissier, P. M. Zarza, A. Petrou, R. A. Henderson, R. W. Harrington and W. Clegg, *Inorg. Chem*., **2004**, 43, 3106.
6. C. Cauquis, A. Deronzier, D. Serve and E. Vieil, *J. Electroanal. Chem. Interfacial Electrochem.*, **1975**, 60, 205.
7. A. Alwaaly and R. A. Henderson, *Chem. Commun*., **2014**, 50, 9669.
8. C. Bonnans-Plaisance and J. C. Gressiw, *J. Chem. Educ.*, **1986**, 65, 93.
9. K. L. C. Grönberg, R. A. Henderson and K. E. Oglieve, *J Chem Soc, Dalton Trans* **1998**, 3093.
10. W. Clegg and R. A. Henderson, *Inorg. Chem*. **2002**, 41, 1128.
11. M. J. Frisch, et al., Gaussian 09, revision D.01, Gaussian, Inc., Wallingford, CT, 2004.
12. Cossi, M; Scalmani, G.; Rega, N.; Barone, V.; *J. chem. Phys*. **2002**, 117, 43.
13. V. Autissier "*Studies on the Protonation Mechanisums of Nickel Complexes*" PhD Thesis. Newcastle University, **2005**.
14. W. Addison, T. Nageswara, J. Rao, J. Reedijk and G. C. Verschoor, *J. Chem. Soc., Dalton Trans*., **1984**, 1349.
15. A. L. Petrou, A. D. Koutselos, H. S. Wahab, W. Clegg, R. W. Harrington and R. A. Henderson, *Inorg Chem*, **2011**, 50, 847.
16. J. H. Espenson, "*Chemical Kinetics and Reaction Mechanism"*; McGraw-Hill Book Company: **1981**.
17. P. W. Atkins, *Physical Chemistry,, Vol. 5th ed*,, Oxford University Press. , p 222, 1994.
18. V. Autissier, P. M. Zarza, A. Petrou, R. A. Henderson, R. Harrington and W. Clegg, *Inorg. Chem.* **2004**, 43, 3098.
19. L. Melander "*Isotope Effect on Reaction Rates*" Vol. 98, Ronald Press, New York, **1960**.
20. G. Parkin and J. E. Bercaw, *Organometallics*, **1989**, 8, 1172.

21. K. Izutsu "*Acid–Base Dissociation Constants in Dipolar Aprotic Solvents*, Blackwell Scientific" Oxford, UK, 1990.
21. B. Garrett, R. A. Henderson, *Dalton Trans* **2005**, 2395.
22. A. Alwaaly and R. A. Henderson, *Chem. Commun*., **2014**, 50, 9669.
23. F. Wilkinson, A. F. Olea, D. J. McGarvey and D. R. Worrall, *J. Braz. Chem. Soc.*, **1995**, 6, 211–220.

# Chapter Three: Kinetic and sterics studies of the rates of proton transfer to $[Ni(XR)\{PhP(CH_2CH_2PPh_2)_2\}]BPh_4$ ($X = Se$, $R = C_6H_6$; $X = S$, $R = Et$, $Bu^t$ or $Cy$; $X = O$, $R = C_6H_5OCH_3$-4, $C_6H_5CH_3$-4, $C_6H_6$ or $C_6H_5Cl$-4)

## 3.1 Introduction.

The study of proton transfer reactions involving metal complexes continues to be fundamental in understanding such reactions when they are part of a complex multistage process such as in the formation of dihydrogen by hydrogenases and nitrogenases. Of particular relevance to these types of metalloenzymes is protonation at coordinated sulfur site. There have been relatively few reports on the rates of proton transfer to sulfur sites but a general feature which has emerged from studies on organic compounds is that rates of proton transfer involving sulfur sites are appreciably slower than the diffusion-controlled limit, even for thermodynamically-favourable reactions [1]. This is because proton transfer is diffusion-controlled only if both the proton donor and acceptor sites are classical hydrogen bond formers and, the electronic and spatial configurations of the acids and their conjugate bases are identical [2].

In this is described the kinetics and mechanisms of protonation of $[Ni(OC_6H_5R\text{-}4)(triphos)]^+$ $[Ni(XR')(triphos)]^+$ {triphos = $PhP(CH_2CH_2PPh_2)_2$} (R = H, $CH_3$, Cl or $OCH_3$; X = Se, R′ = $C_6H_6$; X = S, R′ = Et, $Bu^t$ or Cy). These investigations complement earlier [3] work on the analogous arylthiolate derivatives, $[Ni(SC_6H_4R\text{-}4)(triphos)]^+$ (R = MeO, Me, H, Cl, $NO_2$).

The kinetics of proton transfer reactions is normally very simple. The general form of a proton transfer mechanism is shown in Equation (3.1) [4]. The diffusion together of the reactants and the diffusion apart of the products are fast and normally the hydrogen bonded species {(a) and (b)} do not attain detectable concentrations. Consequently, the associated rate law is that shown in Equation (3.2), where $k_f$ and $k_b$ are the second order rate constants for the reactions of A with $BH^+$ and of B with $AH^+$, respectively. Thus, normally, little mechanistic information can be obtained from the form of the rate law and most information results from interpretation of the rate constants for a series of analogous reactions where systematic changes to the reactants are introduced. An unusual feature of the studies reported in this chapter is that although we are studying the simple transfer of a proton to and from the complex, the rate laws for the proton transfer reactions with the alkyl thiolate derivatives differ from those with the aryl thiolate complexes. However, the differences vary depending on the nature of the phosphine co-ligand.

$$BH^+ + A \rightleftharpoons \underset{(a)}{BH^+....A} \rightleftharpoons \underset{(b)}{B....HA^+} \rightleftharpoons B + AH^+ \qquad (3.1)$$

$$\text{Rate} = \left(k_f[\text{BH}^+] + k_b[\text{B}]\right)[\text{A}] \quad (3.2)$$

## 3.2 Experimental and Methods.

### 3.2.1 General Experimental.

The manipulations, drying of solvents and NMR spectroscopy were performed as described in Experimental of Chapter 2.

#### 3.2.1.1 Preparation of Compounds.

The following chemicals were purchased from Sigma-Aldrich and used as received: $NiCl_2.6H_2O$, 2,6-dimethylpyridine = lut, ethanethiol = EtSH, *tert*-butanethiol = $Bu^t$, bis(diphenylphosphinoethyl)phenylphosphine) = triphos, cyclohexanethiol = Cyh, sodium tetraphenylborate = $NaBPh_4$, phenylselenol = PhSeH, phenol, 4-methylphenol, 4-chlorophenol, 1,2-bis(diphenylphosphino)ethane (dppe) 4-methoxyphenol. The deuterated solvents, ethanol-$d_1$ and $D_2O$ were purchased from Sigma-Aldrich and used as received and $CD_3CN$ was purchased from Goss Scientific and used as received.

#### 3.2.1.2 Synthesis of $[lutH]BPh_4$ [5].

To a stirring solution of lutidine (8.3 ml, 100 mmol) in THF (*ca* 100 ml) was added methanol (4.05 ml, 100 mmol) followed by $Me_3SiCl$ (12.7 ml, 100 mmol). A white solid was formed immediately and the solution was stirred for 30 minutes then filtered. The white solid obtained, [lutH]Cl, was washed with THF and dried *in vacuo* (equation 3.3 and 3.4).

$$CH_3OH + (CH_3)_3SiCl \xrightarrow{THF} (CH_3)_3SiOCH_3 + HCl \qquad (3.3)$$

$$lut + HCl \xrightarrow{THF} [lutH]Cl \qquad (3.4)$$

The following reaction is then carried out in air. In a typical preparation, [lutH]Cl (10.4 g, 0.096 mol) was dissolved in minimum volume of methanol (40 ml) and filtered through celite to remove a fine suspension. The required quantity of sodium tetraphenylborate ($NaBPh_4$) (33.07 g, 0.096 moles) was dissolved in the minimum volume of methanol (60

ml) and filtered through celite to remove any insoluble material, then added slowly to the solution of [lutH]Cl. The resulting mixture was left to stand overnight to complete the formation of a white crystalline precipitate which is a mixture of [lutH]$BPh_4$ and NaCl. The white solid was removed by filtration. In order to remove the contaminating NaCl side product the white solid was washed with approximately 300 ml of distilled water and finally with 100 ml of methanol before drying *in vacuo* (equation 3.5).

$$[lutH]Cl + NaBPh_4 \xrightarrow{CH_3OH} [lutH]BPh_4 + NaCl \qquad (3.5)$$

The identity and purity of the product was confirmed by the $^1$H NMR NMR spectrum:
$^1$H NMR (400 MHz, DMSO) δ 15.93 – 13.46 (broad, H, lut*H*), 8.38 – 6.73 (m, *Ph*), 2.68 – 2.47 (s, $CH_3$).

### 3.2.1.3 Synthesis of [lutD]$BPh_4$ [5].

The deuterated acid, $[lutD]^+$ was prepared by the same method used above for $[lutH]^+$ but using MeOD and $D_2O$. The isotopic purity of the product was determined by $^1$H NMR spectroscopy.
$^1$H NMR (400 MHz, DMSO) δ 16.5 – 14.0 (s, broad, , lut*D*), 6.84 - 8.18 (m, *Ph*) , 2.7 – 2.5 (s, $CH_3$).
By the comparison the $^1$H NMR spectrum of [lutH][$BPh_4$] and [lutD][$BPh_4$] (Figure 3.1) using the same concentration, the spectrum is identical except that the resonance at 16.5 – 14.0 is significantly weaker. Integration of this peak and comparison with the integration of the signal due to the Me group at δ 15.4 allowed us to calculate that the deuterium isotopic purity was more than 80%.

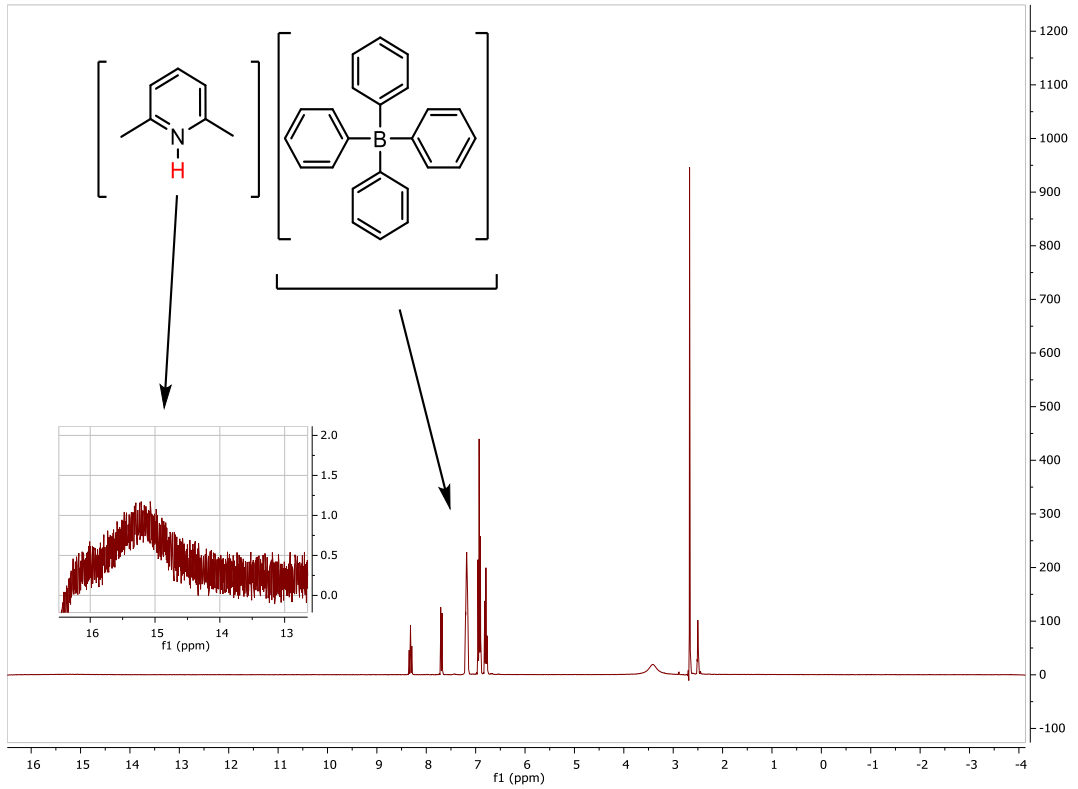


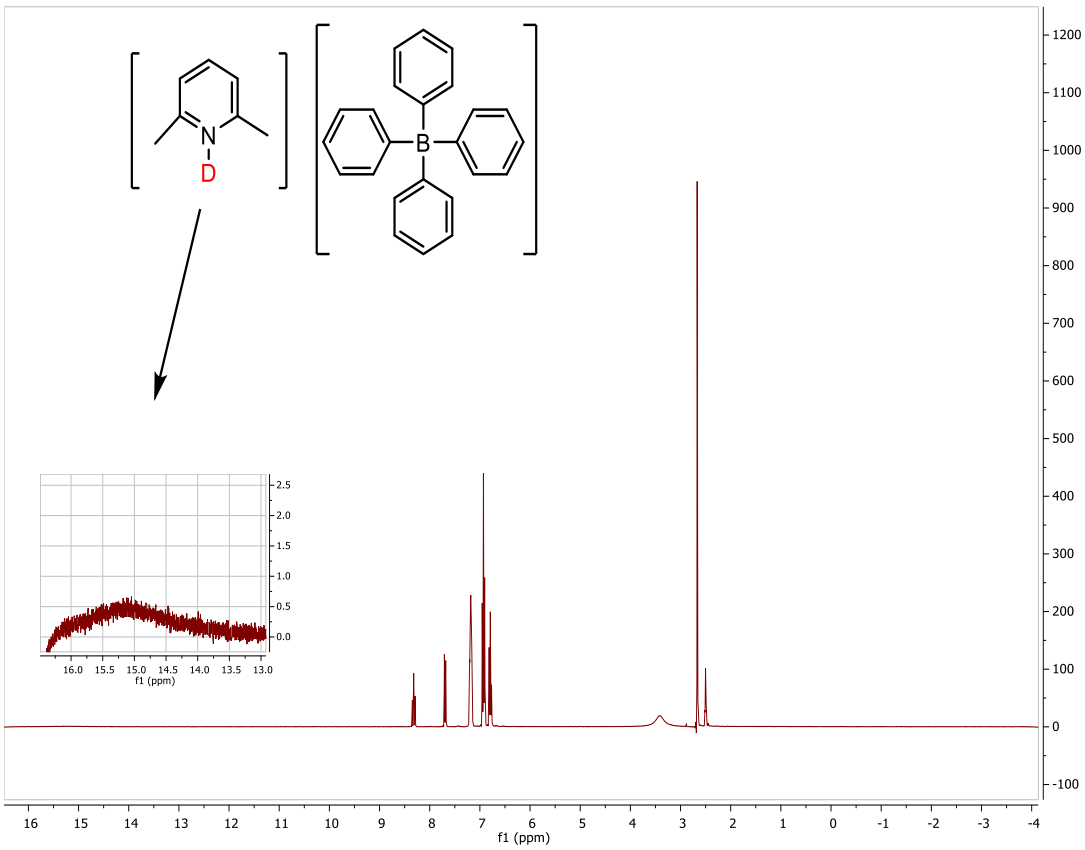


Figure 3.1: Comparison of the presence of the acidic proton in the $^{1}H$ NMR spectra of $[lutH]BPh_4$ (top) $[lutD]BPh_4$ (bottom) in $CD_3CN$.

### 3.2.1.4 Synthesis of $C_6H_5SeNa$, RSNa and $NaOC_6H_4R'$-4 (R = Et, $Bu^t$ or Cyh; R′ = $Cl^-$, H, $CH_3$, $OCH_3$).

All manipulations were performed under an atmosphere of dinitrogen and must be inside fume cupboard.

Sodium metal (2.3 g, 100 mmol) was cut into small pieces (2-4 mm diameter), then the oil on the sodium was removed by quickly washing in diethyl ether, and then the sodium was added to a Schlenk flask containing diethyl ether (100 ml) that had been degassed and was under an atmosphere of dinitrogen. To the stirred solution of sodium pellets, RXH (X = O, R = H, $CH_3$, $OCH_3$, $Cl^-$; X = S R = Et, $Bu^t$, Cyh or X = Se) (100 mmol) was added. The solution was left stirring, at room temperature, for several days until all of the sodium had reacted. The white solid was removed by filtration, washed with diethyl ether, and then the solid was dried *in vacuo.*

$$2RXH + 2Na \xrightarrow{\text{ether}} 2RXNa + H_2 \qquad (3.6)$$

### 3.2.1.5 Synthesis of Nickel Complexes.

#### 3.2.1.5.1 Synthesis of [NiCl(triphos)]$BPh_4$.

The complex was prepared as described in chapter two sections 2.2.1.3.

#### 3.2.1.5.2 Synthesis of [Ni(SEt)(triphos)]$BPh_4$ [6].

$$[NiCl(triphos)]BPh_4 + NaSEt \longrightarrow [NiSEt(triphos)]BPh_4 + NaCl \qquad (3.7)$$

To a suspension of [NiCl(triphos)][$BPh_4$] (0.7435 g, 0.5 mmol) in THF (*ca*. 20 mL) was added NaSEt (0.504 g, 6 mmol). The colour changed rapidly from bright yellow to dark red, and the mixture became homogeneous. After the solution was stirred for 0.5 h, it was concentrated *in vacuo* to ca. 10 ml. Addition of an excess of MeOH produced a dark red microcrystalline solid. The solid was removed by filtration, washed with MeOH, and then dried *in vacuo*. Recrystallization of the complex was accomplished by dissolving the solid in the minimum amount of THF and then adding a large excess of MeOH. Leaving the solution undisturbed at room temperature for 48 h produced well-formed red crystals. These crystals were removed by filtration, washed with MeOH, and dried *in vacuo*. Crystals grown in such a manner were suitable for X-ray crystallographic analysis.
The identify and purity of the product was confirmed by the $^1$H NMR spectrum of [Ni(SEt)(triphos)]$BPh_4$ and X-ray crystallography.
$^1$H NMR (400 MHz, $CD_3CN$) δ 8.24 – 6.75 (m, *Ph*, 45H), 3.5 – 2.3 (broad, $CH_2$, 8H), 2.16 (q, $J_{pp}$ = 7.3 Hz, S$CH_2$, 2H), 0.68 (t, $J_{pp}$ = 7.3 Hz, $CH_3$, 3H).
$^{31}$P{$^1$H} NMR (162 MHz, $CD_3CN$) δ 105.6 (t, $J_{pp}$ = 26.2 Hz), 54.3 (d, $J_{pp}$ = 25.9 Hz)

#### 3.2.1.5.3 Synthesis of [Ni($SC(CH_3)_3$)(triphos)]$BPh_4$.

This complex was prepared in a similar manner to that described above for [Ni(SEt)(triphos)]$BPh_4$. Crystals grown of the complex was accomplished by using mixture of THF and ether.
The identify and purity of the product was confirmed by the $^1$H NMR spectrum of [Ni($SC(CH_3)_3$)(triphos)]$BPh_4$ and X-ray crystallography.

$^{1}$H NMR (400 MHz, $CD_3CN$) δ 8.30 – 6.79 (m, *Ph*, 45H), 3.4 – 2.2 (broad, $CH_2$, 8H), 0.8 (s, ($CH_3$) 9H).

$^{31}P\{^{1}H\}$ NMR (162 MHz, $CD_3CN$) δ 104.7 (t, $J_{pp}$ = 26.3 Hz), 41.9 (d, $J_{pp}$ = 26.2 Hz).

### 3.2.1.5.4 Synthesis of [Ni(SCyh)(triphos)]$BPh_4$.

This complexes was prepared in a similar manner to that described above for [Ni(SEt)(triphos)]$BPh_4$.

The identify and purity of the product was confirmed by the $^{1}$H NMR spectrum of [Ni(SCyh)(triphos)]$BPh_4$ and X-ray crystallography.

$^{1}$H NMR (400 MHz, $CD_3CN$) δ 8.26 – 6.79 (m, -*Ph*), 3.29 – 2.49 (broad, $CH_2$, 8H), 3.8 – 3.5 (m, SC*H*, 1H), 1.9 – 1.7 (m, $CH_2$, 2H), 1.4 – 1.1 (m, $CH_2$, 5H), 1.05 – 0.6 (m, $CH_2$, 3H).

$^{31}P\{^{1}H\}$ NMR (162 MHz, $CD_3CN$) δ 105.6 (t, $J_{pp}$ = 21.1 Hz), 53.8 (d, $J_{pp}$ = 21.0 Hz).

### 3.2.1.5.5 Synthesis of [Ni($OC_6H_5$)(triphos)]$BPh_4$.

$$[NiCl(triphos)]BPh_4 + NaOC_6H_5 \longrightarrow [Ni(OC_6H_5)(triphos)]BPh_4 + NaCl \qquad (3.8)$$

$NaOC_6H_5$ (0.127 g, 1.1 mmol) was added to a suspension of [NiCl(triphos)]$BPh_4$ (0.947 g, 1.0 mmol) in THF (ca. 30 ml) at room temperature,. The mixture was stirred for 2 hrs, and the solution changed from yellow to red. All volatiles were removed *in vacuo*, to produce a red solid. The dry solid was extracted with the minimum amount of dry $CH_2Cl_2$ to form a red solution. The sodium salts were removed by filtration and washed with more $CH_2Cl_2$ to ensure complete extraction of the desired red product. Layering EtOH on the red solution produced (after several days of slow diffusion) red crystals. The crystals were removed by filtration and dried *in vacuo*.

$^{1}$H NMR (400 MHz, $CD_3CN$) δ 8.42 – 6.74 (m, *Ph*, 50H), 3.76 – 2.43 (broad, $CH_2$, 8H).

$^{31}P\{^{1}H\}$ NMR (162 MHz, $CD_3CN$) δ 111.57 (t, $J_{pp}$ = 51.46 Hz), 47.5 (d, $J_{pp}$ = 51 Hz)

### 3.2.1.5.6 Synthesis of [Ni($OC_6H_5$Me-4)(triphos)]$BPh_4$.

This complex was prepared in a similar manner to that described above for [Ni($OC_6H_5$)(triphos)]$BPh_4$.

The purity and the identification of the product were confirmed by the $^{1}H$ NMR spectrum and $^{31}P\{^{1}H\}$ NMR spectrum.

$^{1}H$ NMR (400 MHz, $CD_3CN$) δ 8.36 – 6.75 (m, *Ph*, 54H), 3.48 – 2.38 (broad, $CH_2$, 8H), 2.01 (s, $CH_3$, 3H).

$^{31}P\{^{1}H\}$ NMR (162 MHz, $CD_3CN$) δ 111.8 (t, $J_{pp}$ = 50.4 Hz), 47.33 (d, $J_{pp}$ = 49.9 Hz).

### 3.2.1.5.7 Synthesis of $[Ni(OC_6H_5Cl\text{-}4)(triphos)]BPh_4$.

This complex was prepared in a similar manner to that described above for $[Ni(OC_6H_5)(triphos)]BPh_4$.

The purity and the identification of the product were confirmed by the $^{1}H$ NMR spectrum and $^{31}P\{^{1}H\}$ NMR spectrum.

$^{1}H$ NMR (400 MHz, $CD_3CN$) δ 8.23- 6.47 (m, *Ph*, 54H), 3.16 – 2.34 (broad, $CH_2$, 8H).

$^{31}P\{^{1}H\}$ NMR (162 MHz, $CD_3CN$) δ 111.9 (t, $J_{pp}$ = 50.12 Hz), 47.06 (d, $J_{pp}$ = 50 Hz).

### 3.2.1.5.8 Synthesis of $[Ni(OC_6H_5OMe\text{-}4)(triphos)]BPh_4$.

This complex was prepared in a similar manner to that described above for $[Ni(OC_6H_5)(triphos)]BPh_4$.

The purity and the identification of the product were confirmed by the $^{1}H$ NMR spectrum and $^{31}P\{^{1}H\}$ NMR spectrum.

$^{1}H$ NMR (400 MHz, $CD_3CN$) δ 8.35 – 6.74 (m, *Ph*, 54H), 3.56 – 2.33 (broad, $CH_2$, 8H), 3.67 (s, $OCH_3$, 3H).

$^{31}P\{^{1}H\}$ NMR (162 MHz, $CD_3CN$) δ 111.53 (t, $J_{pp}$ = 50.43 Hz), 47.81 (t, $J_{pp}$ = 50.02 Hz).

### 3.2.1.5.9 Synthesis of $[Ni(SeC_6H_5)(triphos)]BPh_4$.

$$[NiCl(triphos)]BPh_4 + NaSePh \longrightarrow [Ni(SePh)(triphos)]BPh_4 + NaCl \quad (3.9)$$

This complex was prepared in a similar manner to that described above for [Ni(SEt)(triphos)]$BPh_4$.

The purity and the identification of the product were confirmed by the $^1$H NMR spectrum and and X-ray crystallography.

$^1$H NMR (400 MHz, $CD_3CN$) δ 8.24 – 6.75 (m, *Ph*, 50H), 3.08–2.07 (broad, $CH_2$,8H).

$^{31}P\{^1H\}$ NMR (162 MHz, $CD_3CN$) δ 112 -110.5(t, $J_{pp}$ = 49.98 Hz), 48.5 – 47(d, $J_{pp}$ = 49.9Hz).

$^{77}$Se NMR (400 MHz, $CD_3CN$) δ 459 (s, Se).

## 3.3 Result and Discussion.

### 3.3.1 Characterization of Complexes.

#### 3.3.1.1 NMR Spectroscopy

In the $^{1}H$ NMR spectra for all complexes, the peaks in the region $\delta$ = 8 - 6 ppm are assigned to the phenyl groups from tetraphenyl borate and triphos ligand. Exact assignment of the peaks is not possible due to the presence of so many overlapping peaks in this region. The $CH_2$ groups of the triphos ligand appear as broad peaks in the region of $\delta$ = 2 - 3.5 ppm. The peaks of the alkyl and the aryl substituents for SR and OR ligands appeared in the region $\delta$ = 3.6 - 0.5 ppm, and the $^{77}Se$ NMR for [Ni(SePh)(triphos)]$BPh_4$ shows a single peak at 459 ppm.

$^{31}P\{^{1}H\}$ NMR spectra for the complexes consist of two sets of peaks. The two terminal phosphorus atoms ($PPh_2$) of the triphos give a doublet in the region $\delta$ = 55.03 – 45.3 ppm which is attributed to the coupling of terminal phosphorus atoms ($PPh_2$) with the single phosphorus atom (PPh) in the middle of the triphos ligand. The central phosphorus atom couples with the two terminal phosphorus and appears as a triplet in the $\delta$ = 113.6–103.09 ppm region. The value of coupling constant ($J_{pp}$) is in the range 45-50 Hz for [Ni(SePh)(triphos)]$BPh_4$ and [Ni($OC_6H_4$R-4)(triphos)]$BPh_4$, while the coupling constant ($J_{pp}$) value for [Ni(SR)(triphos)]$BPh_4$ is between 20-30 Hz and is consistent with that previously reported for [Ni(SEt)(triphos)]$BPh_4$ (36 Hz)[6].

### 3.3.1.2 X-Ray Crystallography.

The X-ray crystal structures of [Ni(SR)(triphos)]$BPh_4$ {R = Et, $Bu^t$ or Cy) have been determined and the cations are shown in Figure (3.2) selected bond lengths and angles are presented in Table (3.1). Also included in Table (3.1) are the dimensions for the previously reported analogous R = Bz [3] and R = Ph [6] complexes, for comparison. Inspection of the data in Table (3.1) show that all the complexes are essentially isostructural with the nickel being four coordinate and the geometry is best described as distorted square-planar as shown in Figure (3.2). There are no systematic structural changes attributable to the different thiolate ligands. It is worth noting that the bond lengths and angles for $[Ni(SEt)(triphos)]^+$ and $[Ni(SCy)(triphos)]^+$ are very similar but there appear to be some minor differences in the $[Ni(SBu^t)(triphos)]^+$ structure. Thus, the Ni-S bond in $[Ni(SBu^t)(triphos)]^+$ is longer than that in $[Ni(SEt)(triphos)]^+$ (0.078 Å) and $[Ni(SCy)(triphos)]^+$ (0.0715 Å). Furthermore, the Ni-S-C angle for $[Ni(SBu^t)(triphos)]^+$ is smaller than that in $[Ni(SEt)(triphos)]^+$ ($6.48^o$) and $[Ni(SCy)(triphos)]^+$ (6.84°). However, similar dimensions to those observed in $[Ni(SBu^t)(triphos)]^+$ are observed in the structure of $[Ni(SPh)(triphos)]^+$, and thus it appears that the changes in the dimensions around the sulfur in $[Ni(SBu^t)(triphos)]^+$ is not due to the steric bulk of the alkyl substituent. The congestion around the sulfur results in change of angles and bond length around the nickel. Thus, the $P_1$-Ni-S angle decreases by 10.34 and 10.28°, and the nickel $P_1$-Ni bond length decreased by 0.0094 and 0.0124 Å. The decrease in the $P_1$-Ni-S angle is associated with an increase in the $P_2$-Ni-S (7.89 and 7.79) and the $P_3$-Ni-S (13.66 and 13.95) angles.

[Ni(SEt)(triphos)]$^{+}$

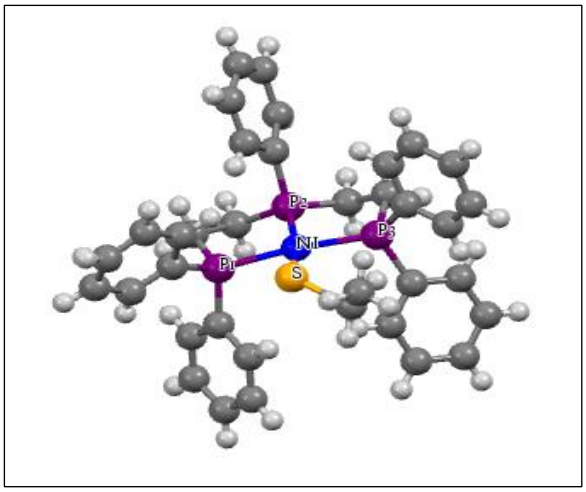


[Ni(SBu$^{t}$)(triphos)]$^{+}$

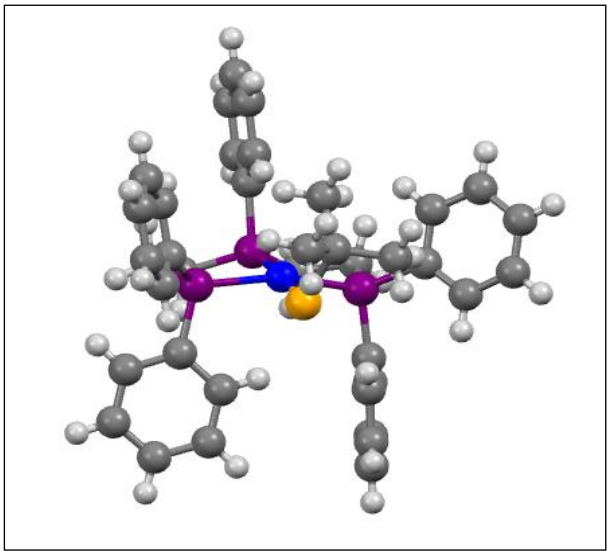

[Ni(SCyh)(triphos)]$^{+}$

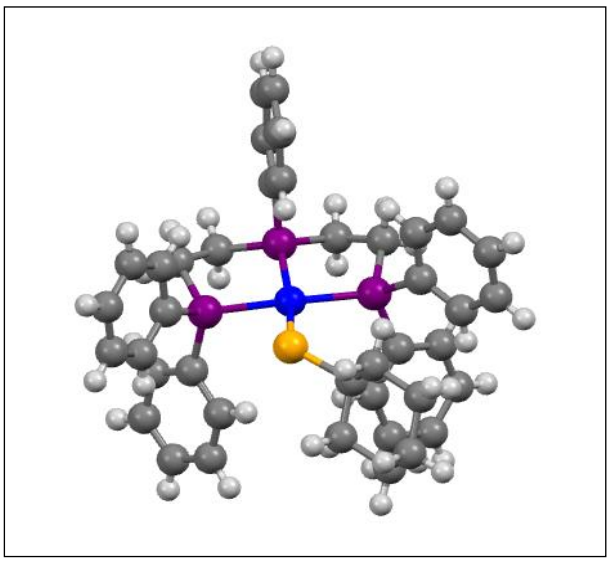

[Ni(SePh)(triphos)]$^+$

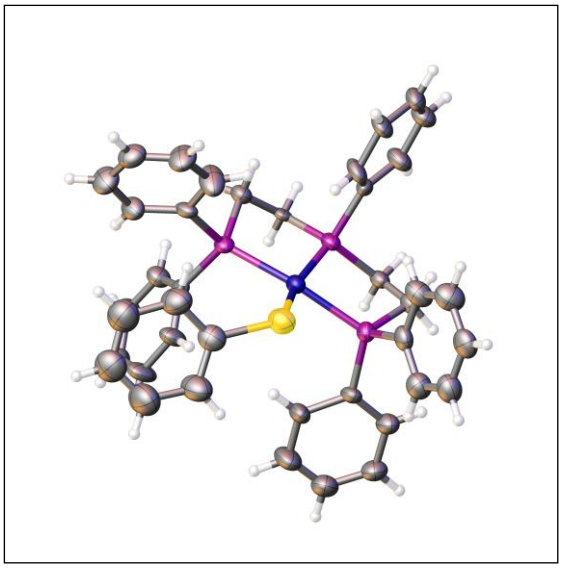

Figure 3.2. Crystal structure of the cation in [Ni(SBu$^t$)(triphos)]$^+$, [Ni(SEt)(triphos)]$^+$, [Ni(SCyh)(triphos)]$^+$ and [Ni(SePh)(triphos)]$^+$ (blue = nickel; orange = sulfur; magena = phosphorus, yellow = selenium).

| [Ni(SR)(triphos)]$^+$ | R = Et | R = Cy | R = Bu$^t$ | R = Bz [3] | R = Ph [6] |
|---|---|---|---|---|---|
| *Bond angles* ° | | | | | |
| $P_1$-Ni-S | 90.22 | 90.28 | 100.56 | 103.95(4) | 99.03(3) |
| $P_2$-Ni-S | 165.82 | 165.90 | 173.79 | 164.01(4) | 173.89(3) |
| $P_3$-Ni-S | 102.43 | 102.72 | 88.77 | 89.66(4) | 89.76(3) |
| $P_1$-Ni- $P_2$ | 85.24 | 84.71 | 85.59 | 84.80(4) | 86.41(2) |
| $P_1$-Ni- $P_3$ | 162.09 | 162.86 | 160.03 | 161.90(4) | 161.50(3) |
| $P_2$-Ni- $P_3$ | 85.23 | 85.04 | 85.11 | 84.96(4) | 85.82(2) |
| Ni-S-C | 117.43 | 117.07 | 110.59 | 115.18(13) | 99.20(8) |
| *Bond lengths* Å | | | | | |
| Ni-S | 2.1599(2) | 2.1664(1) | 2.2379(1) | 2.1689(10) | 2.2456(7) |
| $P_1$-Ni | 2.1962(1) | 2.1932(1) | 2.2056(1) | 2.2042(10) | 2.2101(7) |
| $P_2$-Ni | 2.1340(1) | 2.1286(1) | 2.1377(1) | 2.1468(10) | 2.1506(6) |
| $P_3$-Ni | 2.1888(2) | 2.1991(1) | 2.1810(1) | 2.1960(10) | 2.1858(7) |

Table 3.1. Comparison of selected bond lengths and angles for [Ni(SR)(triphos)]$BPh_4$ (R = Et, Bu$^t$, Cy, Bz or Ph)

### 3.3.2 Kinetics and Mechanism.

Earlier kinetic studies on the equilibrium reaction between the square-planar complexes, $[Ni(SC_6H_4R\text{-}4)(triphos)]^+$ (R = MeO, Me, H, Cl or $NO_2$; triphos = $PhP(CH_2CH_2PPh_2)_2$) and mixtures of $lutH^+$ and lut (lut = 2,6-dimethylpyridine) gave an insight into the mechanism of these protonation reactions. The reactions involve a single protonation of the complex [3] but show complicated kinetics as described by the rate law shown in Equation (3.10). The mechanism is shown in Figure (3.3) and involves two coupled equilibria. In the first step there is rapid formation of a species in which the $lutH^+$ associates (hydrogen-bonds) with the sulfur of the thiolate ($K_1^R$) and the second step involves the intramolecular transfer of the proton to the sulfur ($k_2^R$) .

$$\text{Rate} = \left\{\frac{K_1^R k_2^R[\text{lutH}^+]}{1 + K_1^R[\text{lutH}^+]} + k_{-2}^R[\text{lut}]\right\}[\text{Ni} - \text{thiolate}] \qquad (3.10)$$

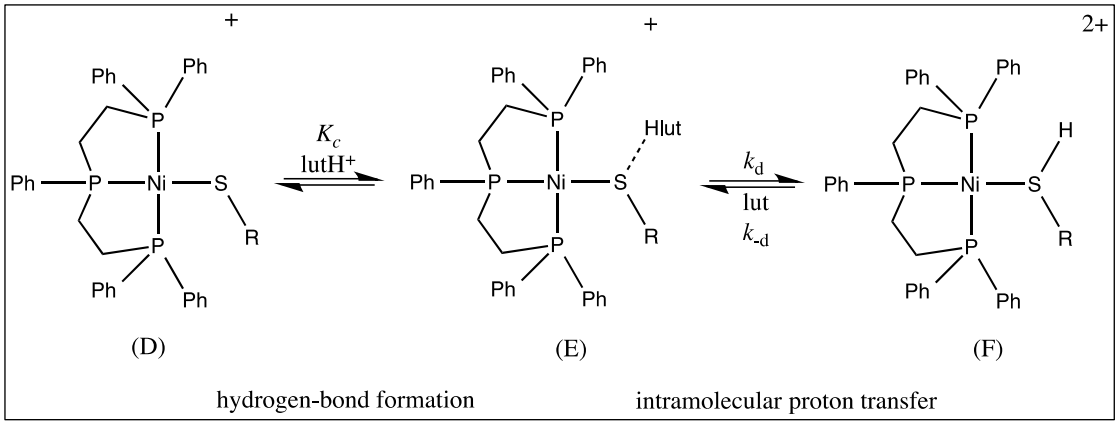


Figure 3.3. Generic mechanism for the equilibrium proton transfer reaction between nickel thiolate and $lutH^+$ showing the involvement of kinetically detected hydrogen-bonding intermediate.

The denominator in Equation (3.12) describes the partitioning between species (D) and (E) as a function of the concentration of $lutH^+$. In deriving this rate law it has been assumed that the formation of the hydrogen-bonded species is a rapid equilibrium ($K_1^R$) and the intramolecular proton transfer step ($k_2^R$) is rate limiting. Thus, when $K_1^R[\text{lutH}^+] < 1$, the rate law simplifies to Equation (3.11).

$$\text{Rate} = \{K_1^R k_2^R[\text{lutH}^+] + k_{-2}^R[\text{lut}]\}[\text{Ni} - \text{thiolate}] \qquad (3.11)$$

### 3.3.2.1 Kinetics of the reaction between $[Ni(SR)(triphos)]^+$ (R = Et, Cyh or $Bu^t$) and $lutH^+$ in the presence of lut.

The kinetics of the protonation of $[Ni(SR)(triphos)]^+$ (R = Et, Cy or $Bu^t$) by $lutH^+$ in the presence of lut (lut = 2,6-dimethylpyridine) have been studied in acetonitrile under conditions where the concentrations of both $lutH^+$ and lut are in an excess over the concentration of complex. The stopped-flow absorbance-time traces can be fitted to a single exponential curve as shown in Figure (3.4).

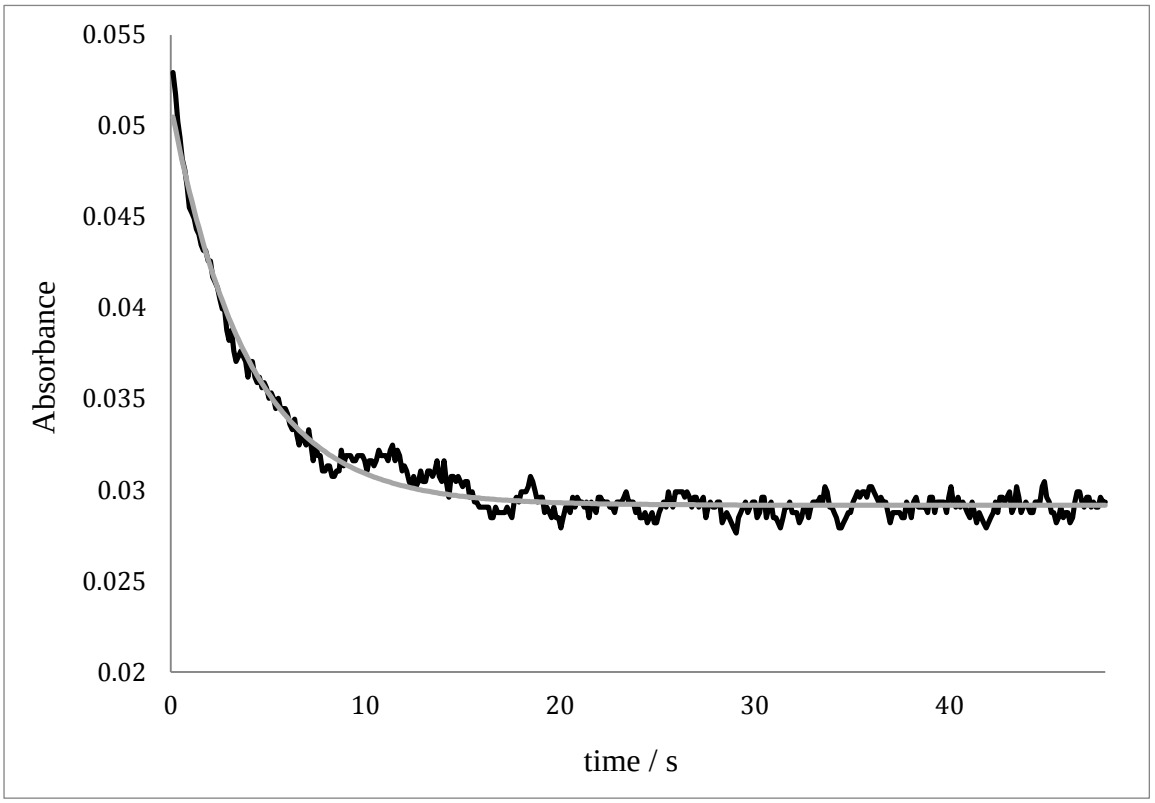


Figure 3.4. Stopped-flow absorbance-time curve for the reaction of [Ni(SEt)(triphos)]+ (0.5 mmol $dm^{-3}$) with $lutH^+$ (5.0 mmol $dm^{-3}$) lut (10.0 mmol $dm^{-3}$) in MeCN at 25.0 $^oC$ ($\lambda$ = 350 nm). The experimental trace is shown in black and the exponential curve fit is shown in grey. The curve fitted to the equation $At = Af + \Delta A.e^{-kobs.t}$

In experiments where the concentrations of $lutH^+$ and lut were varied in a systematic manner, it was observed that $k_{obs}$ depends on the concentrations of both acid and base. For the reactions of each $[Ni(SR)(triphos)]^+$ (R =Et, Cyh and $Bu^t$), graphs of $k_{obs}$/[lut] *versus* $[lutH^+]$/[lut] are linear as shown by the example in Figure (3.5).

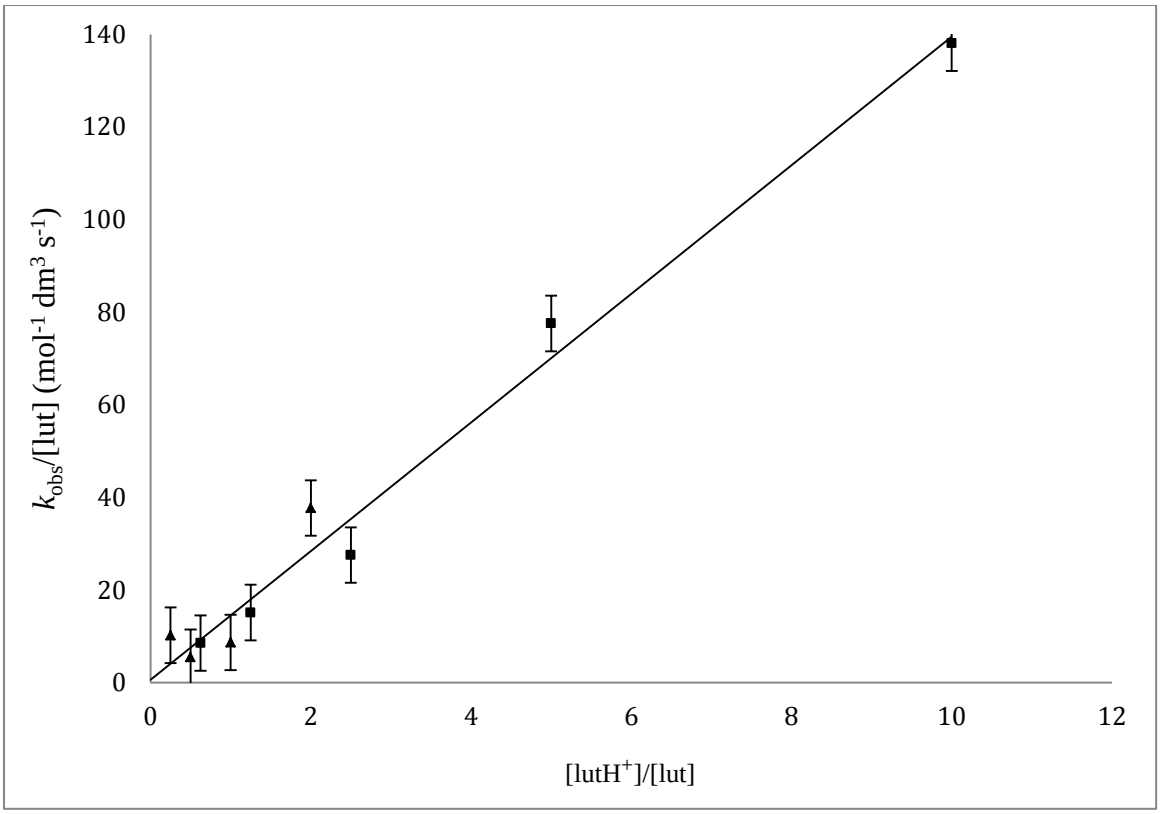


Figure 3.5. Dependence of $k_{obs}$/[lut] on [lutH$^+$]/[lut] for the reaction of [Ni(SEt)(triphos)]$^+$ with mixtures of lutH$^+$ and lut in MeCN at 25.0 $^o$C. Data points correspond to: [lutH$^+$] = 12.5 mmol dm$^{-3}$, [lut] = 2.5 – 40 mmol dm$^{-3}$ (▲); [lutH$^+$] = 25 mmol dm$^{-3}$, [lut] = 2.5 – 40 mmol dm$^{-3}$ (■).The error bars correspond to ± 5% deviation.

All data can be fitted to a single straight-line graph with a small positive intercept, and analysis of the graph gives the rate law shown in Equation (3.11). The values of $K_1^{\mathrm{R}}k_2^{\mathrm{R}}$ and $k_{-2}^{\mathrm{R}}$ are presented in Table (3.2). For comparison, also included in this table are the corresponding rate constants for [Ni($SC_6H_4$R-4)(triphos)]$^+$, which have been reported earlier [3].

| R | $K_1^R$ /dm$^3$ mol$^{-1}$ | $k_2^R$ /$s^{-1}$ | $K_1^R k_2^R$ /dm$^3$ mol$^{-1}$ s$^{-1}$ | $k_{-2}^R$ /dm$^3$ mol$^{-1}$ s$^{-1}$ | $K_1^R K_2^R$ | p$K_a^R$ |
|---|---|---|---|---|---|---|
| [Ni(SR)(triphos)]$^+$ | | | | | | |
| Et | | | 12.0 | 0.6 | 20.0 | 16.7 |
| Cy | | | 5.0 | 1.2 | 4.2 | 16.0 |
| Bu$^t$ | | | 13.0 | 0.7 | 18.6 | 16.7 |
| [Ni(SC$_6$H$_4$R-4)(triphos)]$^{+\,3}$ | | | | | | |
| $NO_2$ | >160 | 7.0 | | 1 x 10$^4$ | | |
| Cl | >160 | 0.19 | | 6 | | |
| H | 200 | 0.10 | 20.0 | 4 | 5.0 | 14.8 |
| Me | >160 | 0.05 | | 1.5 | | |
| MeO | 55.5 | 0.07 | 3.9 | 2.5 | 1.6 | 14.3 |

Table 3.2. Summary of the kinetic data for the reactions between mixtures of lutH$^+$ and lut and [Ni(SR)(triphos)]$^+$ in MeCN at 25.0 $^o$C.

From the data in Table (3.2) it is evident in the reactions of lutH$^+$ with the complexes [NiSC$_6$H$_4$R-4)(triphos)]$^+$ (R = $NO_2$, Cl, H, Me or MeO) that $K_1^R$ is significantly larger than in the reactions with the analogous alkyl thiolate complexes, [Ni(SR)(triphos)]$^+$ (R = Et, Cy or Bu$^t$). Furtheremore, in the reactions of lutH$^+$ with [Ni(SC$_6$H$_4$R-4)(triphos)]$^+$, $K_1^R$ is smaller with electron-donating 4-R-substituents (e.g. [Ni(SC$_6$H$_4$OMe-4)(triphos)]$^+$; $K_1^{MeO}$ = 55.5 dm$^3$ mol$^{-1}$) than with more electron-withdrawing 4-R-substituents (e.g. [Ni(SC$_6$H$_4$NO$_2$-4)(triphos)]$^+$ ($K_1^{NO_2}$ > 160 dm$^3$ mol$^{-1}$). Thus, there is a relationship between the electron donation ability of the 4-R-substituent and $K_1^R$: those containing the least electron-donating thiolates are associated with the largest $K_1^R$. The equilibrium constant for the protonation of [Ni(SR)(triphos)]$^+$ is $K_1^R K_2^R = K_1^R k_2^R / k_{-2}^R$. These values are presented in Table (3.2). Using the literature p$K_a$ of lutH$^+$ in MeCN (15.4), the value of p$K_a^R$ of the coordinated thiol can be calculated using the relationship shown in Equation (3.14).

$$[Ni(SR)(triphos)]^+ + lutH^+ \overset{K_0^R}{\rightleftharpoons} [Ni(SHR)(triphos)]^{2+} + lut \qquad (3.12)$$

$$\frac{[Ni(SHR)(triphos)^{2+}]\,[lut]}{[Ni(SR)(triphos)^+]\,[lutH^+]} = K_0^R = K_1^R \frac{k_2^R}{k_{-2}^R} = K_1^R K_2^R \qquad (3.13)$$

$$K_0^{\mathrm{R}} = \frac{K_{\mathrm{a}}^{\mathrm{lutH}^+}}{K_{\mathrm{a}}^{\mathrm{R}}} \qquad (3.14)$$

The p$K_a$ of all protonated [Ni(Salkyl)$_2$(triphos)] are the same, the coordinated alkylthiol is less acidic than coordinated arylthiols as shown in Table (3.2). This is because the rate of deprotonated ($k_{-2}^{\mathrm{R}}$) of alkylthiolate is slower than arylthiolate complexes.

The intermediate, {[Ni(thiolate)(triphos)]---Hlut}$^{2+}$ (E), associated with $K_1^{\mathrm{R}}$ is formed in the equilibrium reaction between the acid and the complex, involving a hydrogen-bond between the acid and the thiolate sulfur, which is predicted by DFT calculations on {[Ni(SR)(triphos)]---Hlut}$^{2+}$ (E, R = Ph [7] or Et), where the calculated structures show such an interaction. If the formation of the intermediate (E) depends only on the strength of the hydrogen-bonding, then it seems reasonable that increasing the electron-donating ability to thiolate will increase $K_1^{\mathrm{R}}$. However, as indicated above, it is complexes containing electron withdrawing thiolates which form the strongest interaction with lutH$^+$ Using DFT calculation and the X-ray crystal structures of [Ni(thiolate)(triphos)]$^+$ reported in this chapter and previously, the binding of lutH$^+$ to [Ni(thiolate)(triphos)]$^+$ have been investigated, and these will give us clear picture on the structures of (E).

The X-ray crystal structures of several [Ni(SR)(triphos)]$^+$ (R = Ph,[6] $C_6H_4NO_2$-4 [3], $CH_2Ph$, [3] Et, Cy and Bu$^t$) have all been reported and are essentially isostructural. In all the complexes the chelate ring of triphos are identical and all the complexes are square-planar with two different faces. One side (containing the phenyl ring of the central phosphorus atom) is more open (the distance between the phenyl groups on terminal phosphorus atoms is ca 5.2 Å). In contrast, the other side of the complex is closer (the distance between the phenyl groups on terminal phosphorus atoms is ca 2.8 Å). In all the X-ray crystal structures the R group of the thiolate sits in the more open face.

Using DFT calculations (GAUSSIAN09 package [8], geometries optimized at the B3LYP/Lanl2dz levels of theory, see appenidx) the structure of {[Ni(SR)(triphos)]---Hlut}$^{2+}$ (E, R = Ph or Et) [7] have been calculated. In addition, the structures of the analogous {[Ni(YPh)(triphos)]---Hlut}$^{2+}$ (Y = O or Se) have been calculated. In all cases the structure is that shown in Figure (3.5) (right hand side). It is evident that the sterically-demanding lutH$^+$ (distance between methyl groups in lutH$^+$ = 6.02 Å) binds to the more open face, and this necessitates that the thiolate rotates around the Ni-S bond to move the thiolate R group to the other side of the square-plane.

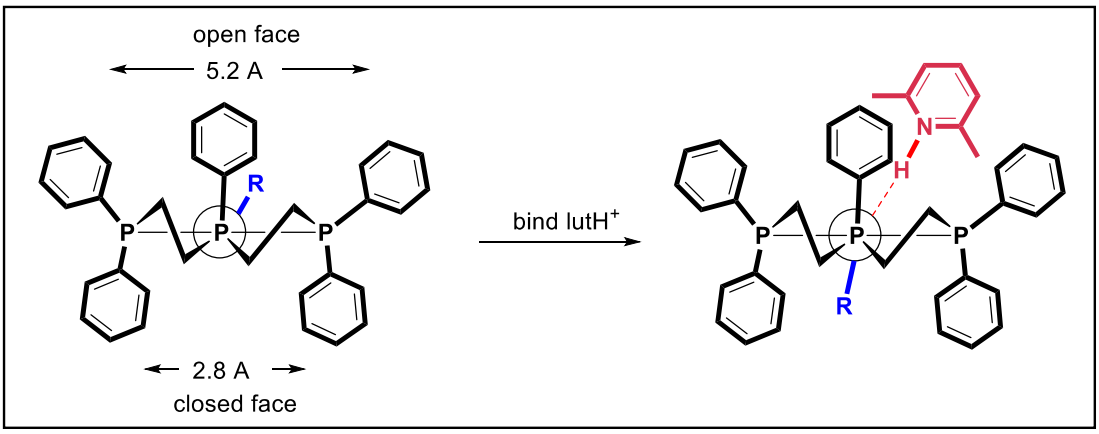


Figure 3.5. Representation of the binding of $lutH^+$ to $[Ni(SR)(triphos)]^+$. Showing how the conformation of the triphos chelate rings differentiates the two sides of the squar-planar complex. The view is down the $P_c$-Ni-S axis ($P_c$ = central P of triphos, Ni and S are behind $P_c$).

The DFT calculations indicate there can be a difference in the orientation of the bound $lutH^+$ with $[Ni(Saryl)(triphos)]^+$ and $[Ni(Salkyl)(triphos)]^+$. With $[Ni(SPh)(triphos)]^+$, the $lutH^+$ is hydrogen-bonded to the sulfur and orientated with the ring parallel to one of the phenyl groups of the triphos, as shown in Figure (3.6) (right hand side). The same orientation is also observed between $lutH^+$ and $[Ni(YPh)(triphos)]^+$ (Y = O or Se, section 3.3.2.8). In contrast, with $[Ni(SEt)(triphos)]^+$, the $lutH^+$ is angled about $90^o$ different so that the plane of the $lutH^+$ is essentially perpendicular to any of the phenyl rings of triphos (Figure 6, left hand side). In $[Ni(SEt)(triphos)]^+$, the distance between phenyl rings on the two terminal phosphorus atoms of triphos are 5.286 Å (open face) and 2.905 Å (closed face), and in $[Ni(SPh)(triphos)]^+$, the distance between phenyl rings on the two terminal phosphorus atoms of triphos are 5.234 Å (open face) and 2.606 Å (closed face). In $\{[Ni(SPh)(triphos)]\text{---}Hlut\}^{2+}$, the phenyl group on the triphos and $lutH^+$ are stacked with a separation of 2.986 – 3.133 Å, whilst in $\{[Ni(SEt)(triphos)]\text{---}Hlut\}^{2+}$, the distance between the methyl groups of $lutH^+$ and the closest phenyl groups of triphos is 3.176 – 3.371 Å. Selected bond lengths and angles for $\{[Ni(SR)(triphos)]\text{---}Hlut\}^{2+}$ (R = Et or Ph) are shown in Table (3.3) and Figure (3.6), and for R = Cy and $Bu^t$ in Appendix B. In $\{[Ni(SPh)(triphos)]\text{---}Hlut\}^{2+}$, the phenyl group on the triphos and $lutH^+$ are stacked with a separation of 2.986 – 3.133 Å, whilst in $\{[Ni(SEt)(triphos)]\text{---}Hlut\}^{2+}$, the distance between the methyl groups of $lutH^+$ and the closest phenyl groups of triphos is 3.176 – 3.371 Å. Selected bond lengths and angles for $\{[Ni(SR)(triphos)]\text{---}Hlut\}^{2+}$ (R = Et or Ph) are shown in Table (3.3) and Figure (3.6), and for R = Cy and $Bu^t$ in Appendix B. From the dimentions there is no difference in the geometry of the interaction of $lutH^+$ and the complexes, just the orientation of $lutH^+$.

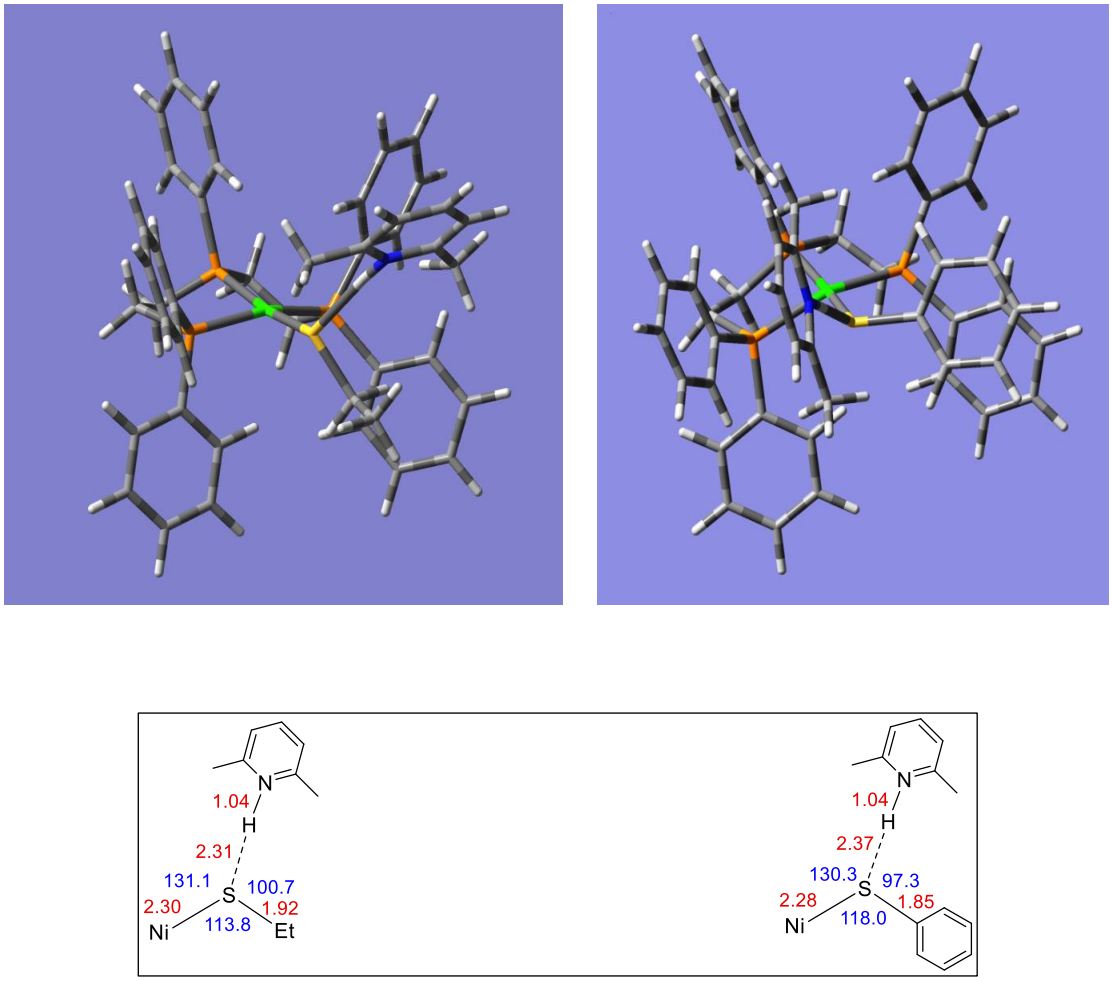


Figure 3.6: Pictures of the {[Ni(SR)(triphos)]---Hlut}$^{2+}$ species obtained from DF calculations (left hand side, R = Et; right hand side, R = Ph[10]). Below each picture is a figure showing the corresponding bond lengths (in red) and angles (in blue) associated with each hydrogen bond.

Studies on organic aromatic molecules have shown that π-stacking (π-stacking or aromatic-aromatic interaction: a noncovalent attractive force between two aromatic rings. Alignment of positive electrostatic potential on one ring with negative electrostatic potential on another ring forms pure benzene or substituent ring [9]) of the aromatic rings is stabilised by electron-withdrawing ring substituents and destabilised by electron-donating substituents [10]. Consequently from the structure of {[Ni($SC_6H_4$R-4)(triphos)]---Hlut}$^{2+}$ , the electronic properties of thiolate ligands (electron-withdrawing or electron-donating) are spread to the phenyl groups of triphos ligand and hence the π-stacking with lutH$^+$ is modulated: electron-withdrawing 4-R-substituents facilitating π-stacking more than electron-donating 4-R-substituents or alkyl thiolates. The binding affinity of [Ni($SC_6H_4$R-4)(triphos)]$^+$ with lutH$^+$ is a combination of the NH---S hydrogen-bond strength and the π-stacking affinity. In contrast, for {[Ni(Salkyl)(triphos)]---Hlut}$^{2+}$, where DFT

calculations indicate there is no π-stacking of $lutH^+$ with any phenyl group of triphos, the binding affinity must be only due to the NH---S hydrogen-bond strength.

| Parameter | $\{[Ni(SR)(triphos)]--lutH\}^{2+}$ | |
|---|---|---|
| | R = Et | R = Ph[10] |
| *bond lengths / Å* | | |
| Ni-P1 | 2.3347 | 2.3238 |
| Ni-P2 | 2.908 | 2.2948 |
| Ni-P3 | 2.3302 | 2.3442 |
| Ni-S | 2.3006 | 2.2839 |
| C-S | 1.9188 | 1.8485 |
| H-S | 2.3132 | 2.3670 |
| N-H | 1.0437 | 1.0368 |
| *bond angles / °* | | |
| P1-Ni-P2 | 85.0666 | 85.2205 |
| P2-Ni-P3 | 85.6279 | 85.6313 |
| P1-Ni-P3 | 158.9249 | 153.4338 |
| P1-Ni-S | 101.2632 | 103.6225 |
| P2-Ni-S | 168.4644 | 167.8539 |
| P3-Ni-S | 91.3332 | 89.7014 |
| Ni-S-C | 113.7776 | 117.9724 |
| Ni-S-H | 131.0537 | 130.3322 |
| C-S-H | 100.6880 | 97.3252 |

Table 3.3. Comparison of selected bond lengths and angles derived from the calculations for the hydrogen-bonded species $\{[Ni(SR)(triphos)]--lutH\}^{2+}$ (R = Et or Ph).

The reactivity pattern described above is also observed in other complexes containing the $\{Ni(triphos)\}^{2+}$ core. Thus, for the reactions of mixtures of $lutH^+$ and lut with $[Ni(YPh)(triphos)]^+$ (Y = Se or O) [7] the kinetics with Y = Se (poorly electron-releasing) exhibits a non-linear dependence on $[lutH^+]$ but the kinetics for Y = O (strongly electron-releasing) exhibits a linear dependence on $[lutH^+]$. Thus, for Y = Se the formation of B is favoured by both the Se---H hydrogen-bond and π-stacking facilitated by the poorly electron-releasing SePh ligand, whilst for Y = O, the π-stacking would be weak (strongly electron-releasing OPh ligand). This will discussed in more detail in section (3.3.2.8).

### 3.3.2.2 Temperature Dependence of the the reactions of [Ni(SR)(triphos)]$^+$ with lutH$^+$ in the presence of lut.

The Arrhenius and Eyring equation is used to describe the affect of changing the temperature on the reaction rate. As shown from the equation 3.15, there is relation between the enthalpy $\Delta H^{\ddagger}$ and the entropy $\Delta S^{\ddagger}$ of the reaction with the rate of the reaction *k*. the value of $\Delta H^{\ddagger}$ and $\Delta S^{\ddagger}$ can be determined from the linear form of Eyring equation as shown in equation 3.16. The derivation of The Arrhenius and Eyring equation are given in appendix B.

$$k = \frac{k_B T}{h} e^{(-\Delta H^{\ddagger}/RT)} e^{(\Delta S^{\ddagger}/R)} \qquad (3.15)$$

$$\ln\left(\frac{k}{T}\right) = -\frac{\Delta H^{\ddagger}}{R}\left(\frac{1}{T}\right) + \ln\frac{k_B}{h} + \frac{\Delta S^{\ddagger}}{R} \qquad (3.16)$$

The value of $\Delta H^{\ddagger}$ and $\Delta S^{\ddagger}$ can be determined from the kinetic data obtained from plot ln(*k*/T) against (1/T). The equation is a straight line with slop equal to ($-\Delta H^{\ddagger}$ / R) and the intercept equal to ln(($k_B$/h) + ($\Delta S^{\ddagger}$ /R)).

The temperature dependence on the rate of the reaction of [Ni(SR)(triphos)]$^+$ (R = Et, Bu$^t$ and Cy) with an excess of lutH$^+$ and lut in MeCN have been studied. Figure (3.7) shows typical graphs of $k_{obs}$/[lut] against [lutH$^+$]/[lut] recorded at different temperatures. The values of $\Delta H^{\ddagger}$, $\Delta S^{\ddagger}$ and $\Delta G^{\ddagger}$ were calculated from the linear Eyring graph as shown in Figure (3.8), and the data presented in Table (3.4).

The data in Table (3.4) correspond to the product of two steps – the binding of lutH$^+$ to the complex ($K_1^R$) and subsequent intramolecular proton transfer ($k_1^R$), Proton transfer from lutH$^+$ to the thiolate ligand. The value of the thermodynamic parameters, $\Delta H^{\ddagger}$ and $\Delta S^{\ddagger}$ will be effected by the electronic structure of the R substituent.

The value of $\Delta H^{\ddagger}$ for the reaction between [Ni(SR)(triphos)]$^+$ and lutH$^+$, will reflect the energy from the hydrogen bond, dissociation of the N-H bond in lutH$^+$ and the formation of the S-H bond. The value of $\Delta H^{\ddagger}$ reflects the transition state where the proton is between the sulfur and the nitrogen atoms and therefore reflects on the relative movment of the proton towards the sulfur in the transition state for formation of the protonated complex.

The negative value of $\Delta S^{\ddagger}$ reflects that the transition state for the protonated complex, The values of $\Delta S^{\ddagger}$ are all negative because the ground state corresponds to two separate reactants (complex and $lutH^{+}$) whilst in the transition state these two species are combined, resulting in a decrease in entropy.

Earlier studies [3] on the temperature dependence of the reactions between $lutH^{+}$ and $[Ni(SC_6H_4R\text{-}4)(triphos)]^{+}$ showed similar values (R = MeO: $\Delta H^{\ddagger}$ = 4.1 kcal $mol^{-1}$, $\Delta S^{\ddagger}$ = -50.1 cal $deg^{-1}$ $mol^{-1}$; R = Me: $\Delta H^{\ddagger}$ = 6.9 kcal $mol^{-1}$, $\Delta S^{\ddagger}$ = -41.2 cal $deg^{-1}$ $mol^{-1}$; R = $NO_2$: $\Delta H^{\ddagger}$ = 11.4 kcal $mol^{-1}$, $\Delta S^{\ddagger}$ = -16.4 cal $deg^{-1}$ $mol^{-1}$).

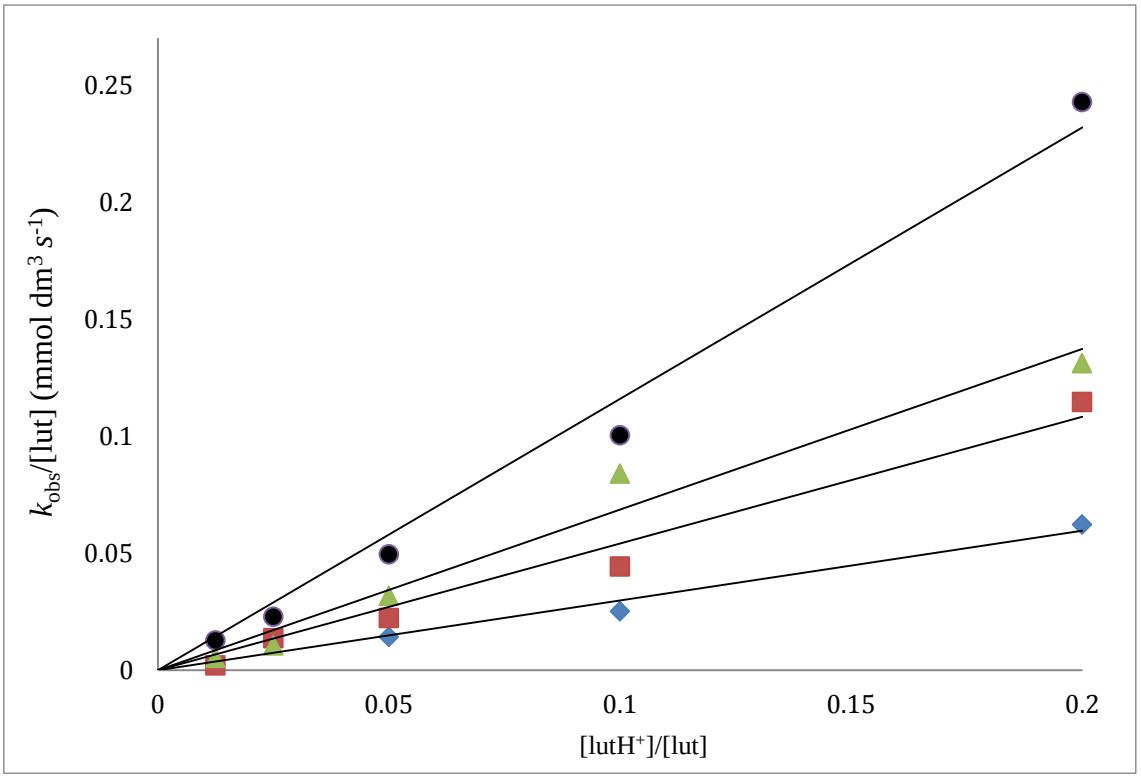


Figure 3.7. graph showing plots of $k_{obs}$/[lut] against [$lutH^{+}$]/[lut] for the reaction between $[Ni(SBu^{t})(triphos)]^{+}$ and mixtures of $[lutH]^{+}$ and lut ($[lutH]^{+}$ = 50 mmol $dm^{-3}$ , [Iut] =5-80 mmol $dm^{-3}$ }, at various temperatures (solvent = MeCN). black, T = 40°C; green, T =30°C; red, T = 25°C; blue, T = 20°C.

| R | $\Delta H^{\ddagger}$/ kcal $mol^{-1}$ | $\Delta S^{\ddagger}$ / cal.$deg^{-1}$ $mol^{-1}$ | $\Delta G^{\ddagger}$/ kcal $mol^{-1}$ at 298 |
|---|---|---|---|
| $Bu^{t}$ | 6.75 | -10.06 | 9.73 |
| Et | 13.04 | -23.03 | 18.89 |
| Cyh | 12.20 | -31.16 | 22.27 |

Table 3.4: Values of $\Delta H^{\ddagger}$, $\Delta S^{\ddagger}$ and $\Delta G^{\ddagger}$ for the reaction between $[Ni(SR)(triphos)]^{+}$ (R = Et, $Bu^{t}$ and Cyh) and $lutH^{+}$ in MeCN.

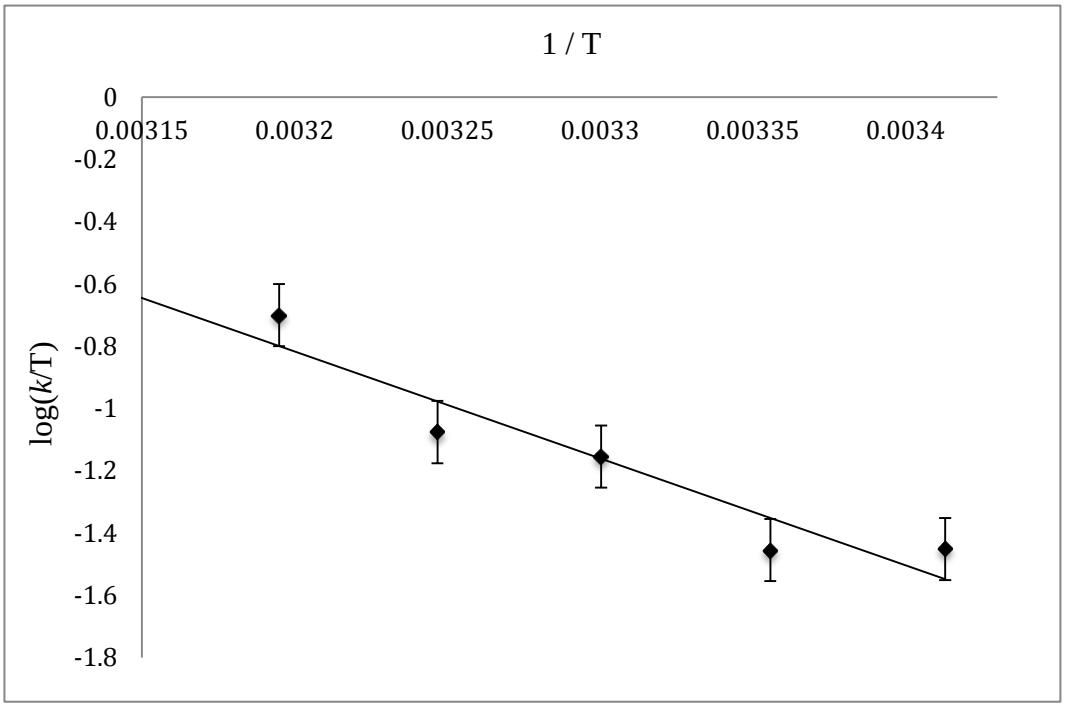


Figure 3.8. Eyring plots of the reaction between $[Ni(SCyh)(triphos)]^+$ and mixture of $lutH^+$ and lut. The error bars corresponded to 5% deviation.

### 3.3.2.3 Kinetic Isotope Effects for the reactions of [Ni(SR)(triphos)]$^+$ with lutD$^+$.

The effect of transferring a deuteron rather than a proton has been studied in the reactions of [Ni(SR)(triphos)]$^+$ with lutD$^+$. The lutD$^+$, used for isotope effects studies, was prepared by the same method as for lutH$^+$ but using MeOD and $D_2O$. Comparison of the broad peaks centred at δ = 15.2 ppm attributed to the acidic proton in the $^1$H NMR spectrum of lutH$^+$ and lutD$^+$ allows estimation of the extent of deuterium labelling in lutD$^+$. It is difficult to estimate an accurate ratio of acidic proton in the deuterated acid due to the broadening of the peak counting for the acidic proton in the spectra. Integration of this peak and comparison with the internal integration of the signal (s, *CH*$_3$) allowed us to calculate that the deuterium isotopic purity less than 80%.

The isotopic effect which is measured in the reactions between [Ni(SR)(triphos)]$^+$ and lutD$^+$ corresponds to the effect on $K_1^{\mathrm{R}}k_2^{\mathrm{R}}$. Thus the observed isotope effect is the nett effect on the isotope effect associated with formation of the hydrogen-bonded species ($K_1^{\mathrm{R}}$) and the isotope effect associated with the intramolecular proton transfer ($k_2^{\mathrm{R}}$). The nett kinetic isotope effect $(k^{\mathrm{R}})^{\mathrm{H}}/(k^{\mathrm{R}})^{\mathrm{D}}$ can thus be written as shown in Equation (3.17). The typical kinetics graph for the reaction [Ni(SR)(triphos)]$^+$ (R = Et, Bu$^t$ and Cyh) with an excess of lutD$^+$ and lut is shown in Figure (3.9).

Kinetic isotope effects for the proton transfer reactions between [Ni(SR)(triphos)]$^+$ and lutH$^+$ were studied using the lutD$^+$. The rate constants obtained with lutH$^+$ ($k^H$) were compared with those obtained with lutD$^+$ ($k^D$). The isotope effect is quantified as the ratio $k^H$ / $k^D$.

We have studied the isotopic effect of both, the formation of hydrogen-bonded ($K_1^{\mathrm{R}}$) reaction and the intramolecular proton transfer ($k_2^{\mathrm{R}}$). The kinetic of isotope $(k^{\mathrm{R}})^{\mathrm{H}}/(k^{\mathrm{R}})^{\mathrm{D}}$ can be written in the term of the formation of hydrogen-bonded ($K_1^{\mathrm{R}}$) reaction and the intramolecular proton transfer reaction ($k_2^{\mathrm{R}}$) as shown in Equation (3.17). The typical kinetics graph for the reaction [Ni(SR)(triphos)]$^+$ (R = Et, Bu$^t$ and Cyh) with an excess of lutD$^+$ and lut is shown in Figure (3.9).

$$\frac{(k^{\mathrm{R}})^{\mathrm{H}}}{(k^{\mathrm{R}})^{\mathrm{D}}} = \frac{(K_1^{\mathrm{R}})^{\mathrm{H}}}{(K_1^{\mathrm{R}})^{\mathrm{D}}} + \frac{(k_2^{\mathrm{R}})^{\mathrm{H}}}{(k_2^{\mathrm{R}})^{\mathrm{D}}} \qquad (3.17)$$

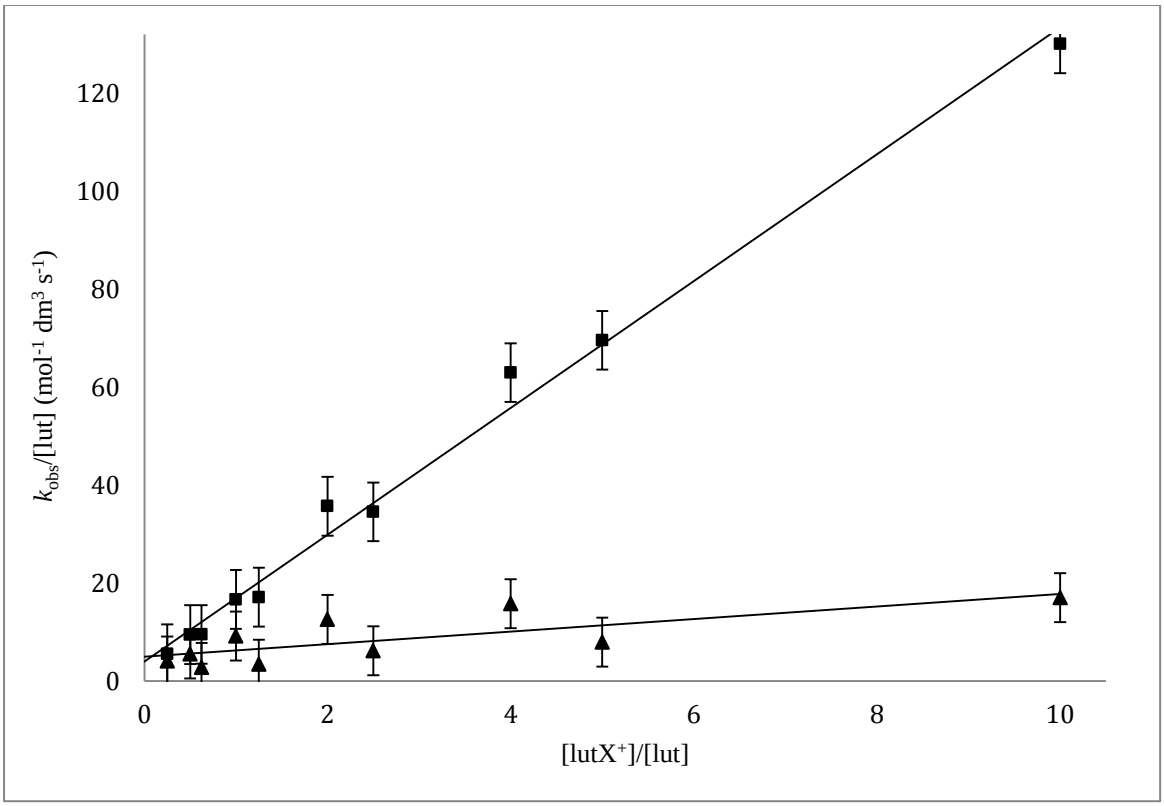


Figure 3.9. Graph of $k_{obs}$/[lut] against [lutX]$^+$/[lut] (X = D ▲; X = H, ■) for the reaction of [Ni(SEt)(triphos)]$^+$ with [lutX]$^+$ = 10 mmol dm$^{-3}$, [lut] = 2.5 - 40 mmol dm$^{-3}$ and [lutX]$^+$ = 25 mmol dm$^{-3}$, [lut] = 2.5 - 40 mmol dm$^{-3}$

The kinetics for the reaction of [Ni(SR)(triphos)]$^+$ show that the reaction is associated with a normal kinetic isotope effect $(k_1^H/k_1^D)$, 25˚C (But = 1.3, Et = 5.9, Cyh = 17.1). Previous kinetic isotope study [3] on the reaction of [Ni($SC_6H_4$-R)(triphos)]$^+$ (R = MeO, $CH_3$, H, Cl or $NO_2$) predict that the electron withdrawing substituents exhibit an inverse primary kinetic isotope effect ($(k_2^{NO_2})^H/(k_2^{NO_2})^D = 0.39$) and as R group become more electron releasing there is change and for R = MeO or Me, a primary isotope effect is observed ($(k_2^{MeO})^H/(k_2^{MeO})^D = 1.2$), ($(k_2^{Me})^H/(k_2^{Me})^D = 1.3$), while the $NO_2$ and Cl substituent shows inverse primary isotope effect.

### 3.3.2.4 Kinetics of the reaction between $[Ni(OC_6H_4R\text{-}4)(triphos)]^+$ (R = H, ) and $lutH^+$ in the presence of lut.

The kinetics of the reactions between $[Ni(OC_6H_4R\text{-}4)(triphos)]BPh_4$ (R = OMe, Me, H or Cl) and $lutH^+$ in the presence of lut has been studied in acetonitrile at 25 °C using stopped-flow spectrophotometry. The kinetic study was performed under pseudo first order conditions where the concentration of $lutH^+$ and lut were present in at least a 10-fold excess over the concentration of complex (0.5 mmol $dm^{-3}$). The absorbance-time curves can be fitted with single exponential as shown in Figure (3.10), indicating the reaction exhibits a first order dependence on the concentration of the complex. To analyse the data a graph $k_{obs}$/[lut] versus [$lutH^+$]/[lut] was plotted which produced a straight-line graph as shown in Figure (3.11).

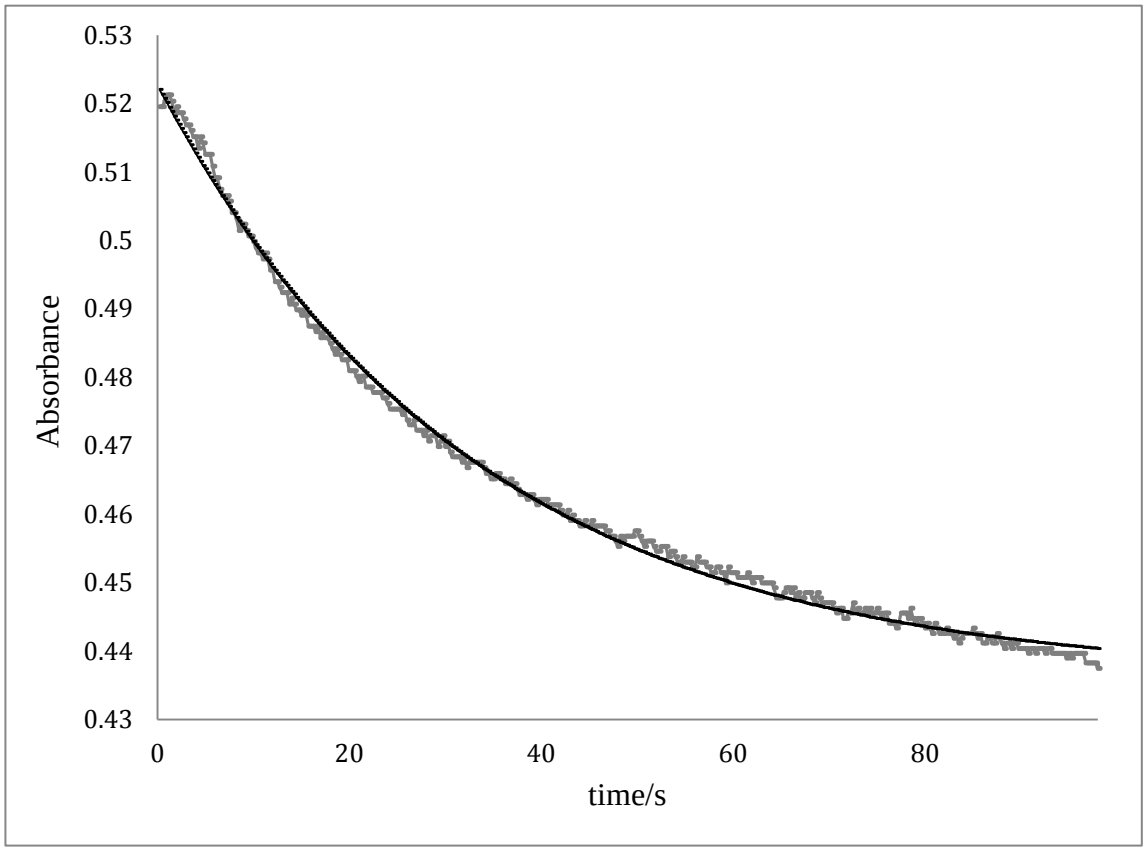


Figure 3.10. Stopped-flow absorbance-time curve for the reaction between $[Ni(OPh)(triphos)]^+$ (0.25 mmol $dm^{-3}$) and $[lutH]^+$ (40.0 mmol $dm^{-3}$)and [lut] (5.0 mmol $dm^{-3}$) in MeCN at 25 C; λ = 350 nm. The curve fitted to the equation $A_t = A_f + \Delta A.e^{-kobs.t}$.

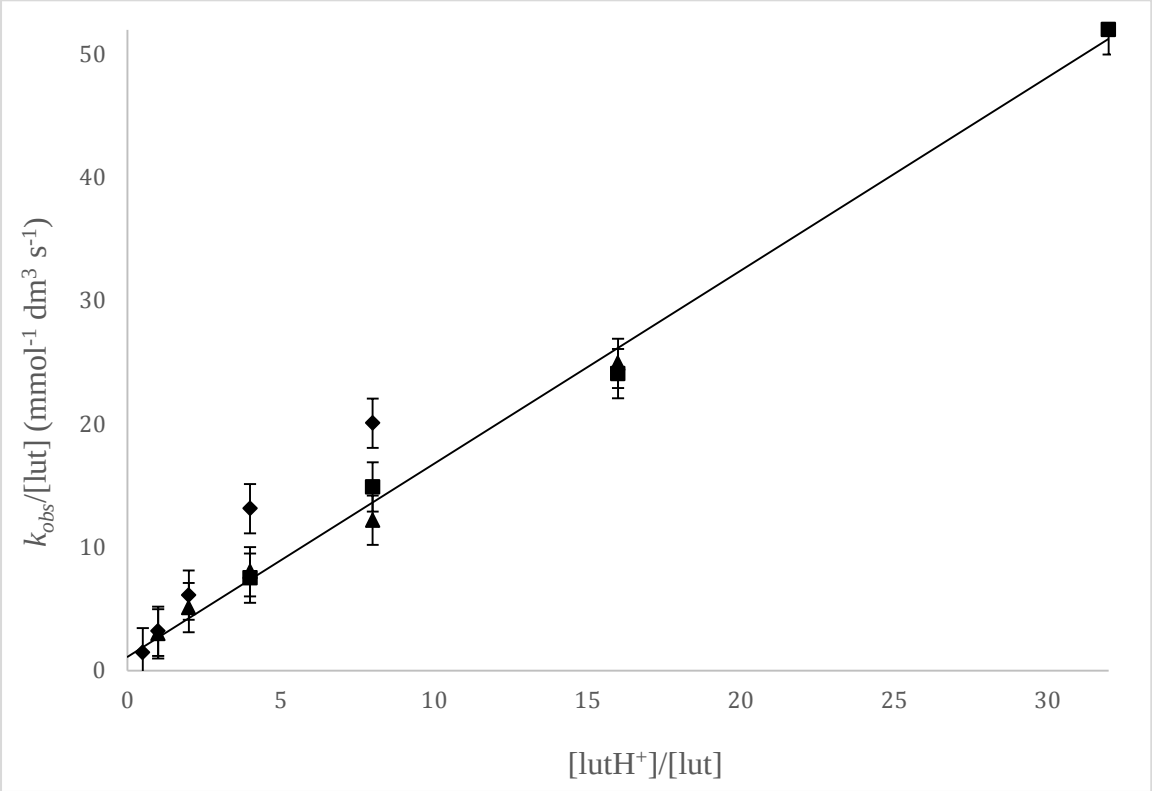


Figure 3.11. Graph of $k_{obs}$/[lut] against [lutH$^+$]/[lut] for the reaction of [Ni($OC_6H_5$)(triphos)]$BPh_4$ (0.5 mmol dm$^{-3}$) with an excess of [lutH$^+$] and [lut] ([lutH$^+$] = 10 mmol$^{-1}$ dm$^3$ s$^{-1}$and [lut] = 1.25 - 20 mmol dm$^{-3}$(◆). [lutH$^+$] = 20 mmol dm$^{-3}$, [lut] = 1.25 – 20 mmol dm$^{-3}$(▲), [lutH$^+$] = 40 mmol dm$^{-3}$, [lut] = 1.25 – 20 mmol dm$^{-3}$(■). The error bars corresponded to 5% deviation. The line is defined by equation 3.31.

Analysis of the straight line graph yielded the experimental rate law shown in Equation (3.18), which is analogous to that described for the nickel thiolate complexes According to the kinetic data the reaction of the complexes with the mixture of lutH$^+$ and lut, Equation (3.18) is consistent with the mechanism in Figure (3.12) and the general rate law show in Equation (3.12). If $K_1^{\mathrm{R}}[\mathrm{lutH}]^+ < 1$, then Equation (3.15) simplified to Equation (3.18). The values of $k_{\mathrm{f}}^{\mathrm{R}}$ and $k_{\mathrm{b}}^{\mathrm{R}}$ are presented in Table (3.5).

$$\mathrm{Rate} = \left(k_{\mathrm{f}}^{\mathrm{R}}[\mathrm{lutH}]^+ + k_{\mathrm{b}}^{\mathrm{R}}[\mathrm{lut}]\right)[\mathrm{Ni(OC_6H_4R-4)(triphos)}]^+ \qquad (3.18)$$

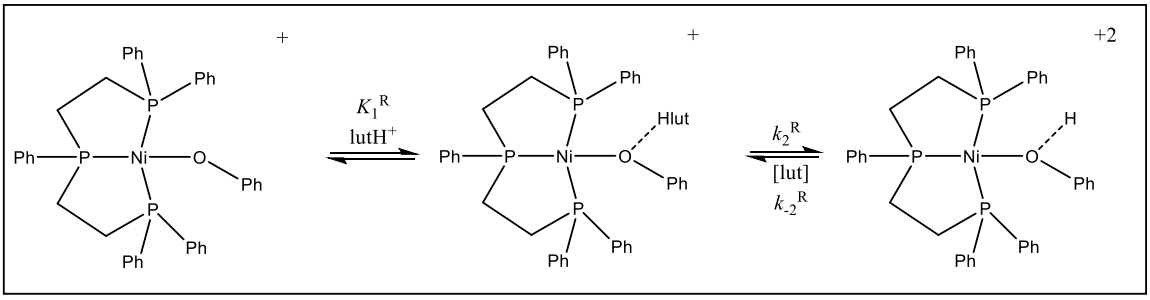


Figure 3.12: Protonation mechanism of $[Ni(OC_6H_4R\text{-}4)(triphos)]^+$.

| R | $k_f^R = K_1^R k_2^R$ /dm$^3$ mol$^{-1}$ s$^{-1}$ | $k_b^R = k_{-2}^R$ /dm$^3$ mol$^{-1}$ s$^{-1}$ | $K_1^R K_2^R$ | p$K_a$ |
|---|---|---|---|---|
| $CH_3$ | 1.16 | 2 | 0.58 | 13.8 |
| H | 1.65 | 1.5 | 1.1 | 14.1 |
| Cl | 0.56 | 1.71 | 0.33 | 13.6 |
| $OCH_3$ | 0.12 | 1.5 | 0.08 | 13.0 |

Table 3.5: The values of $k_f^R$ and $k_b^R$ for the reaction of $[Ni(OC_6H_4R\text{-}4)(triphos)]^+$ and mixture of $lutH^+$ and in $CH_3CN$ at 25 $^0$C.

The acidity of all $[Ni(HOC_6H_4R\text{-}4)(triphos)]^{2+}$ were calculated using Equation (3.19) and the p*K*a for $lutH^+$ which is known in acetonitrile ($pK_a^{[lutH]^+} = 14.1$). The p$K_a$s of the complexes are shown in Table (3.5). There is little variation in the p$K_a$, indicating that the 4-R substituent has little effect on the acidity of the complexes.

$$K_1 K_2 = \frac{K_a^{[lutH]^+}}{K_a^{[Ni-complex]}} \qquad (3.19)$$

### 3.3.2.5 Kinetics of the reaction between $[Ni(SeC_6H_5)(triphos)]^+$ and $lutH^+$ in the presence of lut.

When the kinetics of the reaction between $[Ni(SePh)(triphos)]^+$ and an excess of $lutH^+$ and lut in $CH_3CN$ at 25 $^oC$ are studied the reaction exhibits a first order dependence on the concentration of the complex, as indicated by the exponential fits to the absorbance-time trace as shown in Figure (3.13).

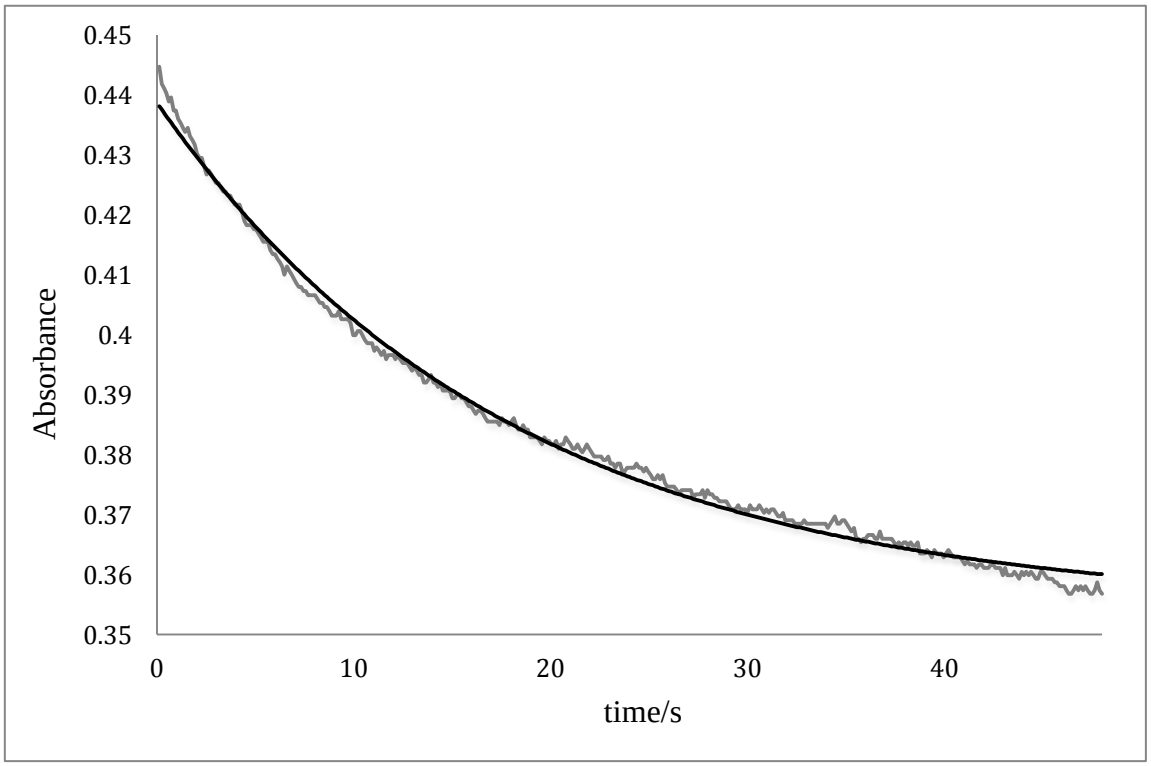


Figure 3.13. Stopped-flow absorbance-time curve for the reaction between $[Ni(SePh)(triphos)]^+$ 0.25 mmol $dm^{-3}$) and $lutH^+$ (5.0 mmol $dm^{-3}$)and lut (40.0 mmol $dm^{-3}$) in MeCN at 25 C; $\lambda$ = 350 nm. The experimental curve is shown in black and the exponential curve is grey. The equation of the exponential curve is $A_t = 0.286+0.339e^{-0.073t}$.

The dependence of the rate on the concentrations of $lutH^+$ and lut is complicated. Plots of $k_{obs}$/[lut] versus [$lutH^+$]/[lut] are straight lines provided the concentration of $lutH^+$ is constant. As the concentration of $lutH^+$ is increased the slope of the line decreases but each line has the same intercept {see Figure (3.14)}.

Analysis of the graphs gives the rate law shown in equation 3.36. A similar behaviour has been observed before in the analogous reactions of $[Ni(SC_6H_4R\text{-}4)(triphos)]^+$ [3]. This rate law is consistent with a mechanism involving two coupled equilibria occur by the

mechanism shown in Figure (3.15) and the rate law as shown in Equation (3.20). The value of $K_1^{Se}$ = 310 dm$^3$ mol$^{-1}$, $k_2^{Se}$ = 0.048 s$^{-1}$, $k_{-2}^{Se}$ = 0.4 dm$^3$ mol$^{-1}$ s$^{-1}$, where $K_1^{Se}[lutH]^+ < 1$.

$$\text{Rate} = \left\{\frac{K_1^R k_2^R [lutH^+]}{1 + K_1^R [lutH^+]} + k_{-2}^R [lut]\right\} [Ni(SeC_6H_5)(triphos)]^+ \qquad (3.20)$$

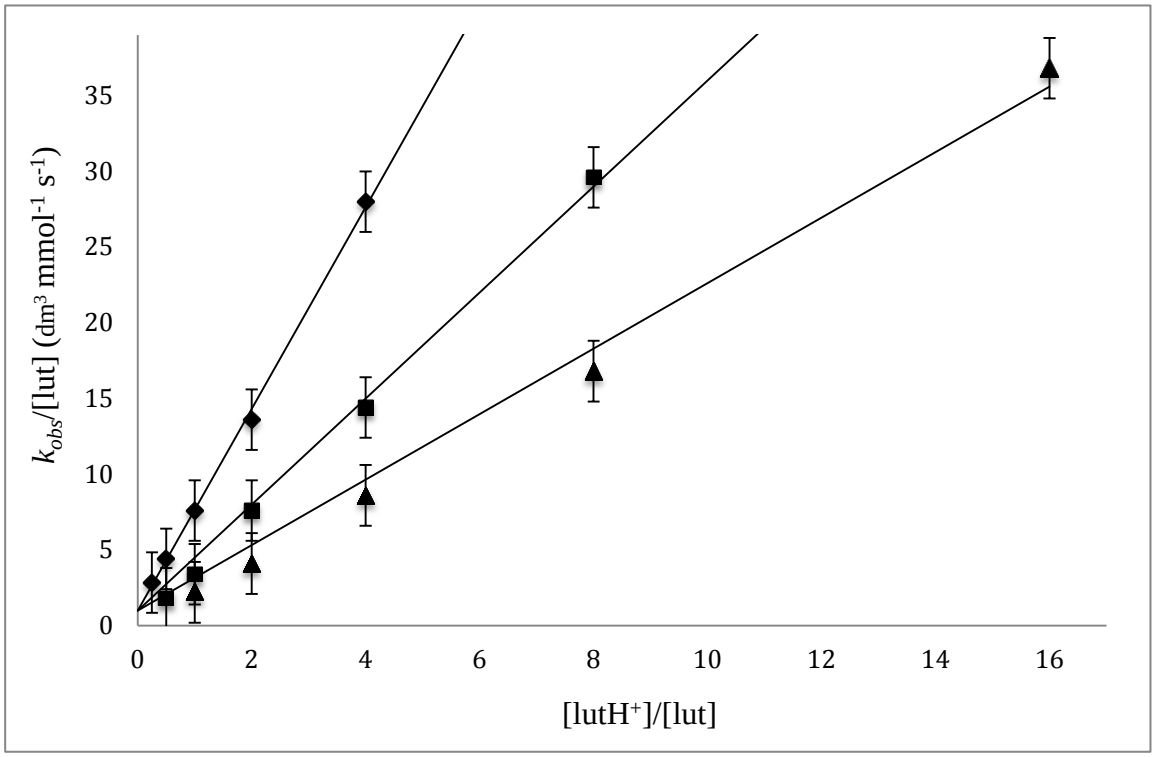


Figure 3.14. Plot of $k_{obs}$/[lut] versus [lutH$^{+1}$]/[lut] for the reacton of [Ni(SePh)(triphos)]$^+$ (0.25 mmol dm$^{-3}$) with mixture of lutH$^+$ and lut in MeCN at 25.0 C. data points correspond to [lutH$^+$] = 5 mmol dm$^{-3}$, [lut] = 2.5-40 mmol dm$^{-3}$(◆), [lutH$^+$] = 10 mmol dm$^{-3}$, [lut] = 2.5-40 mmol dm$^{-3}$(■), [lutH$^+$] = 20 mmol dm$^{-3}$, [lut] = 2.5-40 mmol dm$^{-3}$(▲).The line is defined by equation 3.36.

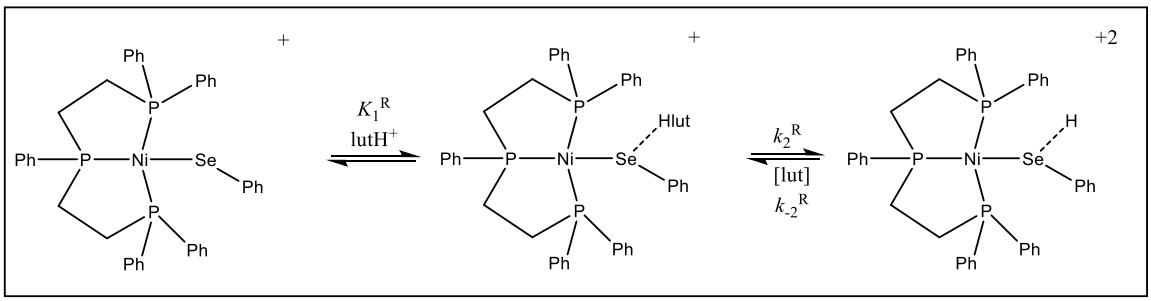


Figure 3.15. The mechanism of the raction of [Ni(SePh)(triphos)]$^+$ with lutH$^+$ in the presence of lut.

### 3.3.2.6 Sterics level the rates of proton transfer to [Ni(XPh)(triphos)]$^+$ (X = O, S or Se).

The kinetics of the reactions between [Ni(XPh)(triphos)]$^+$ (X = O, S or Se) and mixtures of lutH$^+$ and lut are all consistent with the proton transfer mechanism occuring by the same mechanism as shown in Figure (3.12) for [Ni($OC_6H_4$R-4)(triphos)]$^+$. For convenience the values of $K_1^R k_2^R$ and $k_{-2}^R$ are summarised in Table 3.7.

| R | $K_1^R k_1^R$ /dm$^3$ mol$^{-1}$ s$^{-1}$ | $k_{-2}^R$ /dm$^3$ mol$^{-1}$ s$^{-1}$ | p$K_a$ |
|---|---|---|---|
| O | 1.65 | 1.5 | 14.1 |
| S | 20.0 | 4.0 | 14.8 |
| Se | 14.9 | 0.4 | 15.7 |

Table 3.7: rate constant for the equilibrium reactions between mixtures of lutH$^+$ and lut and [Ni(XPh)(triphos)]$^+$ (X = O, S or Se) in MeCN at 25℃.

It is clear from the data in Table (3.7) that the rates of proton transfer to [Ni(XPh)(triphos)]$^+$ and from [Ni(HXPh)(triphos)]$^{2+}$ are much slower than the diffusion-controlled limit and, more unexpectedly, are essentially all the same ($K_1^O k_2^O$: $K_1^S k_2^S$: $K_1^{Se} k_2^{Se}$ = 1:12:9; $k_{-2}^O$: $k_{-2}^S$: $k_{-2}^{Se}$ = 3.8:10:1). This behavior is unprecedented. The rates of proton transfer to oxygen sites are usually diffusion controlled with transfer to analogous sulfur and selenium sites being slightly slower [1].

Typically, in proton transfer reactions, the acid and base can approach one another essentially unhindered to achieve the optimal hydrogen-bonding configuration, prior to proton transfer [11]. However, in systems where both the acid and base contain sterically demanding substituents (in our case, methyl groups on lutH$^+$ and phenyl groups on triphos), such an optimal geometry may be difficult to achieve, resulting in a decrease in the rate.

Using DFT calculations (The geometry optimization of the complexes was achieved by performing DFT calculation using Gaussian 09 package [8], at the B3LYP/Lanl2dz levels of theory used for the optimization for H, C, N, S, P and Ni, with the terminal condition being a root mean sequare (RMS) < 0.001 kcal mol$^{-1}$. The experimental studies has been done in acetonitrile solvent, so we have considered the solvent effect in the geometry

optimization by means of the well- known polarized continuum model (IEFPCM) [12] with the default parameters embedded in Gaussian 09 to obtain a valid approximation of chemical environment) we have investigated the interactions between $[Ni(XPh)(triphos)]^+$ and $lutH^+$ in search for the origins of these slow proton transfer rates. The calculations show that the interaction between $lutH^+$ and $[Ni(XPh)(triphos)]^+$ involves hydrogen bonding of the acid to X as shown in Figure (3.16) (dimensions and angles for the optimised structures are summarised in Appendix B).

Calculations on the $\{[Ni(XPh)(triphos)]^+ \text{---} lutH^+\}$ adducts show that the N---X distances ($R_{NX}$) are: N---O, $R_{NO}$ = 2.75 Å; N---S, $R_{NS}$ = 3.41 Å; N---Se, $R_{NSe}$ = 3.59 Å (see Figure (3.16) and Appendix Table A13). Earlier theoretical studies on systems of the type $\{H_nX\text{---}H\text{---}YH_m\}^+$ have calculated the proton transfer potentials for a series of hydrogen bond lengths and shown that the energy barrier to proton transfer increases dramatically as the hydrogen bond is elongated [14]. The optimal N----X distances are markedly different (X = O, $R_{NO} \approx 2.9$ Å; X = S, $R_{NS} \approx 3.3$ Å) [13]. The calculations on $\{[Ni(XPh)(triphos)]^+ \text{--} lutH^+\}$ indicate that the N---X distances are in good agreement with the earlier calculated optimal distances necessary for rapid proton transfer.

Other calculations for $\{H_nX\text{---}H\text{---}YH_m\}^+$ (where $XH_n$ and $YH_m$ $OH_2$, $NH_3$ and $SH_2$) system have indicated that deviations of the N--X angle from the optimal (pointing directly at the lone pair of electrons) also result in an increase to the barrier for proton transfer. The calculated geometries for the $\{[Ni(XPh)(triphos)]^+ \text{--} lutH^+\}$ {Figure (3.16) } show that the $lutH^+$ is orientated away from the bulky triphos substituents (angles: Ni–O–H = 133.6°; Ni–S–H = 148°; Ni–Se–H = 123°; see Appendix), presumably because of steric issues between the triphos ligand and $lutH^+$. This enforced orientation of the associated $lutH^+$ compromises the optimal angle for proton transfer. However, the angular deviation from the optimal is, in all cases, less than 10°.

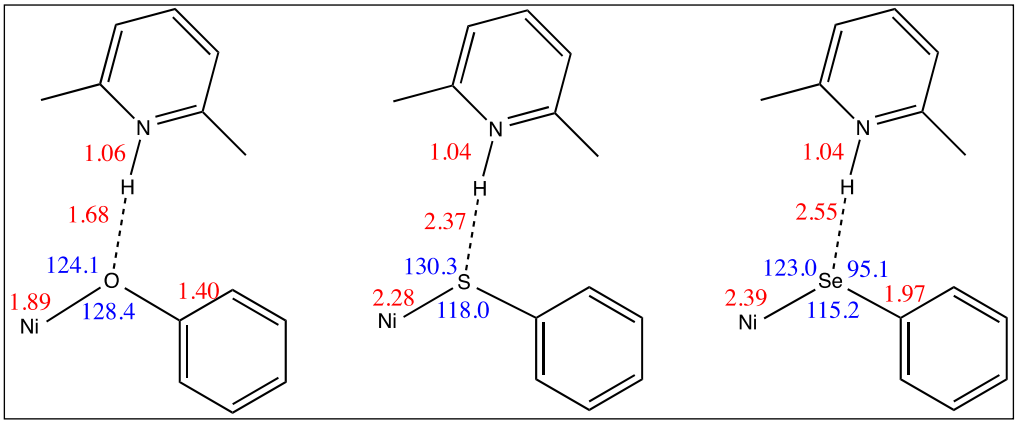


Figure 3.16. The optimal geometries for the angles (in blue) and distances (in red) for the adducts with X = O, S or Se.

The calculations indicate that $lutH^+$ and $[Ni(XPh)(triphos)]^+$ can associate in a manner which essentially achieves both the optimal hydrogen bonding distance and the correct angle for rapid proton transfer. Consequently, it appears that the reason for slow proton transfer between $[Ni(XPh)(triphos)]^+$ and $lutH^+$ is not because the optimal geometry of the hydrogen-bonded precursor cannot be achieved but, rather, an issue with the trajectory that $lutH^+$ must follow to achieve this optimal hydrogen-bonded geometry. The calculations show that the optimal geometries for $\{[Ni(XPh)(triphos)]^+$----$lutH^+\}$ involve inserting the $lutH^+$ between the phenyl substituents of the triphos ligand, and this is a tight fit (Figure 3.17). Thus, the closest non-bonding H----H distance ($R_{HH}$) between the methyl group (on $lutH^+$) and the phenyl substituent (on triphos) {left hand side of Figure 3.17} are: X = O, $R_{HH}$ = 2.73 Å; X = S, $R_{HH}$ = 2.99 Å; X = Se, $R_{HH}$ = 3.76 Å. the non-bonding H----H distance between the methyl group (top of $lutH^+$ in figure 3.17) and the phenyl substituent on the central phosphorus of triphos is short (X = O, $R_{HH}$ = 2.38 Å; X = S, $R_{HH}$ = 3.10 Å; X = Se, $R_{HH}$ = 2.81 Å); (see appendix) These nonbonding interactions must reduce the degrees of rotational freedom of the $lutH^+$ on its trajectory to forming the hydrogen bond and hence impedes proton transfer. It could be that the trajectory to form the optimal geometries shown in Figure (3.16) is so difficult (slow) to achieve that proton transfer actually occurs through an association which is geometrically non-optimal, involving proton transfer over long distances at non-optimal angles.

Finally, the apparent $pK_a^X$ values of $[Ni(XHPh)(triphos)]^+$ have been calculated using the kinetic data presented in Table (3.7). It is to be noted that the values of these apparent $pK_a^X$ s follow a trend completely the opposite to that of the free PhXH ($pK_a^O$ = 28.5, $pK_a^S$ = 21.5 and $pK_a^S$ = 18.1) [15], with coordinated PhOH being most acidic and PhSeH least acidic. This is because the equilibrium constants ($K$) for equation (3.34), calculated from

the kinetic data ($K = \frac{k_f^X}{k_b^X} = \frac{K_1^X k_2^X}{k_{-2}^X}$), reflect the rates of proton transfer to and from the XPh ligand and not the acidity of this ligand, and hence are not true p$K_a^X$s.

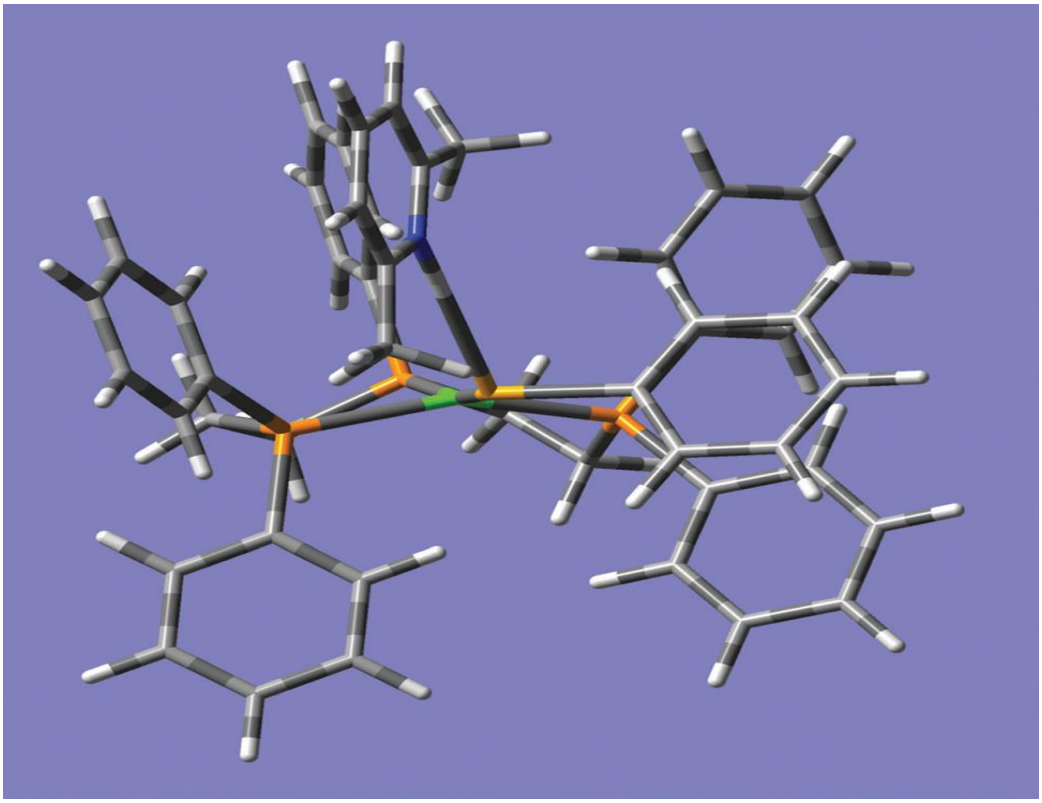

Figure 3.17. Calculated optimsed geometries for the association between lutH$^+$ and [Ni(XPh)(triphos)]$^+$ (X = O, S or Se; Ni =green, P = orange, Se = dark yellow, N = blue, H = white, C = grey).

# 3.4 Conclusion.

The kinetic studies on the protonation reactions of $[Ni(SR)(triphos)]^+$ (R = Et, Cy or $Bu^t$), $[Ni(OC_6H_4R\text{-}4)(triphos)]^+$ (R = Cl, H, Me or OMe) and $[Ni(SeC_6H_5)(triphos)]^+$ with $lutH^+$ have been studied. These are all equilibrium reactions and the kinetic analysis allows the determination of the rate constants for protonation of the coordinated thiolate and deprotonation of the corresponding coordinated thiol. The kinetics of all complexes is consistent with a mechanism where initial hydrogen bond formation between $lutH^+$ and the complex is followed by intramolecular proton transfer. This mechanism has been described before for the reactions of the analogous aryl thiolate complexes, $[Ni(SAr)(triphos)]^+$ and the studies reported in this thesis allow investigation of the changes to the elementary rate and equilibrium constants which occur when an aryl thiolate is replaced by an alkyl thiolate and changing the protonation site (O, S or Se).

The most notable feature of the kinetics is the different rate laws observed when comparing the alkyl and aryl thiolate complexes. The pattern is not systematic. Thus, $[Ni(SeC_6H_5)(triphos)]^+$ shows the full form of the rate law as shown in equation (3.20), but $[Ni(SR)(triphos)]^+$ and $[Ni(OC_6H_4R\text{-}4)(triphos)]^+$ shows the simpler rate law shown in equation 3.12. The reason for this pattern is that weaker hydrogen-bond formation will give rise to the simpler rate law, but the same mechanism operates.

The activation parameters for the intramolecular proton transfer in $\{[Ni(SR)(triphos)]\ldots Hlut\}^{2+}$ have been studied . The values of $\Delta H^{\ddagger}$ and $\Delta S^{\ddagger}$ are affected by the electronic characteristics of the R substituent. Furthermore, the isotope effect for the intramolecular proton transfer step within the hydrogen bond adduct indicate that the reaction is associated with a normal kinetic isotope effect.

The rates of proton transfer within this series of complexes shows that the reactions are markedly slower than the diffusion-controlled rate ($k_{diff}$ = 4 x $10^{10}$ $dm^3$ $mol^{-1}$ $s^{-1}$). DFT calculations indicate that the reason for this behaviour is because steric factors make it difficult for the acid to position itself correctly in preparation for proton transfer.

## 3.5 References.


1. M. Eigen, *Angew. Chem., Int. Ed. Engl.* **1964**, 3, 1.
2. R. A. Henderson, D. L. Hughes, R. L. Richards and C. Shortman, *J. Chem. Soc., Dalton Trans*. **1987**, 1115;
3. V. Autissier, W. Clegg, R. W. Harrington, R. A. Henderson, P. M. Zarza, A. Petrou, *Inorg. Chem*., **2004**, 43, 3106.
4. R. P. Bell, "*The Proton in Chemistry*" 2nd edition, Chapman and Hall, London, **1973**.
5. R. A. Henderson and K. E. Oglieve, *J. Chem. Soc. Dalton Trans*. **1998**, 3093.
6. W. Clegg and R. A. Henderson, *Inorg. Chem*. **2002**, 41, 1128.
7. A. Alwaaly and R. A. Henderson, *Chem Commun.*, **2014**, 50, 9669.
8. M. J. Frisch *et al., Gaussian 09, revision D.01,* Gaussian, Inc., Wallingford, CT, 2004.
9. S. L. Cockroft, C. A. Hunter, K. R. Lawson, J. Perkins and C. J. Urich, *J. Am. Chem. Soc*., **2005**, 127 (24), 8594.
10. J. Hwang, P. Li, W. R. Carroll, M. D. Smith, P. J. Pellechia and K. D. Shimizu, *J. Am. Chem. Soc.,* **2014**, 136, 14060.
11. R. A. Henderson, *Bioinorg. React. Mech.,* **2012**, 8, 1.
12. C. E. Bugg and U. Thewalt, *J. Am. Chem. Soc.*, **1970**, 92, 7441
13. S. Scheiner, *Acc. Chem. Res*., *1985*, 18, 174.
11. P. W. Atkins, *Physical Chemistry*, Vol. 5th ed, Oxford University Press. , 1994.
14. S. Scheiner, *Acc. Chem. Res*., **1985**, 18, 174.
15 B. G. Cox, "*Acids and Bases Solvent Effects on Acid-Base Strength*", Oxford University Press, UK, 2013.

# Chapter Four: Protonation reaction studies of $[Ni(SR)(Ph_2PCH_2CH_2PPh_2)]BPh_4$ (R = Et, $Bu^t$ or Cy)

## 4.1 Introduction.

In the previous chapter we discussed the kinetics of the reaction between the complexes $[Ni(SR)(triphos)]^+$, $[Ni(OC_6H_4R\text{-}4)(triphos)]^+$ and $[Ni(SeC_6H_5)(triphos)]^+$ with excess of a mixture of $lutH^+$ and lut in acetonitrile at 25 °C . The reactions exhibit a first order reaction dependence on the concentration of the nickel complexes, and the reaction shows a mechanism with two steps, where the acid $lutH^+$ combined to the sulfur, oxygen or selenium in the complex through hydrogen bonding and in the second step the hydrogen moved completely from the $lutH^+$ to the complex. The protonation of nickel complexes with two sulfur sites has been invistegated on $[Ni(MeN(CH_2CH_2S)_2)]_2$. The reaction between $[Ni(MeN(CH_2CH_2S)_2)]_2$ and one equivalent of acid has been characterised using X-ray, UV-visible and $^1H$ and $^{13}C$ NMR spectroscopy which indicats that the protonation involves only single proton.

In this work we describe the kinetics and mechanisms of protonation of $[Ni(SR)_2(dppe)]$ (R = Et, $Bu^t$ or Cy; dppe = $Ph_2PCH_2CH_2PPh_2$). From the structure of these complexes there are two site for the protonation reaction, however, only single protonation observed as shown in previous work by Henderson [1] and these investigations complement earlier work on the analogous arylthiolate derivatives, $[Ni(SC_6H_4R\text{-}4)_2(dppe)]$.

## 4.2 Experimental and Methods.

### 4.2.1 General Experimental.

The manipulations, drying of solvents and NMR spectroscopy were performed as described in Experimental section in Chapter 2.

### 4.2.2 Preparation of Compounds.

The experimental conditions used for the preparation of $[Ni(SR)_2(dppe)]$ were the same as used for the preparation of $[Ni(SR)(triphos)]^+$, $[lutH^+]$, $lutD^+]$ and NaSR (Et, $Bu^t$ or Cy) in chapter two and three section (3.2.12, 3.2.1.3 and 3.2.1.4).

### 4.2.2.1 Preparation of $[NiCl_2(dppe)]$ [2].

$$NiCl_2.6HCl + dppe \longrightarrow NiCl_2(dppe) + 6H_2O \qquad (4.1)$$

To a solution of dppe (0.4 g, 1 mmol) in ethanol (30 ml) was added an equimolar amount of $NiCl_2.6H_2O$ (0.237 g, 1 mmol), which is dissolved in hot ethanol. The orange crystalline precipitate appears after stirring for one hour. The orange solid was filtered under vacuum and washed with large excess of ethanol.

The purity and the identification of the product were confirmed by the $^1H$ NMR spectrum.

$^1H$ NMR (400 MHz, $CD_3CN$) δ 8.3 – 7.1 (m, *Ph*, 20H), 1.36 – 1.08 (m, $CH_2$, 4H).

$^{31}P\{^1H\}$ NMR (162 MHz, $CD_3CN$) δ 57.84 (s).

### 4.2.2.2 Preparation of $[Ni(SEt)_2(dppe)]$ [3].

$$NiCl_2.6H_2O + dppe \longrightarrow [NiCl_2(dppe)] + 6H_2O \qquad (4.2)$$

To a suspension of complex $[NiCl_2(dppe)]$ ( 0.528 g, 1 mmol) in THF (*ca* 30ml) an excess of NaSEt (0.504 g, 6 mmol) was added. The solution turned dark red and the mixture were stirred for an hour to allow the mixture to become homogenous. The solution was reduced in volume to *ca* 10 ml and then a large excess of ethanol was added

forming red crystalline solid. The red precipitate was removed by filtration and washed with a large excess of ethanol and dried *in vacuo*.

The purity and the identification of the product were confirmed by the $^{1}$H NMR spectrum.

$^{1}$H NMR (400 MHz, $CD_3CN$) δ 8.1 – 7.2 (m, *Ph*, 20H), 2.37(t, 2.5, $CH_2$, 4H) 2.13 (d, $J_{PP}$= 2.81, $CH_2$, 4H), 1.19 (s, $CH_3$, 6H).

$^{31}$P{$^{1}$H} NMR (162 MHz, $CD_3CN$) δ 56.1 (s).

### 4.2.2.3 Preparation of [Ni(SBu$^{t}$)$_2$(dppe)].

This complexes was prepared in a similar manner to that described above for [Ni(SEt)$_2$(dppe)].

The purity and the identification of the product were confirmed by the $^{1}$H NMR spectrum and $^{31}$P{$^{1}$H} NMR spectrum.

$^{1}$H NMR (400 MHz, $CD_3CN$) δ 7.9 – 7.1 (m, *Ph*, 20H), 2.38 (d, 2.45, $CH_2$, 4H), 2.15 (s, $CH_3$, 18H).

$^{31}$P{$^{1}$H} NMR (162 MHz, $CD_3CN$) δ 55.3 (s).

### 4.2.2.4 Preparation of [Ni(SCyh)$_2$(dppe)].

This complexes was prepared in a similar manner to that described above for [Ni(SEt)$_2$(dppe)].

The purity and the identification of the product were confirmed by the $^{1}$H NMR spectrum and $^{31}$P{$^{1}$H} NMR spectrum.

$^{1}$H NMR (400 MHz, $CD_3CN$) δ 8.3 – 6.8 (m, *Ph*, 20H), 3.6 – 3.4 (m, *CH*, 2H), 2.2 – 2.0 (m, $CH_2$, 4H), 1.51 – 1.47 (m, *CH*, 8H), 1.39 – 1.33 (m, $CH_2$, 5H), 1.15 – 1.02 (m, *CH*, 7H).

$^{31}$P{$^{1}$H} NMR (162 MHz, $CD_3CN$) δ 59.4 (s).

## 4.3 Results and Discussion.

### 4.3.1 Characterization of Complexes.

The $^{1}H$ and $^{31}P\{^{1}H\}$NMR spectrum for all complexes $[Ni(SR)_2(dppe)]$ (R = Et, $Bu^t$ or Cyh) have been run in MeCN. All spectra show doublet peaks in the $^{1}H$ NMR spectrum in the range 2.0 – 2.4 ppm for the $CH_2$ group in dppe ligands. The spectra of phenyl groups in dppe appear in 8.3 – 6.8 ppm region. Figure (4.1) shows the $^{1}H$ NMR spectrum for $[Ni(SBu^t)_2(dppe)]$.

The $^{31}P\{^{1}H\}$NMR spectra for all complexes $[Ni(SR)_2(dppe)]$ (R = Et, $Bu^t$ or Cyh) shows a singlet peak in the range 50-60 ppm region as shown in Figure (4.2) for $[Ni(SBu^t)_2(dppe)]$.

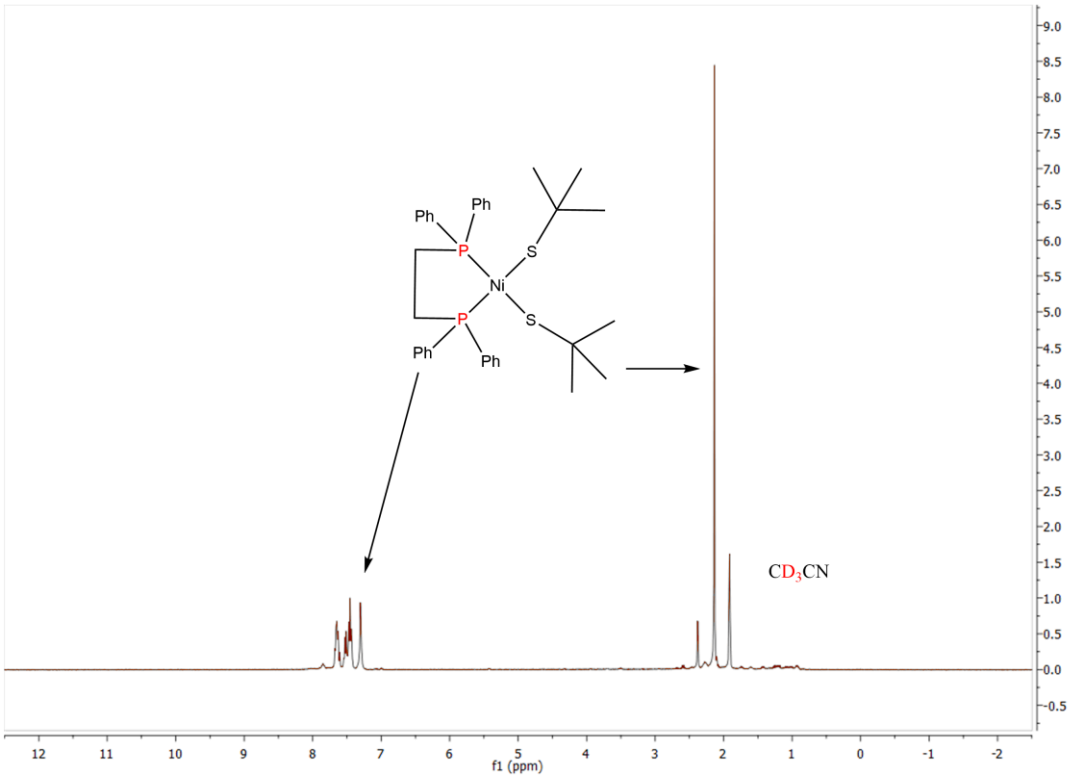


Figure 4.1. $^{1}H$ NMR spectra for $[Ni(SBu^{t})_2(dppe)]$.

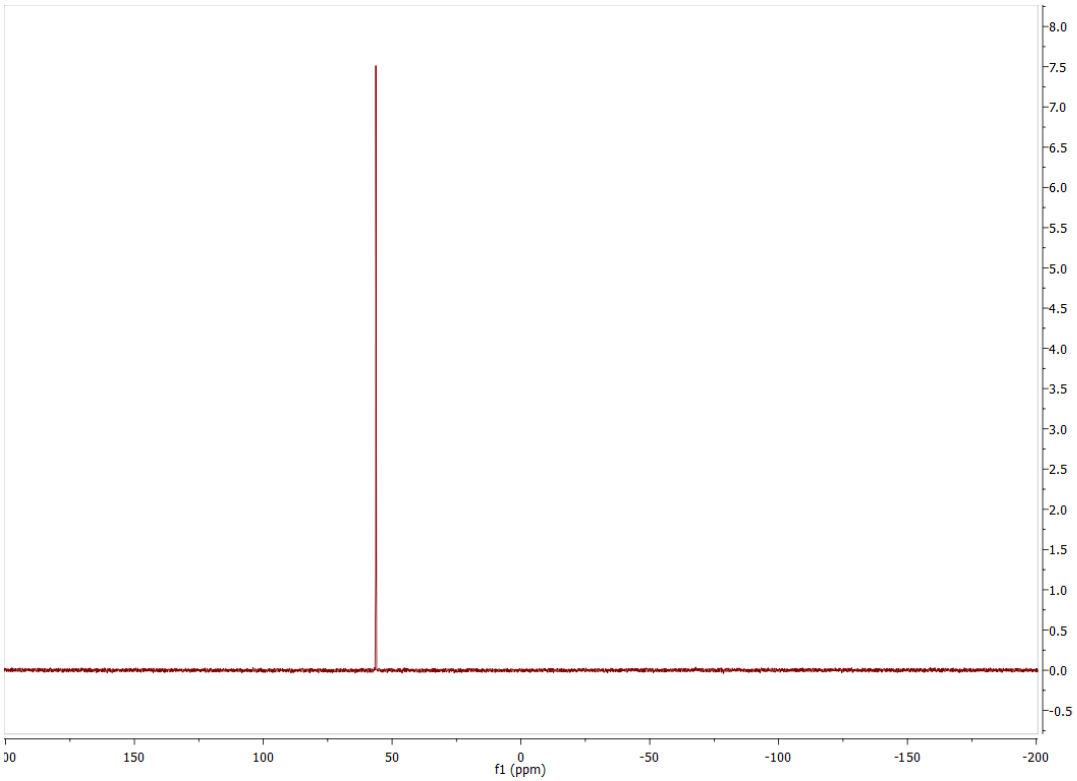


Figure 4.2. $^{31}P\{^{1}H\}$NMR spectra for $[Ni(SBu^{t})_2(dppe)]$

### 4.3.2 Kinetics of the reaction between [Ni(SR)$_2$(dppe)] (R = Et, Cyh or Bu$^t$) and lutH$^+$ in the presence of lut.

The kinetic studies for the reactions of [Ni(SR)$_2$(dppe)] (R = Et, Bu$^t$ or Cyh) with mixtures of lutH$^+$ and lut were performed at 25.0 ℃. The kinetics was performed in dry acetonitrile. The concentration of the complexes, lutH$^+$ and lut used in the kinetic studies are as follows: [Ni(SR)$_2$(dppe)] = 0.5 mmol dm$^{-3}$, [lutH$^+$] = 5 mmol dm$^{-3}$, [lut] = 1.25 – 20 mmol dm$^{-3}$, [lutH$^+$] = 10 mmol dm$^{-3}$, [lut] = 1.25 – 20 mmol dm$^{-3}$, [lutH$^+$] = 20 mmol dm$^{-3}$, [lut] = 1.25 – 20 mmol dm$^{-3}$. All solutions were used within one hour of being prepared.

A typical absorbance-time trace for the reaction of [Ni(SR)$_2$(dppe)] with lutH$^+$ and lut is shown in Figure (4.3).

The dependence of the kinetics on the concentrations of lutH$^+$ and lut was determined using graphs of $k_{obs}$/[lut] versus [lutH$^+$]/[lut]. However, the behaviour is complicated. The plots are linear but only if the concentration of lutH$^+$ is constant. The straight-line plots have a positive intercept. Increasing the concentration of lutH$^+$ defines a new straight line, with the same intercept but a smaller gradient. A typical example of this behaviour is shown, for the reaction of [Ni(SEt)$_2$(dppe)], in Figure (4.3). These data are consistent with the rate law in Equation (4.3). There are two features of Equation (4.3) important to note. First, the intercept of all lines (at various [lutH$^+$]) is the same ($k_{-2}^R$). Secondly, at a constant concentration of lutH$^+$, the dependence of $k_{obs}$/[lut] on [lutH$^+$]/[lut] is linear, but a change in the concentration of lutH$^+$ produces a new line because the gradient of the line is modulated by the factor (1 + $K_1^R$[lutH$^+$]).

$$\text{Rate} = \left\{ \frac{K_1^R k_2^R [\text{lutH}^+]}{1 + K_1^R [\text{lutH}^+]} + k_{-2}^R [\text{lut}] \right\} [\text{Ni} - \text{thiolate}] \qquad (4.3)$$

A summary of the values of the elementary rate and equilibrium constants is presented in Table (4.1). For comparison, Table (4.1) also includes the values of the corresponding elementary rate and equilibrium constants for the reaction of [Ni(SC$_6$H$_4$NO$_2$-4)$_2$(dppe)] with lutH$^+$ and lut.

According to the analysis of the data, the proposed mechanism is shown in Figure (4.4) which is consistent with two coupled equilibria. In the first step there is rapid bonded of lutH$^+$ to sulfur site through the hydrogen-bonding and in the second step the hydrogen moved completely to sulfur site as shown in Figure (4.4).

| R | $K_1^R$ /dm$^3$ mol$^{-1}$ | $k_2^R$ /$s^{-1}$ | $K_1^R k_2^R$ /dm$^3$ mol$^{-1}$ s$^{-1}$ | $k_{-2}^R$ /dm$^3$ mol$^{-1}$ s$^{-1}$ | $K_1^R K_2^R$ | p$K_a^R$ |
|---|---|---|---|---|---|---|
| Et | 420 | 1.12 | 470 | 15.0 | 31.3 | 15.6 |
| Cy | 1000 | 0.083 | 83 | 4.0 | 20.8 | 15.4 |
| Bu$^t$ | 1100 | 0.26 | 286 | 7.0 | 40.9 | 15.7 |
| $C_6H_4NO_2$-4 [(1)] | 200 | 9.9 | 1980 | 4000 | 0.5 | 13.8 |

Table 4.1: Summary of the elementary rate and equilibrium constants for reactions of [Ni(SR)$_2$(dppe)] (R = Et, Cy, Bu$^t$ or $C_6H_4NO_2$-4 [1]) with mixtures of lutH$^+$ and lut in MeCN at 25.0 $^o$C.

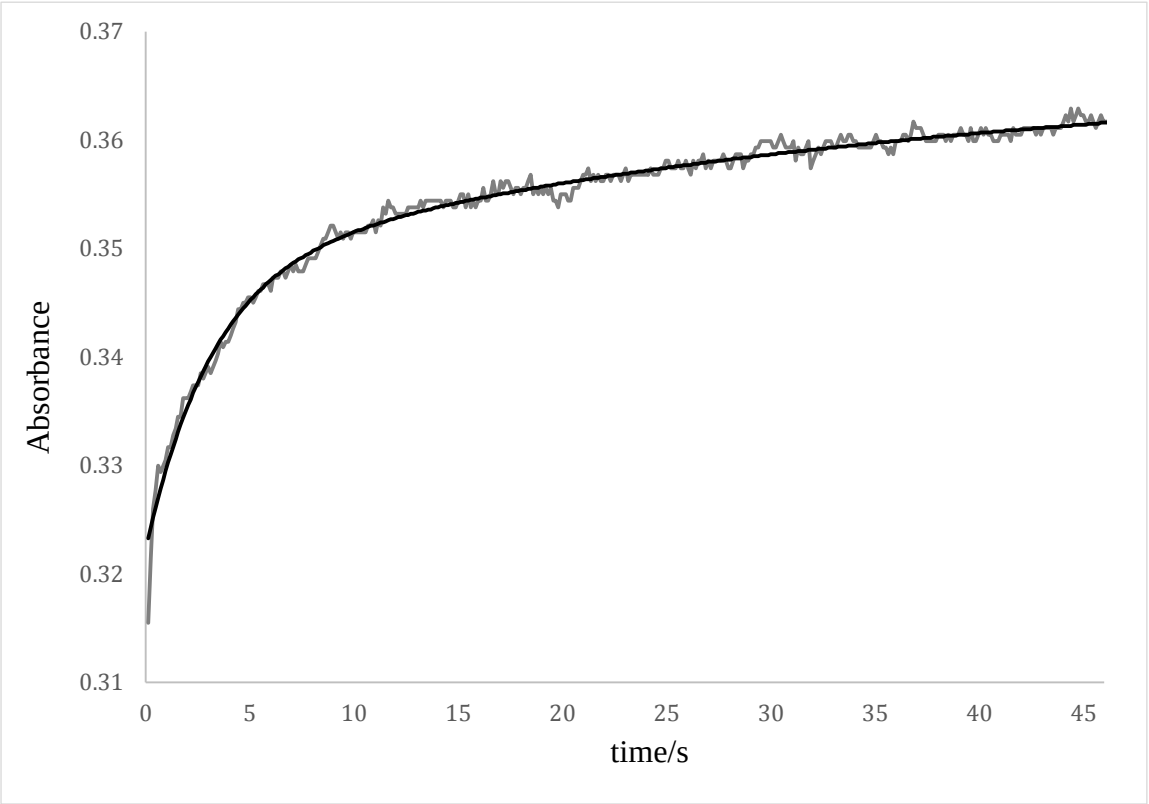


Figure 4.3. Stopped-flow absorbance-time curve for the reaction of [Ni(SEt)$_2$(dppe)] (0.5 mmol dm$^{-3}$) with lutH$^+$ (5.0 mmol dm$^{-3}$) and lut (10.0 mmol dm$^{-3}$) in MeCN at 25.0 $^o$C. The experimental trace is shown in grey and the exponential curve fit is shown in black. The curve fitted to the equation $A_t = A_f + \Delta A.e^{-kobs.t}$.

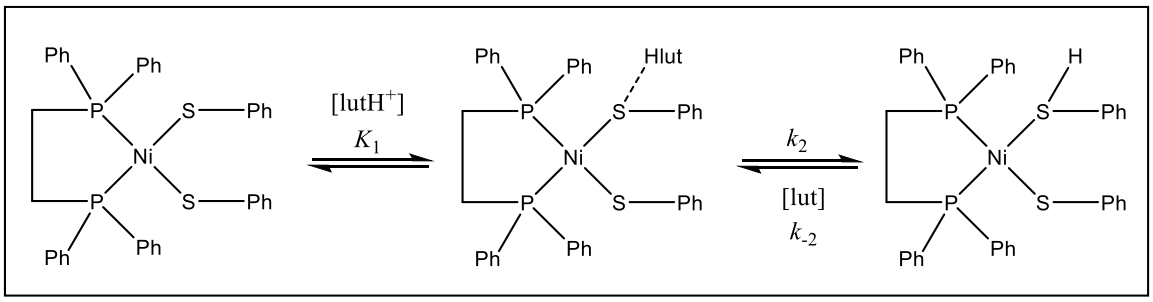


Figure 4.4. Protonation mechanism of $[Ni(SC_6H_5\text{-}NO_2)_2(dppe)]$.

Earlier studies on the equilibrium reaction between the square-planar complexes, $[Ni(SC_6H_4R\text{-}4)_2(dppe)]$ (R = MeO, Me, H, Cl or $NO_2$) and mixtures of $lutH^+$ and lut (lut = 2,6-dimethylpyridine) were consistent with the mechanism of the reaction involving two coupled equilibria. In the first step there is rapid formation of a species in which the $lutH^+$ associates (hydrogen-bonds) with the sulfur of the thiolate and the second step involves the intramolecular transfer of the proton to the sulfur as shown in Figure (4.4). The full rate law (as shown in Equation 4.4) is only observed with $[Ni(SC_6H_4NO_2\text{-}4)_2(dppe)]$. The reactions of the other $[Ni(SC_6H_4R\text{-}4)_2(dppe)]$, with more electron releasing 4-R substituents, are associated with the same rate law but with $K_1^R[lutH^+] < 1$.

The studies reported in this section on the protonation reactions of $[Ni(SR)_2(dppe)]$ complement the studies on $[Ni(SC_6H_4R\text{-}4)_2(dppe)]$. For comparison, Table (4.1) also includes the values of the corresponding elementary rate and equilibrium constants for the reaction of $[Ni(SC_6H_4NO_2\text{-}4)_2(dppe)]^+$ with $lutH^+$ and lut. $[Ni(SC_6H_4NO_2\text{-}4)_2(dppe)]^+$ is the only aryl thiolate complex of this type which shows a dependence of $k_{obs}$/[lut] as described by Equation (4.3). Other derivatives of the type, $[Ni(SC_6H_4R\text{-}4)_2(dppe)]$ show a dependence of $k_{obs}$/[lut] on $[lutH^+]$/[lut] as described by Equation (4.4).

$$\text{Rate} = \{K_1^R k_2^R[\text{lutH}^+] + k_{-2}^R[\text{lut}]\}[\text{Ni} - \text{thiolate}] \qquad (4.4)$$

Because the rate law for the reactions between $lutH^+$ and $[Ni(Salkyl)_2(dppe)]$ is that shown in Equation (4.3) and for the reactions between $lutH^+$ and $[Ni(Saryl)_2(dppe)]$ is that shown in Equation (4.4) one can directly compare the rate constants for protonation ($K_1^R k_2^R$) and deprotonation of the corresponding thiol complexes ($k_{-2}^R$). Interestingly, for $[Ni(SC_6H_4R\text{-}4)_2(dppe)]$ the rate constants for protonation and deprotonation are essentially independent of the 4-R-substituent ($K_1^R k_2^R$ = 338 – 924 $dm^3\ mol^{-1}\ s^{-1}$ and $k_{-2}^R$ = 220 – 400 $dm^3\ mol^{-1}\ s^{-1}$) [1]. Interestingly, for the analogous $[Ni(SR)_2(dppe)]$ the rate constants for protonation vary little with the alkyl substituent and are little different to

those observed with the arylthiolate complexes ($K_1^R k_2^R$ = 83 – 470 dm$^3$ mol$^{-1}$ s$^{-1}$). However, the rate constants for deprotonation of the coordinated alkylthiols are slower than the corresponding reactions with the coordinated arylthiols and ($k_{-2}^R$ = 4.0 – 15.0 dm$^3$ mol$^{-1}$ s$^{-1}$).

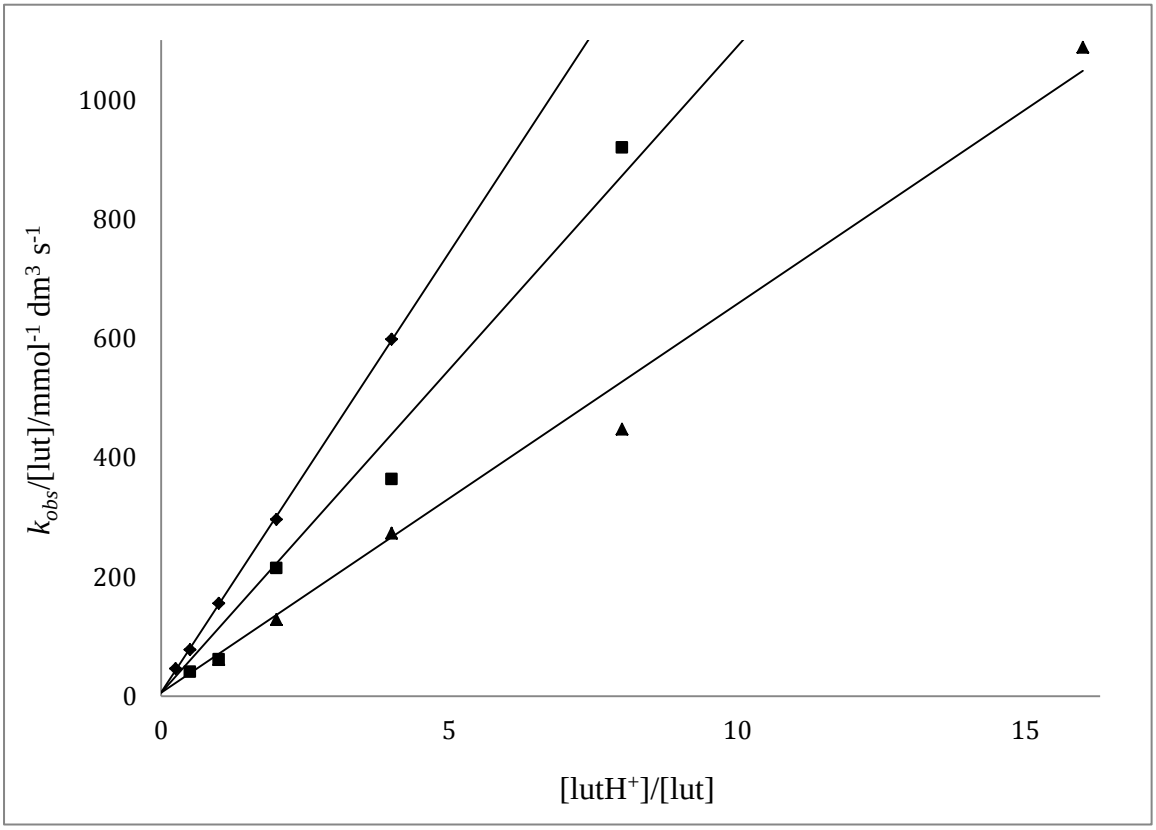


Figure 4.5. Dependence of $k_{obs}$/[lut] on [lutH$^+$]/[lut] for the reaction of [Ni(SEt)$_2$(dppe)] with mixtures of lutH$^+$ and lut in MeCN at 25.0 oC. Data points correspond to: [lutH$^+$] = 5.0 mmol dm-3, [lut] = 1.25 – 20 mmol dm-3 (♦); [lutH$^+$] = 10.0 mmol dm-3, [lut] = 1.25 – 20 mmol dm-3 (■); [lutH$^+$] = 20.0 mmol dm-3, [lut] = 1.25 – 20 mmol dm-3 (▲). The line is defined by equation 4.3.

The p$K_a$s of the thiols coordinated to the [Ni(SHR)(dppe)]$^+$ sites and the earlier work ([Ni(SHC$_6$H$_4$NO$_2$-4)$_2$(dppe)]$^{2+}$) have been calculated using equilibrium in equation 4.5.

$$[Ni(SR)_2(dppe)] + lutH^+ \longrightarrow [Ni(SHR)(SR)(dppe)]^+ + lutH^+ \qquad (4.5)$$

$$\frac{[\mathrm{Ni(SHR)_2(dppe)}]^+\,[\mathrm{lut}]}{[\mathrm{Ni(SR)_2(dppe)}]\,[\mathrm{lutH}^+]} = K_0^{\mathrm{R}} = K_1^{\mathrm{R}}.\frac{k_2^{\mathrm{R}}}{k_{-2}^{\mathrm{R}}} = K_1^{\mathrm{R}}.K_2^{\mathrm{R}} \qquad (4.6)$$

$$K_0^{\mathrm{R}} = \frac{K_{\mathrm{a}}^{\mathrm{lutH}^+}}{K_{\mathrm{a}}^{\mathrm{R}}} \qquad (4.7)$$

For the equilibrium in Equation (4.5), $K_0{}^{\mathrm{R}}$ can be calculated using the relationships shown in equation 4.6 for the [Ni(Salkyl)$_2$(dppe)] and for this systems, using the kinetic data for the reactions of lutH$^+$ it is possible to calculate $K_0{}^{\mathrm{R}}$. Knowing that for lutH$^+$, p$K_{\mathrm{a}}{}^{\mathrm{lut}}$ = 14.1, in MeCN, we can calculate the p$K_{\mathrm{a}}{}^{\mathrm{R}}$ of the coordinated thiol using the relationship shown in equation 4.7. The values of p$K_{\mathrm{a}}{}^{\mathrm{R}}$ for protonated [Ni(Salkyl)$_2$(dppe)] are presented in Table (4.1). The p$K_{\mathrm{a}}{}^{\mathrm{R}}$ of all protonated [Ni(Salkyl)$_2$(dppe)] are essentially the same, p$K_{\mathrm{a}}{}^{\mathrm{R}}$ = 15.6 ± 0.2. The differences in the p$K_{\mathrm{a}}$s of the coordinated alkylthiols and arylthiols in the Table (4.1) are attributable to the slower rates of deprotonation of the coordinated alkylthiols compared to the coordinated arylthiols.

## 4.4 Conclusions.

The kinetics on the protonation reactions of $[Ni(SR)_2(dppe)]$ (R = Et, Cy or $Bu^t$) with $lutH^+$ have been studied to get more information on the reactivity of this type of complex. The kinetics observed with this type of complex is consistent with a two-step equilibrium mechanism. The first step involves formation of a hydrogen-bond between $lutH^+$ and sulfur site lone pair of electrons and this is followed by proton transfer from the bound acid to the sulfur. The intramolecular proton transfer is the rate-limiting step. The change of the R group seems to have only a slight effect on the basicity of the sulfur (*i.e.* the differences in the p$K_a$s of the coordinated alkylthiols are small).

## 4.5 Refrences.


1. V. Autissier, W. Clegg, R. W. Harrington, R. A. Henderson, *Inorg. Chem*. **2004**, 43, 3098.
2. G. Booth, J. Chatt, *J. Chem. Soc*. **1965**, 3238.
3. R. G. Hayter, F. S. Humiec, *J. Inorg. Nucl.Chem*. **1964**, 26, 807.

# Chapter Five: Substitution and protonation reactions of $[Fe_4S_4(OPh)_4]^{2-}$ and $[\{MoFe_3S_4(OPh)_3\}_2(\mu\text{-}SPh)_3]^{3-}$

## 5.1 Introduction.

Proton transfer is a common reaction in chemistry and biology, and understanding the factors controlling the rates of these reactions is fundamental to a wide range of complex processes [1] in the reactions of enzymes. In order to understand proton transfer steps in the multi-step reactions of enzymes it is necessary to study the protonation chemistry of simpler synthetic analogous of the active site (biomimetic chemistry).

A variety of enzymes and proteins contain Fe-S-based clusters as their active sites [2]. Such proteins are involved in a number of biological transformations and reactions: from simple electron-transfer agents to the active sites in enzymes such as aconitase, hydrogenases, nitrogenases, carbon monoxide dehydrogenase, and sulfite reductase.

In this chapter the substitution and protonation reactions of the clusters $[Fe_4S_4(OPh)_4]^{2-}$ and $[\{MoFe_3S_4(SPh)_3\}_2(\mu\text{-}OPh)_3]^{2-}$ have been studied in the hope of providing an insight into the effect of changing the terminal sulfur substituent on the reactivity in these most mono and heterometallic iron-sulfur based clusters. Studies on the cuboidal cluster types have already shown that the presence of heterometals can modulate the reactivity of the cluster. In addition DFT calculations are used to understand that the p$K_a$s of all clusters ($[Fe_4S_4(OPh)_4]^{2-}$, $[S_2Mo(\mu\text{-}S_2)Fe(OPh)_2]^{2-}$ and $[\{MoFe_3S_4(SPh)_3\}_2(\mu\text{-}OPh)_3]^{2-}$) fall in the same range, which is unexpected result, because $[Fe_4S_4(OPh)_4]^{2-}$ contains triply-bridging S ($\mu_3$-$SFe_3$), while $[S_2Mo(\mu\text{-}S_2)Fe(OPh)_2]^{2-}$ contains only doubly-bridging S ($\mu$-$SFe_2$).

## 5.2 Experimental.

Because of the air sensitivity of the Fe-S-based clusters studied in this work all preparations were performed under an atmosphere of dinitrogen using Schlenk and syringe techniques.

### 5.2.1 Solvents

All solvents were dried and distilled under dinitrogen immediately prior to use. Acetonitrile was distilled from calcium hydride and methanol from $Mg(OMe)_2$ (generated *in situ*). Tetrahydrofuran (THF) and diethyl ether (ether) were dried over sodium.

### 5.2.2 Proton Nuclear Magnetic Resonance Spectroscopy.

$^1$H NMR spectra of iron-sulfur clusters are difficult to analyse due to broadening and shifting of resonances arising from the paramagnetism from the iron. Most of the compounds prepared have been reported earlier and the isolated products have been identified by comparison with those reported in the literature.
$^1$H NMR spectra were recorded on a 300 MHz Brücker Avance spectrometer. Samples were prepared in dry, degassed $CD_3CN$ under an atmosphere of dinitrogen and chemical shifts are determined relative to tetramethylsilane (TMS).

### 5.2.3 Preparation of Compounds.

The following chemicals were purchased from Sigma-Aldrich and used as received: $FeCl_3$, $NEt_3$, $NaBPh_4$, $[NH_4]_2[MoS_4]$, PhCOCl, $[NEt_4]]SPh$. The deuterated solvents, $CD_3CN$, MeOD and $D_2O$ were purchased from Goss Scientific and used as received.

#### 5.2.3.1 Synthesis of $[NEt_4]SPh$ [3].

Sodium metal (2.3 g, 0.1 mmol) was dissolved in methanol (~50 ml) forming a colourless solution. When the solution had cooled to room temperature, benzenethiol (11 ml, 100 mmol) was added to the stirring solution forming a colourless solution and the reaction

mixture was left to stir for 30 minutes. Dried [$NEt_4$]Br (3.1 g, 100 mmol) was added to the reaction mixture which was stirred for a further 30 minutes. The solvent was removed *in vacuo* leaving a white solid. MeCN (~80 ml) was added to dissolve the [$NEt_4$][SPh] but not the NaBr side product and the mixture was stirred for 30 minutes and then filtered through celite.

The volume of the filtrate was reduced to ~30 ml *in vacuo* and a large excess of diethyl ether (~150 ml) was added. The flask is cooled to -20 $^oC$ overnight. The white precipitate is isolated by filtration, washed with diethyl ether and dried *in vacuo*. The crude product is dissolved in the minimum volume of cold MeCN (~ 50 ml) and a three-fold excess of diethyl ether was added. Upon cooling to -20 $^oC$ a white solid was observed. The white solid was isolated by filtration, washed with cold diethyl ether and dried *in vacuo.*

The identity and purity of the product was confirmed by $^1H$ NMR spectra: $^1H$ NMR (400 MHz, Acetonitrile-$d_3$) δ 7.19 – 6.32 (m, 5H), 3.11 (q, $J_{PP}$ = 7.3 Hz, 2H), 1.17 – 1.01 (t, $J_{PP}$ = 7.42 Hz, 3H).

### 5.2.3.2 Synthesis of [$NHEt_3$]$BPh_4$ [4].

To a stirring solution of triethylamine (13.5 g, 100 mmol) in THF (~ 100 ml) was added methanol (4.05 ml, 100 mmol) followed by $Me_3SiCl$ (12.7 ml, 100 mmol). A white solid was formed immediately and the solution was stirred for ~30 minutes then filtered. The white solid obtained, [$NHEt_3$]Cl, was filtered, washed with THF and dried *in vacuo*.

In a typical preparation, [$NHEt_3$]Cl (8.7 g, 63 mmol) was dissolved in the minimum volume of methanol (~ 40ml) and filtered through celite to remove a fine suspension. The required quantity of Na[$BPh_4$] (20.0 g, 63 mmoles) was dissolved in the minimum volume of methanol (~ 60 ml) and filtered through celite to remove any insoluble material and added to the solution of [$NHEt_3$]Cl. The solution was left to stand overnight and formation of a white precipitate ([$NHEt_3$]$BPh_4$ and NaCl mixture) was observed. The white solid was isolated by filtration. In order to remove the contaminating NaCl side product the solid is washed with approximately 3 L of distilled water and finally with 1 L of methanol before drying *in vacuo*.

The identity and purity of the product was confirmed by $^1H$ NMR spectra:

$^1H$ NMR (300 MHz, Acetonitrile-$d_3$) δ 7.30 – 6.81 (m, 1H), 3.13 (q, $J$ = 7.3, 4.3 Hz, 2H), 1.24 (t, $J$ = 7.3 Hz, 3H).

### 5.2.3.3 Synthesis of $[NBu^n_4]_2[Fe_4S_4(SPh)_4]$ [5].

Sodium (1.38 g, 60 mmol), was dissolved in methanol (40 ml). The solution was allowed to cool to room temperature and then thiophenol (6.2 ml, 60 mmol) was added to give a clear solution. Anhydrous $FeCl_3$ (2.43 g, 15 mmol) dissolved in methanol (20 ml) was added to the thiolate solution giving a dark green mixture. After stirring for about 20 minutes, sulfur (0.48 g, 15 mmol) was added. The mixture was then stirred for 12-18 hrs during which time it became a dark brown-red colour.

The mixture was filtered and a solution of $[NBu^n_4]Br$ (3.23 g, 10 mmol) in methanol (20 ml) was added to the filtrate. A black precipitate was immediately formed. The mixture was left for about half an hour at room temperature to ensure complete crystallization. The mixture was then filtered and the black precipitate washed with methanol, anhydrous diethyl ether and dried *in vacuo*.

The solid was recrystallised by dissolving in the minimum (~30 ml) of warm (~50 $^oC$) MeCN then adding an excess (~100 ml) of warm (~50 $^oC$) methanol. The solution was allowed to cool slowly to room temperature, and left overnight to give black crystals.

The identity and purity of the product was confirmed by $^1H$ NMR spectra; δ 8.11 (*meta*-H), δ 5.81 (*ortho*-H), δ 5.21 (*para*-H). An example of a typical $^1H$ NMR spectra obtained for $[NBu_4]_2[Fe_4S_4(SPh)_4]$ is included in appendix B (spectra B1).

### 5.2.3.4 Synthesis of $[NBu^n_4]_2[Fe_4S_4Cl_4]$ [6].

$[NBu^n_4]_2[Fe_4S_4(SPh)_4]$ (3.2 g, 2.5 mmol) was suspended in MeCN (30 ml). Benzoyl chloride (previously dried over anhydrous magnesium sulfate) (7.0 ml, 50 mmol) was added to the stirred slurry. The solid $[NBu^n_4]_2[Fe_4S_4(SPh)_4]$ gradually dissolved and the solution developed a deep brown colour with a purple black cast.

After stirring the solution for 1 hr, anhydrous diethyl ether (100 ml) was added, causing the product to separate as a dark solid. This material was collected by filtration under dinitrogen and washed with anhydrous diethyl ether, then dried *in vacuo*. The crude product is dissolved in a minimum volume (20 ml) of warm (50 $^oC$) MeCN. Precipitation of the product was effected by addition of a threefold excess of warm (50 $^oC$) isopropyl alcohol and slow cooling to room temperature. The resulting black crystals were filtered and washed with cold isopropyl alcohol then cold diethyl ether and dried *in vacuo*.

The identity and purity of the product was confirmed by comparison to the $^1$H NMR spectra of $[NBu^n_4]_2[Fe_4S_4(SPh)_4]$. The loss of the signals associated with the terminal thiolate ligands was observed, indicating that successful substitution of the terminal ligands had occurred. An example of a typical $^1$H NMR spectra obtained for $[NBu^n_4]_2[Fe_4S_4Cl_4]$ is included in appendix B (spectra B2).

### 5.2.3.5 Synthesis of $[NBu^n_4]_2[Fe_4S_4(OPh)_4]$ [7].

A mixture of (1.46 g, 2.52 mmol) of $[Bu^n_4N]_2[Fe_4S_4Cl_4]$ and (1.23 g, 10.6 mmol) of anhydrous NaOPh in 80 ml of MeCN. An immediate color change from green brown to orange-brown was observed, accompanied by formation of a white precipitate. The reaction mixture was stirred for 2 hr and the precipitate removed by filtration and washed with a small portion of MeCN. The combined filtrate was concentrated *in vacuo* until a dark crystalline precipitate began to form. Addition of several volumes of THF and cooling to -20 ºC caused complete precipitation of the microcrystalline product, which was collected by filtration and washed with THF or i-PrOH. Recrystallization was achieved by dissolving the compound in MeCN and cooling the solution to -20 ºC.

The identity and purity of the product was confirmed by $^1$H NMR spectra: $^1$H NMR (300 MHz, $CD_3CN$) δ 9.4 (*meta*-H), δ 4.52 (*ortho*-H), δ 4.2 (*para*-H). An example of a typical $^1$H NMR spectra obtained for $[NBu_4]_2[Fe_4S_4(OPh)_4]$ is included in appendix B (spectra B3).

### 5.2.3.6 Synthesis of $[NEt_4]_3[\{MoFe_3S_4(SPh)_3\}_2(\mu\text{-}SPh)_3]$ [8].

Sodium (0.92 g, 40 mmol) was dissolved in methanol (40 ml) forming a colourless solution. When this solution had cooled to room temperature thiophenol (4.11 ml, 40 mmol) was added followed by $FeCl_3$ (1.62 g, 10 mmol) dissolved in 20 ml of methanol. The solution immediately turned a dark yellow/black colour. Addition of $[NH_4]_2[MoS_4]$ (0.87 g, 3.3 mmol) resulted in the rapid formation of a red/brown solution. The solution was stirred at room temperature overnight.

After approximately 18 hours the solution was filtered through celite giving a pale solid and deep brown/black filtrate. A solution of $[NBu^n_4]I$ (3.69 g, 10 mmol) in 20 ml of methanol was added to the filtrate resulting in the immediate formation of a dark brown/black precipitate. The mixture was left for 30 minutes to ensure complete

crystallization then the dark brown solid was removed by filtration. The solid was washed with 100 ml of methanol then dried *in vacuo*.

The crude product was recrystallised from the minimum volume (30 ml) of warm ( 50 $^{o}$C) MeCN and a three-fold excess of warm ( 50 $^{o}$C) methanol. After cooling to room temperature overnight the mixture was filtered and the black precipitate were washed with cold methanol and dried *in vacuo*.

The identity and purity of the product was confirmed by $^{1}$H NMR spectra: $^{1}$H NMR (300 MHz, $CD_3CN$). For the bridging thiophenolate ligands: δ 8.2 (*ortho*-H), δ 5.9 (*meta*-H) , δ 5.2 (*para*-H). For the terminal thiophenolate ligands: δ 13.9 (*meta*-H), δ -3.8 (*ortho*-H)/(*para*-H). An example of a typical $^{1}$H NMR spectra obtained for $[NEt_4]_3[\{MoFe_3S_4(SPh)_3\}_2(\mu\text{-}SPh)_3]$ is included in appendix B (spectra B4).

### 5.2.3.7 Synthesis of $[NEt_4]_3[\{MoFe_3S_4Cl_3\}_2(\mu\text{-}SPh)_3]$ [6].

To a stirred solution of $[NEt_4]_3[\{MoFe_3S_4(SPh)_3\}_2(\mu\text{-}SPh)_3$ ] (0.66 g, 0.35 mmol) in MeCN (40 ml) was added PhCOCl (0.41 ml, 3.5 mmol). The solution was stirred for 1 hr. Addition of a solution of $Et_2O$/THF (50 ml of 50/50) produced a black precipitate which was removed by filtration, washed with $Et_2O$/THF (50/50) and dried *in vacuo*. The solid was recrystallized by dissolving in the minimum volume of warm MeCN (*ca*. 50 $^{\circ}$C) and allowing the solution to cool slowly. The identity and purity of the product was confirmed by $^{1}$H NMR spectra: The loss of the signals associated with the terminal thiolate ligands was observed, indicating that successful substitution of the terminal ligands had occurred. For the bridging thiophenolate ligands: δ 5.8 (*meta*-H), δ 5.22 (*para*-H).

An example of a typical $^{1}$H NMR spectra obtained for $[NEt_4]_3[\{MoFe_3S_4Cl_3\}_2(\mu\text{-}SPh)_3]$ is included in appendix B (spectra B5).

#### 5.2.3.8 Synthesis of $[NEt_4]_3[\{MoFe_3S_4(OPh)_3\}_2(\mu\text{-}SPh)_3]$.

This complexes was prepared in a similar manner to that described above for $[Fe_4S_4(OPh)_4]^{2-}$. The identity and purity of the product was confirmed by $^{1}$H NMR spectra: $^{1}$H NMR (300 MHz, $CD_3CN$). For the bridging thiophenolate ligands: δ 8.2 (*ortho*-H), δ 5.9 (*meta*-H), δ 5.2 (*para*-H). For the terminal thiophenolate ligands: δ 13.9 (*meta*-H), δ -3.8 (*ortho*-H)/(*para*-H).

An example of a typical $^{1}H$ NMR spectra obtained for $[NEt_4]_3[\{MoFe_3S_4(OPh)_3\}_2(\mu\text{-}SPh)_3]$ is included in appendix B (spectra B6).

## 5.3 Kinetic studies on reactions of $[Fe_4S_4(OPh)_4]^{2-}$ involving protonation.

The cuboidal $[Fe_4S_4X_4]^{2-}$ clusters occur widely in biology (X = cysteine), and therefore synthetic analogous of these clusters (X = halide, S-aryl, S-alkyl or phenolate) have been investigated in detail since the first preparation described by Holm et al. in 1972 [9]. One particular general reaction of these clusters is protonation and the effect that protonation of the cluster has on its lability.

Direct study of proton transfer to Fe-S-based clusters is difficult because of the negligible spectroscopic changes upon protonation. Therefore, the protonation of synthetic Fe-S-based clusters has been investigated indirectly, by analyzing the effect that protonation has on the rates of substitution of terminal ligands as shown in Equation (5.1) [10].

$$[Fe_4S_4X_4]^{2-} + 4PhS^- \xrightarrow{NHR_3^+} [Fe_4S_4(SPh)_4]^{2-} + 4X^- \qquad (5.1)$$

The first study on the mechanism of substitution of synthetic Fe-S clusters was on the reactions of $[Fe_4S_4(SR)_4]^{2-}$ (R = Et or $Bu^t$) with 4-R′$C_6H_4SH$ (R′ = $NH_2$, Me or $NO_2$). The study showed that the rate of the reactions correlated with the acidity of the arylthiol and the arylthiol was both the acid and the nucleophile [10].

Later studies used mixtures of $NHEt_3^+$ (acid) and $PhS^-$ (nucleophile) hence allowing distinction between the acid and nucleophile. In this system, the nucleophile and the acid can be distinguished. The nucleophile is introduced as a thiolate salt (a tetraalkylammonium salt). The acid used was $[NHEt_3]^+$ . The acid is provided as the $[BPh_4]^-$ salt since this anion is effectively inert and does not interfere with either the protonation or substitution reactions. The acids are relatively weak acids in MeCN but sufficiently strong to protonate the clusters. However, the acids are not so strong that they will result in decomposition of the cluster.

In mixtures containing $RS^-$ and $[NHEt_3]^+$ , the equilibrium shown in Equation (5.2) is rapidly established, and the concentrations of all reactants can be calculated from the relationships shown in Equations (5.3 - 5.5). The concentrations of all these reagents can be controlled independently, and the kinetic dependence on each can be determined.

$$PhS^- + NHEt_3^+ \underset{}{\overset{K}{\rightleftharpoons}} PhSH + NEt_3 \qquad (5.2)$$

As the concentration of $[NHEt_3]^+$ is further increased over $[PhS^-]$ then the equilibrium in Equation (5.2) lies completely to the right hand side and all thiolate ($PhS^-$) is converted to thiol (PhSH). Any excess acid can then protonate the cluster core $[Fe_4S_4(OPh)_4]^{2-}$ increasing the rate of substitution of the terminal $PhO^-$ ligands. The equilibrium amounts of each of these species (PhSH, $[NHEt_3]^+$ and $NEt_3$ in solution) can be determined from the simple relationships in Equations (5.3), (5.4) and (5.5), where the subscript (i) corresponds to the initial added concentrations and the subscript e represent the concentration in the equilibrium mixture.

$$[NHEt_3^+]_e = [NHEt_3^+]_i - [PhS^-]_i \quad (5.3)$$

$$[NEt_3]_e = [NEt_3]_i + [PhS^-]_i \quad (5.4)$$

$$[PhSH]_e = [PhS^-]_i + [PhSH]_i \quad (5.5)$$

In the presence of an acid (*e.g.* $NHEt_3^+$, p$K_a$ = 18.46 in MeCN [11], where protonation is thermodynamically-favourable) the substitution mechanisms of terminal ligands in $[Fe_4S_4X_4]^{2-}$ in MeCN are most accurately described as acid-catalysed substitution mechanisms, in which the act of substitution is rate-limiting and is preceded by a rapid proton transfer to the cluster. Such mechanisms are readily identified from the kinetics. Thus, in the reactions of $[Fe_4S_4X_4]^{2-}$ with the nucleophile Y, using $NHEt_3^+$ as the acid, the rate of the reaction depends on the ratio $[NHEt_3^+]/[NEt_3]$ but, not the absolute concentrations of either acid or base (Figure 5.2). Such behaviour has been described for X = SEt, $SBu^t$, SPh, Cl and Br [12]. To further extend the types of terminal ligands, the analogous reactions of $[Fe_4S_4X_4]^{2-}$ {Equation (5.1), X = OPh} have been studied with mixtures of $NHEt_3^+$ and $PhS^-$.

### 5.3.1 Kinetics of the reaction of $[Fe_4S_4(OPh)_4]^{2-}$ with $PhS^-$ in the presence of $NHEt_3^+$.

The kinetics of the reaction of $[Fe_4S_4(OPh)_4]^{2-}$ with $PhS^-$ (5.0, 10.0 and 20.0 mmol $dm^{-3}$) in the presence of $[NHEt_3]^+$ (0.0 – 100.0 mmol $dm^{-3}$) have been studied. The absorbance-

time traces were found to be excellent fits to two exponential curves under all conditions It is proposed that the two phases correspond to the substitution of the first two phenoxide ligands of $[Fe_4S_4(OPh)_4]^{2-}$ by $PhS^-$ in the presence of $[NHEt_3]^+$. The study will consider just the first exponential which corresponds to the substitution of the first phenoxide ligand, because the protonation of other sites on the cluster may occur, but they apparently do not affect the rate of substitution. A typical absorbance-time trace is shown in Figure (5.1).

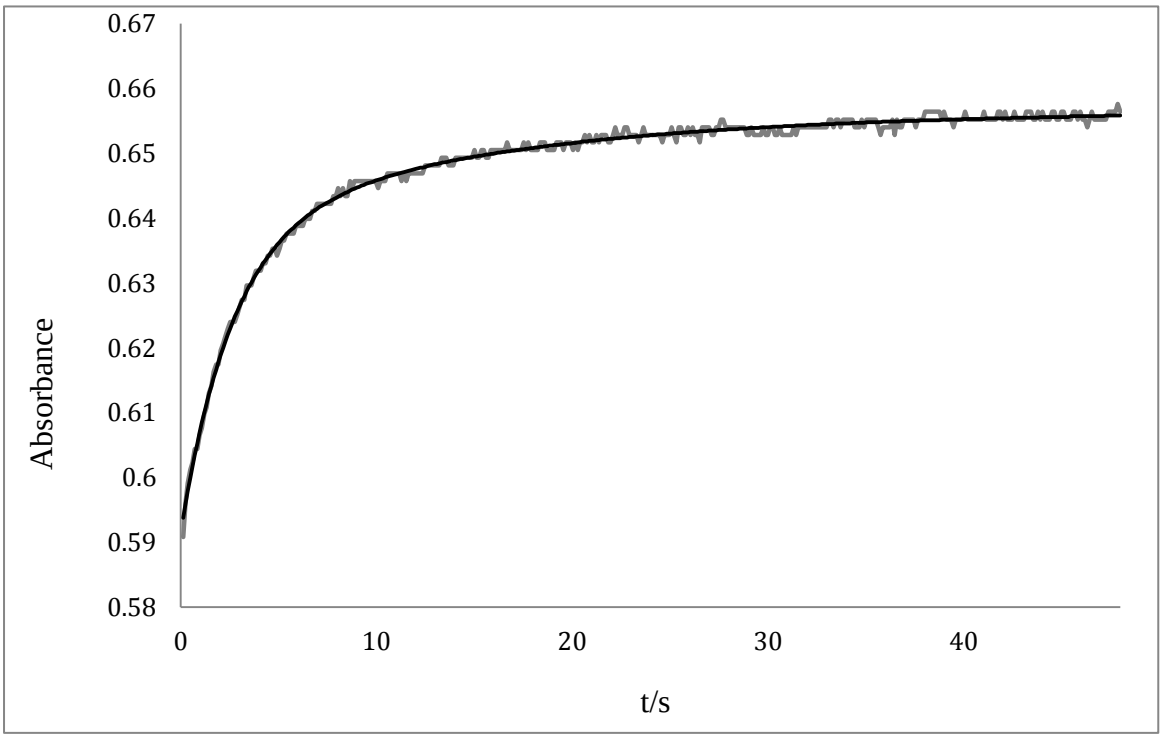


Figure 5.1. Stopped-flow absorbance-time curve for the reaction of $[Fe_4S_4(OPh)_4]^{2-}$ (0.5 mmol $dm^{-3}$) with $[PhS^-]$ (5.0 mmol $dm^{-3}$) and $[NHEt_3]^+$ (40.0 mmol $dm^{-3}$) in MeCN at 25.0 $^oC$ ($\lambda$ = 350 nm). The experimental trace is shown in black and the exponential curve fit is shown in grey. The curve fitted to the equation $A_t = 0.65 - 0.06.e^{-076.t}$.

The rate of the reaction between $[Fe_4S_4(OPh)_4]^{2-}$ and $PhS^-$ in the presence of $NHEt_3^+$ shows a non-linear dependence on the ratio $[NHEt_3^+]/[NEt_3]$, and is independent of the concentration of nucleophile (PhSH) Figure (5.2).

Inspection of Figure (5.2) indicates that when $[NHEt_3^+] = 0$, the reaction occurs at a finite rate, which corresponds, to the acid-independent pathway, (where $PhS^-$ is the nucleophile). In the presence of an excess of $NHEt_3^+$, PhSH is the nucleophile, and as $[NHEt_3^+]/[NEt_3]$ is increased the rate increases. At low $[NHEt_3^+]/[NEt_3]$ the rate exhibits a first order dependence on $[NHEt_3^+]/[NEt_3]$ but at high $[NHEt_3^+]/[NEt_3]$ the rate is

independent of $[NHEt_3^+]/[NEt_3]$. The rate constant at this point for the reaction of $[Fe_4S_4(OPh)_4]^{2-}$ with PhSH is equal to $k = 0.15\ s^{-1}$.

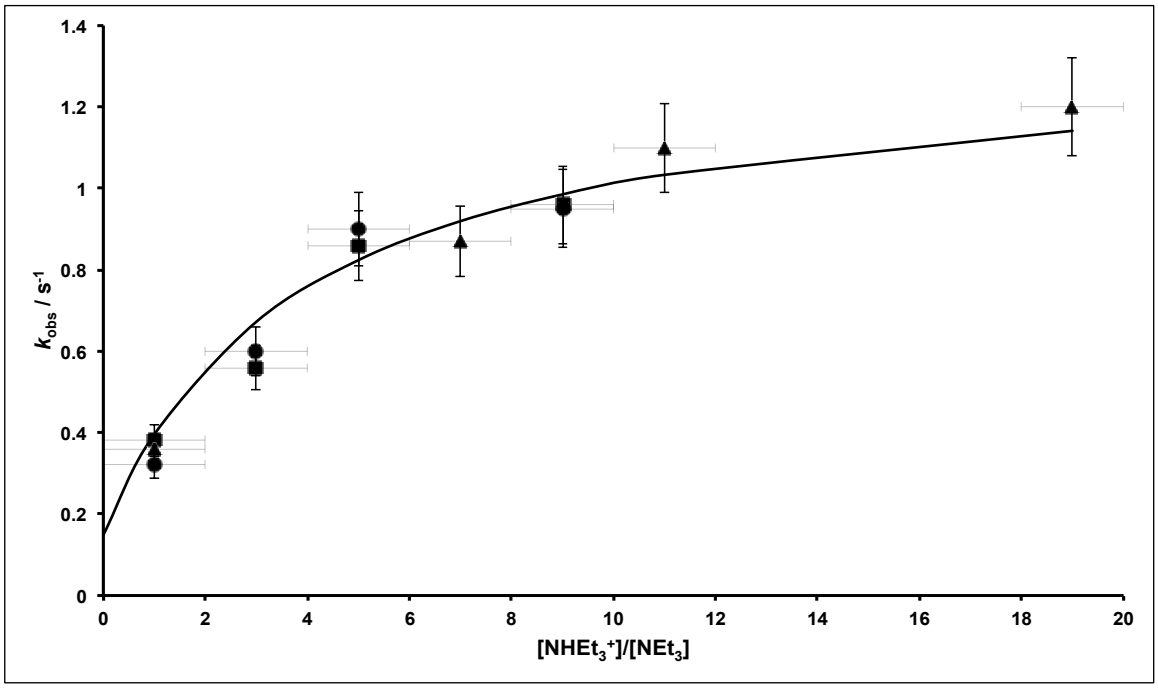


Figure 5.2. Dependence of $k_{obs}$ on the ratio $[NHEt_3^+]/[NEt_3]$ for the reaction of $[Fe_4S_4(OPh)_4]^{2-}$ with PhSH in MeCN at 25 °C, showing the independence of the rate on the concentration of PhSH; [PhSH] = 2.5 mmol $dm^{-3}$ (■), [PhSH] = 5.0 mmol $dm^{-3}$ (●), [PhSH] = 10.0 mmol $dm^{-3}$ (▲).The error bars corresponded to 5% deviation. The curve is defined by equation 5.6.

The mechanism associated with the data in Figure (5.2) is shown in Figure (5.4). The rate law associated with the reaction mechanism shown in Figure (5.4) is given by Equation (5.6). (Derivation of the rate law can be seen in appendix B)

$$\text{Rate} = \left\{ k_0 + \frac{K_1 k_2 \dfrac{[\text{NHEt}_3^+]_e}{[\text{NEt}_3]_e}}{1 + K_1^R \dfrac{[\text{NHEt}_3^+]_e}{[\text{NEt}_3]_e}} \right\} [\text{Fe}_4\text{S}_4(\text{OPh})_4]_T^{2-} \qquad (5.6)$$

The dependence of $k_{obs}$ on the ratio $[NHEt_3^+]_e/[NEt_3]_e$ can be analysed by the usual double-reciprocal graph [13], as shown in Figure (5.3) from which the value of $K_1$ and $k_2$ are found. Note that the data in the graph has been fitted using a value for $k_0 = 0.15\ s^{-1}$

when $[NHEt_3^+]_e/[NEt_3]_e$ = 0 as this corresponds to the measured rate when no acid is present.

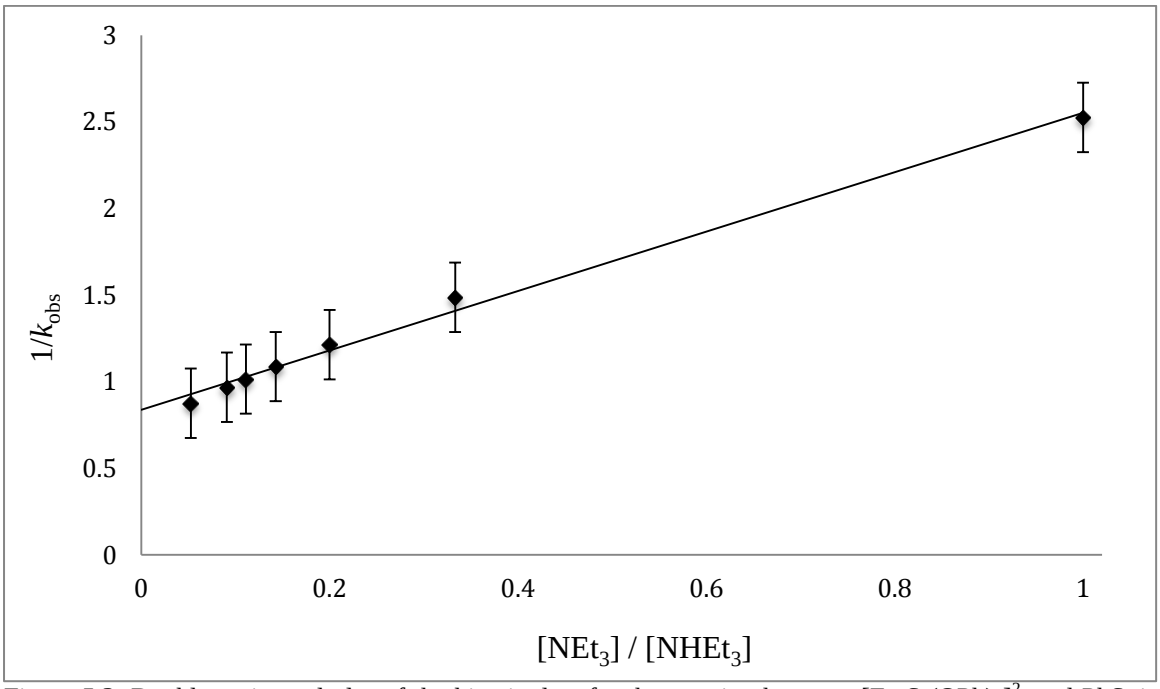


Figure 5.3. Double reciprocal plot of the kinetic data for the reaction between $[Fe_4S_4(OPh)_4]^{2-}$ and $PhS^-$ in the presence $NHEt_3^+$.

Analysis of the kinetic data in Figure (5.3) leads to rate law shown in Equation (5.7).

$$\text{Rate} = \left\{ 0.15 + \frac{0.312\dfrac{[\text{NHEt}_3^+]_e}{[\text{NEt}_3]_e}}{1 + \ 0.26\dfrac{[\text{NHEt}_3^+]_e}{[\text{NEt}_3]_e}} \right\} [\text{Fe}_4\text{S}_4(\text{OPh})_4]_{\text{T}}^{2-} \qquad (5.7)$$

Comparison Equation (5.7) with Equation (5.6) gives the protonation constant ($K_1$ = 0.26) and the rate constant for the substitution step ($k_2$ = 1.2 $s^{-1}$).

The dependence of the rate on $[NHEt_3^+]/[NEt_3]$ indicates that the cluster only binds a single proton and at high values of $[NHEt_3^+]/[NEt_3]$, the observed kinetics correspond to the substitution of this protonated cluster. The interpretation of the kinetics only reflects the protonation which labilises the substitution step. Protonation of other sites on the cluster may occur, but they apparently do not affect the rate of substitution.

Using the value of $K_1$ and p$K_a$ = 18.46 of $NHEt_3^+$ in MeCN [11], p$K_a$ = 17.9 for the protonated cluster, $[Fe_4S_3(SH)(OPh)_4]^-$, can be calculated.

The p$K_a$ of the protonated cluster is determined using Equation (5.8) (the derivation of the Equation (5.8) shown in section 4.3.2.

$$K_1 = \frac{K_a^{NHEt_3^+}}{K_a^{ClusterH^+}} \qquad (5.8)$$

Rearranging Equation (5.7) and solving for $K_a^{cluster-H^+}$ using $K_1$ = 0.26 gives $K_a^{cluster-H^+}$ = 1.25 x $10^{-18}$ and therefore a p$K_a$ of 17.9 for the protonated cluster.

Similar kinetics have been observed for $[Fe_4S_4X_4]^{2-}$ (X = SEt, $SBu^t$ and SPh) [14]. In all these clusters it has been suggested that the substitution occurs by a dissociative mechanism because the rate is independent of the concentration of nucleophile. The mechanism and associated rate law is shown in Figure (5.4). In contrast, for $[Fe_4S_4X_4]^{2-}$ where X = Cl or Br, the kinetics of the acid-catalysed substitution reactions also exhibit a non-linear dependence on $[NHEt_3^+]/[NEt_3]$ but exhibit a first order dependence on the concentration of nucleophile, suggesting an associative substitution pathway (Figure 5.4).

The interesting feature about all these studies is that protonation of the cluster facilitates both associative and dissociative substitution reactions. This is unusual, especially since the site of protonation is remote from the terminal ligand. It would be anticipated that the electron-pulling effect of the positive charge from the protonation would have different effects on the lability of different types of donors. It is difficult to rationalise the observed behaviour with the simple mechanisms shown in Figure (5.4). Another anomalous characteristic is that the p$K_a$ calculated for $[Fe_4S_4H(OPh)_4]^-$ is typical of all $[Fe_4S_3(SH)X_4]^-$ (X = SPh, p$K_a$ = 18.6; X = SEt, p$K_a$ = 18.0; X = $SBu^t$, p$K_a$ = 17.9; X = Cl, p$K_a$ = 18.8; X = Br, p$K_a$ = 18.8). The p$K_a$s of all protonated synthetic Fe-S-based clusters fall in the narrow range p$K_a$ = 17.9 – 18.9 [15], irrespective of the cluster composition. Furthermore, the $[Fe_2S_2Cl_4]^{-2}$ cluster also has a p$K_a$ in the same range [16]. This is unexpected since $[Fe_4S_4X_4]^{-2}$ contains only triply-bridging sulfurs ($\mu_3$-S), while $[Fe_2S_2Cl_4]^{-2}$ contains only doubly-bridging sulfurs (μ-S), and these structurally different sulfur atoms would be expected to have different basicity. Finally, it is worth noting that the rates of protonation of $[Fe_2S_2Cl_4]^{2-}$ and $[Fe_4S_4Cl_4]^{2-}$ are considerably less than the diffusion-controlled limit even for thermodynamically-favourable reactions ($k \leq$ 1x $10^7$ $dm^3$ $mol^{-1}$ $s^{-1}$) [17], and show no significant primary isotope effect [18].

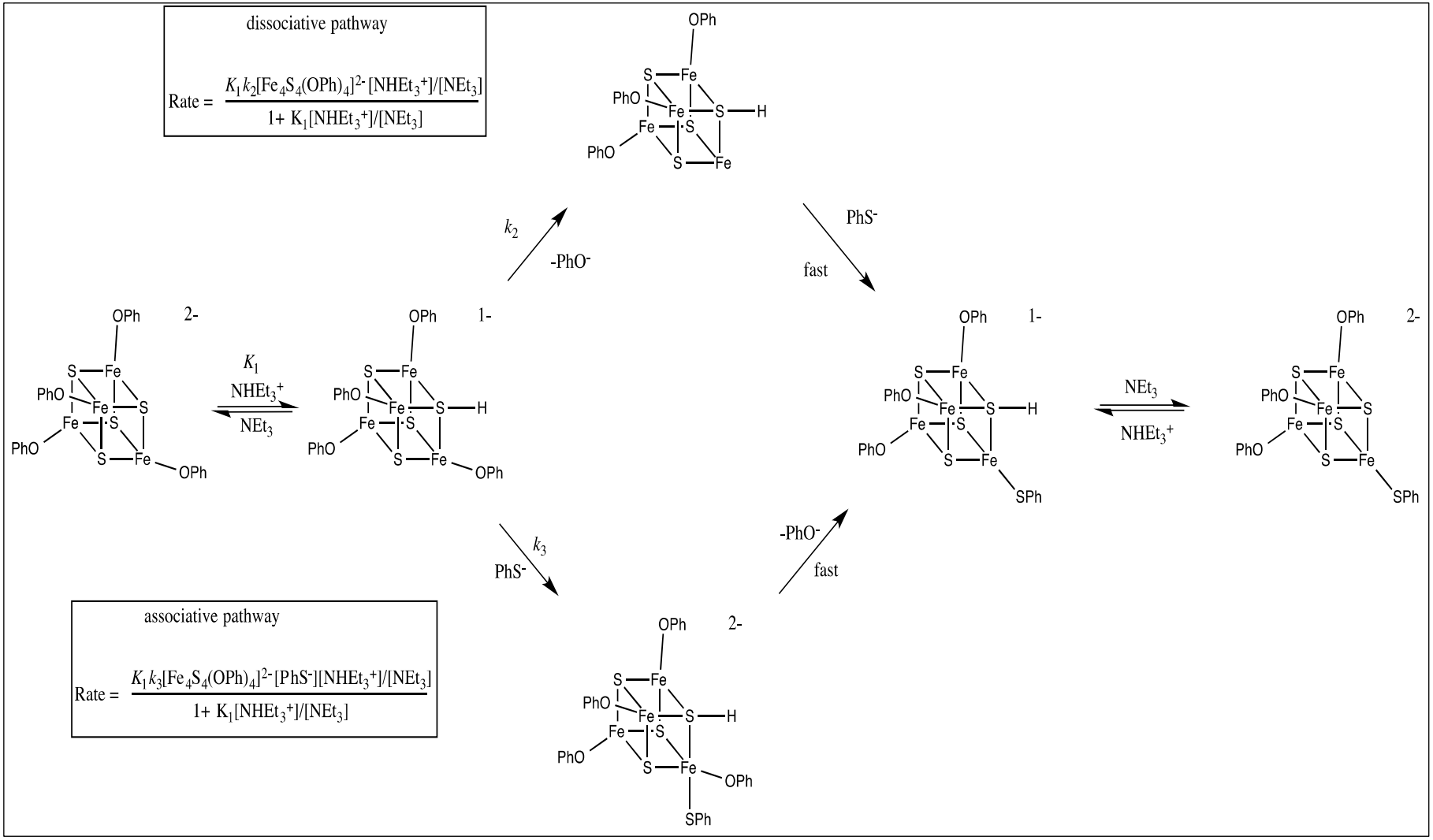


Figure 5.4. Suggested mechanisms for the acid-catalysed substitution reactions of $[Fe_4S_4X_4]^{2-}$ prior to DFT calculations.

Recent theortical investigation [19] has been performed by Professor Ian Dance, School of Chemistry, University of New South Wales, Sydney, Australia (Density functional simulations [20] were performed using DMol3 [21], the blyp functional, numerical basis sets (dnp), unrestricted spins, and fine integration grid) of the protonation of the active site of the nitrogenase enzyme that showed that $\mu_3$-S-Fe bond will be elongate on protonation and becomes doubly-bridging $\mu_2$-SH-Fe bond upon protonation as shown in Figure (5.5). This result suggested that protonation of $\mu_3$-S in $[Fe_4S_4X_4]^{2-}$ should also be investigated, to establish whether a similar disruption to the structure of the cluster core occurs.

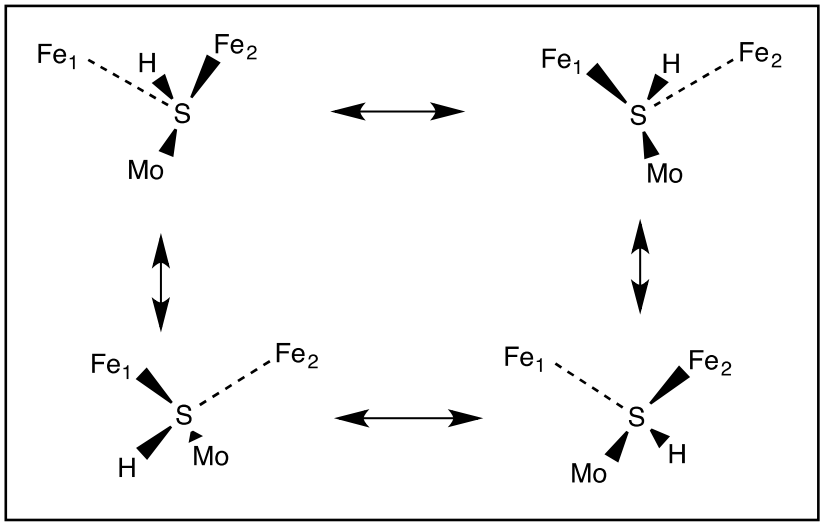


Figure 5.5. The four trigonal pyramidal conformers of S-H after protonation of Sulfur site in the cluster.
.

The result from the calculations is that, upon protonation a $\mu_3$-S-Fe bond elongates or breaks in all $[Fe_4S_4X_4]^{2-}$ (X = phenoxide, halide or thiolate) to $\mu_3$-SH in $[Fe_4S_3(SH)X_4]^-$ as shown in Figure (5.6) for the two conformations calculated for $[Fe_4S_3(SH)X_4]^-$. The SH function has pyramidal trigonal stereo chemistry, and the distance of the Fe-S bond changed from ca 2.3 Å to at least 2.85 Å in the most stable electronic states. The changing in the structure with protonation of the cluster $[Fe_4S_4X_4]^{2-}$ is reversible.

This result suggests simple explanations for the enigmatic reactivity observed with these clusters. The unexpectedly slow rate of proton transfer to $[Fe_4S_4X_4]^{2-}$ is now more understandable, because the measured or estimated rate constant does not correspond to the simple transfer of a proton from acid to $\mu_3$-S, but rather is a proton transfer step coupled to elongation/cleavage of an Fe–S bond. For the same reason there is no significant isotope effect. Moreover, it is now clear that the similarity in the p$K_a$s of $\mu_3$-SH and μ-SH is illusory. The apparent p$K_a$ values measured for protonation of

$[Fe_4S_4X_4]^{2-}$ (containing only $\mu_3$-S) are, in fact, not true p$K_a$s because the process being measured is protonation of a $\mu_3$-S coupled to cleavage of an Fe–S bond. In contrast, the p$K_a$s measured for $[Fe_2S_2X_2]^{2-}$ (containing only μ-S) are true p$K_a$s since the reaction only involves protonation of a μ-S.

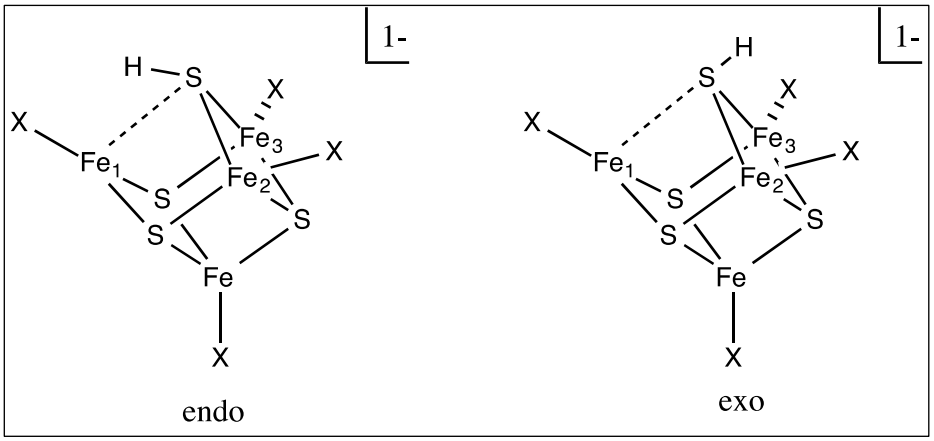


Figure 5.6. Endo and exo isomers of $[Fe_4S_3(SH)X_4]^-$.

The results of the DFT [18] calculations suggest a reason for the enigmatic reactivity observed with cluster upon protonation. Thus, the unexpected slow rate of proton transfer to $[Fe_4S_4X_4]^{2-}$ is because the measured rate constant will correspond to the coupled transfer of a proton from acid to $\mu_3$-S and the S-Fe bond cleavage. Furthermore, it is now clear that the calculated p$K_a$s for the protonated clusters are not valid because the measured equilibrium constant corresponds to protonation of a $\mu_3$-S with cleavage of a Fe-S bond, rather than the simple addition of a proton. The calculations also indicate that protonation of $\mu_3$-S will make Fe in the cluster $[Fe_4S_3(SH)(OH)_4]^-$ essentially planar three-coordination, therefore, it might be anticipated that this Fe becomes more susceptible to binding of nucleophiles than is the four coordinate Fe in the parent $[Fe_4S_4X_4]^{2-}$. The general mechanism for the protonation and substitution reactions of $[Fe_4S_4X_4]^{2-}$ , incorporating the Fe-S bond cleavage step is shown in Figure (5.7). That protonation of $[Fe_4S_4X_4]^{2-}$ involves formation of a three coordinate Fe site suggests that this site will undergo substitution by an associative mechanism. To accommodate this proposal, it has been suggested that the substitution mechanism of $[Fe_4S_3(SH)X_4]^-$ (X = SEt, $SBu^t$ and SPh; where the rate of substitution is independent of the concentration of nucleophile) is not a dissociative pathway but rather involves attack by the solvent MeCN to produce a solvento-intermediate and the solvent ligand is subsequently rapidly replaced by $PhS^-$. For $[Fe_4S_4X_4]^{2-}$ (X = Cl or Br; where the rate of substitution depends on the concentration of PhSH), it has been suggested that because the coordinated halide is much

more labile, displacement of halide by MeCN is fast and displacement of the coodinated solvent by PhSH becomes rate-limiting.

In summary, the key features of the mechanism in Figure (5.7) are: (1) protonation of $\mu_3$-S generates a three-coordinate Fe site which is primed to be the site of substitution because it is susceptible to attack by a nucleophile; (2) coordination of acetonitrile (present as solvent) to the three-coordinate Fe prior to dissociation of $X^-$; (3) displacement of coordinated MeCN by PhSH.

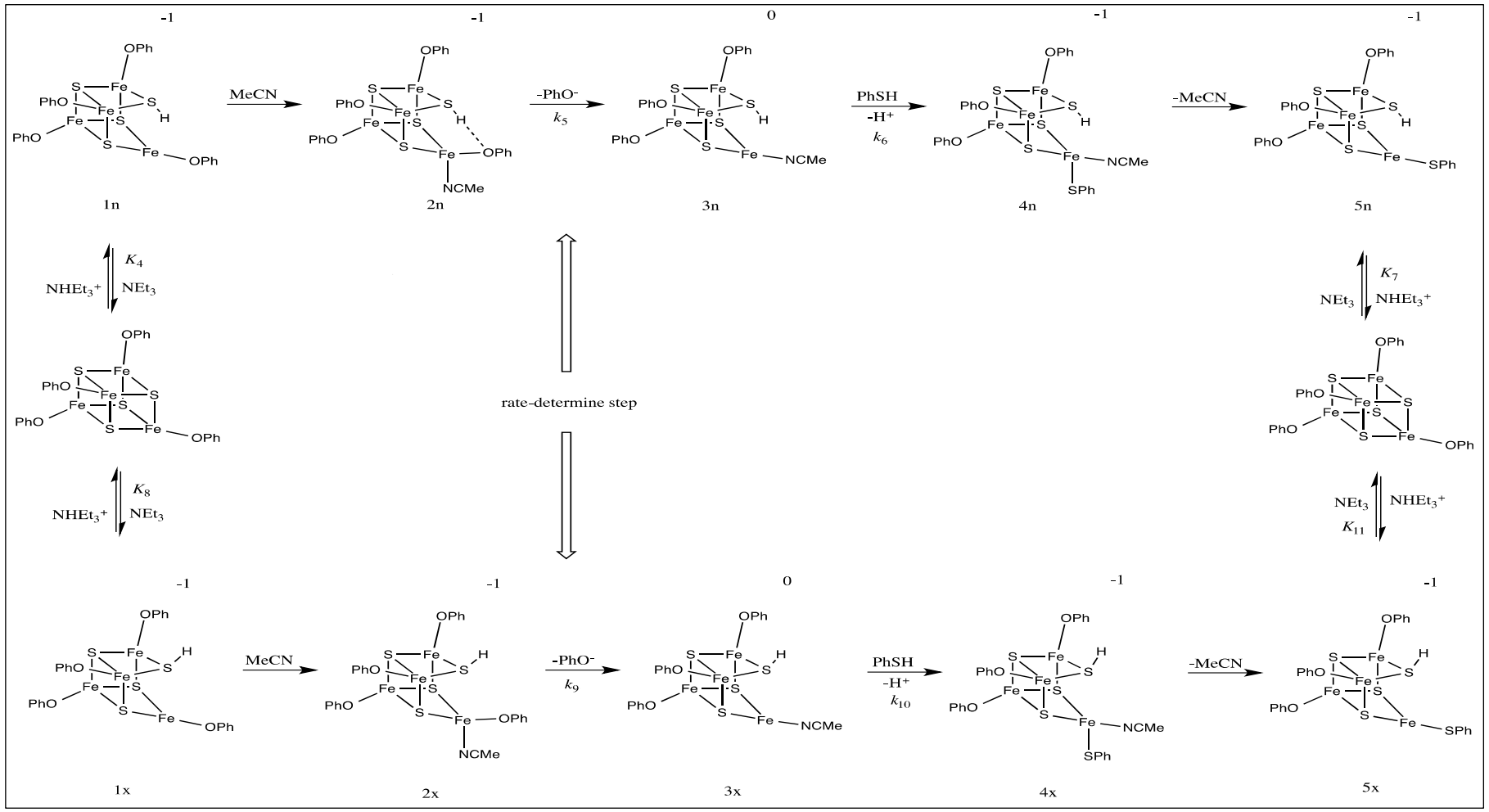


Figure 5.7. The proposed mechanism for acid-catalyzed substitution of $[Fe_4S_4(OPh)_4]^{2-}$ to form $[Fe_4S_4(OPh)_3(SPh)]^{2-}$ in MeCN, passing through either endo or exo $[Fe_4S_3(SH)(OPh)_4]^-$. The structures of all intermediates have been confirmed by DFT optimisation.

## 5.3.2 Kinetics of the reaction of $[\{MoFe_3S_4(OPh)_3\}_2((\mu\text{-}SPh)_3]^{3-}$ with $PhS^-$ in the presence of $NHEt_3^+$.

The effect of Mo on the reactivity of Fe cluster has been studied previously [3], and in clusters of the type $[\{MoFe_3S_4Y_3\}_2(\mu\text{-}X)_3]^{3-}$(Y = Cl, SPh or SEt and X = SEt or SPh) it has been shown that the bridging thiolate ligands do not undergo substitution. Although $[\{MoFe_3S_4Y_3\}_2(\mu\text{-}X)_3]^{3-}$ are structurally simpler than the FeMo-cofactor, kinetics studies on the clusters, $[\{MoFe_3S_4Y_3\}_2(\mu\text{-}X)_3]^{3-}$, will provide insights into how the Mo in FeMo-cofactor may modulate the substitution, substrate binding and protonation characteristics of Fe-S-based clusters [22].

The kinetics of the reaction of $[\{MoFe_3S_4(OPh)_3\}_2(\mu\text{-}SPh)_3]^{3-}$ with $PhS^-$ (2.5, 5.0 and 10 mmol $dm^{-3}$) in the presence of an excess of $[NHEt_3]^+$ (2.5 – 40 mmol $dm^{-3}$) have been studied. The absorbance-time traces were good fits to double exponentials. The values of $k_{obs1}$ and $k_{obs2}$ were found to vary with the concentration of PhSH and $[NHEt_3]^+$ in a manner similar to that described above for $[Fe_4S_4(OPh)_4]^{2-}$. This behaviour (for the first phase of the reaction) is shown in Figure (5.8).

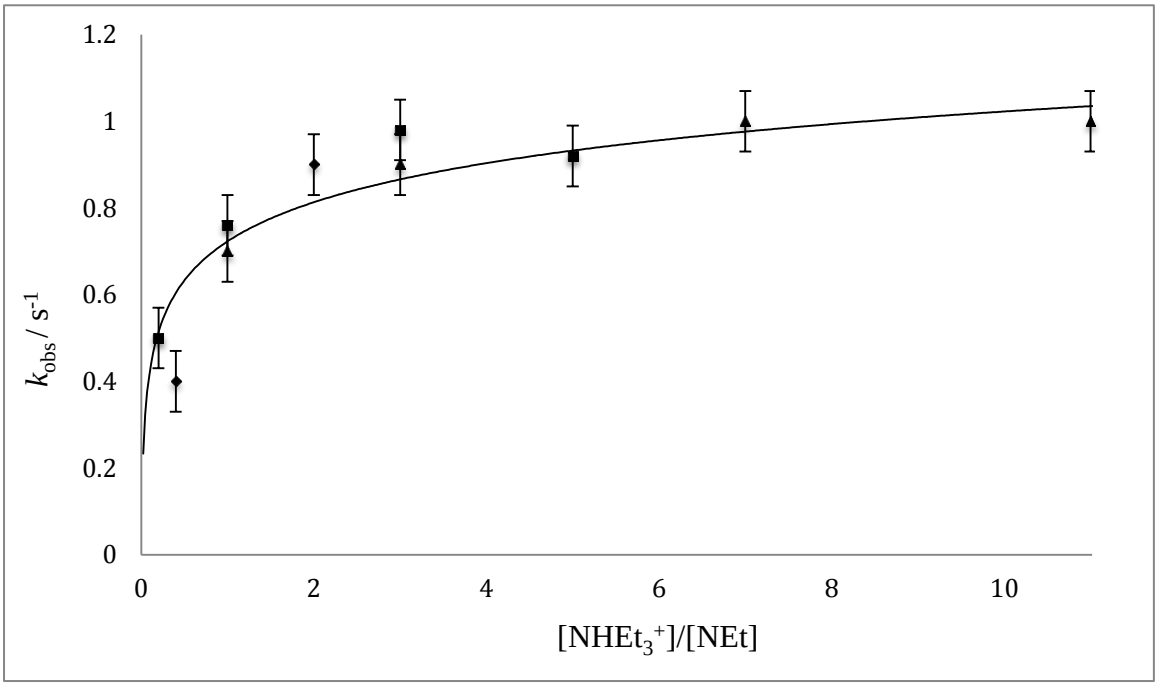


Figure 5.8. Dependence of $k_{obs}$ on the ratio $[NHEt_3^+]/[NEt_3]$ for the reaction of $[\{MoFe_3S_4(OPh)_3\}_2((\mu\text{-}SPh)_3]^{3-}$ with PhSH in MeCN at 25 °C. Data points correspond to: $[PhS^-]$ = 2.5 mmol dm-3, $[NHEt_3^+]$ = 2.5 – 30 mmol dm-3 (■); $[PhS^-]$ = 5.0 mmol dm-3, $[NHEt_3^+]$ = 2.5 – 30 mmol dm-3 (▲);$[PhS^-]$ = 10.0 mmol dm-3, $[NHEt_3^+]$ = 10 - 40 mmol dm-3 (♦). The curve is defined by equation 5.21. The error bar corresponded to 5% deviation.

Analysis of the data in Figure (5.8) leads to the rate law shown in Equation (5.21).

$$Rate = \left\{ 0.38 + \frac{1.31\,\frac{[\mathrm{NHEt_3^+}]}{[\mathrm{NEt_3}]}}{1 + \ 1.43\,\frac{[\mathrm{NHEt_3^+}]}{[\mathrm{NEt_3}]}} \right\} [cluster] \qquad (5.21)$$

From mechanism of the reaction of $[\{MoFe_3S_4(OPh)_3\}_2(\mu\text{-}SPh)_3]^{3-}$ with $PhS^-$ in the presence of $[NHEt_3]^+$ which is associated with the data in Figure (5.8) is similar to the mechanism of $[Fe_4S_4X_4]^{2-}$ in Figure (5.7) and the rate law which is a match with the mechanism in Figure (5.7) is given by Equation (5.22). The derivation of Equation (5.22) in the same way for $[Fe_4S_4X_4]^{2-}$.

$$\mathrm{Rate} = \left\{ \frac{K_1^R k_2^R\,\frac{[\mathrm{NHEt_3^+}]}{[\mathrm{NEt_3}]}}{1 + \ K_1^R\,\frac{[\mathrm{NHEt_3^+}]}{[\mathrm{NEt_3}]}} \right\} [\mathrm{cluster}] \qquad (5.22)$$

The comparison of equation 5.21 with equation 5.22 the value of $K_1$ and $k_2$ can be found, 1.43 and 0.91 respectively. The p$K_a$ of the cluster (18.66) can be calculated using Equation (5.7) and using the value of the p$K_a$ for $[NHEt_3]^+$ in MeCN (18.46) [14].

Comparison of the result with those $[Fe_4S_4(OPh)_4]^{2-}$ indicate. Firstly the equilibrium constants for a $PhS^-$ ion binding to the cluster is 7 times greater for the $[\{MoFe_3S_4(OPh)_3\}_2(\mu\text{-}SR)_3]^{3-}$ clusters than the $[Fe_4S_4(OPh)_4]^{2-}$ cluster. The increased affinity is a result of both an increase in the rate of binding ($k_1$) and a decrease in the rate of dissociation ($k_{-1}$) [23]. Such behaviour is general and has been noted for the binding of a variety of molecules and ions (halides and $PhS^-$) [24]. Secondly, a comparison of the proton transfer values show the proton transfer from $[NHEt_3]^+$ to the cluster is affected by the presence of Mo with proton transfer to the Mo di-cubane clusters being slower than to the $[Fe_4S_4(OPh)_4]^{2-}$ cluster.

## 5.4 Conclusions.

In this chapter the substitution and protonation reactions of the cuboidal $[Fe_4S_4(OPh)_4]^{2-}$ and dicubane $[\{MoFe_3S_4(OPh)_3\}_2(\mu\text{-}SPh)_3]^{3-}$ clusters are presented. Previous studies have shown that the bridging thiolate ligands in dicubane clusters do not undergo substitution [3] and so in both $[Fe_4S_4(OPh)_4]^{2-}$ and $[\{MoFe_3S_4(OPh)_3\}_2(\mu\text{-}SPh)_3]^{3-}$ the substitution reactions are limited to the Fe-OPh sites. For both clusters the reactions with mixtures of $NHEt_3^+$ and $PhS^-$ were studied. The observed kinetics are similar to those observed with other Fe-S-based clusters using the same system and exhibit a non-linear dependence on the ratio $[NHEt_3^+]/[NEt_3]$ but are independent of the concentration of nucleophile (PhSH). This kinetics suggests an acid-catalyzed substitution mechanism. In line with earlier studies it is suggested that a $\mu_3$-S on the cluster is protonated and this is followed by the rate-limiting dissociation of a phenoxide ligand.

Recent DFT calculations (by Dance) indicate that Fe–S clusters undergo large structural changes {cleavage of the Fe-($\mu_3$-SH)} when protonated at a $\mu_3$-S. The kinetic results reported in this chapter are discussed in the light of this proposal.

## 5.5 References.


1. *Recent Advances in Hydride Chemistry*; Peruzzini, M., Poli, R., Eds.; Elsevier: Amsterdam, **2001**; Chapters 2.
2. S. C. Lee and R. H. Holm, *Chem. Re*v. **2005**, 104, 135.
3. R. E. Palermo, P. P. Power and R. H. Holm, *Inorg. Chem*., **1982**, 21, 173.
4. J. R. Dilworth, R. A. Henderson, P. Dahlstrom, T. Nicholson and J. A. Zubieta, *J. Chem. Soc., Dalton Trans.* **1987**, 529.
5. G. Christou and C. D. Garner. *J.Chem.Soc. Dalton Trans*., **1979**, 1093.
6. G.B. Wong, M.A. Bobrick and R.H. Holm., *Inorg.Chem*., **1978**, 17, 578.
7. W. E. Cleland, D. A. Holtman, M. Sabat, A. James and B. A. Averill; *J. Am. Chem. Soc.*, **1983** 105 (19), 6021.
8. G. Christou and C. D. Garner, *J.Chem.Soc., Dalton Trans*., **1980**, 2354.
9. T. Herskovitz, B.A. Averill, R. H. Holm, J. A. Ibers, W. D. Phillips and J. F. Weiher, *Proc. Natl. Acad. Sci. U. S. A*., **1972**, 69, 2437
10. R. A. Henderson, *Chem. Rev*., **2005**, 105, 2365
11. K. Izutsu, *Acid - Base Dissociation Constants in Dipolar Aprotic Solvents*. Blackwell Scientific: Oxford, U.K., **1990**.
12. R. H. Holm, S. Ciurli and J. A. Weigel, *Prog. Inorg. Chem*., **1990**, 38, 1
13. R. G. Wilkins, *Kinetics and Mechanism of Reactions of Transition Metal Complexes*. VCH: Weinheim, **1991**; p 24.
14. J. Dunford and R. A. Henderson, *Chem. Commun.*, **2002**, 360.
15. A. Alwaaly, I Dance and R. A. Henderson, *Chem. Commun*., **2014**, 50, 4799.
16. R. A. Henderson, *Bioinorg. React. Mech*., **2012**, 8, 1.
17. R. A. Henderson and K. E. Oglieve, *J. Chem. Soc., Dalton Trans*., **1999**, 3927.
18. A. J. Dunford, and R. A. Henderson, *J. Chem. Soc., Dalton Trans*., **2002**, 2837
19. I, Dance, *Inorg. Chem*., **2013**, 52, 13068.
20. I, Dance, *J. Am. Chem. Soc.* **2005**, 127, 10925.
21. B. Delley, *J. Chem. Phys*. **1990**, 92, 508.
22. J. Bell, A. J. Dunford, E. Hollis and R. A. Henderson, *Angew. Chem. Int. Ed.* **2003,** 42, 1149.
23. R. A. Henderson, *Chem. Rev.* **2005**, 2365.
24. R. A. Henderson, and K. E. Oglieve, *J. Chem. Soc., Dalton Trans.* **1993**, 1473.

# Chapter Six: Conclusion

## 6.1 General Conclusions.

The work presented in this thesis has covered some aspects of the kinetic and mechanistic chemistry of the substitution and protonation chemistry of Ni-thiolate complexes and Fe-S-based clusters which have a cuboidal structure: $\{Fe_4S_4\}$ or $\{MoFe_3S_4\}$. This work is part of a longer-term investigation into the intrinsic reactivity associated with these types of compounds.

In the first chapter an overview of the importance of protonation reactions at metal sites in biological systems was presented which laid the foundations for the work presented in later chapters of the thesis. Throughout the thesis a summary of the most important points in each chapter has been presented. Here the key results are summarized with indications of possible future work.

In chapter 2 studies on $[Ni(S_2CR)(triphos)]^+$ are presented. The rates of protonation of coordinated carboxydithioates by HCl in MeCN are *ca.* $10^7 - 10^{10}$ slower than the diffusion-controlled limit ($k_{diff} \sim 3.7 \times 10^{10}$ dm$^3$ mol$^{-1}$ s$^{-1}$ in MeCN) [(1)]. The reason for the slowness is the reactions are thermodynamically-unfavourable. Although the slow proton transfer observed in the reactions of $[Ni(XPh)(triphos)]^+$ (X = O, S or Se) [(2)] with $lutH^+$ has been attributed to unfavourable steric interactions between the $lutH^+$ and the phenyl group on the triphos ligand, it seems unlikely that with the smaller HCl such issues are relevant.

The kinetics for the protonation of $[Ni(S_2CR)(triphos)]^+$ (R = alkyl or aryl) with HCl has been investigated and the results indicate a two-step equilibrium mechanism. The initial step involves the rapid formation of a hydrogen-bonded precursor ($K_1^R$) and this is followed by intramolecular proton transfer ($k_2^R$) as shown in Figure (6.1) and the rate law associated with this mechanism is shown in Equation (6.1). The kinetic isotope effects measured for the complete transfer of a proton from HCl to $[Ni(S_2CR)(triphos)]^+$ (R = Me, Et or Bu$^n$) are small $\{(K_1^R k_2^R)^H / (K_1^R k_2^R)^D = 0.79–1.14\}$. This is the result of a small inverse equilibrium isotope effect for the formation of the precursor hydrogen-bonded adduct $\{(K_1^R)^H / (K_1^R)^D = 0.44–0.85\}$ and a significant kinetic primary isotope effect for the intramolecular proton transfer step $\{(k_2^R)^H / (k_2^R)^D = 1.33–1.81\}$. Finally, DFT calculations indicate that protonation can occur at either the equatorial or the axial sulfur sites, but that chelate ring opening of the carboxydithionic acid occurs only after protonation of the equatorial sulfur.

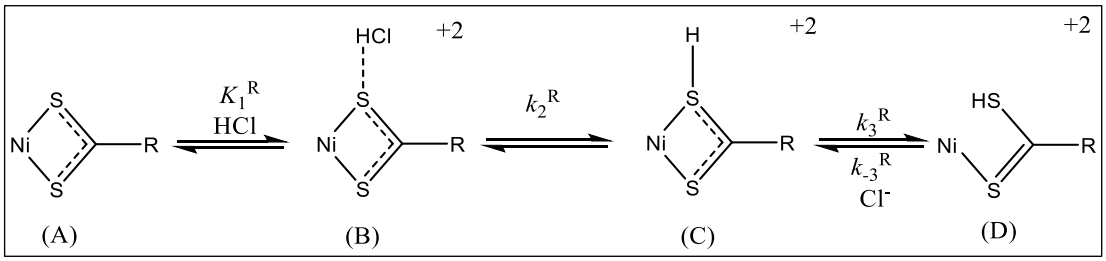


Figure 6.1. Mechanisms of protonation of $[Ni(S_2CR)(triphos)]^+$ (R = Me, Et , $Bu^n$ or Ph).

$$\text{Rate} = \{\frac{K_1^R k_2^R[\text{acid}]}{1 + K_1^R[\text{acid}]} + k_{-2}^R[\text{base}]\}[\text{Ni} - \text{thiolate}] \qquad (6.1)$$

For comparison, the protonation of $[Ni(O_2CR)(triphos)]^+$ have been studied. The reactions are much faster and require the use of the weaker acid $lutH^+$ for the reactions to be studied by the stopped-flow technique. The mechanism is the same as shown for carboxydithiolate and the rate law is analogous to that shown for carboxydithiolate but that $K_1^R < 1$ (no accumulation of the hydrogen bonded precursor intermediate) as show in Equation (6.2).

$$\text{Rate} = \{K_1^R k_2^R\ [lutH^+] + k_{-2}^R[lut]\}[Ni(O_2CPh)(triphos)^+] \qquad (6.2)$$

The rates of proton transfer to O $\{(K_1^{Et}k_2^{Et})^O/(K_1^{Ph}k_2^{Ph})^O = 1.4\}$ are less sensitive to the R-substituent than the rates of proton transfer to S $\{(K_1^{Et}k_2^{Et})^S/((K_1^{Ph}k_2^{Ph}))^S = 18$.

The basicity calculation indicate that the coordinated carboxylate is *ca* 3.2 x $10^6$ (R = Ph) and *ca* 0.6 x $10^6$ (R = Et) times more basic than the corresponding coordinated dithioate.

The work presented in this chapter focused on the reactivity of thiolate complexes (alkylthiolate and carboxydithioate) with Ni-triphos and Ni-dppe, and has focused mainly on studying the factor, which affect the protonation chemistry of Ni-triphos complexes. During these studies the dithiocarbamate complex $[Ni(S_2CNPh)(dppe)]$ was prepared. This complex has an interesting structure as shown (X-ray crystal structure) in Figure (6.2) where $C_7$-$S_1$ and $C_7$-$S_2$ are single bonds and $N_9$-$C_7$ is double bond.

The synthesis and study of the protonation reactions of $[Ni(S_2CNR_2)(triphos)]^+$ and $[Ni(S_2CNR)(triphos)]$ would be worthwhile to explore further some of the features that were observed in the dithioate complexes (*i.e.* chelate ring-opening upon protonation and the consequences of protonating different sulfur sites in trigonal bipyramidal complexes).

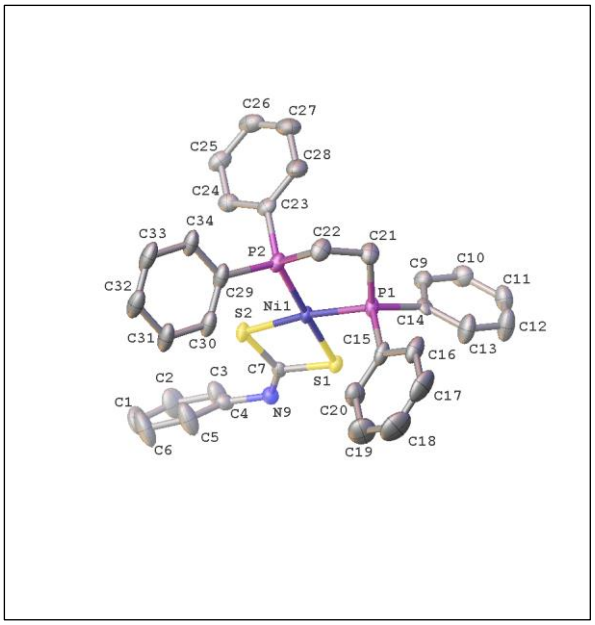


Figure 6.2. X-ray crystal structure for [Ni($S_2$CNPh)(dppe)]

In chapter 3 the kinetics of the protonation reactions of [Ni(SR)(triphos)]$^+$ and [Ni(SR)$_2$(dppe)] (R = Et, Cy or Bu$^t$) with lutH$^+$ are discussed, which are all equilibrium reactions. The kinetics of the reactions of both [Ni(SR)(triphos)]$^+$ and [Ni(SR)$_2$(dppe)] are consistent with a single mechanism in which initial hydrogen bond formation between lutH$^+$ and the complex is followed by intramolecular proton transfer. This mechanism has been described before for the reactions of the analogous aryl thiolate complexes, [Ni(SAr)(triphos)]$^+$ [3] and [Ni(SAr)$_2$(dppe)] [4].

The most notable feature of the kinetics of the protonation reactions of [Ni(SR)(triphos)]$^+$ and [Ni(SR)$_2$(dppe)] is the different rate laws observed when comparing the analogous alkyl and aryl thiolate complexes. [Ni(SR)$_2$(dppe)] shows the full form of the rate law {Equation (6.1)} but [Ni(SR)(triphos)]$^+$ shows the simpler rate law {Equation (6.2)}. The different rate laws are a consequence of the strength of the association of lutH$^+$ with the complex.

The kinetic isotope reaction of [Ni(SR)(triphos)]$^+$ (R = Et, Cy or Bu$^t$) with lutD$^+$ has been studied and shows that the reaction is associated with a normal kinetic isotope effect $(k_1^H/k_1^D)$ , 25°C (But = 1.3, Et = 5.9, Cyh = 17.1) in comparison with previous studies on the reaction of [Ni(SC$_6$H$_4$-R)(triphos)]$^+$ (R = MeO, CH$_3$, H, Cl or NO$_2$) where the isotope effect depends on type of substituent.

The rates of proton transfer between [Ni(XPh)(triphos)]$^+$ (X = O, S, Se) and lutH$^+$ are markedly slower than the diffusion-controlled rate ($k_{diff}$ ~ 3.7 x 10$^{10}$ dm$^3$ mol$^{-1}$ s$^{-1}$), and

essentially the same for each complex. DFT calculation indicate that the reason for this behaviour is because steric factors make it difficult for the acid to position itself correctly in preparation for proton transfer.

Further work in this area should explore further the ability to control the rates of proton transfer because of steric effects. It would be of interest to study the reactions of $[Ni(XPh)(triphos)]^+$ (X = O, S or Se) with the series of acids $NHMe_3^+$, $NHEt_3^+$ and $NHBu^n{}_3^+$. These acids all have approximately the same p$K_a$ (17.8 – 18.4) but the length of the alkyl groups varies the steric factors. Other work would be to study complexes of the type $[Ni(SAr)(triphos)]^+$ where Ar = 2-substituted phenyl and 2,6-disubstituted phenyl groups, to investigate whether the substituents interact with the nickel site and modulate its reactivity.

The final chapter of the thesis focuses on the substitution reactions of Fe-S-based clusters with phenoxide ligands: the cuboidal $[Fe_4S_4(OPh)_4]^{2-}$ and Mo dicubane $[\{MoFe_3S_4(OPh)_3\}_2(\mu\text{-}SPh)_3]^{3-}$. The reactions of these clusters with $PhS^-$ in the presence of $NHEt_3^+$ result in the replacement of the phenoxide ligands by $PhS^-$ Both clusters follow the same mechanism which involves rapid protonation of the cluster (presumanbly at a $\mu_3$-S site), followed by rate-limiting substitution of a phenoxide ligand.

Density functional calculations suggest that Fe–S clusters undergo unexpected large structural changes when protonated at $\mu_3$-S. Thus, it is proposed that protonation of all cuboidal $[Fe_4S_4X_4]^2$ to $[Fe_4S_3(SH)X_4]^-$ (X = Cl, SR, OR) results in formation of doubly-bridging SH, severance of one Fe–S bond, and creation of a three-coordinate Fe. The kinetics of the acid-catalysed substitution reaction of $[Fe_4S_4(OPh)_4]^{2-}$ are discussed in the light of the DFT calculations.

## 6.2 References.


1. F. Wilkinson, A. F. Olea, D. J. McGarvey and D. R. Worrall, *J. Braz. Chem. Soc*., **1995**, 6, 211.
2. A. Alwaaly and R. A. Henderson, *Chem. Commun*., **2014**, 50, 9669.
3. A. Valerie, M. Z. Pedro, P. Athinoula, R. A. Henderson, R. W. Harrington and W. C. Clegg, *Inorg. Chem.*, **2004**, 43, 3106.
4. Valerie A.; Pedro M. Z.; Athinoula P.; Henderson, R. A.; Harrington R. W.; Clegg, W. C., *Inorg. Chem.*, **2004**, 43, 3098.

# Appendix A: Kinetic data

## Chapter two

Table A2.1. Kinetic data of for the reaction of [Ni($S_2$CR)(triphos)] with HCl (R = Me, Et, $Bu^n$) in $CH_3CN$ at 25˚C.

| R | [HCl] /mmol $dm^{-3}$ | $k_{obs}$ /$s^{-1}$ |
|---|---|---|
| Me | 5 | 17.12 |
| Me | 10 | 22.4 |
| Me | 20 | 35.39 |
| Me | 30 | 37.19 |
| Me | 40 | 31.55 |
| Me | 60 | 37.83 |
| Me | 80 | 53.56 |
| Me | 100 | 45.53 |

| R | [HCl] /mmol $dm^{-3}$ | $k_{obs}$ /$s^{-1}$ |
|---|---|---|
| Et | 2.5 | 0.1 |
| Et | 5 | 0.14 |
| Et | 10 | 0.2 |
| Et | 20 | 0.27 |
| Et | 30 | 0.33 |
| Et | 40 | 0.35 |
| Et | 50 | 0.4 |
| Et | 60 | 0.38 |
| Et | 80 | 0.4 |
| Et | 100 | 0.43 |

| R | [HCl] /mmol $dm^{-3}$ | $k_{obs}$ /$s^{-1}$ |
|---|---|---|
| $Bu^n$ | 2.5 | 0.08 |
| $Bu^n$ | 5 | |
| $Bu^n$ | 10 | 0.11 |
| $Bu^n$ | 20 | 0.13 |
| $Bu^n$ | 30 | 0.18 |
| $Bu^n$ | 40 | 0.19 |
| $Bu^n$ | 50 | 0.194 |
| $Bu^n$ | 60 | 0.2 |
| $Bu^n$ | 80 | 0.21 |

Table A2.2. Kinetic data of for the reaction of [Ni($S_2$CR)(triphos)] with HCl/DCl (R = Me, Et, $Bu^n$) in $CH_3CN$ at 25˚C.

| R | [XCl] /mmol $dm^{-3}$ | $k_{obs}^{H}$ /$s^{-1}$ | $k_{obs}^{D}$ /$s^{-1}$ |
|---|---|---|---|
| Me | 5 | 0.11 | 0.12 |
| Me | 10 | 0.12 | 0.24 |
| Me | 20 | 0.16 | 0.30 |
| Me | 30 | 0.16 | 0.37 |
| Me | 50 | 0.23 | 0.39 |

| R | [XCl] /mmol $dm^{-3}$ | $k_{obs}^{H}$ /$s^{-1}$ | $k_{obs}^{D}$ /$s^{-1}$ |
|---|---|---|---|
| Et | 2.5 | 0.14 | 0.08 |
| Et | 5 | 0.20 | 0.12 |
| Et | 10 | 0.24 | 0.12 |
| Et | 20 | 0.32 | 0.16 |
| Et | 30 | 0.35 | 0.16 |
| Et | 40 | 0.39 | 0.25 |
| Et | 60 | 0.34 | 0.23 |

| R | [XCl] /mmol $dm^{-3}$ | $k_{obs}^{H}$ /$s^{-1}$ | $k_{obs}^{D}$ /$s^{-1}$ |
|---|---|---|---|
| $Bu^n$ | 5 | | 0.053 |
| $Bu^n$ | 10 | 0.11 | 0.03 |
| $Bu^n$ | 20 | 0.13 | 0.24 |
| $Bu^n$ | 30 | 0.18 | 1.01 |
| $Bu^n$ | 40 | 0.19 | 0.2322 |
| $Bu^n$ | 60 | 0.194 | 0.22 |
| $Bu^n$ | 80 | 0.2 | 0.223 |
| $Bu^n$ | 100 | 0.21 | 0.2 |

Table A2.3. Kinetic data of for the reaction of [Ni($S_2$CR)(triphos)] with HCl in the presence of $Cl^-$ (R = Me, Et, $Bu^n$) in $CH_3CN$ at 25˚C.

| R | $[HCl]_0$ /mmol $dm^{-3}$ | $[Cl^-]_0$ /mmol $dm^{-3}$ | $[HCl]_e$ /mmol $dm^{-3}$ | $[Cl^-]_e$ /mmol $dm^{-3}$ | $k_{obs}$ /$s^{-1}$ |
|---|---|---|---|---|---|
| Me | 50 | 2.5 | 0.0478 | 0.00029 | 72.3 |
| Me | 50 | 5 | 0.0456 | 0.00061 | 64.2 |
| Me | 50 | 10 | 0.0413 | 0.00132 | 58.7 |
| Me | 50 | 20 | 0.0332 | 0.0032 | 48.4 |
| Me | 50 | 30 | 0.0259 | 0.0059 | 38.9 |
| Me | 50 | 50 | 0.0149 | 0.0149 | 26.8 |
| Me | 100 | 2.5 | 0.0976 | 0.00006 | 77.1 |
| Me | 100 | 5 | 0.0953 | 0.00032 | 65 |
| Me | 100 | 10 | 0.0907 | 0.00066 | 57.9 |
| Me | 100 | 20 | 0.0814 | 0.00144 | 56.6 |
| Me | 100 | 30 | 0.0724 | 0.00241 | 48.6 |
| Me | 100 | 50 | 0.055 | 0.005 | 40.7 |

| R | [HCl] /mmol $dm^{-3}$ | $[Cl^-]$ /mmol $dm^{-3}$ | $[HCl]_e$ /mmol $dm^{-3}$ | $[Cl^-]_e$ /mmol $dm^{-3}$ | $k_{obs}$ /$s^{-1}$ |
|---|---|---|---|---|---|
| Et | 25 | 1 | 0.0242 | 0.0002 | 0.37 |
| Et | 25 | 2.5 | 0.023 | 0.00053 | 0.4 |
| Et | 25 | 5 | 0.0212 | 0.00115 | 0.69 |
| Et | 25 | 10 | 0.0176 | 0.00264 | 1.34 |
| Et | 50 | 2.5 | 0.0478 | 0.00029 | 0.5 |
| Et | 50 | 5 | 0.0456 | 0.00061 | 0.5 |
| Et | 50 | 10 | 0.0413 | 0.00132 | 0.69 |
| Et | 50 | 20 | 0.0332 | 0.0032 | 1.4 |
| Et | 50 | 30 | 0.0259 | 0.0059 | 2.75 |
| Et | 100 | 2.5 | 0.0976 | 0.00006 | 0.39 |
| Et | 100 | 5 | 0.0953 | 0.00032 | 0.6 |
| Et | 100 | 10 | 0.0907 | 0.00066 | 0.85 |
| Et | 100 | 20 | 0.0814 | 0.00144 | 1.08 |
| Et | 100 | 30 | 0.0724 | 0.00241 | 1.24 |

| R | $[HCl]_0$ /mmol $dm^{-3}$ | $[Cl^-]_0$ /mmol $dm^{-3}$ | $[HCl]_e$ /mmol $dm^{-3}$ | $[Cl^-]_e$ /mmol $dm^{-3}$ | $k_{obs}$ /$s^{-1}$ |
|---|---|---|---|---|---|
| $Bu^n$ | 50 | 2.5 | 0.0477 | 0.00029 | 0.22 |
| $Bu^n$ | 50 | 5 | 0.045 | 0.0006 | 0.23 |
| $Bu^n$ | 50 | 10 | 0.0413 | 0.0013 | 0.29 |
| $Bu^n$ | 50 | 20 | 0.033 | 0.0031 | 0.43 |
| $Bu^n$ | 50 | 30 | 0.025 | 0.0058 | 0.58 |
| $Bu^n$ | 50 | 50 | 0.0148 | 0.014 | 1.2 |
| $Bu^n$ | 100 | 2.5 | 0.097 | 0.00015 | 0.21 |
| $Bu^n$ | 100 | 5 | 0.095 | 0.0003 | 0.24 |
| $Bu^n$ | 100 | 10 | 0.0906 | 0.00064 | 0.40 |
| $Bu^n$ | 100 | 20 | 0.081 | 0.0014 | 0.40 |

Table A2.4. Kinetic data of for the reaction of [Ni($S_2CC_6H_4R$-4)(triphos)] with HCl in the presence of $Cl^-$ (R = H, Me, OMe, Cl) in $CH_3CN$ at 25˚C.

| R | $[HCl]_0$ /mmol $dm^{-3}$ | $[Cl^-]_0$ /mmol $dm^{-3}$ | $[HCl]_e$ /mmol $dm^{-3}$ | $[Cl^-]_e$ /mmol $dm^{-3}$ | $k_{obs}$ /$s^{-1}$ |
|---|---|---|---|---|---|
| $C_6H_5$ | 100 | 1 | 0.099 | 0.00006 | 0.23 |
| $C_6H_5$ | 100 | 2.5 | 0.098 | 0.00012 | 0.28 |
| $C_6H_5$ | 100 | 5 | 0.097 | 0.00018 | 0.29 |
| $C_6H_5$ | 100 | 10 | 0.096 | 0.00024 | 0.48 |
| $C_6H_5$ | 100 | 15 | 0.095 | 0.00031 | 0.24 |
| $C_6H_5$ | 150 | 1 | 0.149 | 0.001 | 0.31 |
| $C_6H_5$ | 150 | 2.5 | 0.148 | 0.0025 | 0.3 |
| $C_6H_5$ | 150 | 5 | 0.147 | 0.005 | 0.31 |
| $C_6H_5$ | 150 | 10 | 0.146 | 0.01 | 0.34 |
| $C_6H_5$ | 150 | 15 | 0.145 | 0.015 | 0.25 |

| R | $[HCl]_0$ /mmol $dm^{-3}$ | $[Cl^-]_0$ /mmol $dm^{-3}$ | $[HCl]_e$ /mmol $dm^{-3}$ | $[Cl^-]_e$ /mmol $dm^{-3}$ | $k_{obs}$ /$s^{-1}$ |
|---|---|---|---|---|---|
| $C_6H_4$Me-4 | 100 | 1 | 0.099 | 0.00006 | 0.23 |
| $C_6H_4$Me-4 | 100 | 2.5 | 0.098 | 0.00012 | 0.28 |
| $C_6H_4$Me-4 | 100 | 5 | 0.097 | 0.00018 | 0.29 |
| $C_6H_4$Me-4 | 100 | 10 | 0.096 | 0.00024 | 0.48 |
| $C_6H_4$Me-4 | 100 | 15 | 0.095 | 0.00031 | 0.24 |
| $C_6H_4$Me-4 | 150 | 1 | 0.149 | 0.001 | 0.31 |
| $C_6H_4$Me-4 | 150 | 2.5 | 0.148 | 0.0025 | 0.3 |
| $C_6H_4$Me-4 | 150 | 5 | 0.147 | 0.005 | 0.31 |
| $C_6H_4$Me-4 | 150 | 10 | 0.146 | 0.01 | 0.34 |
| $C_6H_4$Me-4 | 150 | 15 | 0.145 | 0.015 | 0.25 |

| R | $[HCl]_0$ /mmol $dm^{-3}$ | $[Cl^-]_0$ /mmol $dm^{-3}$ | $[HCl]_e$ /mmol $dm^{-3}$ | $[Cl^-]_e$ /mmol $dm^{-3}$ | $k_{obs}$ /$s^{-1}$ |
|---|---|---|---|---|---|
| $C_6H_4OMe$-4 | 100 | 1 | 0.099 | 0.00006 | 0.23 |
| $C_6H_4OMe$-4 | 100 | 2.5 | 0.098 | 0.00012 | 0.28 |
| $C_6H_4OMe$-4 | 100 | 5 | 0.097 | 0.00018 | 0.29 |
| $C_6H_4OMe$-4 | 100 | 10 | 0.096 | 0.00024 | 0.48 |
| $C_6H_4OMe$-4 | 100 | 15 | 0.095 | 0.00031 | 0.24 |

| | | | | | |
|---|---|---|---|---|---|
| $C_6H_4OMe$-4 | 150 | 1 | 0.149 | 0.001 | 0.31 |
| $C_6H_4OMe$-4 | 150 | 2.5 | 0.148 | 0.0025 | 0.3 |
| $C_6H_4OMe$-4 | 150 | 5 | 0.147 | 0.005 | 0.31 |
| $C_6H_4OMe$-4 | 150 | 10 | 0.146 | 0.01 | 0.34 |
| $C_6H_4OMe$-4 | 150 | 15 | 0.145 | 0.015 | 0.25 |

| R | $[HCl]_0$ /mmol $dm^{-3}$ | $[Cl^-]_0$ /mmol $dm^{-3}$ | $[HCl]_0$ /mmol $dm^{-3}$ | $[Cl^-]_0$ /mmol $dm^{-3}$ | $k_{obs}$ /$s^{-1}$ |
|---|---|---|---|---|---|
| $C_6H_4Cl$-4 | 100 | 0 | 0.1 | 0 | 0.32 |
| $C_6H_4Cl$-4 | 100 | 1 | 0.1 | 0.001 | 0.31 |
| $C_6H_4Cl$-4 | 100 | 2 | 0.1 | 0.002 | 0.17 |
| $C_6H_4Cl$-4 | 100 | 3 | 0.1 | 0.003 | 0.03 |
| $C_6H_4Cl$-4 | 100 | 4 | 0.1 | 0.004 | 0.22 |
| $C_6H_4Cl$-4 | 100 | 5 | 0.1 | 0.005 | 0.13 |

| | | | | | |
|---|---|---|---|---|---|
| $C_6H_4Cl$-4 | 150 | 0 | 0.15 | 0 | 0.20 |
| $C_6H_4Cl$-4 | 150 | 1 | 0.15 | 0.001 | 0.18 |
| $C_6H_4Cl$-4 | 150 | 2 | 0.15 | 0.002 | 0.41 |
| $C_6H_4Cl$-4 | 150 | 3 | 0.15 | 0.003 | 0.21 |
| $C_6H_4Cl$-4 | 150 | 4 | 0.15 | 0.004 | 0.27 |
| $C_6H_4Cl$-4 | 150 | 5 | 0.15 | 0.005 | 0.26 |

Table A2.5. Kinetic data of for the reaction of [Ni($O_2$CEt)(triphos)] with $lutH^+$ in the presence of lut in $CH_3CN$ at 25˚C.

| [$lutH^+$] /mmol $dm^{-3}$ | [lut] /mmol $dm^{-3}$ | $k_{obs}$ /$s^{-1}$ |
|---|---|---|
| 2.5 | 0.05 | 68.2 |
| 2.5 | 0.1 | 70.3 |
| 2.5 | 0.2 | 70.7 |
| 2.5 | 0.3 | 78.5 |
| 2.5 | 0.5 | 83.7 |
| | | |
| 5 | 0.05 | 138 |
| 5 | 0.1 | 147 |
| 5 | 0.2 | 148 |
| 5 | 0.3 | 160 |
| 5 | 0.5 | 169 |

Table A2.6. Kinetic data of for the reaction of [Ni($O_2CC_6H_5$)(triphos)] and with $lutH^+$ in the presence of lut in $CH_3CN$ at 25˚C.

| [$lutH^+$] /mmol $dm^{-3}$ | [lut] /mmol $dm^{-3}$ | $k_{obs}$ /$s^{-1}$ |
|---|---|---|
| 2.5 | 0.0 | 38.2 |
| 2.5 | 0.05 | 44.4 |
| 2.5 | 0.1 | 44.0 |
| 2.5 | 0.2 | 48.4 |
| 2.5 | 0.3 | 52.9 |
| 2.5 | 0.5 | 57.7 |
| | | |
| 5 | 0.0 | 93.1 |
| 5 | 0.05 | 101.5 |
| 5 | 0.1 | 90.9 |
| 5 | 0.2 | 93.9 |
| 5 | 0.3 | 104.2 |
| 5 | 0.5 | 107.8 |
| | | |
| 10 | 0.0 | 222.6 |
| 10 | 0.05 | 242.1 |
| 10 | 0.1 | 177.9 |
| 10 | 0.2 | 231.4 |
| 10 | 0.3 | 229.7 |
| 10 | 0.5 | 231.7 |

Table A3.1. Kinetic data for the reaction of $[Ni(SR)(triphos)]BPh_4$ with $[lutH]BPh_4$ and lut at 25 °C in MeCN.(R = $Bu^t$, Et, Cyh).

| R | $[lutH]^+$ / $mmol^{-1}$ $dm^{-3}$ | [lut] / $mmol^{-1}$ $dm^{-3}$ | $k_{obs}$ / $s^{-1}$ |
|---|---|---|---|
| $Bu^t$ | 10 | 2.5 | 0.10 |
| $Bu^t$ | 10 | 5 | 0.11 |
| $Bu^t$ | 10 | 10 | 0.12 |
| $Bu^t$ | 10 | 20 | 0.11 |
| $Bu^t$ | 10 | 40 | 0.12 |
| | | | |
| $Bu^t$ | 25 | 2.5 | 0.32 |
| $Bu^t$ | 25 | 5 | 0.36 |
| $Bu^t$ | 25 | 10 | 0.36 |
| $Bu^t$ | 25 | 20 | 0.33 |
| $Bu^t$ | 25 | 40 | 0.35 |

| R | $[lutH]^+$ / $mmol^{-1}$ $dm^{-3}$ | [lut] / $mmol^{-1}$ $dm^{-3}$ | $k_{obs}$ / $s^{-1}$ |
|---|---|---|---|
| Et | 10 | 2.5 | 0.24 |
| Et | 10 | 5 | 0.18 |
| Et | 10 | 10 | 0.08 |
| Et | 10 | 20 | 0.10 |
| Et | 10 | 40 | 0.40 |
| | | | |
| Et | 25 | 2.5 | 0.34 |
| Et | 25 | 5 | 0.38 |
| Et | 25 | 10 | 0.27 |
| Et | 25 | 20 | 0.30 |
| Et | 25 | 40 | 0.34 |

| R | $[lutH]^+$ / $mmol^{-1}$ $dm^{-3}$ | [lut] / $mmol^{-1}$ $dm^{-3}$ | $k_{obs}$ / $s^{-1}$ |
|---|---|---|---|
| Cyh | 10 | 2.5 | 0.13 |
| Cyh | 10 | 5 | 0.14 |
| Cyh | 10 | 10 | 0.12 |
| Cyh | 10 | 20 | 0.13 |
| Cyh | 10 | 40 | 0.11 |
| | | | |
| Cyh | 25 | 2.5 | 0.23 |
| Cyh | 25 | 5 | 0.47 |
| Cyh | 25 | 10 | 0.36 |
| Cyh | 25 | 20 | 0.30 |
| Cyh | 25 | 40 | 0.34 |

Table A3.2. Kinetic data for the reaction of $[Ni(OC_6H_4R\text{-}4)(triphos)]BPh_4$ with $lutH^+$ and lut at 25 °C in MeCN and λ = 350.(R = H, $CH_3$, Cl, $OCH_3$).

| R | $[lutH]^+$ / $mmol^{-1}$ $dm^{-3}$ | [lut] / $mmol^{-1}$ $dm^{-3}$ | $k_{obs}$ / $s^{-1}$ |
|---|---|---|---|
| H | 5 | 0.6125 | 0.02 |
| H | 5 | 1.25 | 0.032 |
| H | 5 | 2.5 | 0.030 |
| H | 5 | 5 | 0.032 |
| H | 5 | 10 | 0.029 |
| | | | |
| H | 10 | 0.6125 | 0.03 |
| H | 10 | 1.25 | 0.03 |
| H | 10 | 2.5 | 0.04 |
| H | 10 | 5 | 0.05 |
| H | 10 | 10 | 0.06 |
| | | | |
| H | 20 | 0.6125 | 0.06 |
| H | 20 | 1.25 | 0.06 |
| H | 20 | 2.5 | 0.07 |
| H | 20 | 5 | 0.075 |
| H | 20 | 10 | 0.08 |

| R | $[lutH]^+$ / $mmol^{-1}$ $dm^{-3}$ | [lut] / $mmol^{-1}$ $dm^{-3}$ | $k_{obs}$ / $s^{-1}$ |
|---|---|---|---|
| $CH_3$ | 5 | 0.6125 | 0.013 |
| $CH_3$ | 5 | 1.25 | 0.017 |
| $CH_3$ | 5 | 2.5 | 0.026 |
| $CH_3$ | 5 | 5 | 0.039 |
| $CH_3$ | 5 | 10 | 0.048 |
| | | | |
| $CH_3$ | 10 | 0.6125 | 0.046 |
| $CH_3$ | 10 | 1.25 | 0.058 |
| $CH_3$ | 10 | 2.5 | 0.063 |
| $CH_3$ | 10 | 5 | 0.063 |
| $CH_3$ | 10 | 10 | 0.09 |
| | | | |
| $CH_3$ | 20 | 0.6125 | 0.038 |
| $CH_3$ | 20 | 1.25 | 0.033 |
| $CH_3$ | 20 | 2.5 | 0.053 |
| $CH_3$ | 20 | 5 | 0.049 |
| $CH_3$ | 20 | 10 | 0.053 |

| R | $[lutH]^+$ / $mmol^{-1}$ $dm^{-3}$ | [lut] / $mmol^{-1}$ $dm^{-3}$ | $k_{obs}$ / $s^{-1}$ |
|---|---|---|---|
| $OCH_3$ | 5 | 0.6125 | 0.013 |
| $OCH_3$ | 5 | 1.25 | 0.008 |
| $OCH_3$ | 5 | 2.5 | 0.013 |
| $OCH_3$ | 5 | 5 | 0.017 |
| $OCH_3$ | 5 | 10 | 0.019 |
| | | | |
| $OCH_3$ | 10 | 0.6125 | 0.06 |
| $OCH_3$ | 10 | 1.25 | 0.065 |
| $OCH_3$ | 10 | 2.5 | 0.067 |
| $OCH_3$ | 10 | 5 | 0.046 |
| $OCH_3$ | 10 | 10 | 0.055 |
| | | | |
| $OCH_3$ | 20 | 0.6125 | 0.32 |
| $OCH_3$ | 20 | 1.25 | 0.32 |
| $OCH_3$ | 20 | 2.5 | 0.41 |
| $OCH_3$ | 20 | 5 | 0.28 |
| $OCH_3$ | 20 | 10 | 0.2 |

| R | $[lutH]^+$ / $mmol^{-1}$ $dm^{-3}$ | [lut] / $mmol^{-1}$ $dm^{-3}$ | $k_{obs}$ / $s^{-1}$ |
|---|---|---|---|
| Cl | 5 | 0.6125 | 0.013 |
| Cl | 5 | 1.25 | 0.01 |
| Cl | 5 | 2.5 | 0.007 |
| Cl | 5 | 5 | 0.027 |
| Cl | 5 | 10 | 0.03 |
| | | | |
| Cl | 10 | 0.6125 | 0.02 |
| Cl | 10 | 1.25 | 0.05 |
| Cl | 10 | 2.5 | 0.01 |
| Cl | 10 | 5 | 0.04 |
| Cl | 10 | 10 | 0.03 |
| | | | |
| Cl | 20 | 0.6125 | 0.02 |
| Cl | 20 | 1.25 | 0.02 |
| Cl | 20 | 2.5 | 0.03 |
| Cl | 20 | 5 | 0.05 |
| Cl | 20 | 10 | 0.049 |

Table A3.3. Kinetic data for the reaction of [Ni(SePh)(triphos)]$BPh_4$ with [lutH]$BPh_4$ and lut at 25 °C in MeCN and λ = 350 nm.

| R | $[lutH]^+$ / $mmol^{-1}$ $dm^{-3}$ | [lut] / $mmol^{-1}$ $dm^{-3}$ | $k_{obs}$ / $s^{-1}$ |
|---|---|---|---|
| SePh | 5 | 0.6125 | 0.035 |
| SePh | 5 | 1.25 | 0.034 |
| SePh | 5 | 2.5 | 0.038 |
| SePh | 5 | 5 | 0.044 |
| SePh | 5 | 10 | 0.057 |
| | | | |
| SePh | 10 | 0.6125 | 0.037 |
| SePh | 10 | 1.25 | 0.036 |
| SePh | 10 | 2.5 | 0.038 |
| SePh | 10 | 5 | 0.034 |
| SePh | 10 | 10 | 0.036 |
| | | | |
| SePh | 20 | 0.6125 | 0.046 |
| SePh | 20 | 1.25 | 0.042 |
| SePh | 20 | 2.5 | 0.043 |
| SePh | 20 | 5 | 0.041 |
| SePh | 20 | 10 | 0.044 |

Table A3.4. Kinetic data of the Temperature Change Studies for the reaction of [Ni(SEt)(triphos)]$BPh_4$ with $lutH^+$ and lut in MeCN and $\lambda = 350$ nm.

| R | $[lutH]^+$ /$mmol^{-1}\,dm^{-3}$ | [Lut] /$mmol^{-1}\,dm^{-3}$ | $k_{obs}$ /$s^{-1}$ | T /°C |
|---|---|---|---|---|
| Et | 25 | 2.5 | 0.31 | 288 |
| Et | 25 | 5 | 0.25 | 288 |
| Et | 25 | 10 | 0.28 | 288 |
| Et | 25 | 20 | 0.38 | 288 |
| Et | 25 | 40 | 0.18 | 288 |
| | | | | |
| Et | 25 | 2.5 | 0.57 | 293 |
| Et | 25 | 5 | 0.44 | 293 |
| Et | 25 | 10 | 0.44 | 293 |
| Et | 25 | 20 | 0.54 | 293 |
| Et | 25 | 40 | 0.16 | 293 |
| | | | | |
| Et | 25 | 2.5 | 0.65 | 298 |
| Et | 25 | 5 | 0.84 | 298 |
| Et | 25 | 10 | 0.63 | 298 |
| Et | 25 | 20 | 0.42 | 298 |
| Et | 25 | 40 | 0.42 | 298 |
| | | | | |
| Et | 25 | 2.5 | 1.21 | 303 |
| Et | 25 | 5 | 1.00 | 303 |
| Et | 25 | 10 | 0.99 | 303 |
| Et | 25 | 20 | 0.92 | 303 |
| Et | 25 | 40 | 1.02 | 303 |
| | | | | |
| Et | 25 | 2.5 | 1.47 | 308 |
| Et | 25 | 5 | 1.16 | 308 |
| Et | 25 | 10 | 1.054 | 308 |
| Et | 25 | 20 | 0.95 | 308 |
| Et | 25 | 40 | 1.22 | 308 |

Table A3.5. Kinetic data of the Temperature Change Studies for the reaction of $[Ni(SBu^t)(triphos)]BPh_4$ with $[lutH]^+$ and lut in MeCN and $\lambda = 350$ nm.

| R | $[lutH]^+$ /mmol$^{-1}$ dm$^{-3}$ | [lut] /mmol$^{-1}$ dm$^{-3}$ | $k_{obs}$ /s$^{-1}$ | T /°C |
|---|---|---|---|---|
| $Bu^t$ | 25 | 2.5 | 0.25 | 293 |
| $Bu^t$ | 25 | 5 | 0.3 | 293 |
| $Bu^t$ | 25 | 10 | 0.26 | 293 |
| $Bu^t$ | 25 | 20 | 0.24 | 293 |
| $Bu^t$ | 25 | 40 | 0.22 | 293 |
| | | | | |
| $Bu^t$ | 25 | 2.5 | 0.26 | 298 |
| $Bu^t$ | 25 | 5 | 0.31 | 298 |
| $Bu^t$ | 25 | 10 | 0.31 | 298 |
| $Bu^t$ | 25 | 20 | 0.318 | 298 |
| $Bu^t$ | 25 | 40 | 0.26 | 298 |
| | | | | |
| $Bu^t$ | 25 | 2.5 | 0.36 | 303 |
| $Bu^t$ | 25 | 5 | 0.37 | 303 |
| $Bu^t$ | 25 | 10 | 0.40 | 303 |
| $Bu^t$ | 25 | 20 | 0.39 | 303 |
| $Bu^t$ | 25 | 40 | 0.44 | 303 |
| | | | | |
| $Bu^t$ | 25 | 2.5 | 0.51 | 308 |
| $Bu^t$ | 25 | 5 | 0.64 | 308 |
| $Bu^t$ | 25 | 10 | 0.55 | 308 |
| $Bu^t$ | 25 | 20 | 0.52 | 308 |
| $Bu^t$ | 25 | 40 | 0.32 | 308 |
| | | | | |
| $Bu^t$ | 25 | 2.5 | 0.51 | 213 |
| $Bu^t$ | 25 | 5 | 0.63 | 213 |
| $Bu^t$ | 25 | 10 | 0.73 | 213 |
| $Bu^t$ | 25 | 20 | 0.72 | 213 |
| $Bu^t$ | 25 | 40 | 0.46 | 213 |

Table A3.6. Kinetic data of the Temperature Change Studies for the reaction of $[Ni(SCyh)(triphos)]BPh_4$ with $[lutH]^+$ and lut in MeCN and $\lambda = 350$ nm.

| R | $[lutH]^+$ /mmol$^{-1}$ dm$^{-3}$ | [lut] /mmol$^{-1}$ dm$^{-3}$ | $k_{obs}$ /s$^{-1}$ | T /°C |
|---|---|---|---|---|
| Cyh | 25 | 2.5 | 0.025 | 293.1 |
| Cyh | 25 | 5 | 0.023 | 293.1 |
| Cyh | 25 | 10 | 0.05 | 293.1 |
| Cyh | 25 | 20 | 0.047 | 293.1 |
| Cyh | 25 | 40 | 0.046 | 293.1 |
| | | | | |
| Cyh | 25 | 2.5 | 0.78 | 298.1 |
| Cyh | 25 | 5 | 0.074 | 298.1 |
| Cyh | 25 | 10 | 0.065 | 298.1 |
| Cyh | 25 | 20 | 0.074 | 298.1 |
| Cyh | 25 | 40 | 0.063 | 298.1 |
| | | | | |
| Cyh | 25 | 2.5 | 0.064 | 303 |
| Cyh | 25 | 5 | 0.078 | 303 |
| Cyh | 25 | 10 | 0.082 | 303 |
| Cyh | 25 | 20 | 0.100 | 303 |
| Cyh | 25 | 40 | 0.080 | 303 |
| | | | | |
| Cyh | 25 | 2.5 | 0.13 | 308 |
| Cyh | 25 | 5 | 0.14 | 308 |
| Cyh | 25 | 10 | 0.14 | 308 |
| Cyh | 25 | 20 | 0.15 | 308 |
| Cyh | 25 | 40 | 0.14 | 308 |
| | | | | |
| Cyh | 25 | 2.5 | | 313 |
| Cyh | 25 | 5 | 0.17 | 313 |
| Cyh | 25 | 10 | 0.21 | 313 |
| Cyh | 25 | 20 | 0.24 | 313 |
| Cyh | 25 | 40 | 0.21 | 313 |

Table A3.7. Kinetic data of the Isotop Effect Studies for the reaction of [Ni(SR)(triphos)]$BPh_4$ (R= Et, $Bu^t$, Cyh) with $[lutH/D]^+$ and lut at 25.0 ˚C in MeCN and $\lambda$ = 350 nm.

| R | $[lutD]^+$ /$mmol^{-1}\,dm^{-3}$ | [lut] /$mmol^{-1}\,dm^{-3}$ | $k_{obs}$ /$s^{-1}$ | T /°C |
|---|---|---|---|---|
| Et | 10 | 2.5 | 0.14 | 298 |
| Et | 10 | 5 | 0.087 | 298 |
| Et | 10 | 10 | 0.09 | 298 |
| Et | 10 | 20 | 0.11 | 298 |
| Et | 10 | 40 | 0.08 | 298 |
| | | | | |
| Et | 25 | 2.5 | 0.062 | 298 |
| Et | 25 | 5 | 0.04 | 298 |
| Et | 25 | 10 | 0.06 | 298 |
| Et | 25 | 20 | 0.068 | 298 |
| Et | 25 | 40 | 0.07 | 298 |
| | | | | |
| $Bu^t$ | 10 | 2.5 | 0.16 | 298 |
| $Bu^t$ | 10 | 5 | 0.11 | 298 |
| $Bu^t$ | 10 | 10 | 0.14 | 298 |
| $Bu^t$ | 10 | 20 | 0.11 | 298 |
| $Bu^t$ | 10 | 40 | 0.12 | 298 |
| | | | | |
| $Bu^t$ | 25 | 2.5 | 0.32 | 298 |
| $Bu^t$ | 25 | 5 | 0.32 | 298 |
| $Bu^t$ | 25 | 10 | 0.31 | 298 |
| $Bu^t$ | 25 | 20 | 0.29 | 298 |
| $Bu^t$ | 25 | 40 | 0.29 | 298 |
| | | | | |
| Cyh | 10 | 2.5 | 0.047 | 298 |
| Cyh | 10 | 5 | 0.017 | 298 |
| Cyh | 10 | 10 | 0.023 | 298 |
| Cyh | 10 | 20 | 0.019 | 298 |
| Cyh | 10 | 40 | 0.016 | 298 |
| | | | | |
| Cyh | 25 | 2.5 | 0.018 | 298 |
| Cyh | 25 | 5 | 0.015 | 298 |
| Cyh | 25 | 10 | 0.017 | 298 |
| Cyh | 25 | 20 | 0.021 | 298 |
| Cyh | 25 | 40 | 0.017 | 298 |

Table A4.1. Kinetic data for the reaction of [Ni(SR)(dppe)] with $[lutH]^+$ and lut at 25 °C in MeCN (R = But, Et, Cyh) and λ = 350 nm.

| R | $[lutH]^+$ /$mmol^{-1}\,dm^{-3}$ | [lut] /$mmol^{-1}\,dm^{-3}$ | | $k_{obs}$ / $s^{-1}$ |
|---|---|---|---|---|
| Et | 5 | 1.25 | | 0.74 |
| Et | 5 | 2.5 | | 0.74 |
| Et | 5 | 5 | | 0.77 |
| Et | 5 | 10 | | 0.78 |
| Et | 5 | 20 | | 0.93 |
| | | | | |
| Et | 10 | 1.25 | | 1.15 |
| Et | 10 | 2.5 | | 0.91 |
| Et | 10 | 5 | | 1.07 |
| Et | 10 | 10 | | 0.62 |
| Et | 10 | 20 | | 0.81 |
| | | | | |
| Et | 20 | 1.25 | | 1.36 |
| Et | 20 | 2.5 | | 1.12 |
| Et | 20 | 5 | | 1.36 |
| Et | 20 | 10 | | 1.28 |
| Et | 20 | 20 | | 1.22 |

| R | $[lutH]^+$ /$mmol^{-1}\,dm^{-3}$ | [lut] /$mmol^{-1}\,dm^{-3}$ | | $k_{obs}$ / $s^{-1}$ |
|---|---|---|---|---|
| $Bu^t$ | 5 | 1.25 | | 0.21 |
| $Bu^t$ | 5 | 2.5 | | 0.18 |
| $Bu^t$ | 5 | 5 | | 0.24 |
| $Bu^t$ | 5 | 10 | | 0.33 |
| $Bu^t$ | 5 | 20 | | 0.36 |
| | | | | |
| $Bu^t$ | 10 | 1.25 | | 0.17 |
| $Bu^t$ | 10 | 2.5 | | 0.21 |
| $Bu^t$ | 10 | 5 | | 0.16 |
| $Bu^t$ | 10 | 10 | | 0.29 |
| $Bu^t$ | 10 | 20 | | 0.24 |
| | | | | |
| $Bu^t$ | 20 | 1.25 | | 0.03 |
| $Bu^t$ | 20 | 2.5 | | 0.31 |
| $Bu^t$ | 20 | 5 | | 0.042 |
| $Bu^t$ | 20 | 10 | | 0.061 |
| $Bu^t$ | 20 | 20 | | 0.24 |
| | | | | |
| R | $[lutH]^+$ /$mmol^{-1}\,dm^{-3}$ | [lut] /$mmol^{-1}\,dm^{-3}$ | | $k_{obs}$ / $s^{-1}$ |
| Cyh | 5 | 1.25 | | 0.074 |
| Cyh | 5 | 2.5 | | 0.076 |
| Cyh | 5 | 5 | | 0.064 |
| Cyh | 5 | 10 | | 0.096 |
| Cyh | 5 | 20 | | 0.139 |
| | | | | |
| Cyh | 10 | 1.25 | | 0.083 |
| Cyh | 10 | 2.5 | | 0.048 |
| Cyh | 10 | 5 | | 0.081 |
| Cyh | 10 | 10 | | 0.124 |
| Cyh | 10 | 20 | | 0.107 |
| | | | | |
| Cyh | 20 | 1.25 | | 0.029 |
| Cyh | 20 | 2.5 | | 0.049 |
| Cyh | 20 | 5 | | 0.03 |
| Cyh | 20 | 10 | | 0.176 |
| Cyh | 20 | 20 | | 0.095 |

Table A5.1. Kinetic data for the reaction of $[Fe_4S_4(OPh)_4]^{2-}$ with $[PhS^-]$ in the presence of $[NHEt_3]^+$ in MeCN at 25.0 $^oC$. Kinetic data was determined at $\lambda$ = 500 nm.

| $[NEt_4]SPh$ /mmol$^{-1}$ dm$^{-3}$ | $[NHEt_3]BPh_4$ /mmol$^{-1}$ dm$^{-3}$ | $k_{obs1}$ /s$^{-1}$ | $k_{obs2}$ /s$^{-1}$ |
|---|---|---|---|
| 5 | 0 | 0.67 | 0.04 |
| 5 | 5 | 0.01 | 0.014 |
| 5 | 10 | 0.29 | 0.008 |
| 5 | 20 | 0.01 | 0.006 |
| 5 | 40 | 0.89 | 0.06 |
| 5 | 60 | 0.76 | 0.08 |
| 5 | 100 | 0.21 | 0.13 |
| | | | |
| 10 | 0 | 0.86 | 0.047 |
| 10 | 5 | 0.52 | 0.03 |
| 10 | 10 | 0.027 | 0.027 |
| 10 | 20 | 0.31 | 0.025 |
| 10 | 40 | 0.77 | 0.051 |
| 10 | 60 | 1.1 | 0.05 |
| 10 | 100 | 0.99 | 0.05 |
| | | | |
| 5 | 0 | 1.77 | 0.06 |
| 5 | 5 | 1.6 | 0.05 |
| 5 | 10 | | |
| 5 | 20 | 2.4 | 0.16 |
| 5 | 40 | 0.66 | 0.04 |
| 5 | 60 | 0.63 | 0.037 |
| 5 | 100 | 0.6 | 0.04 |
| | | | |
| 10 | 0 | 2.6 | 0.034 |
| 10 | 5 | 1.6 | 0.06 |
| 10 | 10 | 2.4 | 0.037 |
| 10 | 20 | 0.31 | 0.028 |
| 10 | 40 | 0.56 | 0.03 |
| 10 | 60 | 0.734 | 0.021 |
| 10 | 100 | 0.66 | 0.03 |

Table A5.2. Kinetic data for the reaction of $[\{MoFe_3S_4(OPh)_3\}_2(SPh)_3]^{3-}$ with $[PhS^-]$ in the presence of $[NHEt_3]^+$ in MeCN at 25.0 $^oC$. Kinetic data was determined at $\lambda$ = 500 nm.

| $[NEt_4]SPh$ /$mmol^{-1}\,dm^{-3}$ | $[NHEt_3]BPh_4$ /$mmol^{-1}\,dm^{-3}$ | $k_{obs1}$ /$s^{-1}$ | $k_{obs2}$ /$s^{-1}$ |
|---|---|---|---|
| 5 | 5 | 0.38 | 0.068 |
| 5 | 10 | 0.7 | 0.087 |
| 5 | 20 | 0.81 | 0.091 |
| 5 | 40 | 0.55 | 0.05 |
| 5 | 60 | 0.54 | 0.13 |
| | | | |
| 10 | 5 | 0.39 | 0.025 |
| 10 | 10 | 0.5 | 0.06 |
| 10 | 20 | 0.76 | 0.076 |
| 10 | 40 | 0.9 | 0.11 |
| 10 | 60 | 0.76 | 0.072 |

## Appendix B: rate law derivation and Arrhenius and Eyring Equations.

## 1. Arrhenius and Eyring Equations.

Arrhenius [1] and Eyring equations can describe the effect of the temperature on the rate of the reaction in Equation (1), A = pre-exponential factor, $E_a$ = activation energy. $k$ = rate constant of the reaction, R = gas constant and T = temperature.

$$\ln k = \ln A - \frac{E_a}{RT} \quad (1)$$

The Eyring equation is dependent on the transition state model and describes all matter phases. The transition state theory described the chemical reaction of two reactants, A and B combine to produce transition state as shown in Equation (2). The transition state ($AB^{\ddagger}$) is unstable species, and there are two pathways: convert this transition state into the product C or go back to the A and B reactants.

$$A + B \underset{k_{-1}}{\overset{k_1}{\rightleftharpoons}} AB^{\ddagger} \xrightarrow{k_2} C \quad (2)$$

From the mechanism in Equation (2) we can derive the rate law as shown in Equation (3), that relates the variation of the concentration of $AB^{\ddagger}$ with time deduced from the mechanism in Equation (2) where, [A], [B] and [$AB^{\ddagger}$] are the equilibrium concentrations of A, Band $AB^{\ddagger}$ respectively.

$$\frac{-d[AB^{\ddagger}]}{dt} = k_1[A][B] - k_{-1}[AB^{\ddagger}] - k_2[AB^{\ddagger}] \quad (3)$$

The equilibrium constant $K^{\ddagger}$ for the equilibrium reaction between reactant (A and B) and the transition state ($AB^{\ddagger}$) can be described by the Equation (4).

$$K^{\ddagger} = \frac{k_1}{k_{-1}} = \frac{[AB^{\ddagger}]}{[A][B]} \quad (4)$$

Thus at the equilibrium $k_1$[A][B] and $k_{-1}$ [$AB^{\ddagger}$] are equal and removed in equation 3 to give Equation (5).

$$\frac{-d[\mathrm{AB}^{\ddagger}]}{d\mathrm{t}} = k_2[\mathrm{AB}^{\ddagger}] \quad (5)$$

According to statistical mechanics, $k_2$ ($s^{-1}$) is derived by Equation (6), where, $k_B$ is the Boltzmann constant ($k_B$= 1.381x10$^{-23}$ J.K$^{-1}$), h is the Planck constant (h = 6.626 x 10$^{-34}$ J.s) and T the temperature.

$$k_2 = \frac{\mathrm{k_B T}}{\mathrm{h}} \quad (6)$$

Using Equations (4) and (6), Equation (5) will become Equation (7).

$$\frac{-d[\mathrm{AB}^{\ddagger}]}{d\mathrm{t}} = \frac{\mathrm{k_B T}}{\mathrm{h}} K^{\ddagger}[\mathrm{A}][\mathrm{B}] \quad (7)$$

The observed rate constant, $k$ ($dm^3$ $mol^{-1}$ $s^{-1}$), is as shown by Equation (8).

$$k_{\mathrm{obs}} = \frac{\mathrm{k_B T}}{\mathrm{h}} K^{\ddagger} \quad (8)$$

From the free activation enthalpy $\Delta G^{\ddagger}$ (kJ $mol^{-1}$) (Equations (9) and (10)), the activation enthalpy ($\Delta H^{\ddagger}$ in kJ $mol^{-1}$) and the activation entropy ($\Delta S^{\ddagger}$ in kJ $mol^{-1}$ $K^{-1}$) can be related to $K^{\ddagger}$ ($dm^3$ $mol^{-1}$) Equation (11).

$$\Delta G^{\ddagger} = -RT\ln(K^{\ddagger}) \quad (9)$$

$$\Delta G^{\ddagger} = \Delta H^{\ddagger} - T\Delta S^{\#} \quad (10)$$

$$\ln k = \frac{-\Delta H^{\ddagger}}{RT} + \frac{-\Delta S^{\ddagger}}{R} \quad (11)$$

Replacing $K^{\ddagger}$ from Equation (11) in Equation (7) gives Equation (12).

$$k = \frac{\mathrm{k_B T}}{\mathrm{h}} \mathrm{e}^{\left(\frac{-\Delta H^{\ddagger}}{RT}\right)} \mathrm{e}^{\left(\frac{-\Delta S^{\ddagger}}{R}\right)} \quad (12)$$

Rearrangement Equation (12) gives Equation (13), which is called Eyring equation.

$$\ln k = \ln\left(\frac{k_B \mathrm{T}}{\mathrm{h}}\right) - \frac{\Delta \mathrm{H}^{\ddagger}}{\mathrm{R}} + \frac{\Delta \mathrm{S}^{\ddagger}}{\mathrm{R}} \quad (13)$$

Rearrange the Equation (13) to find the linear form as shown Equation (14).

$$\ln\left(\frac{k}{\mathrm{T}}\right) = -\frac{\Delta \mathrm{H}^{\ddagger}}{\mathrm{R}}\left(\frac{1}{\mathrm{T}}\right) + \ln\frac{k_{\mathrm{B}}}{\mathrm{h}} + \frac{\Delta \mathrm{S}^{\ddagger}}{\mathrm{R}} \quad (14)$$

We can find the activation enthalpy ($\Delta H^{\ddagger}$) and the activation entropy ($\Delta S^{\ddagger}$), From the slope (m) and the intercept (b) of the plot of ln(*k*/T) against 1/T.

$$\mathrm{m} = -\frac{\Delta \mathrm{H}^{\ddagger}}{\mathrm{R}}$$

$$\mathrm{b} = \ln\frac{k_{\mathrm{B}}}{\mathrm{h}} + \frac{\Delta \mathrm{S}^{\ddagger}}{\mathrm{R}}$$

The value of the Gibbs free energy of activation ($\Delta G^{\ddagger}$) can be determined from ($\Delta H^{\ddagger}$) and $\Delta S^{\ddagger}$) at any temperature T using Equation (10).

1. Atkins, P. W. *Physical Chemistry, 5th ed, Oxford University Press.* **1994**.

## 2. Rate law derivation for $[Fe_4S_4(OPh)_4]^{2-}$.

The rate law associated with this acid-catalysed dissociative substitution mechanism is derived as follows.

From the mechanism in Figure (4.6), if it is assumed that the dissociation of (OPh) group is the rate-limiting step of the reaction.

$$\text{Rate } = k_0 + k_2[\text{Fe}_4\text{S}_3(\text{SH})(\text{OPh})_4]_e^{2-} \quad \text{(B1)}$$

(The subscript 'e' refers to a concentration at equilibrium)

The equilibrium constant $K_1$ can be defined as shown in Equation (B2).

$$K_1 = \frac{[\text{Fe}_4\text{S}_3(\text{SH})(\text{OPh})_4]_e^{2-}[\text{NEt}_3]}{[\text{Fe}_4\text{S}_4(\text{OPh})_4]_e^{2-}[\text{NHEt}_3^+]} \quad \text{(B2)}$$

Rearranging equation (B2) and replaceing the $[\text{Fe}_4\text{S}_3(\text{SH})(\text{OPh})_4]_e^{2-}$term, equation (B3) is obtained.

$$\text{Rate } = K_1\, k_2[\text{Fe}_4\text{S}_4(\text{OPh})_4]_e^{2-}\frac{[\text{NHEt}_3^+]}{[\text{NEt}_3]} \quad \text{(B3)}$$

The total initial concentration of cluster ($[\text{Fe}_4\text{S}_4(\text{OPh})_4]_\text{T}^{2-}$) must equal the sum of the equilibrium concentrations of the intermediate species. This is expressed mathematically by equation (B4).

$$[\text{Fe}_4\text{S}_4(\text{OPh})_4]_\text{T}^{2-} = [\text{Fe}_4\text{S}_4(\text{OPh})_4]_e^{2-} + [\text{Fe}_4\text{S}_3(\text{SH})(\text{OPh})_4]_e^{2-} \quad \text{(B4)}$$

Rearranging equation (B2) and substituting into equation (B4) gives equation (B5).

$$[\text{Fe}_4\text{S}_4(\text{OPh})_4]_\text{T}^{2-} = [\text{Fe}_4\text{S}_4(\text{OPh})_4]_e^{2-} + K_1[\text{Fe}_4\text{S}_4(\text{OPh})_4]_e^{2-}\frac{[\text{NHEt}_3^+]}{[\text{NEt}_3]} \quad \text{(B5)}$$

A rearranged form of equation (B5) is shown below.

$$[\text{Fe}_4\text{S}_4(\text{OPh})_4]_e^{2-} = \frac{[\text{Fe}_4\text{S}_4(\text{OPh})_4]_\text{T}^{2-}}{1 + \frac{K_1[\text{NHEt}_3^+]}{[\text{NEt}_3]}} \quad \text{(B6)}$$

Finally substituting (B6) into equation (B3) yields the theoretical rate law (B7).

$$\text{Rate} = \left\{ \frac{K_1 k_2 \frac{[\text{NHEt}_3^+]_e}{[\text{NEt}_3]_e}}{1 + K_1^R \frac{[\text{NHEt}_3^+]_e}{[\text{NEt}_3]_e}} \right\} [\text{Fe}_4\text{S}_4(\text{OPh})_4]_\text{T}^{2-} \qquad \text{(B7)}$$

# 3. Cluster $^{1}$H NMR spectra.

1. $[Fe_4S_4(SPh)_4]^{2-}$

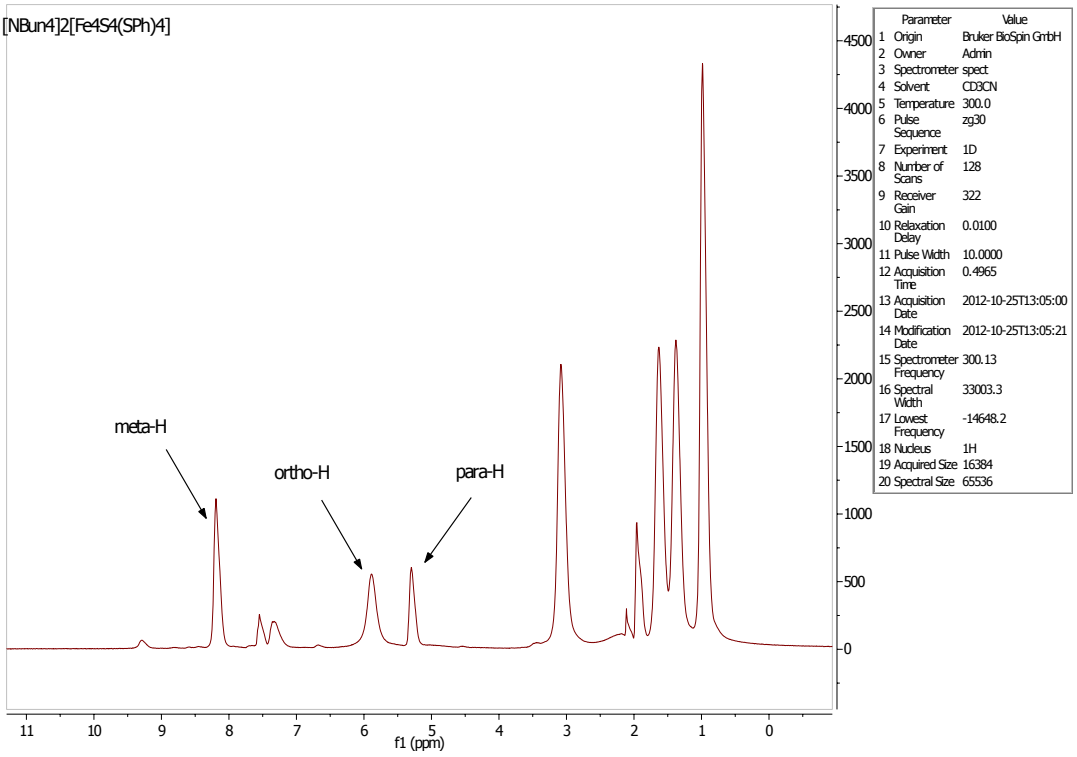


2. $[Fe_4S_4Cl_4]^{2-}$

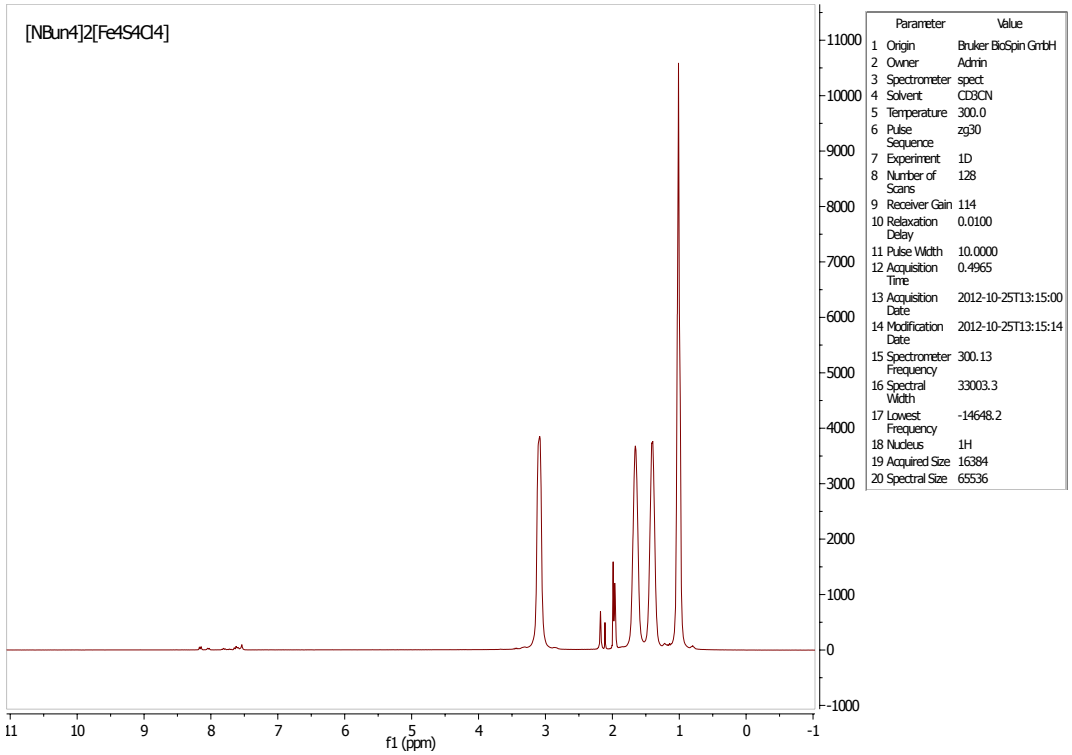


$[Fe_4S_4(OPh)_4]^{2-}$

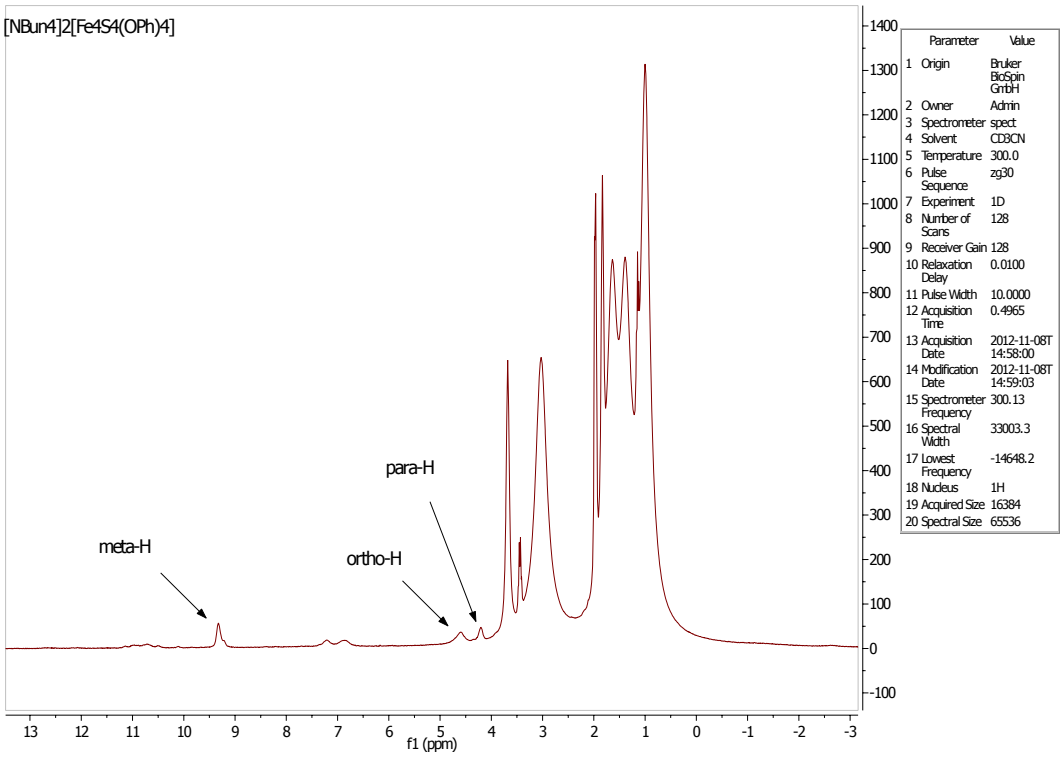


$[\{MoFe_3S_4(SPh)_3\}_2(\mu\text{-}SPh)_3]^{3-}$

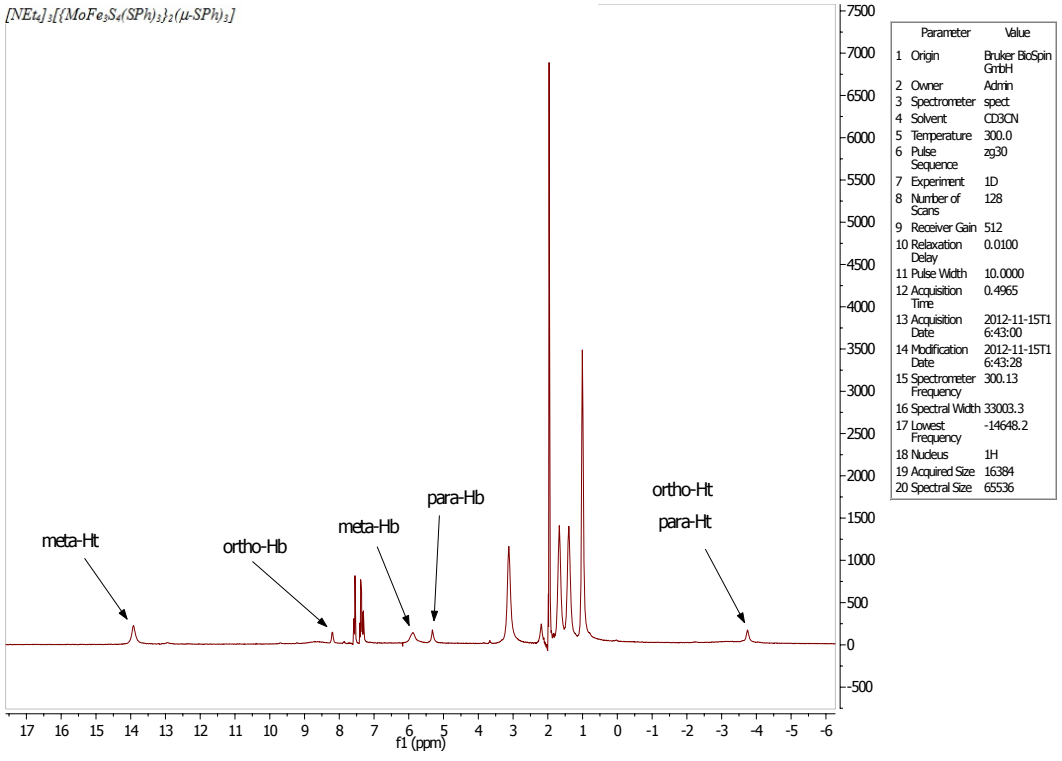

$[\{MoFe_3S_4Cl_3\}_2(\mu\text{-}SPh)_3]^{3-}$

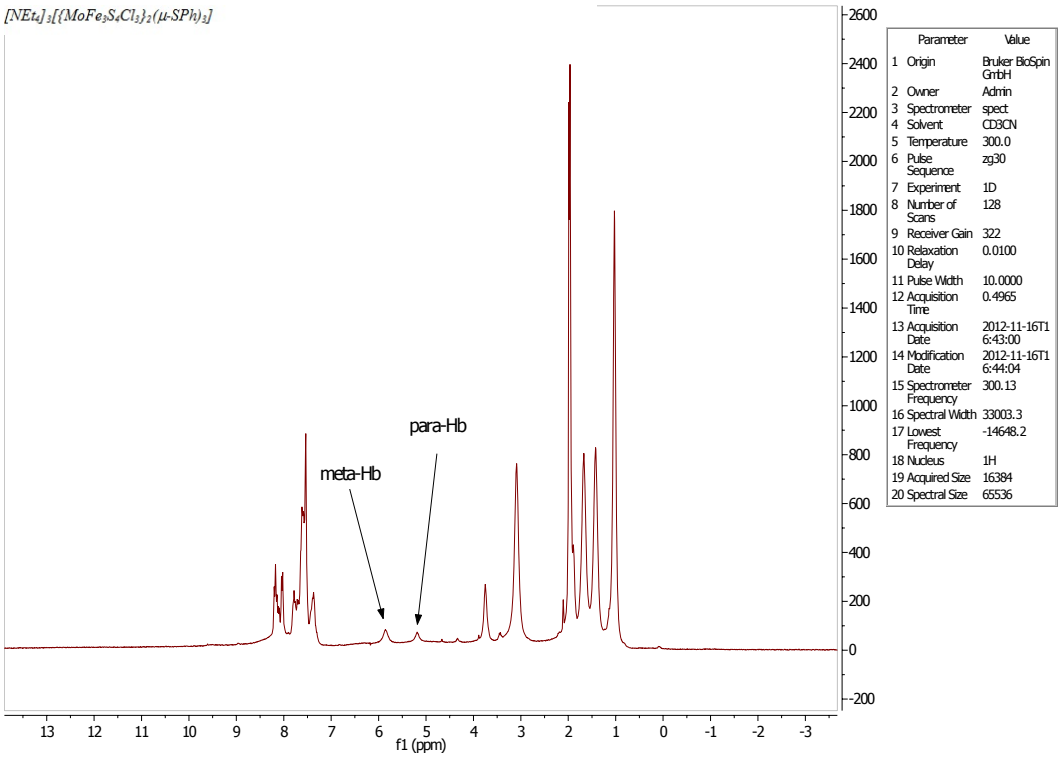


| | Parameter | Value |
|---|---|---|
| 1 | Origin | Bruker BioSpin GmbH |
| 2 | Owner | Admin |
| 3 | Spectrometer | spect |
| 4 | Solvent | CD3CN |
| 5 | Temperature | 300.0 |
| 6 | Pulse Sequence | zg30 |
| 7 | Experiment | 1D |
| 8 | Number of Scans | 128 |
| 9 | Receiver Gain | 322 |
| 10 | Relaxation Delay | 0.0100 |
| 11 | Pulse Width | 10.0000 |
| 12 | Acquisition Time | 0.4965 |
| 13 | Acquisition Date | 2012-11-16T16:43:00 |
| 14 | Modification Date | 2012-11-16T16:44:04 |
| 15 | Spectrometer Frequency | 300.13 |
| 16 | Spectral Width | 33003.3 |
| 17 | Lowest Frequency | -14648.2 |
| 18 | Nucleus | 1H |
| 19 | Acquired Size | 16384 |
| 20 | Spectral Size | 65536 |

# 4. DFT calculation

## Chapter two

All theoretical calculations in this work were performed using the computational methods implemented in the GAUSSIAN09 package [1] and the geometries of the compounds were optimized at the B3LYP/Lanl2dz levels of theory.


1. M. J. Frisch, G. W. Trucks, H. B. Schlegel, G. E. Scuseria, M. A. Robb, J. R. Cheeseman, J. A. Montgomery, Jr., T. Vreven, K. N. Kudin, J. C. Burant, J. M. Millam, S. S. Iyengar, J. Tomasi, V. Barone, B. Mennucci, M. Cossi, G. Scalmani, N. Rega, G. A. Petersson, H. Nakatsuji, M. Hada, M. Ehara, K. Toyota, R. Fukuda, J. Hasegawa, M. Ishida, T. Nakajima, Y. Honda, O. Kitao, H. Nakai, M. Klene, X. Li, J. E. Knox, H. P. Hratchian, J. B. Cross, V. Bakken, C. Adamo, J. Jaramillo, R. Gomperts, R. E. Stratmann, O. Yazyev, A. J. Austin, R. Cammi, C. Pomelli, J. W. Ochterski, P. Y. Ayala, K. Morokuma, G. A. Voth, P. Salvador, J. J. Dannenberg, V. G. Zakrzewski, S. Dapprich, A. D. Daniels, M. C. Strain, O. Farkas, D. K. Malick, A. D. Rabuck, K. Raghavachari, J. B. Foresman, J. V. Ortiz, Q. Cui, A. G. Baboul, S. Clifford, J. Cioslowski, B. B. Stefanov, G. Liu, A. Liashenko, P. Piskorz, I. Komaromi, R. L. Martin, D. J. Fox, T. Keith, M. A. Al-Laham, C. Y. Peng, A. Nanayakkara, M. Challacombe, P. M. W. Gill, B. Johnson, W. Chen, M. W. Wong, C. Gonzalez and J. A. Pople, *Gaussian 09, revision D.01; Gaussian, Inc.: Wallingford, CT*, 2004.


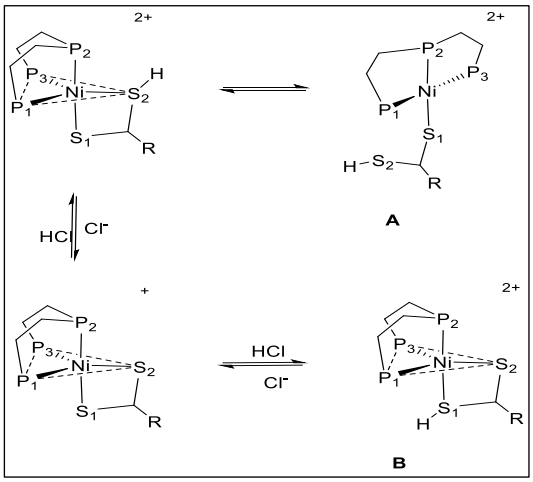


Figure B2.1. Summary of the results of DFT calculations showing the different structural consequences of protonation at axial and equatorial sulfur sites in $[Ni(S_2CR)(triphos)]^+$. Selected bond lengths and bond angles of $A^R$ and $B^R$ (R = Me or Ph) are presented in Tables B2.1 and B2.2, respectively, and pictures of the corresponding $A^R$ are shown in Figures B2.2 and B2.3, respectively.

| | Complex $\mathbf{A}^{\mathbf{Me}}$ | Complex $\mathbf{B}^{\mathbf{Me}}$ |
|---|---|---|
| *bond lengths* | | |
| Ni-$P_1$ | 2.3369 | 2.2971 |
| Ni-$P_2$ | 2.3034 | 2.2110 |
| Ni-$P_3$ | 2.3295 | 2.2519 |
| Ni-$S_1$ | 2.3187 | 2.2988 |
| Ni-$S_2$ | 3.4270 | 2.5345 |
| *bond angles* | | |
| $P_1$-Ni-$P_2$ | 85.085 | 87.13 |
| $P_1$-Ni-$P_3$ | 152.052 | 127.98 |
| $P_1$-Ni-$S_1$ | 94.845 | 95.98 |
| $P_1$-Ni-$S_2$ | | 100.92 |
| $P_2$-Ni-$P_3$ | 85.785 | 86.92 |
| $P_2$-Ni-$S_1$ | 179.017 | 173.19 |
| $P_2$-Ni-$S_2$ | | 119.82 |
| $P_3$-Ni-$S_1$ | 93.840 | 95.83 |
| $P_3$-Ni-$S_2$ | | 106.54 |

Table B2.1. Selected bond lengths and angles of $Ni(HS_2CMe)(triphos)]^{2+}$ from DFT calculations

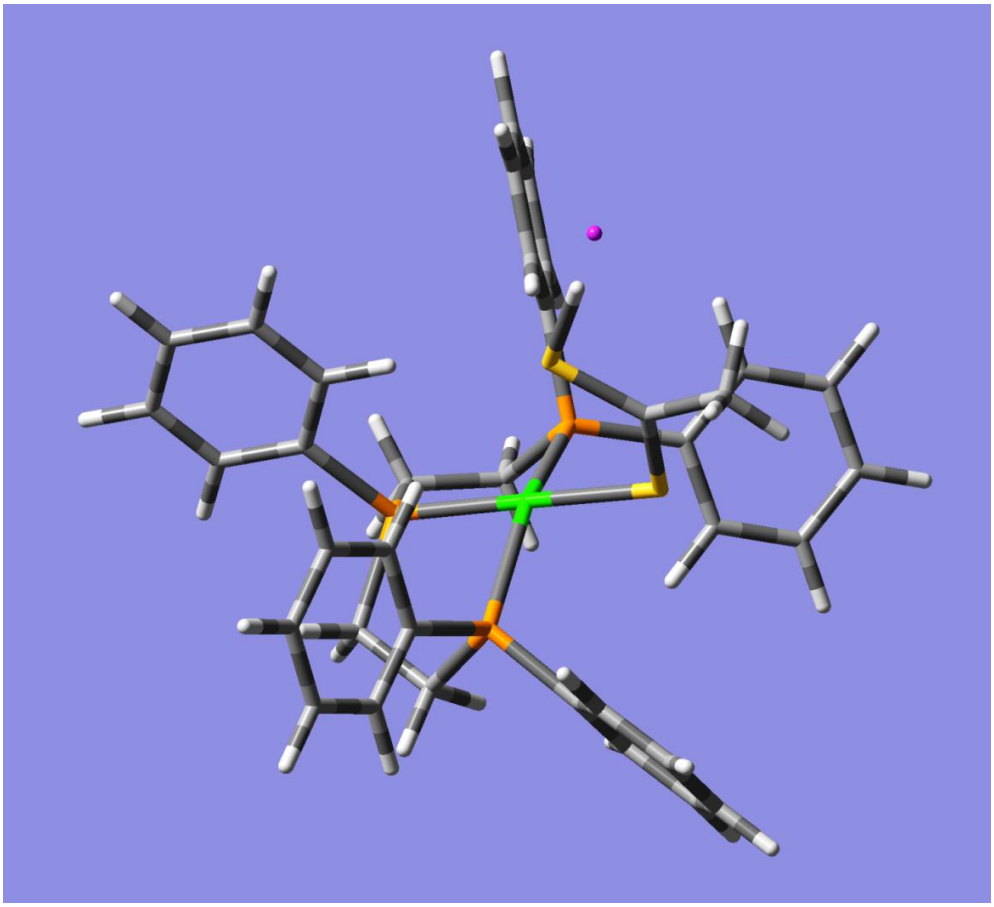

**Figure B2.2.** Picture of the optimised structure of $[Ni(HS_2CMe)(triphos)]^{2+}$ ($\mathbf{A^{Me}}$) showing the protonated carboxydithioate ligand has undergone chelate ring opening. Key: Ni = green; P = orange; S = yellow; H = white, C = grey and Cl = magenta.

| | Complex $E^{Ph}$ | Complex $F^{Ph}$ |
|---|---|---|
| *bond lengths* | | |
| Ni-$P_1$ | 2.2665 | 2.2665 |
| Ni-$P_2$ | 2.2176 | 2.2630 |
| Ni-$P_3$ | 2.2630 | 2.2176 |
| Ni-$S_1$ | 2.2865 | 2.0423 |
| Ni-$S_2$ | 3.5122 | 2.4400 |
| *bond angles* | | |
| $P_1$-Ni-$P_2$ | 85.90 | 85.90 |
| $P_1$-Ni-$P_3$ | 152.31 | 152.31 |
| $P_1$-Ni-$S_1$ | 94.17 | 90.91 |
| $P_1$-Ni-$S_2$ | | 104.47 |
| $P_2$-Ni-$P_3$ | 85.25 | 85.25 |
| $P_2$-Ni-$S_1$ | 179.93 | 167.33 |
| $P_2$-Ni-$S_2$ | | 123.24 |
| $P_3$-Ni-$S_1$ | 94.69 | 92.04 |
| $P_3$-Ni-$S_2$ | | 102.33 |

**Table B2.2.** Selected bond lengths and angles of $Ni(HS_2CPh)(triphos)]^{2+}$ from DFT calculations

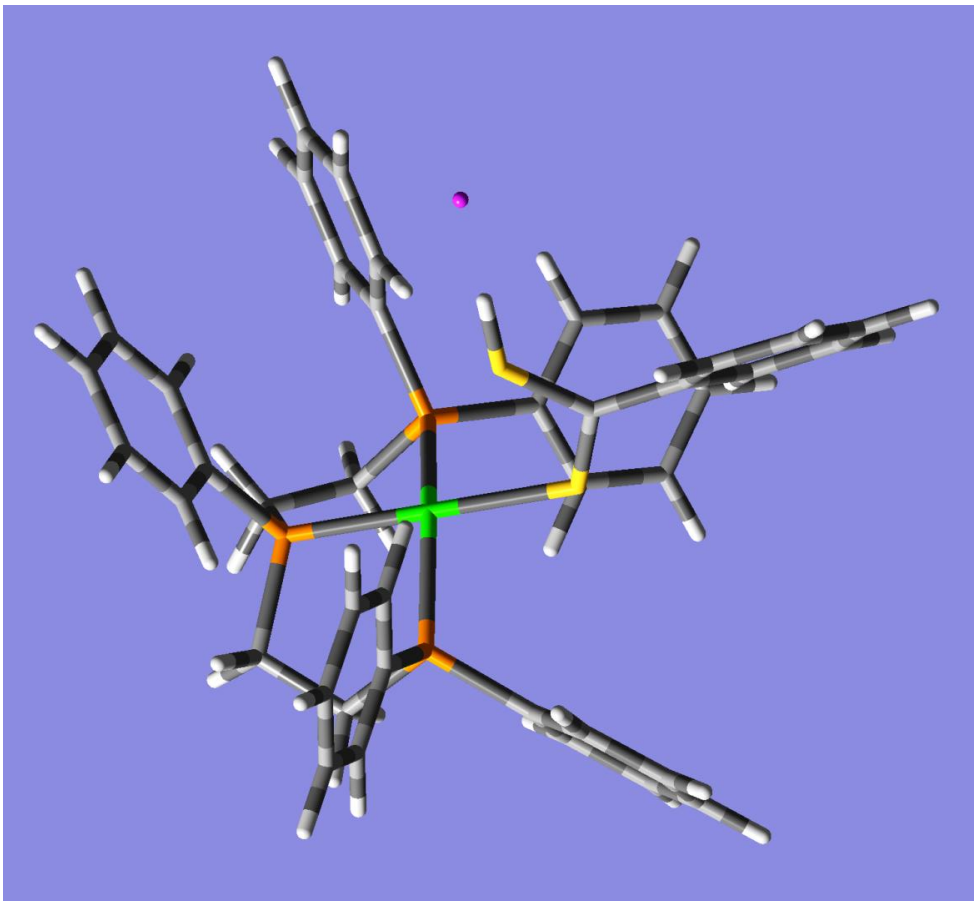

**Figure B2.3.** Picture of the optimised structure of $[Ni(HS_2CPh)(triphos)]^{2+}$ ($\mathbf{A^{Ph}}$) showing the protonated carboxydithioate ligand has undergone chelate ring opening. Key: Ni = green; P = orange; S = yellow; H = white, C = grey and Cl = magenta.

Table B3.1. Selected bond lengths and angles derived from the calculations for the hydrogen-bonded species {[Ni(XPh)(triphos)]$^+$---lutH$^+$} (R= O, S or Se).

| Parameter | Complex | | |
|---|---|---|---|
| Bond lengths/Å | [Ni(OPh)(triphos)]$^+$ | [Ni(SPh)(triphos)]$^+$ | [Ni(SePh)(triphos)]$^+$ |
| Ni-P1 | 2.3835 | 2.3238 | 2.3215 |
| Ni-P2 | 2.3067 | 2.2948 | 2.3002 |
| Ni-P3 | 2.3610 | 2.3442 | 2.3409 |
| Ni-X | 1.8944 | 2.2839 | 2.3901 |
| C-X | 1.3958 | 1.8485 | 1.9716 |
| H-X | 1.6842 | 2.3670 | 2.5471 |
| N-H | 1.0609 | 1.0368 | 1.0354 |
| | | | |
| Bond angles/° | | | |
| P1-Ni-P2 | 84.2774 | 85.2205 | 85.1328 |
| P2-Ni-P3 | 84.5498 | 85.6313 | 85.5031 |
| P1-Ni-P3 | 151.9061 | 153.4338 | 154.4351 |
| P1-Ni-X | 101.8269 | 103.6225 | 103.5088 |
| P2-Ni-X | 171.6689 | 167.8539 | 167.5933 |
| P3-Ni-X | 92.3319 | 89.7014 | 90.0012 |
| Ni-X-C | 128.3714 | 117.9724 | 115.2255 |
| Ni-X-H | 124.1439 | 130.3322 | 123.0030 |
| C-X-H | 101.8936 | 97.3252 | 95.1183 |

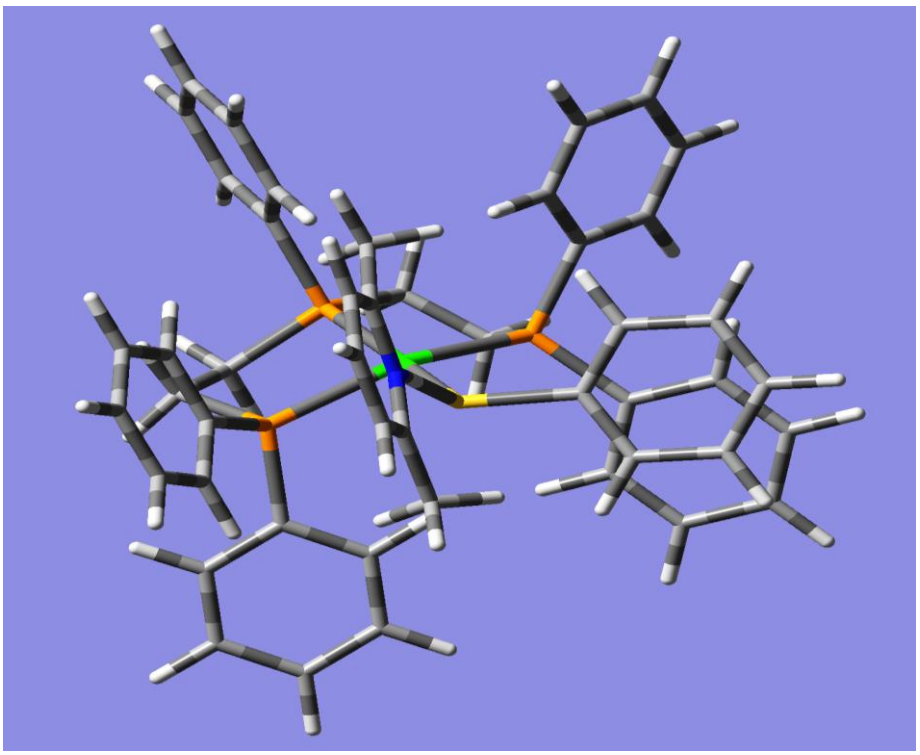

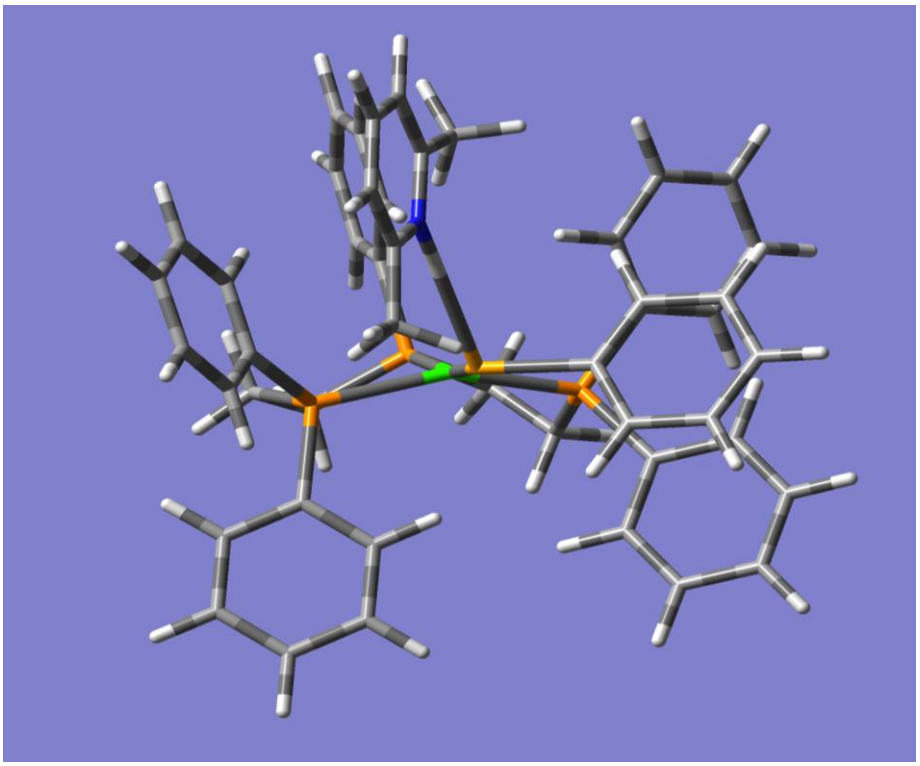

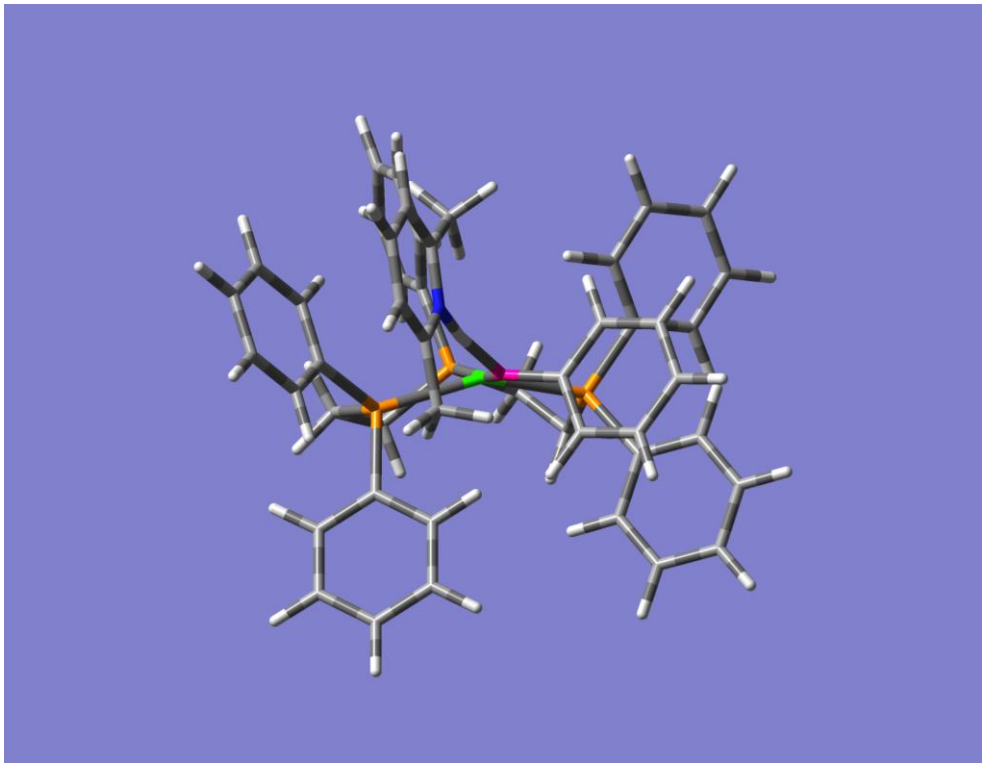

Figure B3.1. Pictures of the optimised structure of {[Ni($SC_6H_5$)(triphos)]$^+$---lutH$^+$}, {[Ni($SeC_6H_5$)(triphos)]$^+$---lutH$^+$} and {[Ni($OC_6H_5$)(triphos)]$^+$---lutH$^+$} showing the geometry of the hydrogen bonding interaction. Key: Ni = green; P = orange; S = yellow; N = blue; H = white and C = grey.

Table B4.1. Selected bond lengths and angles derived from the calculations for the hydrogen-bonded species {[Ni(SHR)(triphos)]---lutH$^{+}$} (R= Et, Bu$^{t}$ or Cyh).

| Parameter | [Ni(HSEt)(triphos)] | [Ni(HSBu$^{t}$)(triphos)] | [Ni(HSCyh)(triphos)] |
|---|---|---|---|
| Ni-P1 | 2.33473 | 2.35311 | 2.32963 |
| Ni-P2 | 2.29079 | 2.32919 | 2.29869 |
| Ni-P3 | 2.33023 | 2.3668 | 2.33649 |
| Ni-S | 2.3006 | 2.31255 | 2.27555 |
| P1-Ni-P2 | 85.06658 | 84.91285 | 84.52393 |
| P2-Ni-P3 | 85.6279 | 85.02603 | 85.50576 |
| P1-Ni-P3 | 158.92493 | 158.74326 | 154.28664 |
| P1-Ni-S | 101.26322 | 102.12949 | 104.03828 |
| P3-Ni-S | 91.33322 | 88.01439 | 90.58002 |
| P2-Ni-S | 168.46444 | 172.78483 | 166.54556 |
| S-C | 1.91881 | 1.97145 | 1.93026 |
| Ni-S-C | 113.77755 | 118.406 | 116.78104 |
| S-H | 2.31315 | 2.14504 | 2.37687 |
| N-H | 1.04372 | 1.05815 | 1.03862 |
| S-H-N | 172.01931 | 169.59028 | 174.58668 |
| Ni-S-H | 131.05371 | 123.73605 | 127.08483 |
| C-S-H | 100.68797 | 106.75615 | 105.06983 |
| H-H | 3.17595 | 3.40154 | 2.92708 |
| Ni-H | 4.19923 | 3.93178 | 4.16539 |
| E | -1920 | -1919 | -2076 |

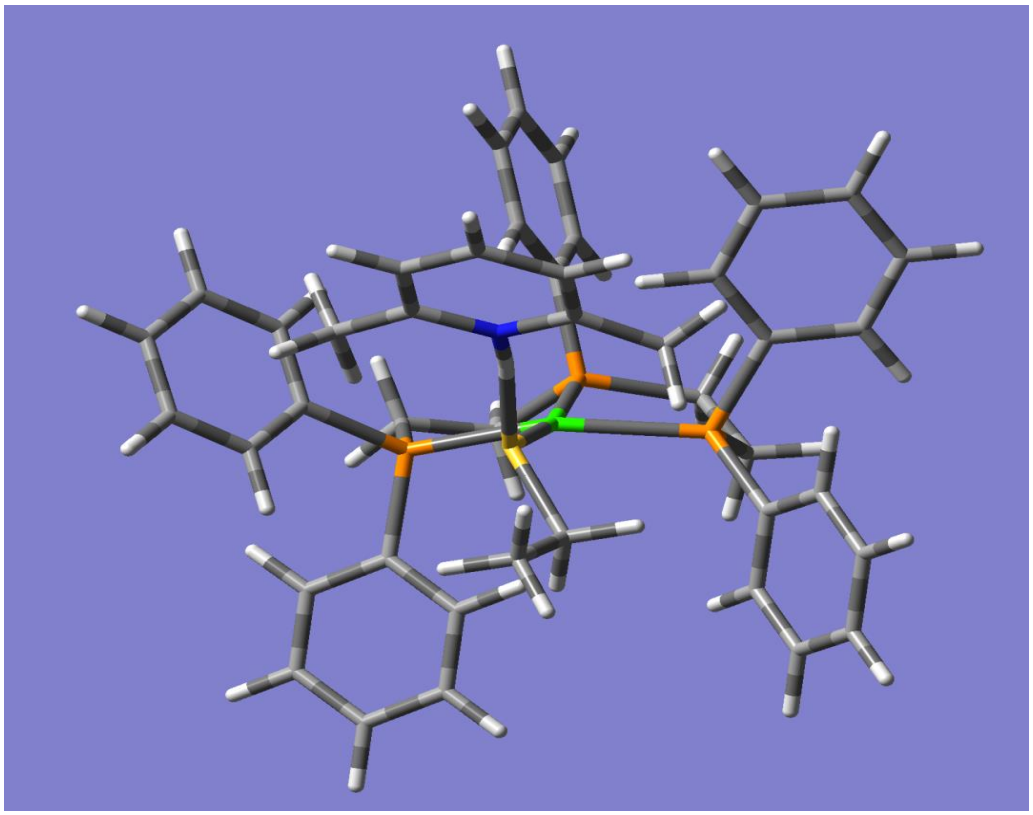

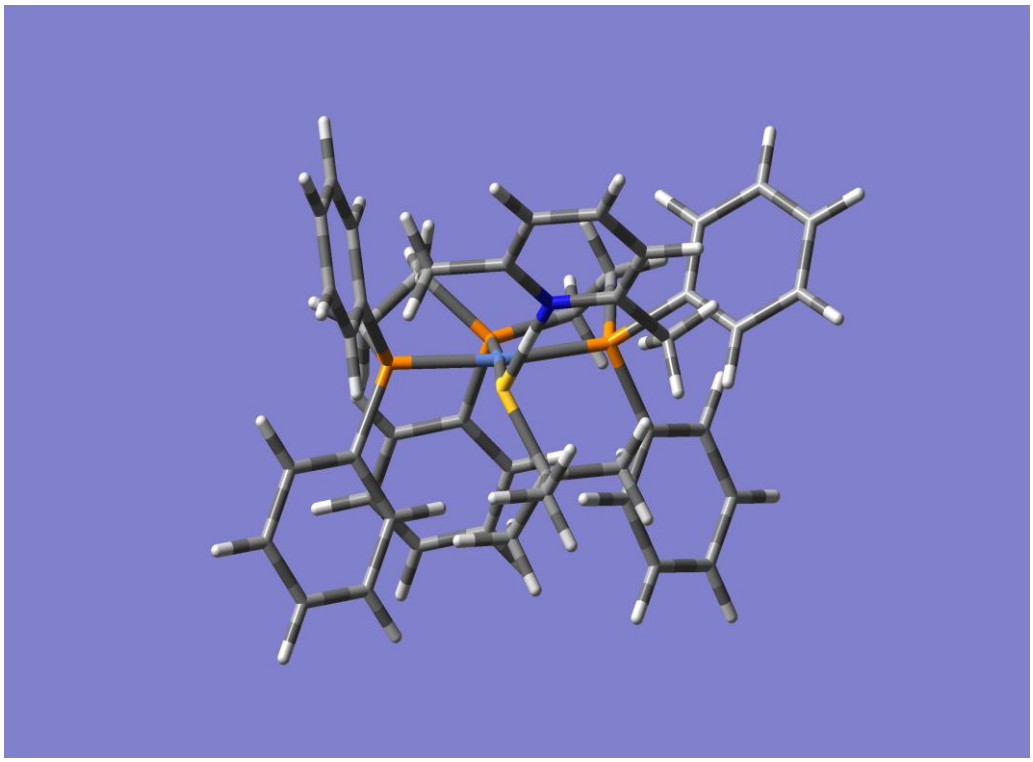

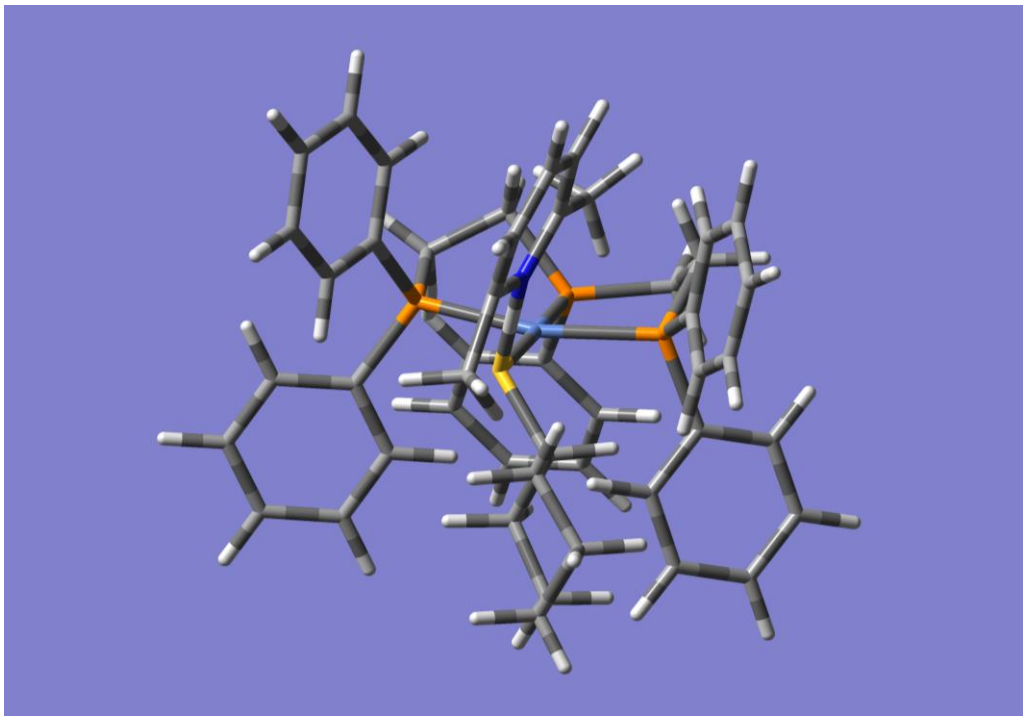

Figure.View of {[Ni(SEt)(triphos)]---Hlut}$^{2+}$, {[Ni(SBu$^{t}$)(triphos)]---Hlut}$^{2+}$ and {[Ni(SCyh)(triphos)]---Hlut}$^{2+}$ respectively, showing the orientation of the hydrogen bonded lutH$^{+}$. Colour key: green = Ni; orange = P; yellow = S and blue = N).